

# CHEMIA

**STUDIA  
UNIVERSITATIS BABEȘ-BOLYAI  
CHEMIA**

**1/2014**

**EDITORIAL BOARD**  
**STUDIA UNIVERSITATIS BABEȘ-BOLYAI**  
**CHEMIA**

**ONORARY EDITOR:**

IONEL HAIDUC - Member of the Romanian Academy

**EDITOR-IN-CHIEF:**

LUMINIȚA SILAGHI-DUMITRESCU

**EXECUTIVE EDITOR:**

CASTELIA CRISTEA

**EDITORIAL BOARD:**

PAUL ȘERBAN AGACHI, Babeș-Bolyai University, Cluj-Napoca, Romania

LIVAIN BREAU, UQAM University of Quebec, Montreal, Canada

HANS JOACHIM BREUNIG, Institute of Inorganic and Physical Chemistry,  
University of Bremen, Bremen, Germany

MIRCEA DIUDEA, Babes-Bolyai University, Cluj-Napoca, Romania

JEAN ESCUDIE, HFA, Paul Sabatier University, Toulouse, France

ION GROSU, Babeș-Bolyai University, Cluj-Napoca, Romania

EVAMARIE HEY-HAWKINS, University of Leipzig, Leipzig, Germany

FLORIN DAN IRIMIE, Babeș-Bolyai University, Cluj-Napoca, Romania

FERENC KILAR, University of Pecs, Pecs, Hungary

BRUCE KING, University of Georgia, Athens, Georgia, USA

ANTONIO LAGUNA, Department of Inorganic Chemistry, ICMA, University of  
Zaragoza, Zaragoza, Spain

JURGEN LIEBSCHER, Humboldt University, Berlin, Germany

KIERAN MOLLOY, University of Bath, Bath, UK

IONEL CĂTĂLIN POPESCU, Babeș-Bolyai University, Cluj-Napoca, Romania

CRISTIAN SILVESTRU, Babeș-Bolyai University, Cluj-Napoca, Romania

<http://chem.ubbcluj.ro/~studiachemia/>; [studiachemia@chem.ubbcluj.ro](mailto:studiachemia@chem.ubbcluj.ro)  
[http://www.studia.ubbcluj.ro/serii/chemia/index\\_en.html](http://www.studia.ubbcluj.ro/serii/chemia/index_en.html)

YEAR  
MONTH  
ISSUE

Volume 59 (LIX) 2014  
MARCH  
1

# STUDIA

## UNIVERSITATIS BABEȘ-BOLYAI

### CHEMIA

1

---

STUDIA UBB EDITORIAL OFFICE: B.P. Hasdeu no. 51, 400371 Cluj-Napoca, Romania,  
Phone + 40 264 405352

---

#### CUPRINS – CONTENT – SOMMAIRE – INHALT

OANA ONIJA, GHEORGHE BORODI, VASILE POP, LELIA CIONTEA, LUCIA RUS, New Solid Form of Promethazine Hydrochloride.....	7
LIVIA PATRAȘCU, CORINA GAMBUȚEANU, PETRU ALEXE, Rheological and Physical Characteristics of Minced <i>Biceps Femoris</i> Muscle in Different Brining Systems .....	13
HAMID REZA FAZLOLLAHI, HOSSEIN SHABANI, A Group Theoretical Method for Computing Harary Index .....	23
LOTFALLAH POURFARAJ, MODJTABA GHORBANI, Remarks on the Reciprocal Degree Distance .....	29
ANCA MUNCEANU, BOTOND NAGY, MARIA TRIF, NORBERT DIMA, <i>Pseudomonas Fluorescens</i> Lipase as Biocatalyst in the Enzymatic Kinetic Resolution of Chiral Phenothiazin Ethanol.....	35
ALINA BRATAN, MANUELA MINCEA, IOANA RODICA LUPSA, MARILEN GABRIEL PIRTEA, VASILE OSTAFE, Quantification of Nicotine and Cotinine in Teenager's Urine .....	47

MIHAIL CHIRA, HORATIU VERMESAN, VASILE RUS, ERNEST GRUNWALD, Corrosion Behavior of Zn-Ni Coatings Electrodeposited in Pulsed Current and Magnetic Field on Different Substrates by Electrochemical Impedance Spectroscopy Techniques .....	63
EDIT FORIZS, ATTILA-ZSOLT KUN, EMESE-ZSUZSÁNNA BOD, FIRUȚA GOGA, JENŐ BÓDIS, Experimental and Theoretical Investigations on Coordination Compounds of Acetazolamide .....	79
ANDRA CRISTINA GAGIU, ELENA MARIA PICA, GHEORGHE BLAGA, PETRU PASCUTA, KERI AGNES, Mineralogical Characterisation and Heavy Metals Assessment of Soils from Urban Recreational Areas in Central Transylvania .....	87
TEODORA ELENA HARSA, QSAR Study on Nitrogen-Containing Flavonoids by Similarity Cluster Prediction.....	99
ALEXANDRA MARIA HARSA, A Novel QSAR Approach in Modeling Hydrophobicity of a Set of Flavonoids .....	111
MANUELA STAN, MARIA LOREDANA SORAN, CODRUȚA VARODI, ILDIKO LUNG, Influence of Microwave Field on the Ascorbic Acid Content in Leaves of Some Common Aromatic Plants in Romania...	125
SZABÓ (PÁLFI) MÁRIA, BÁLINT EMESE-ÉVA, SZILÁGYI LÁSZLÓ, ÁBRAHÁM BEÁTA, Comparative Study of Green Fluorescent Protein Mutants .....	135
TATYANA S. TISHAKOVA, Extraction in CCl <sub>4</sub> of Ionic Associates of Iodine-Iodide Complexes with the Cationic Dye Brilliant Green .....	149
MARIN AMĂREANU, LARISA MELIȚĂ, Organic Polymer-Modified Cement Conceret .....	159
DEJAN PRVULOVIĆ, RUDOLF KASTORI, IMRE KÁDÁR, The Effect of Zinc from the Seed on Antioxidant Defense System in Winter Wheat ( <i>Triticale aestivum</i> L.) Seedlings .....	171
ANDREA (IUHASZ) FAZAKAS, ZSOLT BODOR, ERIKA KOVÁCS, ÉVA LASLO, SZABOLCS LÁNYI, BEÁTA ÁBRAHÁM, Isolation of Succinic Acid-Producing <i>Escherichia Coli</i> from Animal Faeces.....	177
TAMARA TOPALĂ, ANDREEA BODOKI, ALEJANDRO PASCUAL-ÁLVAREZ, LUMINIȚA OPREAN, RADU OPREAN, Design, Synthesis and Characterization of New Cu(II) Complexes with <i>N</i> -Substituted Sulfonamide Ligands .....	187
NAHID YAVARI, HOSSEIN SHABANI, HAMID REZA FAZLOLLAHI, MIRCEA V. DIUDEA, Computing the Harary Index of a Class of Nanostar Dendrimers .....	201

Studia Universitatis Babes-Bolyai Chemia has been selected for coverage in Thomson Reuters products and custom information services. Beginning with V. 53 (1) 2008, this publication is indexed and abstracted in the following:

- Science Citation Index Expanded (also known as SciSearch®)
- Chemistry Citation Index®
- Journal Citation Reports/Science Edition



## NEW SOLID FORM OF PROMETHAZINE HYDROCHLORIDE

OANA ONIJA<sup>a, b, \*</sup>, GHEORGHE BORODI<sup>a</sup>, VASILE POP<sup>b</sup>,  
LELIA CIONTEA<sup>b</sup>, LUCIA RUS<sup>c</sup>

**ABSTRACT.** The main objective of the present paper was to obtain new solid forms of Promethazine Hydrochloride (PTZ). The preparation was performed by grinding in a ball mill equipment Promethazine Hydrochloride and acetic acid (1:1). To evidence this new solid form of Promethazine Hydrochloride, different investigation techniques have been used: X-ray diffraction (XRD), Fourier transformed infrared (FTIR) spectroscopy, and Differential Thermal Analysis (DTA). XRPD data allowed the determination of the crystallographic system and lattice parameters. The new solid form crystallizes in a monoclinic system having the following unit cell parameters:  $a=14.52\text{\AA}$ ,  $b=9.33\text{\AA}$ ,  $c=14.21\text{\AA}$ ,  $\alpha=90^\circ$ ,  $\beta=110.59^\circ$ ,  $\gamma=90^\circ$ . In the FTIR spectra of PTZ and PTZ-acetic acid the displacement of the bands, indicating the formation of a new compound, appears in the  $1500\text{--}4000\text{ cm}^{-1}$  spectral range. In the DTA thermograms, the difference between the onset temperatures suggests that these two samples represent different solid forms.

**Keywords:** *Promethazine Hydrochloride, solid form.*

## INTRODUCTION

The new solid forms of API-active pharmaceutical ingredient are important in the field of pharmaceuticals because of their potential to modify the physico-chemical properties of the drug for a desired therapeutic use. Significant improvements of the API properties can often be achieved by the development of new solid forms [1].

PTZ, (RS)-dimethyl [1-methyl-2-(phenothiazine-10-yl) ethyl] amine hydrochloride is a phenothiazine derivate, a first-generation antihistamine of the phenothiazine family [2]. It is used for the amelioration of the allergic

---

<sup>a</sup> National Institute for Research and Development of Isotopic and Molecular Technologies, 65-103 Donath St., 400293 Cluj-Napoca, Romania, \* oana.onija@itim-cj.ro

<sup>b</sup> Technical University of Cluj-Napoca, 28 Memorandumului St., 400114 Cluj-Napoca, Romania

<sup>c</sup> Iuliu Hațieganu University of Medicine and Pharmacy, 8 Babeș St., 400012 Cluj-Napoca, Romania



reactions, the treatment of motion sickness and the prevention and control of nausea and vomiting, associated with certain types of anesthesia and surgery [3].

Recently, two crystalline structures of PTZ were determined by single crystal XRD and revealed a case of intergrowth of polymorphic domains. The two crystal structures of PTZ have been characterized and the conformation and crystal packing have been determined [4]. It was established that due to disorder, one form is less stable and it transforms into the more stable, but still disordered polymorph. In order to improve the stability of PTZ we investigated the possibility of obtaining new solid forms.

This study is focused on the preparation and characterization of a new solid form of PTZ. The preparation method consists in grinding the mixture PTZ - acetic acid (1:1) in a vibratory ball mill apparatus. For such a preparation method, it is not easy to describe the process leading to the formation of a new compound; an evaluation of the potential interaction between molecules is necessary. In our case, the most probable interaction is that of the carbonyl from acetic acid which may form hydrogen bonds with the nitrogen from the aliphatic part of PTZ. The component mixture is mechanically activated in the vibratory ball mill [5].

The resulted compound was investigated by X-ray powder diffraction (XRPD), infrared (FTIR) spectroscopy and differential thermal analysis (DTA).

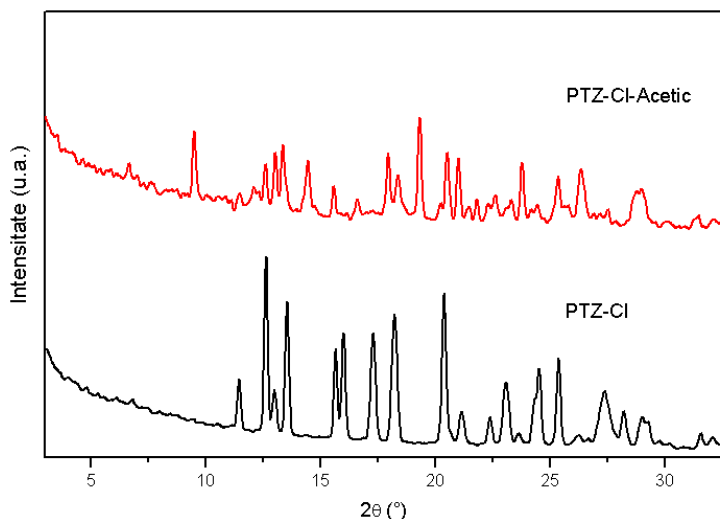
## RESULTS AND DISCUSSIONS

Figure 1 presents the X-Ray diffraction pattern of Promethazine Hydrochloride (PTZ) and of the PTZ - acetic acid form obtained as a result of the grinding preparation. The XRPD pattern for acetic acid is not necessary to be shown in the figure because of its liquid nature. Figure 1 indicates that the XRPD pattern of PTZ - acetic acid form is different from the XRPD pattern of PTZ, indicating that a new solid form was obtained. Indexing of the X-ray powder diffraction pattern was carried out using X-Cell indexing algorithm [6]. From the powder diffraction indexing it was obtained that the new solid form crystallizes in a monoclinic system having the following unit cell parameters:  $a=14.52\text{\AA}$ ,  $b=9.33\text{\AA}$ ,  $c=14.21\text{\AA}$ ,  $\alpha=90^\circ$ ,  $\beta=110.59^\circ$ ,  $\gamma=90^\circ$ .

In order to characterize the new solid form, the first technique was the FTIR spectroscopy. The FTIR spectra of PTZ and of the PTZ- acetic acid are presented in Figure 2.

The characteristic vibrational frequencies corresponding to the PTZ and PTZ-acetic acid are presented. The spectra of the PTZ contain the characteristic absorption bands due to CH stretching ( $2800\text{--}3000\text{ cm}^{-1}$ ),  $\text{NH}^+$  stretching ( $2200\text{--}2480\text{ cm}^{-1}$ ), aromatic C=C stretching ( $1591\text{ cm}^{-1}$ ),  $\text{CH}_3$  and  $\text{CH}_2$  bending ( $1430\text{--}1470\text{ cm}^{-1}$ ), C-N stretching of tertiary amine ( $1334\text{ cm}^{-1}$ ), out plane CH bending of distributed aromatic ( $1378\text{ cm}^{-1}$ ), according to literature [7].

## NEW SOLID FORM OF PROMETHAZINE HYDROCHLORIDE



**Figure 1.** X-ray powder diffraction for PTZ and PTZ-acetic acid.

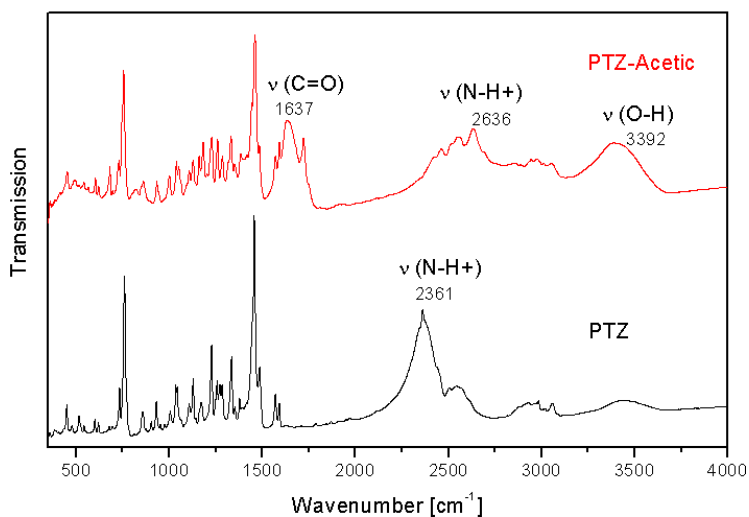


**Figure 2.** FTIR spectra of Promethazin Hydrochloride and its new solid form with acetic acid in the 350-4000 cm<sup>-1</sup> spectral range.

It is to notice that the FTIR spectra of PTZ and PTZ-acetic acid are quite similar in the spectral region 350-1500 cm<sup>-1</sup> and that displacement of the bands is appearing in the 1500-4000 cm<sup>-1</sup> spectral range. The carbonyl stretch of acetic acid appears as an absorption band at 1637cm<sup>-1</sup>. Concerning the O-H stretch, it is present in the spectrum as a wide band at 3392 cm<sup>-1</sup> [8], [9].

The PTZ crystal structure was solved by Borodi et al. [4]. The molecular configuration of the PTZ molecule and the intermolecular hydrogen bond with the Cl atom are shown in Figure 3. The organic cation interact with Cl<sup>-</sup> anion via N-H<sup>+</sup>... Cl hydrogen bond.

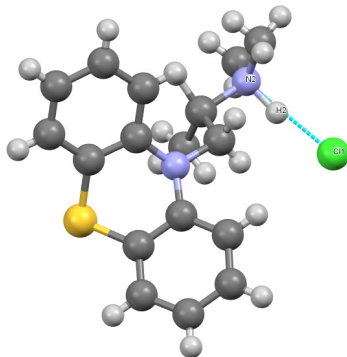


**Figure 3.** Model of molecular structure of PTZ

Based on the as determined crystal structure of PTZ, the IR spectrum was simulated and assignments were made. For the N-H<sup>+</sup> bond a vibration feature at 2361 cm<sup>-1</sup> is observed. In the FTIR spectrum of the PTZ-acetic acid form a significant reduction in the band intensity was found. In the meantime, a considerable band shift from 2361 cm<sup>-1</sup> to a higher wave number (2636 cm<sup>-1</sup>) is taking place. This is due to structural changes in the vicinity of the nitrogen ion, most likely generated by its interaction with the acetic acid.

Another way to characterize the new solid form is Differential Thermal Analysis. The DTA thermogram of PTZ (see Figure 4) shows a sharp endothermic peak at 230 °C, corresponding to the melting point.

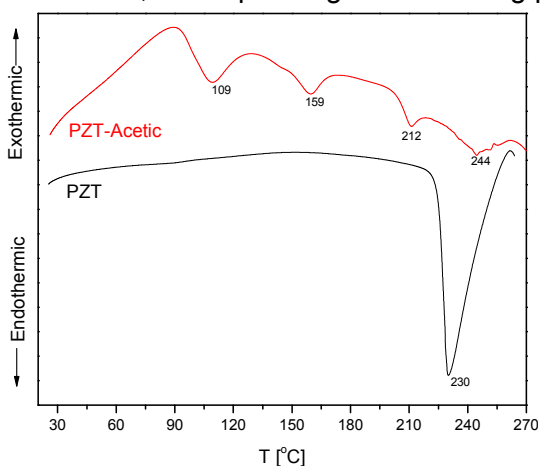


**Figure 4.** DTA curves of PTZ and PTZ-acetic acid.

The new form with acetic acid presents a different DTA thermogram as compared to that of PTZ. This thermogram shows a broad endothermic peak below 109°C due to acetic acid and water elimination by evaporation, and another broad endothermic peak at 159°C probably corresponding to a hydrochloride acid elimination [10]. The next thermal event, occurring at 212°C, corresponds to the melting of the sample, followed by another sharp endothermic peak with maximum around 244°C which corresponds to the decomposition of the compound. The difference between the onset temperatures and the heat of fusions suggests that these two samples represent different solid forms.

## CONCLUSIONS

A new solid form Promethazin–Acetic acid was prepared by a grinding procedure. XRD analysis, FTIR spectroscopy and DTA indicate the formation of new solid form. Based on the X-ray powder diffraction the lattice parameters for the new compound were determined.

## EXPERIMENTAL SECTION

Pure acetic acid was purchased from *Sigma Aldrich* and started material Promethazine Hydrochloride by Microsin. Both compounds were used without further purification. Based on grinding in a ball mill procedure [7], the new solid form was prepared by milling a mixture of 1:1 Promethazine Hydrochloride and acetic acid. Vibratory ball mill was used to prevent evaporation of acetic acid. Milling occurs for 90 minutes at a frequency of 27.5 Hz. The solid mixture it was maintained at room temperature until the next day to dry.

X-Ray powder pattern was obtained using D8 Advanced diffractometer equipped with Ge (111) monochromator in the incident beam and EyeLynx position detector using Cu tube (Cu  $K\alpha_1$  radiation;  $\lambda=1.54056 \text{ \AA}$ ).

The FTIR absorption spectra of the studied samples were obtained with a JASCO FTIR 6200 spectrometer in the 4000 - 400  $\text{cm}^{-1}$  spectral range with a resolution of 4  $\text{cm}^{-1}$ . The IR absorption measurements were performed using the KBr pellet technique.

The thermal behaviour of studied samples was carried out using a Perkin Elmer TG/DTA 6300 thermal analyzer under Ar gas atmosphere. About 25 mg of sample was heated in Pt-holder with another Pt-holder containing  $\alpha$ -alumina as a reference material. A uniform heating rate of 10 °C/ min. was adopted.

## ACKNOWLEDGMENTS

This paper was supported by the project "Improvement of the doctoral studies quality in engineering science for development of the knowledge based society-QDOC" contract no. POSDRU/107/1.5/S/78534, project co-funded by the European Social Fund through the Sectoral Operational Program Human Resources 2007-2013.

## REFERENCES

1. S. Childs, P.G. Stahly, A. Park, *Molecular Pharmaceutics*, **2007**, 4(3), 323.
2. A.P. Feinberg, S. Snyder, *Proceedings of the National Academy of Science of the United States of America*, **1975**, 1899.
3. D. Brown, R. Brown, H. Patel, H. Srinivasan, *US 2005/0232986 A1*, **2005**.
4. G. Borodi, M. Pop, O. Onija, X. Filip, *Cristal Growth & Design*, **2012**, 12, 5846.
5. A.V.Trash, W. Jones, *Top Curr Chem*, **2005**, 254:41.
6. M.N. Neuman, *X-Cell: J. Appl. Cryst.*, **2003**, 36, 356.
7. G. Sharma, V.K. Pawar, G. Garg, R. Awasthi, G. Kulkarni, *Der Pharmacia Letre*, **2010**, 2(3), 83.
8. N. Alpert, W. Keiser, H. Szymanski, *IR Theory and Practice of Infrared Spectroscopy*, **1970**, Plenum Press, New York.
9. M. Avram, Gh. Mateescu, *Spectroscopia in infrarosu si aplicatii in chimia organica*, **1966**, Ed. Tehnica, Bucuresti, p. 448.
10. M. Pop, I. Kacso, C. Tripon, Z. Moldovan, Gh. Borodi, S. Simon, I. Bratu, *J Therm. Anal. Calorim.*, **2011**, 104, 299.

## RHEOLOGICAL AND PHYSICAL CHARACTERISTICS OF MINCED *BICEPS FEMORIS* MUSCLE IN DIFFERENT BRINING SYSTEMS

LIVIA PATRAȘCU<sup>a,\*</sup>, CORINA GAMBUȚEANU<sup>a</sup>, PETRU ALEXE<sup>a</sup>

**ABSTRACT.** The effect of brine rate (20, 30, 40 and 50 %) and k-carrageenan addition (0, 0.25 and 0.5 %) on rheological and physical characteristics of pork *Biceps femoris* muscle was investigated. Minced muscle was mixed with different types of brine so that a total of 12 samples resulted in order to obtain meat restructured products without fat addition. Water holding capacity of admixtures was determined. After cooking process samples in the form of meat restructured products were subjected to textural analysis determining samples' hardness. Rheological tests were carried out by applying oscillatory dynamic tests and behavior of  $G'$ ,  $G''$  and  $\delta$  angle was characterized. Results showed that water holding capacity, represented by expressible moisture (EM, %), significantly increased ( $p < 0.05$ ) with k-carrageenan addition for samples with 20 and 30% of added brine. Samples' hardness was also significantly influenced ( $p < 0.05$ ) by k-carrageenan addition with exception of samples with 40 and 50% of added brine. Rheological data showed a higher  $G'$  versus  $G''$  in all cases when subjected to frequency sweep and temperature ramp tests. For every percent of added k-carrageenan  $G'$  values had a decreasing tendency in most of the cases when more brine was added to the system.

**Keywords:** *Hardness, water holding capacity, viscoelastic moduli, k-carrageenan.*

### INTRODUCTION

Meat restructured products are wide spread on the food market and the majority of meat available nowadays is processed to some extent [1]. For economic benefits and for the fact that consumers judge quality based on tenderness, products made from chopped meat have various types of lipids added, from animal or vegetable sources. On the other hand consumers demand healthier products with low fat content [2]. Reducing fat content

---

<sup>a</sup> Department of Biotechnology, Faculty of Food Science and Engineering, Dunărea de Jos University of Galati, 111, Domnească Street, 800201, Romania, \* livia.mantoc@ugal.ro

without affecting water holding capacity and texture can be achieved by using fat replacers such as hydrocolloids, vegetable and connective-tissue proteins [3].

Carrageenans are widely used in the food industry because of its water binding, thickening and gelling properties [4-6], with *kappa* form being the most common. More, Warrand [7] reported health benefits of hydrocolloids presence in food products (including carrageenans).

Rheological tests in food industry are important because of the possibility to characterize raw material before processing, intermediary product before manufacturing but also the final product itself [8].

The objective of this study was to investigate the effect of k-carrageenan addition and brine rate on water holding capacity; textural and rheological characteristics of minced *Biceps femoris* muscle in order to obtain a meat restructured product with no added fat.

## RESULTS AND DISCUSSIONS

### *Physical characteristics*

Results showed in figure 1 present the effect of k-carrageenan addition and brine rate on samples water holding capacity. Adding k-carrageenan to *Biceps femoris* muscle–brine system significantly ( $p < 0.05$ ) decreased quantity of brine lost during centrifugation at little brine rates used.

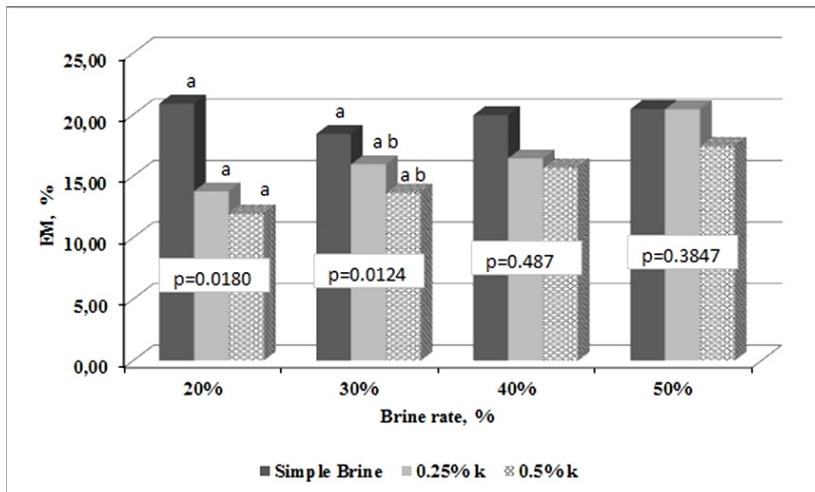


**Figure 1.** Expressible moisture of samples treated with different types of brine added in four rates. K-stand for k-carrageenan. Values marked with same letter within same block of columns differ significantly ( $p < 0.05$ ).

Contrary, when 40 and further 50 % of brine was added to the system the effect of k-carrageenan addition in low quantities decreased, values being insignificantly different ( $p > 0.05$ ). More, increasing brine intake resulted in a linear increase in expressible moisture values for samples were k-carrageenan was added ( $R^2 = 0.905$  for samples with 0.25 % of added k-carrageenan and  $R^2 = 0.998$  for samples with 0.5 % of added k-carrageenan). Verbeken, et al. [5] reported that increasing carrageenan concentration led to an increase in water holding capacity (WHC) of meat extracts. An improvement in WHC of meat emulsified systems/sausages with different concentrations of added k-carrageenan was also reported by Ayadi, et al. [9] and Patraşcu, et al. [10].

When speaking of samples' texture, results presented in figure 2 showed tendencies similar to those encountered for expressible moisture. Therefore, hardness significantly decreased ( $p < 0.05$ ) with k-carrageenan addition for samples mixed with 20 and 30 % of brine. Further increasing brine rate led to a smoothing in hardness's values. Analyzing hardness for every type of brine used in the survey when increasing brine rates from 20 to 50 % denoted linear regression in all cases.

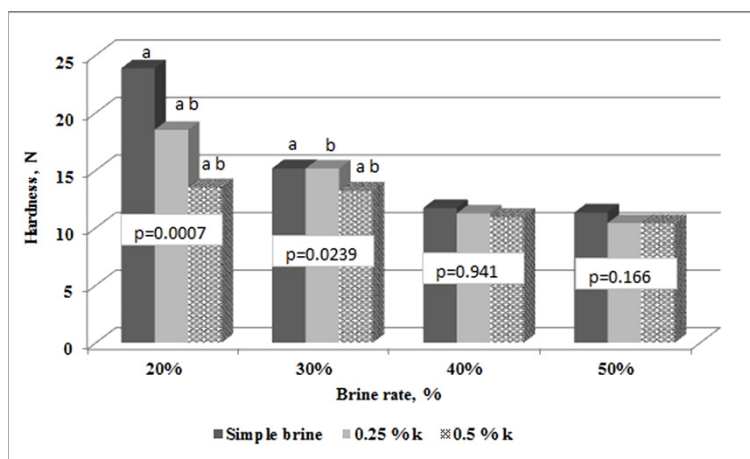


**Figure 2.** Hardness for samples treated with different types of brine added in four rates. K - stand for k-carrageenan. Values marked with same letter within same block of columns differ significantly ( $p < 0.05$ ).

Thus, for samples with simple brine in the system, increasing brine rate showed a linear decrease in hardness with  $R^2 = 0.828$ , for samples with 0.25 % of added k-carrageenan  $R^2 = 0.946$ , and for samples with 0.5% of added k-carrageenan  $R^2 = 0.902$ . A slightly decreasing effect of k-carrageenan addition on hardness was reported by Alexa, et al. [11], & Patraşcu, et al. [10]. Cierach, et al. [3] reported that sausages containing carrageenan, independently of the amount of the addition were characterized by significantly higher values



for hardness. It seems that k-carrageenan presence in products containing any amount of fat strengthens the final product. Fat being softer than the muscle itself, it is expected for k-carrageenan to soften texture of any meat product with no added fat, as reported by Patrașcu, et al. [12], when addition of k-carrageenan to ham like products determined a decrease of product's hardness. The influence of fat level on the texture of sausage has been previously reported by Hensley & Hand [13], and Candogan & Kolsarici [14] who noted that hardness was correlated with fat content.

### **Rheological data analyses**

When speaking of food products with hard texture (named solids in rheology), there can be performed creep tests over a range of time and oscillatory tests over a range of frequency. So that the short times will correspond to high frequencies and long times will relate to low frequencies [15]. The data presented in figure 3 (A, B, C), show admixtures' rheological behavior during frequency sweep test. It can be seen that for every type of brine used, increasing brine rate led to a decrease in  $G'$  values. However, for the entire experiment,  $G'$  values were higher than those of  $G''$ , including samples in solid-like materials. When looking at  $G'$  curves for samples with similar brine level and different k-carrageenan concentration there seem to be no effect of hydrocolloid addition. But, at a lower frequency, the data showed different tendencies. For samples with 20 % of added brine  $G'$  values recorded at 0.1 Hz, decreased with increasing k-carrageenan concentration from 2160 Pa to 1392 Pa ( $R^2=0.966$ ). For samples with 30 % of added brine at 0.1 Hz  $G'$  values decreased from 1343 Pa to 843 Pa ( $R^2=0.895$ ). For samples with 40 % of added brine  $G'$  values decreased from 1434 Pa to 807 Pa ( $R^2=0.842$ ) and for 50 % of added brine  $G'$  values decreased from 940 Pa to 697 Pa ( $R^2=0.981$ ) confirming that k-carrageenan addition softened admixtures structure. Delta values recorded during frequency sweep test, presented significant differences with k-carrageenan addition (Table 1) increasing from  $\sim 20^\circ$  for simple brine to  $\sim 30^\circ$  for samples with 0.5 % of k-carrageenan. Delta values below  $45^\circ$  enclose the mixtures in solid-like materials.

**Table 1.** Effect of brine rate and k-carrageenan addition on delta values ( $\delta^\circ$ ) during frequency sweep test

Sample type	Injection rate			
	20 %	30 %	40 %	50 %
Simple Brine	20.66±1.2 <sup>a</sup>	21.26±1.51 <sup>a</sup>	20.49±1.12 <sup>a</sup>	21.73±0.99 <sup>a</sup>
0.25% k-carrageenan	19.85±1.68 <sup>b</sup>	29.94±2.9 <sup>a</sup>	31.61±2.47 <sup>a</sup>	34.04±0.68 <sup>a</sup>
0.5% k-carrageenan	27.79±2.6 <sup>ab</sup>	32.06±1.83 <sup>a</sup>	33.4±1.35 <sup>a</sup>	34.05±0.17 <sup>a</sup>
<b>p value</b>	<b>0.0453</b>	<b>0.0314</b>	<b>0.0094</b>	<b>0.0006</b>

Values represent means ± Standard Deviation

Means with same superscript within same column differ significantly ( $p<0.05$ )

Temperature ramp test highlighted the moment of protein denaturation which took place at  $\sim 50\div 60$  °C, as seen in figure 3 (D, E, F). After that moment  $G'$  curve showed a sudden growing tendency until the final test temperature of 72 °C. Rheological tests with rising temperature are often utilized for observing material behavior during heat treatment, being possible determination of proteins' nature preventing destruction of the system [16, 17]. All samples began to form a gel like structure as seen from viscoelastic moduli curves at about 40 °C, similar to findings of Westphalen, et al. [18]. This tendency continued till  $\sim 60$  °C. The inflexion points are associated with myosin denaturation [19]. The mechanism through myosin form a gel is thought to involve the aggregation of the heavy meromyosin (HMM), which is the head of the protein, and the formation of a network amongst the LMM, or tail portions of the protein [20]. The exact temperature of these transitions was observed from  $G'$  data recorded at temperatures indicated to be the inflection points (41, 50 and 57 °C) as reported by Westphalen, et al. [18]. Elasticity of paste meat products continued to develop after gelling point. This corresponds to reinforcement of the gel network [21].

Delta curves during temperature ramp test showed tendencies similar to those of viscoelastic moduli, presenting significantly different values ( $p < 0.05$ ) between temperature range of  $4 \div 50.7$  °C and  $51 \div 72$  °C, as seen in table 2. With exception of samples with 20% of added brine in other cases (samples with 30, 40 and 50 % brine) k-carrageenan addition significantly increased delta values ( $p < 0.05$ ).

**Table 2.** Effect of brine rate and k-carrageenan addition on delta values ( $\delta^\circ$ ) during temperature ramp test, before and after protein denaturation

Injection rate	Temperature range, °C	Simple Brine	0.25 % k-carrageenan	0.5 % k-carrageenan	<i>p</i> value
20 %	4 ÷ 50.7	19.34±1.36 <sup>a</sup>	19.46±1.51 <sup>b</sup>	26.96±3.36 <sup>ab</sup>	0.0686
	51 ÷ 72	15.31±0.85 <sup>a</sup>	15.39±0.84 <sup>b</sup>	19.64±1.91 <sup>ab</sup>	0.0713
30 %	4 ÷ 50.7	19.7±1.4 <sup>a</sup>	29.58±2.85 <sup>a</sup>	31.79±1.88 <sup>a</sup>	0.0209
	51 ÷ 72	15.44±0.83 <sup>a</sup>	21.41±1.68 <sup>a</sup>	22.7±1.39 <sup>a</sup>	0.0239
40 %	4 ÷ 50.7	19.38±0.93 <sup>a</sup>	29.38±2.46 <sup>a</sup>	30.32±2.16 <sup>a</sup>	0.0198
	51 ÷ 72	15.47±0.60 <sup>a</sup>	21.13±1.55 <sup>a</sup>	21.48±1.29 <sup>a</sup>	0.0265
50 %	4 ÷ 50.7	20.12±0.85 <sup>a</sup>	30.71±0.84 <sup>a</sup>	31.13±0.71 <sup>a</sup>	0.0014
	51 ÷ 72	15.78±0.57 <sup>a</sup>	21.36±0.60 <sup>a</sup>	22.07±0.55 <sup>a</sup>	0.0029

Values represent means ± Standard Deviation

Means with same superscript within same row differ significantly ( $p < 0.05$ )

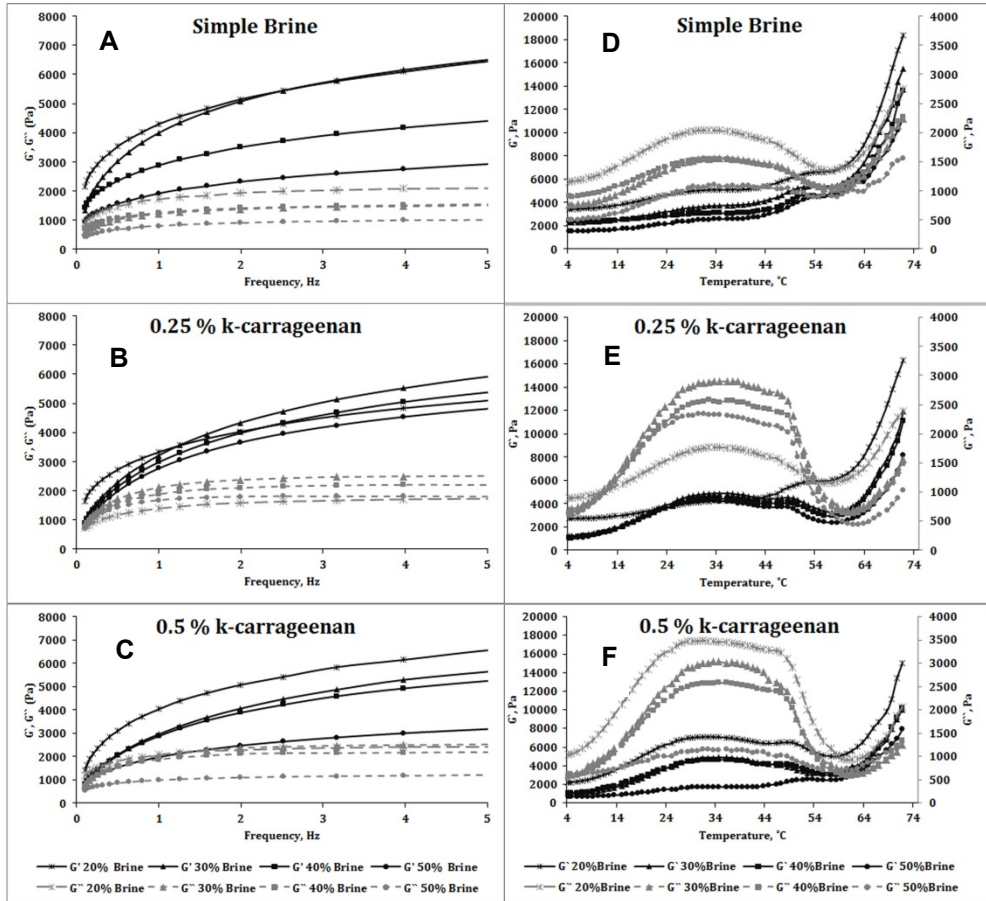


**Figure 3.** Samples' rheological behavior during frequency sweep (A, B, C) and temperature ramp (D, E, F) tests.

## CONCLUSIONS

K-carrageenan addition to minced meat - brine system improved water holding capacity and texture of samples from *Biceps femoris* pork muscle, by decreasing hardness's values, when small amount of brine is desired (20 or 30 % of added brine). However, in order to add more brine to the system there are needed higher quantities of k-carrageenan in order to improve water retention. Rheological analyses showed softer structure for samples mixed with more brine. Also, a higher quantity of k-carrageenan led to significantly higher values for delta angle ( $p < 0.05$ ) both for frequency sweep test and for temperature ramp test. Results showed that products from minced/restructured meat with proper binding characteristics and texture can be produced without fat addition.

## EXPERIMENTAL SECTION

### ***Raw material***

*Biceps femoris* muscles obtained from one side of pork carcass (24 h after slaughter) were purchased from a local distributor (pH=5.78 ± 0.05; total lipids: 2.51 ± 0.12 g/100 g). Meat, a total of 7 kg (3 muscles) per batch, was processed immediately after collecting in refrigeration conditions at a temperature of +4 °C. Any seen fat or conjunctive tissue was removed. The meat was chopped through Philips HR7625/70/AC home chopper, for two minutes at second speed, obtaining a homogenous batter. Obtained mass was separated into 12 samples (500 g per sample).

### ***Mixture formation and processing***

The study was projected with variation of two factors:

- a. Four brine rates used – 20, 30, 40 and 50 %.
- b. Three types of brine added – simple brine with no added hydrocolloid, brine containing 0.25 kg of k-carrageenan/100 kg meat and brine containing 0.5 kg of k-carrageenan/100 kg meat.

Brine used for injection contained sodium chloride, sodium nitrite, sodium tripolyphosphate, sugar, water and k-carrageenan when needed. The ingredients were added in different proportions, depending on the type of brine used and the percentage of added brine so that in finished product the following quantities could be found: 1.8 % salt; 0.3 % sodium tripolyphosphate; 0.015 % sodium nitrite; 0.3 % sugar and 0.25 % or 0.5 % of k-carrageenan as described by Patraşcu, et al. [12]. Brine temperature was kept at +4 °C. Samples were subjected to rheological analyses immediately after forming the mixture, allowing a resting time of 30 min at room temperature. In order to perform textural analysis, mixture was stuffed in cylindrical impermeable casings with 2 cm in diameter, and pasteurized in a water bath (MEMMERT, WNB-45, Germany) gradually increasing water temperature with ~1.5 °C per min from 20 °C ± 2 °C to 75 °C until the internal temperature of the sample reached 72 °C, measured with a thermocouple. After heat treatment, the samples were cooled down in running water to about 20 °C.

### **Expressible moisture**

Meat samples of known weight (3.0 ± 0.5 g) were placed in centrifuge tubes fitted with thimbles of filter paper and centrifuged (Refrigerated Centrifuge TGL-16M) at 2400 rpm for 20 min at 4 °C. Expressible moisture was calculated as the percentage of moisture lost during centrifugation as described by Pietrasik & Shand [22].

$$\%,EM = (initial\ weight - final\ weight) / (initial\ weight) \times 100 \quad (1)$$

### **Textural analyzing**

The textural characteristics of samples were analyzed using a TA.XT. Plus Texture Analyzer. The technical parameters of the apparatus were: Compression Test Mode; Test Speed of 1.5 mm/s. Maximum force recorded during the test was reported as *hardness* (*N*).

### **Rheological analyses**

Samples were assessed rheologically by oscillatory tests using a control–stress rheometer (AR2000ex, TA Instruments, Ltd). The temperature was set at 20 °C using a Peltier temperature control system. The procedure was conducted using con - plate geometry with an angle of 2°, 40 mm diameter and a gap of 2000 μm was used. Samples' viscoelastic domain was determined by a strain sweep test (frequency set to 1 Hz). Dynamic viscoelastic characterization was performed by a frequency sweep test increasing the oscillations frequency from 0 to 5 Hz, at an imposed strain of 0.5%. Temperature ramp step was performed from 4 to 72 °C (increased with 5 °C/min), changing the sample between tests, at an imposed strain of 0.5 % and oscillations' frequency of 1 Hz.

### **Statistical analyses**

Statistical analyses were carried out using Microsoft Excel Software with application of Anova Single Factor ( $\alpha=0.05$ ), and Regression tests. Each experiment was carried out in duplicate and the results were reported as mean values. The Fisher's least significant difference (LSD) test was used to determine differences between treatment means with Statgraphics Centurion XVI.I software.

## **REFERENCES**

1. H.J. Andersen, What is pork quality? *Quality of meat and fat in pigs as affected by genetics and nutrition. Proceedings of the joint session of the EAAP commissions on pig production, animal genetics and animal nutrition, Zurich, Switzerland, 2000*, 100, 15.
2. J. Weiss, M. Gibis, V. Schuh, H. Salminen, *Meat Science*, **2010**, 86(1), 196.
3. M. Cierach, M. Modzelewska-Kapituła, K. Szaciło, *Meat Science*, **2009**, 82(3), 295.
4. A.D. Anderson, C.R. Daubert, B.E. Farkas, *Journal of Food Science*, **2002**, 67(2), 649.

5. D. Verbeken, N. Neirinck, P. Van Der Meeren, K. Dewettinck, *Meat Science*, **2005**, 70(1), 161.
6. L. Gonzalez-Tomas, E. Costell, *Journal of Dairy Science*, **2006**, 89(12), 4511.
7. J. Warrand, *Food Technology and Biotechnology*, **2006**, 44(3), 355.
8. G. Tabilo-Munizaga, G.V. Barbosa-Cánovas, *Journal of Food Engineering*, **2005**, 67(1), 147.
9. M.A. Ayadi, A. Kechaou, I. Makni, H. Attia, *Journal of Food Engineering*, **2009**, 93(3), 278.
10. L. Patraşcu, I. Dobre, P. Alexe, *Studia UBB Chemia*, **2010**, 55(3), 75.
11. R.I. Alexa, J.S. Mounsey, B.T. O'Kennedy, J.C. Jacquier, *LWT - Food Science and Technology*, **2010**, 43, 843.
12. L. Patraşcu, I. Dobre, P. Alexe, *The Annals of the University Dunarea de Jos of Galati, Fascicle VI: Food Technology*, **2013**, 37(1), 69.
13. J.L. Hensley, L.W. Hand, *Journal of Food Science*, **1995**, 60(1), 55.
14. K. Candogan, N. Kolsarici, *Meat Science*, **2003**, 64(2), 199.
15. H.A. Barnes, "A Handbook of Elementary Rheology". Institute of Non-Newtonian Fluid Mechanics, University of Wales, **2000**, chapter 13.
16. M.H. Tunick, *Journal of Agricultural and Food Chemistry*, **2011**, 59, 1481.
17. L. Marchetti, S.C. Andrés, A.N. Califano, *LWT - Food Science and Technology*, **2013**, 51, 514.
18. A.D. Westphalen, J.L. Briggs, S.M. Lonergan, *Meat Science*, **2006**, 72(6), 97.
19. E. Tornberg, *Meat Science*, **2005**, 70, 493-508.
20. K. Samejima, M. Ishioroshi, T. Yasui, *Journal of Food Science*, **1981**, 46, 1412.
21. E. Çakir, A. Foegeding, *Food Hydrocolloids*, **2011**, 25, 1538.
22. Z. Pietrasik, P.J. Shand, *Meat Science*, **2004**, 66(4), 871.



## A GROUP THEORETICAL METHOD FOR COMPUTING HARARY INDEX

HAMID REZA FAZLOLLAHI<sup>a</sup>, HOSSEIN SHABANI<sup>a,\*</sup>

**ABSTRACT.** The Harary index of a molecular graph  $G$  is defined as the sum of the inverse of distances between the pair vertices of  $G$ . In this paper we report a group theoretical method for computing Harary index in some classes of dendrimers.

**Keywords:** *Graph automorphism, Harary index, Dendrimer.*

### INTRODUCTION

A graph  $G$  is called a molecular graph if the set of vertices  $V(G)$  represent atoms and the set of edges  $E(G)$  collect the chemical bonds ( $uv$ ) joining the atoms  $u$  and  $v$  in the molecule. The length of the shortest path between two vertices is called the topological distance and is denoted by  $d(u,v)$ ; the maximum distance between the vertex  $u$  and any vertex  $v$  in  $G$  is named the eccentricity of  $u$  and is denoted  $e(u)$ .

Denote by  $Aut(G)$  the automorphism group of  $G$ . A topological index  $TI$  is a number that is invariant under the  $Aut(G)$ . A variety of  $TIs$  have been proposed for characterization of chemical structures and used for structure-property correlations in QSPR models [1-3].

In particular, the Harary index of a graph,  $H(G)$ , has been introduced in 1993, independently by Ivanciuc *et al.*[4] and by Plavšić *et al.* [5] Even earlier, the QSAR group in Timisoara, Romania, particularly Ciubotariu, [6] have used this index to express the decay of interactions between pair atoms in molecules as the distances between them increased. It has been named in the honor of Professor Frank Harary, on the occasion of his 70<sup>th</sup> birthday. The Harary index is defined as follows:

$$H(G) = \sum_{u,v \in V(G)} \frac{1}{d_G(u,v)}$$

---

<sup>a</sup> *Institute of Nanoscience and Nanotechnology, University of Kashan, Kashan 87317-51167, I.R. Iran, \* shabai@grad.kashanu.ac.ir*



where the summation runs over all unordered pairs of vertices of the graph  $G$  and  $d_G(u,v)$  denotes the topological distance between any two vertices  $u$  and  $v$  of  $G$  (i.e., the number of edges in a shortest path connecting  $u$  and  $v$ ). Mathematical properties and some applications of  $H$  the reader can find in refs [7-14].

Dendrimers are hyper-branched synthetic polymers (i.e. macromolecules) with a well-defined molecular topology [4-6].

In this paper, we use a group theoretical method [15-19] for computing the Harary index.

According to this method, we compute the Harary index of the dendrimers  $\mathcal{T}[h,m]$  (Figure 1, 2). This dendrimer has a central vertex (denoted  $x_0$ ) of degree  $h + 1$  and every non-pendent vertex (i.e. branching vertex/atom) has degree  $h + 1$ , and  $m$  denote to the distance between the central vertex and each pendent vertices. The number of vertices of  $\mathcal{T}[h,m]$  is equal to  $1+h \frac{(h-1)^m - 1}{(h-2)}$ .

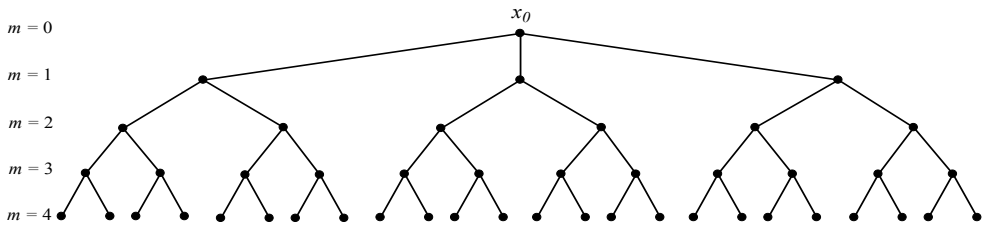


Figure 1. Dendrimer  $\mathcal{T}[2,4]$

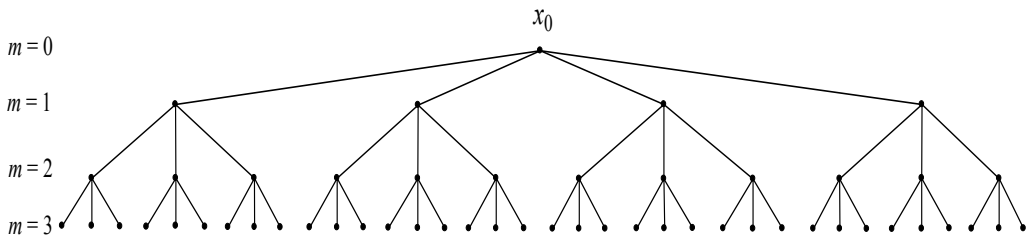


Figure 2. Dendrimer  $\mathcal{T}[3,3]$ .

Throughout this paper, our notation is standard and taken mainly from the standard books of graph theory as like as [20].

## RESULTS AND DISCUSSION

Let  $v$  be a vertex of graph  $G$ . We write  $N_i(v)$  for the set of vertices at distance  $i$  (of which maximum equals  $e(v)$ ) from  $v$ .  $N_1(v)$  is called the neighborhood of  $v$ . We call the partition of the vertex set  $V(G) = N_0(v) \cup N_1(v) \cup \dots \cup N_{e(v)}(v)$  a representation of  $G$  with respect to  $v$  and denoted by  $n_i(v)$ , the cardinality of  $N_i(v)$ . Now set

$$Rd(v) = 1^{-1}n_1(v) + 2^{-1}n_2(v) + \dots + e(v)^{-1}n_{e(v)}(v)$$

and then rewrite the Harary index as

$$H(G) = \sum_{v \in V} Rd(v).$$

**Lemma.** If the action of automorphism group of  $G$  on  $V(G)$  contains the orbits  $V_1, V_2, \dots, V_k$ , then  $H(G) = \sum_{i=1}^k |V_i| Rd(v_i)$ , where  $v_i$  is a vertex of

the  $i$ -th orbit. In particular, if the action is transitive and  $v$  is a vertex of  $G$  then  $H(G) = |V(G)|Rd(v)$ .

**Proof.** Suppose  $v$  is a vertex of  $G$ . Consider the level representation of  $G$  with respect to  $v$ . For each vertex  $v_1$  and  $v_2$  in the same orbit, there exists an automorphism  $f$  such that  $f(v_1) = v_2$ . Thus they have the same level representation and  $n_i(v_1) = n_i(v_2)$ , so  $Rd(v_1) = Rd(v_2)$ . Since  $V(G)$  is partitioned by orbits, then  $H(G) = \sum_{i=1}^k \sum_{v_i \in V_i} Rd(v_i) = \sum_{i=1}^k |V_i| Rd(v_i)$ . This completes the proof.

**Example.** Consider  $Q_n$  be the hypercube with  $2^n$  vertices and  $n2^{n-1}$  edges. The set vertex of  $Q_n$  is consist of the sequences  $v = (v_1, v_2, \dots, v_n)$  where  $v_i$  is equals to 0 or 1 and two vertices  $u$  and  $v$  are adjacent if and only if they differ in an one place. This graph is vertex transitive and the automorphism group is isomorphic to group  $Z_2 \sim S_n$ . The distance of two vertices are  $i$  if and only if they differ in  $i$  places. Take  $0 = (0, 0, \dots, 0)$  then  $Rd(0) = F([1,1,1-n], [2,2], -1)_n$  where  $F$  is the generalized hyper geometric function. Then the Harary index of  $Q_n$  is as follow:

$$H(Q_n) = 2^n Rd(0).$$

In this section, we describe our computational method for computing Harary index of dendrimer  $T_m = T[h, m]$ . Choose the node  $x_0$  of  $T_m$ , with minimum eccentricity, as the root and then consider the sets,  $S[i]$  containing all vertices at the distance  $i$  from  $x_0$  and  $1 \leq i \leq m$ . Therefore  $V(T_m) = S[1] \cup S[2] \cup \dots \cup S[m]$ . In order to characterize the symmetry of  $T_m$ , we notice that each dynamical symmetry operation of  $S[1]$ , considering the rotations of elements of  $T_1$ , in

different generations of the whole  $T_m$ , is composed of  $m$  sequential physical operations. We first have a physical symmetry of the framework. Such operations form the group  $T_m$  of order  $(h + 1)!$ , which is isomorphic to  $S_{h+1}$  or  $Sym(h + 1)$ . We can see that, after accomplishing the first framework symmetry operation, there are two reflections isomorphic to  $S_h$ , for each  $i \in T_m$ . Therefore, we find a group isomorphic to

$$H = ((\dots(S_h \sim S_h) \sim S_h) \sim \dots) \sim S_h \sim S_h$$

with  $n$  components. Thus, the automorphism graph of  $T_m$  is isomorphic to the wreath product  $H \sim G$  of order  $(h + 1)! \times h^{(h+1)((h)^n - 1)}$ .

If  $Aut(T_m)$  acts on  $V(T_m)$  then the orbits of  $Aut(T_m)$  are  $S[i]$  for  $0 \leq i \leq k$ . Then, it is sufficient to obtain  $R(v)$  for each vertices in  $S[i]$ .

Let  $\alpha_x(y, y + 1 + m) = x^y / (y + 1 + m)$ . Then for vertex in  $m = 0$  we have:

$$Rd(v_0) = (h + 1)[\alpha_h(0, 1) + \alpha_h(1, 2) + \dots + \alpha_h(k - 1, k)];$$

and if  $m \neq 0$  then for any vertex in row  $m$ :

$$\begin{aligned} Rd(v_m) &= h[\alpha_h(0, 1) + \alpha_h(1, 2) + \dots + \alpha_h(k - m - 1, k - m)] + h[\alpha_h(0, 1 + m) \\ &+ \alpha_h(1, 2 + m) + \dots + \alpha_h(k - 1, k + m)] + [1 + \frac{1}{2} + \dots + \frac{1}{m}] \\ &+ 2^{h-2} \sum_{l=0}^{m-2} [\sum_{t=0}^{k-m+l} \alpha_h(t, t + l + 2)]; \end{aligned}$$

so, the Harary index of  $T_m$  is equals to:

$$\begin{aligned} H(T[h, m]) &= Rd(v_0) + \sum_{m=1}^k ((h + 1) \times h^{(m-1)}) Rd(v_m) \\ &= \frac{(h + 1)}{2} \left\{ \sum_{\alpha=0}^{k-1} v_h(\alpha, \alpha + 1) + \sum_{m=1}^k [h^m \left[ \left( \sum_{\alpha=0}^{k-m-1} v_h(\alpha, \alpha + 1) \right) \right. \right. \\ &+ \sum_{\alpha=0}^{k-1} v_h(\alpha, \alpha + m + 1)) \\ &+ \left. \left. \frac{1}{h} \left( \sum_{p=1}^m \frac{1}{p} + 2^{(h-2)} \sum_{\alpha=0}^{k-m+l} \left[ \sum_{l=0}^{m-2} v_h(\alpha, \alpha + l + 2) \right] \right) \right] \right\}. \end{aligned}$$

For example, the Harary index of the two dendrimers  $T[2, m]$  and  $T[3, m]$  is equals to:

A GROUP THEORETICAL METHOD FOR COMPUTING HARARY INDEX

$$H(T[2,m]) = \frac{3}{2} \left\{ \sum_{\alpha=0}^{k-1} v_2(\alpha, \alpha+1) + \sum_{m=1}^k [2^m \left[ \left( \sum_{\alpha=0}^{k-m-1} v_2(\alpha, \alpha+1) + \sum_{\alpha=0}^{k-1} v_2(\alpha, \alpha+m+1) \right) + \frac{1}{2} \left( \sum_{p=1}^m \frac{1}{p} + \sum_{\alpha=0}^{k-m+l} \left[ \sum_{l=0}^{m-2} v_2(\alpha, \alpha+l+2) \right] \right) \right] \right\};$$

$$H(T[3,m]) = 2 \left\{ \sum_{\alpha=0}^{k-1} v_3(\alpha, \alpha+1) + \sum_{m=1}^k [3^m \left[ \left( \sum_{\alpha=0}^{k-m-1} v_3(\alpha, \alpha+1) + \sum_{\alpha=0}^{k-1} v_3(\alpha, \alpha+m+1) \right) + \frac{1}{3} \left( \sum_{p=1}^m \frac{1}{p} + 2 \sum_{\alpha=0}^{k-m+l} \left[ \sum_{l=0}^{m-2} v_3(\alpha, \alpha+l+2) \right] \right) \right] \right\}.$$

In Table 1, 2, the Harary index of  $T[2,m]$  and  $T[3,m]$  are computed, respectively.

**Table 1.** Computed Harary index

$m$	$H(T[2,m])$	$m$	$H(T[2,m])$
1	4.5	11	1064563.395
2	22	12	3802983.327
3	77.6	13	13753209.73
4	224.2285714	14	50236271.01
5	775.6190476	15	185005359.71
6	2442.472727	16	685960877.82
7	7855.125142	17	2557954484.97
8	25906.94426	18	9585125382.98
9	87570.42562	19	36068194256.98
10	302532.8129	20	136219894944.35

**Table 2.** Computed Harary index

$m$	$H(T[3,m])$	$m$	$H(T[3,m])$
1	7	11	3138719374.89
2	56.5	12	25643446199.96
3	291.4	13	211367664294.6
4	1527.128571	14	1754974615408.66
5	15634.53571	15	14661259143345.1
6	110475.5422	16	123126656175525
7	815803.798	17	1038739505017990
8	6228620.769	18	8798075520380730
9	48738232.29	19	74781213850513200
10	388404328.77	20	637606433725983000

## ACKNOWLEDGMENTS

This work was partially supported by of the University of Kashan, I.R. Iran.

## REFERENCES

1. M.V. Diudea, Ed., *QSPR/QSAR Studies by Molecular Descriptors*, Nova, Huntington, N.Y., **2001**.
2. E. Estrada and E. Molina, *QSPR/QSAR by Graph Theoretical Descriptors beyond the Frontiers*. In: M.V. Diudea, Ed., *QSPR/QSAR Studies by Molecular Descriptors*, Nova Science, Huntington, New York, **2001**, 83–107.
3. I. Lukovits, *Int. J. Quantum. Chem.: Quantum Biology Symp.*, **1992**, 19, 217–223.
4. O. Ivanciuc, T.S. Balaban and A.T. Balaban, *J. Math. Chem.*, **1993**, 12, 309.
5. D. Plavšić, S. Nikolić, N. Trinajstić and Z. Mihalić, *J. Math. Chem.*, **1993**, 12, 235.
6. D. Ciubotariu, PhD thesis, 1987, Timisoara, Romania; D. Ciubotariu, M. Medeleanu, V. Vlaia, T. Olariu, C. Ciubotariu, D. Dragos and C. Seiman, *Molecules*, **2004**, 9, 1053.
7. K.C. Das, B. Zhou and N. Trinajstic, *J. Math. Chem.*, **2009**, 46, 1369.
8. M.V. Diudea, *J. Chem. Inf. Comput. Sci.*, **1997**, 37, 292.
9. L. Feng and A. Ilic, *Appl. Math. Lett.*, **2010**, 23, 943.
10. I. Gutman, *Indian J. Chem.*, **1997**, 36 A, 128.
11. B. Lucić, A. Miličević, S. Nikolić and N. Trinajstić, *Croat. Chem. Acta*, **2002**, 75, 847.
12. K. Xu, *Discrete Appl. Math.*, **2012**, 160, 321.
13. K. Xu and K.C. Das, *Discrete Appl. Math.*, **2011**, 159, 1631.
14. B. Zhou, X. Cai and N. Trinajstić, *J. Math. Chem.*, **2008**, 44, 611.
15. M.R. Darafsheh, *Acta Appl. Math.*, **2010**, 110 1225.
16. H. Shabani, A.R. Ashrafi and M.V. Diudea, *Croat. Chem. Acta*, **2010**, 83, 439.
17. H. Shabani, A. R. Ashrafi and I. Gutman, *Studia UBB Chemia*, **2010**, 55, 107.
18. A.R. Ashrafi, H. Shabani, M.V. Diudea, *MATCH, Commun. Math. Comput. Chem.*, **2013**, 69, 151.
19. A.R. Ashrafi, H. Shabani and M.V. Diudea, *Studia UBB Chemia*, **2010**, 4, 137.
20. F. Buckley, F. Harary, *Addison-Wesley, Reading, MA*, **1990**.

## REMARKS ON THE RECIPROCAL DEGREE DISTANCE

LOTFALLAH POURFARAJ<sup>a,\*</sup> AND MODJTABA GHORBANI<sup>b</sup>

**ABSTRACT.** In the present paper we study some properties of a new graph invariant named reciprocal degree distance of some molecular graphs. This new topological index is defined by Hua et al. as

$RDD(G) = \sum_{u,v \in E(G)} (d(u) + d(v))[d(u,v)]^{-1}$ , where the  $d(u,v)$  denotes the distance between vertices  $u$  and  $v$ .

**Key Words:** reciprocal degree distance, graph invariants, octane isomers.

### INTRODUCTION

Theoretical chemistry has many branches. Among them, Mathematical chemistry is an important tool for which applies mathematical methods to predict chemical phenomena without necessarily referring to quantum mechanics. Chemical graph theory is a branch of mathematical chemistry for studying molecular structures [1-3]. This theory had an important effect on the development of the chemical sciences [4,5].

Throughout this paper all graphs are simple and connected. We denote the vertex and edge sets of a graph  $G$  by  $V(G)$  and  $E(G)$ , respectively. Suppose  $\mathcal{G}$  denotes the class of all graphs. A topological index is a real function  $\Lambda: \mathcal{G} \rightarrow \mathbb{R}^+$  by this property that if  $G \cong H$  then  $\Lambda(G) = \Lambda(H)$ . Obviously, the maps  $\Lambda_1 = |V(G)|$  and  $\Lambda_2 = |E(G)|$  are topological indices. If  $x, y \in V(G)$  then the distance  $d(x, y)$  between  $x$  and  $y$  is defined as the length of a minimum path connecting  $x$  and  $y$ . The Wiener index [6] is the first reported distance based topological index and is defined as half sum of the distances between all the pairs of vertices in a molecular graph. In other words, the Wiener index is defined as follows:

---

<sup>a</sup> Department of Mathematics, Islamic Azad University, Central Tehran Branch (IAUCTB), Tehran, I.R. Iran

<sup>b</sup> Department of Mathematics, Faculty of Science, Shahid Rajaei Teacher Training University, Tehran, 16785 – 136, I.R. Iran

\* Corresponding author: l.pourfaraj@iauctb.ac.ir

$$W(G) = \frac{1}{2} \sum_{x,y \in V(G)} d(x,y).$$

The reciprocal degree distance  $RDD(G)$  of a molecular graph  $G$  was proposed by Hua and Zhang [7] as

$$RDD(G) = \sum_{u,v \in V(G)} (d(u) + d(v)) \frac{1}{d(u,v)},$$

where  $d(u)$  denotes the degree of the vertex  $u$  in  $G$ . The eccentricity of a vertex  $u$  is also defined as  $\varepsilon(u) = \text{Max}\{d(x,u) \mid x \in V(G)\}$ . The maximum eccentricity over all vertices of  $G$  is called the diameter of  $G$  and denoted by  $d(G)$  and the minimum eccentricity among the vertices of  $G$  is called radius of  $G$  and denoted by  $r(G)$ .

The Harary index  $H(G)$  of a graph  $G$  on  $n$  vertices is based on the concept of reciprocal distance and is defined the half-sum of the off-diagonal elements of the reciprocal distance matrix  $RD(G)$ :

$$H(G) = \frac{1}{2} \sum_{uv \in V(G)} \frac{1}{d(u,v)},$$

where the  $ij$ -th entry of reciprocal distance matrix  $RD(G)$  is

$$RD(G)_{ij} = \frac{1}{d(v_i, v_j)}.$$

Here, our notations are standard and mainly taken from standard book of graph theory such as [8] as well as [9 – 13].

## RESULTS AND DISCUSSION

In this section we compute some bounds of reciprocal degree distance of graphs. The following theorem presents a sharp bound of reciprocal degree distance. Here, the complete graph and a star graph on  $n$  vertices are denoted by  $K_n$  and  $S_n$ , respectively.

### Example 1.

$$RDD(K_n) = n(n-1)^2 \text{ and } RDD(S_n) = n(3n+1)/2.$$

In generally, for regular graph we have:

**Lemma 1.** Let  $G$  be a regular graph of degree  $r$ , then

$$RDD(G) = 4r \times H(G).$$

### Vertex Transitive Graphs

A bijection  $\sigma$  on vertices set of graph  $G$  is named an automorphism of graph, if it preserves the edge set. In other word,  $\sigma$  is an automorphism if for every edge  $e = uv$  of  $E$  then  $\sigma(e) = \sigma(u)\sigma(v)$  be an edge of  $E$ . Let  $Aut(G) = \{\alpha : V \rightarrow V, \alpha \text{ is bijection}\}$ , then  $Aut(G)$  under the composition of mappings forms a group.  $Aut(G)$  acts transitively on  $V$  if for any vertices  $u$  and  $v$  in  $V$  there is  $\alpha \in Aut(G)$  such that  $\alpha(u) = v$ . For given vertex  $u$ , let

$$T(u) = \sum_{v \in V(G)} d(u, v)^{-1}.$$

Then we have the following Lemma:

**Lemma 2.** If  $G$  be a vertex transitive graph, then for any pair of vertices such as  $u$  and  $v$ ,  $T(u) = T(v)$ .

**Proof.** Since  $G$  is vertex transitive, so there is an automorphism  $\alpha$  in  $Aut(G)$  such that  $\alpha(u) = v$ . Hence,

$$\begin{aligned} T(v) &= \sum_{x \in V(G)} \frac{1}{d(x, v)} = \sum_{x \in V(G)} \frac{1}{d(x, \alpha(u))} \\ &= \sum_{y \in V(G)} \frac{1}{d(\alpha(y), \alpha(u))} = \sum_{y \in V(G)} \frac{1}{d(y, u)} = T(u). \end{aligned}$$

**Theorem 3.** If  $G$  be a vertex transitive graph on  $n$  vertices, then for a given vertex  $u$ ,

$$RDD(G) = 2nrT(u).$$

**Proof.** Since  $G$  is vertex transitive graph,  $G$  is regular. So the reciprocal degree distance is:

$$\begin{aligned} RDD(G) &= \sum_{u, v \in V(G)} (d(u) + d(v)) \frac{1}{d(u, v)} = 2r \times \sum_{u, v \in V(G)} \frac{1}{d(u, v)} \\ &= 2r \times \sum_{u \in V(G)} T(u) = 2nrT(u). \end{aligned}$$

As a result of Theorem 3, we compute reciprocal degree distance of well-known fullerene namely  $C_{60}$ , see Figure 1.

The graph of this fullerene is a three connected cubic graph whose faces are pentagons and hexagons. One can prove easily by Euler's theorem that numbers of pentagonal and hexagonal faces are 12 and 20, respectively. This fullerene is the only vertex transitive IPR (Isolated Pentagonal Rule) fullerene. The smallest fullerene is dodecahedron  $C_{20}$  and it is composed of exactly 12 pentagons. In other word,  $C_{20}$  is the only fullerene without any hexagonal faces. The fullerene  $C_{20}$  is non-IPR vertex transitive. By a direct computation we get for every vertex  $u$ ,  $T(u) = 179/20$ . Hence, by using Theorem 4  $RDD(C_{20}) = 1074$ . By using a similar way for the fullerene  $C_{60}$ , for any vertex  $u$  in  $V(C_{60})$ ,  $T(u) = 4259/168$  and thus  $RDD(C_{60}) = 63885/7$ .





**Figure 1.** 3-D graph of fullerene  $C_{60}$ .

A hypercube (Figure 2) is a regular graph, where its vertex set consisted of all  $n$ -tuples  $b_1b_2\dots b_n$  with  $b_i \in \{0,1\}$  and Two vertices are adjacent if and only if the corresponding tuples differ in precisely one place. Darafsheh in [14] proved that hypercube is a vertex transitive graph of order  $n$  and hence by using Theorem 3, we have:

**Theorem 4.**  $RDD(H_n) = 2^{n+2} - 2(n+1)$ .

**Proof.** The number of vertices of a hypercube  $H_n$  is  $2^n$  and the number of pair of vertices at distance  $i$  is  $C(n,i) = \frac{n!}{i!(n-i)!}$ . This implies that for every vertex  $u$ ,  $T(u) = \sum_{i=1}^n C(n,i)/i = (2^{n+1} - n - 1)/n$ . Since every vertex has degree  $n$ , by using Theorem 3 the proof is completed.

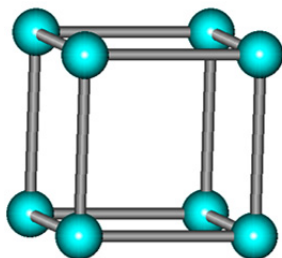


**Figure 2.** 3-D graph of a hypercube, where  $n = 3$ .

### RECIPROCAL DEGREE DISTANCE OF OCTANE ISOMERS

The aim of this section is to compute the reciprocal degree distance of octane isomers. Then we obtain a good linear correlation between  $RDD$ , acentric factor and entropy( $S$ ) of the octane isomers, e.g.  $R^2 = 0.9726$ . These values are reported in Table 1. All isomers of octane are depicted in Figure 3.

REMARKS ON THE RECIPROCAL DEGREE DISTANCE

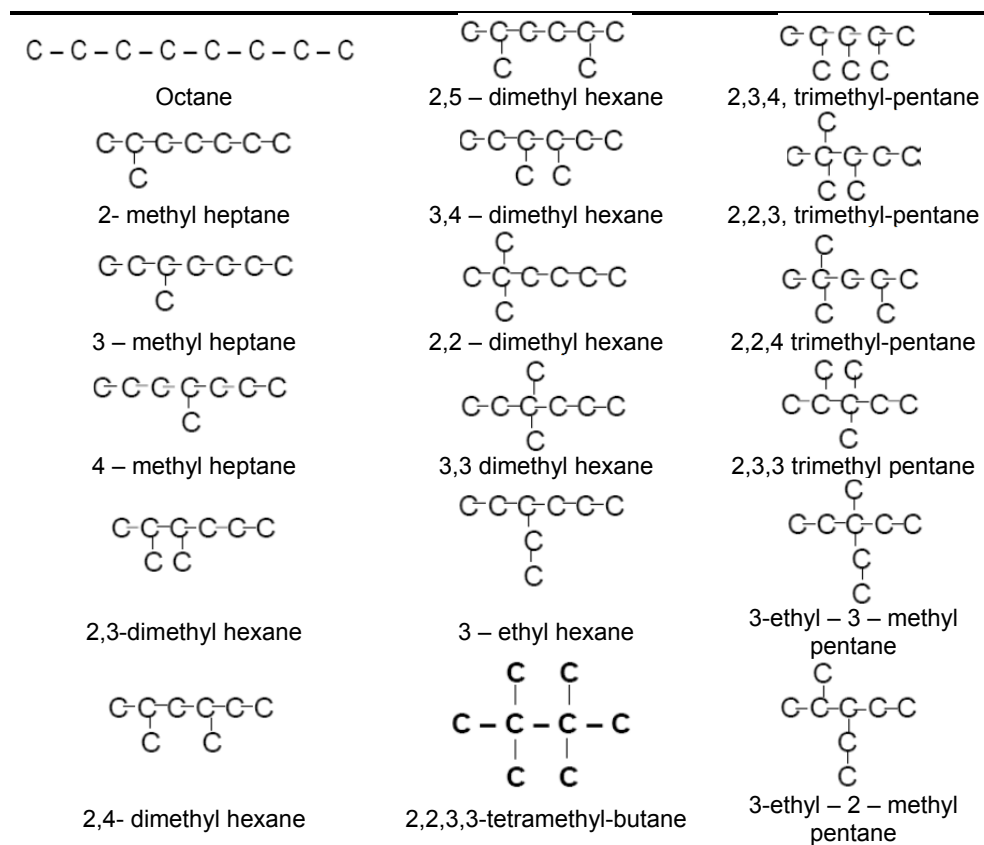


Figure 3. All octane isomers.

Table 1. Acen Fac, S and RRD of the octane isomers.

Molecule	Acent Fac	S	RRD
octane	0.397898	111	99.57
2-methyl-heptane	0.377 916	109.84	104.33
3-methyl-heptane	0.371002	111.26	106.2
4-methyl-heptane	0.371504	109.32	112.27
3-ethyl-hexane	0.362472	109 .43	108.6
2,2-dimethyl-hexane	0.339426	103.42	113.4
2,3-dimethyl-hexane	0.348247	108.02	112.27
2,4-dimethyl-hexane	0.344 223	106.98	112.27
2,5-dimethyl-hexane	0.35683	105.72	109.2
3,3-dimethyl-hexane	0.322596	104.74	116.47
3,4-dimethyl-hexane	0.340 345	106.59	113.8
2-methyl-3-ethyl-pentane	0.332433	106.06	114.33
3-methyl-3-ethyl-pentane	0.306 899	101.48	119
2,2,3-trimethyl-pentane	0.300816	101.31	121.67

Molecule	Acent Fac	S	RRD
2,2,4-trimethyl-pentane	0.30537	104.09	118.67
2,3,3-trimethyl-pentane	0.293 177	102.06	122.67
2,3,4-trimethyl-pentane	0.317422	102.39	118
2,2,3,3-tetramethylbutane	0.255294	93.06	130

## CONCLUSION

Topological descriptors are very important tools in chemical graph theory. Among them topological indices play a fundamental role in predicting chemical phenomena. The reciprocal degree distance is a topological index was defined by Hua and Zhang. In this paper reciprocal degree distance of some vertex transitive chemical graphs were computed.

## ACKNOWLEDGMENTS

The results in this paper are part of "On The Reciprocal Degree Distance Of Graphs" project. Support of this work was provided for L. Pourfaraj and M. Ghorbani by grant from Islamic Azad University, Central Tehran Branch, Tehran. Iran. Also the authors would like to thank Islamic Azad University, Central Tehran Branch, Tehran. Iran.

## REFERENCES

1. M.V. Diudea, (Ed.), *QSPR/QSAR Studies by Molecular Descriptors*, NOVA, New York, **2001**.
2. M.V. Diudea, I. Gutman, L. Jäntschi, *Molecular Topology*, NOVA, New York, **2002**.
3. M.V. Diudea, M.S. Florescu, P. V. Khadikar, *Molecular Topology and Its Applications*, EFICON, Bucharest, **2006**.
4. I. Gutman, O.E. Polansky, *Mathematical Concepts in Organic Chemistry*, Springer - Verlag, New York, **1986**.
5. M.A. Johnson, G.M. Maggiora, *Concepts and Applications of Molecular Similarity*, Wiley Interscience, New York, **1990**.
6. H. Wiener, *J. Am. Chem. Soc.*, **1947**, 69, 17.
7. H. Hua, S. Zhang, *Discrete Appl. Math.*, **2012**, 160, 1152.
8. S. Gupta, M. Singh, A.K. Madan, *J. Math. Anal. Appl.*, **2002**, 275, 386.
9. N. Trinajstić, *Chemical Graph Theory*, CRC Press, Boca Raton, FL, **1992**.
10. S. Sardana, A.K. Madan, *MATCH Commun. Math. Comput. Chem.*, **2001**, 43, 85.
11. A.R. Ashrafi, M. Saheli, M. Ghorbani, *Journal of Computational and Applied Mathematics*, **2011**, 235, 4561.
12. M. Jalali, M. Ghorbani, *Studia UBB Chemia*, **2009**, 4(2), 145.
13. I. Gutman, N. Trinajstić, *Chem. Phys. Lett.*, **1972**, 17, 535.
14. M.R. Darafsheh, *Acta. Appl. Math.*, **2010**, 110, 1225.

## **PSEUDOMONAS FLUORESCENS LIPASE AS BIOCATALYST IN THE ENZYMATIC KINETIC RESOLUTION OF CHIRAL PHENOTHIAZIN ETHANOLS**

**ANCA MUNCEANU<sup>a,\*</sup>, BOTOND NAGY<sup>a</sup>,  
MARIA TRIF<sup>a</sup>, NORBERT DIMA<sup>a</sup>**

**ABSTRACT.** The synthesis of both enantiomers of 1-(10-ethyl-10*H*-phenothiazin-2-yl)-1-ethanol by enzymatic kinetic resolution of the racemic alcohol or his corresponding acetate was performed using lipase from *Pseudomonas fluorescens* (PFL) as biocatalyst. PFL was next immobilized by sol-gel encapsulation. The stability, activity and reusability of the obtained enzyme preparations were also determined.

**Keywords:** enzymatic kinetic resolution, lipase from *Pseudomonas fluorescens*, sol-gel encapsulation, chiral phenothiazine derivatives

### **INTRODUCTION**

Phenothiazines and related compounds have shown diverse biological activities.<sup>1</sup> They bind to physiological targets or receptors, producing many possible mechanisms of actions. Due to the chiral nature of pharmacological receptors, their interaction with the individual enantiomer of the same compound could be significantly different and the synthesis of each of them is an important target in the modern medicinal chemistry.

Enantiopure secondary alcohols are key intermediates in the synthesis of a large number of pharmaceutical products. In particular, non-racemic alcohols and their derived amines containing heterocyclic fragments are known for their biological activity.<sup>2</sup> The lipase mediated kinetic resolution of some heteroaryl-1-ethanols have been already successfully performed.<sup>3,5,8</sup>

Kinetic resolution (KR) of racemates is by far the most common transformation catalyzed by lipases in which the enzyme discriminate between the two enantiomers of racemic mixture, so that one enantiomer is transformed to the product faster than the other one. In the ideal case, at 50% conversion, a final mixture of 50% reactant and 50% product, both in optically pure form,

---

<sup>a</sup> "Babeş-Bolyai" University, Faculty of Chemistry and Chemical Engineering, M. Kogălniceanu 1, RO-400084 Cluj-Napoca, Romania, \* Anca.Munceanu@farmec.ro

can be obtained. For example, starting from the racemic ethyl 3-hydroxy-3-(10-alkyl-10*H*-phenothiazin-3-yl)propanoates as substrates, a multienzymatic procedure was developed for the efficient synthesis of the corresponding highly enantiomerically enriched (*R*)- and (*S*)-3-heteroaryl-3-hydroxypropanoic acids.<sup>4</sup> Lipase A and B from *Candida antarctica* were found as efficient catalyst not only for KR and dynamic kinetic resolution (DKR)<sup>5</sup> of the enantiomer selective resolution of various heteroaryl cyanohydrins, including *N*-alkylated phenothiazin-3-yl-cyanohydrins,<sup>6</sup> but also for phenothiazine based 3-hydroxypropanoic acids,<sup>7</sup> methanols and ethanols.<sup>8, 10</sup>

The synthesis of 2-substituted *N*-acylphenothiazines derivatives and their antibacterial and antifungal activities was reported.<sup>9</sup> The chiral heteroaryl-ethanol obtained by carbonyl reduction represent an interesting compound in the field of medicinal chemistry, especially if the individual enantiomers are used as optically active intermediates.

To obtain highly enantiomerically enriched or optically pure heterocyclic ethanols,<sup>10</sup> the synthesis of both enantiomers of 1-(10-ethyl-10*H*-phenothiazin-2-yl)-1-ethanol by enzymatic kinetic resolution of the racemic alcohol or his corresponding acetate was our object of enquiry. We note that the enzymatic kinetic resolution of racemic 1-(10-ethyl-10*H*-phenothiazin-2-yl)-1-ethanol and their acetate with the lipase A and B from *Candida antarctica* was reported by our group recently.<sup>11</sup> However, to apply these results in industrial processes, the use of an efficient, cheap and stable catalyst is necessarily.

Thus, the most used method for improvement of biocatalysts performance is their immobilization. Many effective immobilization methods have been developed, including binding to a carrier, cross-linking and encapsulation in an organic or inorganic polymeric matrix.

Lipases from *Pseudomonas fluorescens* (PFL) belongs to commonly used commercial lipases. Their immobilization using adsorption,<sup>12</sup> cross-linking,<sup>13</sup> sol-gel encapsulation,<sup>14</sup> combination of the methods<sup>15</sup> or other techniques<sup>16</sup> has been under extensive studies.

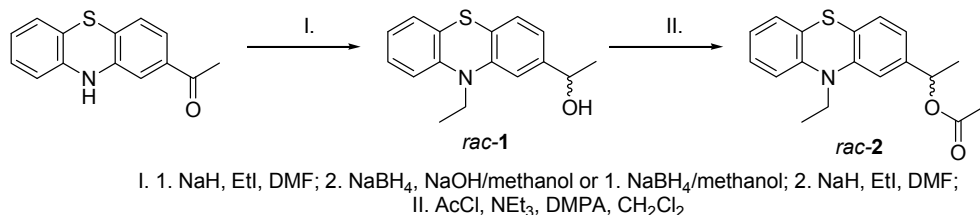
In the present work, PFL encapsulated in sol-gels was prepared and studied for the enzymatic kinetic resolution of racemic 1-(10-ethyl-10*H*-phenothiazin-2-yl)ethanol and their acetate, for obtaining both enantiomers of the heterocyclic ethanol, a valuable intermediate for different chiral active compounds. The stability, activity and reusability of enzyme preparations were determined.

## RESULTS AND DISCUSSION

### 1. Chemical synthesis

The 1-(*N*-ethyl-phenothiazin-2-yl)ethanol *rac*-1 was chosen as model compound for this study, due to its availability by simple reaction starting from the commercial ketone. The racemic substrate was prepared using a modified previously described method,<sup>17</sup> as shown in Scheme 1. By alkylation of

1-(10*H*-phenothiazin-2-yl)ethanone with ethyl iodide in DMF in presence of sodium hydride at room temperature, followed by chemical reduction of the carbonyl group with sodium borohydride in methanol at reflux or by reduction followed by *N*-alkylation in the same conditions, the racemic ethanol can be obtained in high yield. Chemical acetylation of the alcohol with acetyl chloride in presence of triethylamine and catalytic amount of DMAP gave the corresponding racemic acetate *rac-2* (Scheme 1).



**Scheme 1.** Chemical synthesis of the racemic substrates

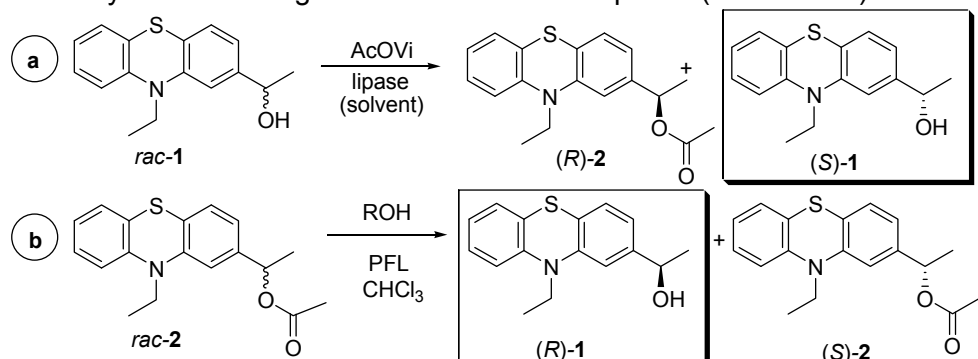
To investigate the stereoselectivity of the subsequent enzymatic reactions, the chromatographic separation of the enantiomers of the racemic 1-(10-ethyl-10*H*-phenothiazin-2-yl)-1-ethanol (*rac-1*) and his acetate (*rac-2*), was first established. The base-line separation of enantiomers was performed by HPLC using a Chiralpack IB column.

## 2. Biotransformations with lipases

### 2.1. Analytical scale biotransformations

#### 2.1.1. Analytical scale enzymatic acetylation of *rac-1*

First, the analytical scale enantiomer selective lipase catalyzed acetylation of racemic 1-(10-ethyl-10*H*-phenothiazin-2-yl)ethanol (*rac-1*) was studied in neat vinyl acetate using commercial available lipases (Scheme 2a).



**Scheme 2.** Lipase mediated enzymatic kinetic resolution processes

Most of them exhibited good enantiomer selectivities and activities. The best results were obtained with immobilized lipases B from *Candida antarctica* (CaL-B), commercialized as Novozym 435 and with lipase from *Pseudomonas fluorescens* (PFL) (Table 1, entry 1-2,  $E \gg 200$ , at 50% conversion). Lipase A from *Candida antarctica* (CaL-A) was also selective and active ( $E = 198$  at 48% conversion), while lipases from *Candida rugosa* (CrL), *Candida cylindracea* (CcL) and from *Thermomyces lanuginosa* (TLIM) were selective but less active (only 15-34 % conversion after 24 h). Other commercial lipases such as that from *Mucor javanicus* and pancreas pig lipase were only moderate active and selective ( $E = 30-70$ , at 10-25% conversion, data not presented in Table 1).

**Table 1.** Lipase catalyzed acetylations of *rac-1* in neat vinyl acetate in the presence of some lipases after 24 h

Entry	Lipase	ee <sub>(R)-2</sub> (%)	ee <sub>(S)-1</sub> (%)	c (%)	<i>E</i>
1	CaL-B	>99	>99	50	>>200
2	PFL	>99	>99	50	>>200
3	CaL-A	89	97	48	198
5	CcL	>99	18	15	>200
6	CrL	>99	31	25	>200
7	TLIM	>99	52	34	>200

It is known that the nature of the solvent could significantly influence the selectivity of the enantiomer selective acylation. Thus the acylation of *rac-1* with vinyl acetate in presence of PFL as selected catalyst was tested in several organic solvents (Table 2). Chloroform proved to be the most appropriate solvent for the acetylation ( $E > 200$ ,  $c = 50\%$  after 24 hours, Table 2, entry 1).

**Table 2.** Lipase catalyzed acetylations of *rac-1* (5 mg) with vinyl acetate (10  $\mu$ L) and PFL (5 mg) in different solvents (200  $\mu$ L) after 24 h

Entry	Solvent	ee <sub>(R)-2</sub> (%)	ee <sub>(S)-1</sub> (%)	c (%)	<i>E</i>
1	Chloroform	>99	96.3	50	>200
2	<i>n</i> -Hexane	>99	77.1	56	44
3	Toluene	>99	72.7	58	36
5	Tetrahydrofuran	>99	87.1	53	85
6	Dichlorometane	>99	45.9	68	14
7	Acetonitrile	95.2	94	50	122

### 2.1.2. Analytical scale enzymatic alcoholysis of *rac-2*

It is known that lipases usually retain their enantiomer preference in hydrolysis or alcoholysis.<sup>18</sup> Consequently, such reactions should result in the opposite enantiomeric forms of the reaction counterparts (Scheme 2b). The degree tested using four alcohols (methanol, ethanol, propan-1-ol and butan-1-ol) of enantioselectivity in alcoholysis of the racemic acetate *rac-2* was

with PFL as catalyst. The highest selectivity was achieved for ethanolysis (Table 3, entry 2), yielding the highly enantiomerically enriched opposite forms: (*R*)-**1** and (*S*)-**2**.

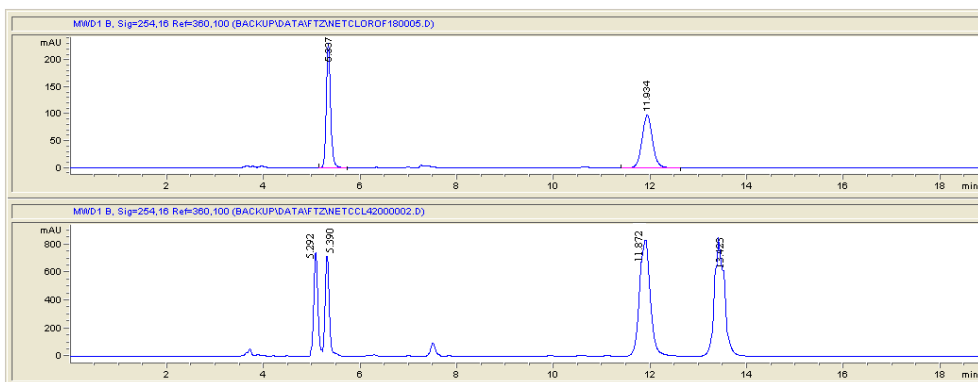


**Figure 1.** The chromatogram of the mixture obtained after the EKR of *rac*-**1** with PFL in chloroform (up) in comparison with the chromatogram of a mixture of *rac*-**1** and *rac*-**2**.

**Table 3.** Lipase catalyzed alcoholysis of *rac*-**2** with PFL in chloroform after 24 h

Entry	Alcohol	ee( <i>S</i> )- <b>2</b> (%)	ee( <i>R</i> )- <b>1</b> (%)	c (%)	<i>E</i>
1	Methanol	95	79	45	94
2	Ethanol	99	99	50	>>200
3	<i>n</i> -Propanol	91	85	48	58
4	<i>n</i> -Butanol	85	75	47	28

## 2.2. The use of immobilized biocatalysts

### 2.2.1. Preparation of immobilized PFL catalysts

Using a combination of methyltrimethoxysilane (MTMS) and tetramethoxysilane (TMOS), a hydrophobic matrix, suitable to enhance the activity of the entrapped lipase, was prepared by using an optimized<sup>19</sup> method of Reetz.<sup>20</sup> This method consists of the base-catalyzed *in situ* polymerization of the silanes. The previously reported optimal conditions (TMOS/MTMS=1/5, molar *ratio*; water/gel= 9/1 molar *ratio* and fluoride ion-catalyzed hydrolysis of silane precursors<sup>19</sup>) were used. The influence of celite and sucrose as additives on the performance and stability of the biocatalyst in the studied EKR processes was also investigated.

### 2.2.2. Acylation of *rac*-**1** and ethanolysis of *rac*-**2** with sol-gel immobilized PFL

PFL sol-gel catalysts were tested for the acylation of *rac*-**1** (0.1 M) with vinyl acetate and ethanolysis of *rac*-**2** (0.1 M) in chloroform. The results were excellent with respect to the applicability of our modified catalyst,



obtained in the presence of both celite and sucrose, in the studied enzymatic resolution processes ( $E \gg 200$  with all enzyme preparations).

### 2.2.3. Reuse of immobilized enzymes

One of the most important features of immobilized enzymes in synthetic applications is their reusability. For testing the recycling capacity, the acylation of *rac*-1 (0.1 M) with vinyl acetate (0.2 M) in chloroform was repeated with the same enzyme preparation up to 4 times. Every reaction was allowed to proceed to approx. 50% conversion before the catalyst was subjected to the next cycle. Between the cycles, the catalyst was washed with dry chloroform and reused without drying. The results (as enantiomeric excesses of the obtained compounds and enantiomeric *ratio E* of each reaction) are presented in Table 4.

**Table 4.** Reuse of the sol-gel PFL enzyme preparations (1.5 mg protein/mL) for the *O*-acylation of *rac*-1 (0.1 M) with vinyl acetate (0.2 M) in chloroform (1 mL) at room temperature

	PFL cycle				
	powder	1	2	3	4
Time (h)	24	20	20	22	22
<i>c</i> (%)	50	49	48	50	49
<i>ee</i> <sub>(S)-1</sub>	96	97	97	96	94
<i>ee</i> <sub>(R)-2</sub>	99	98	96	95	93
<i>E</i>	$\gg 200$	$>200$	$>200$	183	115

The enzymatic activity decreased slowly (5%) after 3 cycles and significantly (10%) after 4 times, respectively. The reuse had no significant effect on enzymatic enantioselectivity, allowing the preparation of (*S*)-1 and (*R*)-2 from *rac*-1 in highly enantiomerically enriched forms ( $ee > 95\%$ ) still on the 4<sup>th</sup> reuse cycle.

### 3. Preparative scale synthesis of both (*R*)- and (*S*)-1

The resulted optimum issued from the analytical scale studies was successfully applied at preparative scale synthesis of both highly enantiomerically enriched stereoisomers of 1-(10-ethyl-10*H*-phenothiazin-2-yl)ethanol and his acetate. To demonstrate the usefulness of these enzymatic procedures, 500 or 600 mg of the racemic substrate were used for each EKR as acetylation and alcoholysis. Whereas the enzymatic acetylation afforded the acetate (*R*)-2 and the alcohol (*S*)-1a in high enantiomeric excess, alcoholysis of the racemic acetate *rac*-2, yielded the opposite enantiomeric forms (*R*)-1 and (*S*)-2.

The absolute configuration of these enantiopure products was assigned using the earlier published data for optically pure enantiomers of **1**.<sup>11,17a</sup>

## EXPERIMENTAL PART

### 1. Analytical methods

High Performance Liquid Chromatography (HPLC) analyses were conducted with a HP 1200 instrument using Chiralpak IB column (4.6 x 250 mm) and a mixture of *n*-hexan: 2-propanol, 90:10 (v/v) as eluent for enantiomeric separation of *rac*-**1,2** at 1 mL/min flow rate. Retention times for (*R*)- and (*S*)-**1,2** are: 5.29 and 5.47 min for **2** and 11.87 and 13.42 min for **1**.

Thin Layer Chromatography (TLC) was carried out using Merck Kieselgel 60F<sub>254</sub> sheets. Spots were visualized by treatment with 5% ethanolic phosphomolybdic acid solution and heating. Preparative chromatographic separations were performed using column chromatography on Merck Kieselgel 60 (63-200 μm). Melting points were determined by hot plate method and are uncorrected. The enantiomeric excess of the resolution products were calculated using the peak area from the chiral HPLC analysis.

The determination of enantiomeric ratio (*E*) is based on the equation  $E = \ln[(1-c)(1-ee_S)]/\ln[(1-c)(1+ee_S)]$  with  $c = ee_S/(ee_S + ee_P)$ <sup>21</sup>

### 2. Materials

Lipozyme TLIM and CaL-B (immobilized and commercialized as Novozym 435) were products of Novozymes, Denmark. Lipases from *Candida rugosa* (CrL) was purchased from Fluka, whereas PPL, lipase from *Candida cylindracea* (CcL) and *Mucor miehei* were obtained from Sigma. Lipase from *P. fluorescens* (PFL) was purchased from Amano Pharmaceuticals Co., Ltd. (Nagoya, Japan) and used as received. All organic, inorganic reagents and solvents were products of Sigma-Aldrich or Fluka. All solvents were purified and dried by standard methods as required.

### A. Chemical synthesis

#### 1. Synthesis of racemic 1-(10-ethyl-10H-phenothiazin-2-yl)ethanol *rac*-**1**

Into a stirred solution of 1-(10H-phenothiazin-2-yl)ethanone (241 mg, 1 mmol) in anhydrous DMF (20 mL) NaH (26.5 mg, 1.1 mmol) was added in small portion maintaining the mixture temperature at 0-5 °C. After 10 min., ethyl iodide (125 μL, 1.25 mmol) was added and the resulted mixture was stirred at 50 °C. After completion of the reaction (TLC monitoring), the solvent was removed under reduced pressure to dryness. The solid resulting residue was dissolved in CH<sub>2</sub>Cl<sub>2</sub> (20 mL), filtered and concentrated *in vacuo*. The crude 1-(10-ethyl-10H-phenothiazin-2-yl)-ethanone was then crystallized from ethanol to provide a yellow semisolid material which was used as such in the next step without further purification.

To a stirred solution of the 1-(10-ethyl-10*H*-phenothiazin-2-yl)ethanone (215 mg, 0.8 mmol) in dry methanol (5 mL) NaBH<sub>4</sub> (38 mg, 1 mmol,) was added in small portion at room temperature with stirring. After the reduction was complete (TLC monitoring), the reaction was quenched by dropwise addition of 2N HCl solution (1 mL), then evaporated to a final volume of about 1 mL. To this mixture water (3 mL) and CH<sub>2</sub>Cl<sub>2</sub> (6 mL) were added. After separating the two layers, the aqueous one was extracted with CH<sub>2</sub>Cl<sub>2</sub> (6 mL). The combined organic layers were dried over anhydrous MgSO<sub>4</sub> and the solvent was removed. The residue was purified by column chromatography on silica gel using CH<sub>2</sub>Cl<sub>2</sub> as eluent to yield the desired product as colorless semisolid.

## **2. Chemical acetylation of the racemic 1-(10-ethyl-10*H*-phenothiazin-2-yl)ethanol *rac*-1**

Into a solution of racemic 1-(10-ethyl-10*H*-phenothiazin-2-yl)ethanol (*rac*-1, 1.5 g, 5.61 mmol) in dry CH<sub>2</sub>Cl<sub>2</sub> (15 mL), Et<sub>3</sub>N (6.16 mmol, 624 mg, 860 μL), acetyl chloride (6.17 mmol, 484.3 mg, 438.7 μL) and DMAP (0.16 mmol, 20 mg) were dropwise added in this order. The mixture was stirred at room temperature overnight and quenched with water (15 mL). After separation, the organic layer was dried over anhydrous sodium sulfate then evaporated to dryness under reduced pressure. The crude product was purified by vacuum-chromatography on neutral aluminum oxide (Brockmann IV) using CH<sub>2</sub>Cl<sub>2</sub> as eluent to give *rac*-2 as semisolid.

The structure of racemic **1,2** was confirmed by spectral analysis. All data are in good accordance with those previously reported in literature.<sup>11</sup>

## **B. Biotransformations with lipases**

### **1. Analytical scale biotransformations**

#### **1.1. Analytical scale enzymatic acetylation of *rac*-1**

Into a solution of racemic 1-(10-ethyl-10*H*-phenothiazin-2-yl)ethanol *rac*-1 (27.1 mg, 0.1 mmol) in vinyl acetate (1 mL), the tested lipase (50 mg) was added. The reaction mixture was shaken at 300 rpm at room temperature. For HPLC analysis, samples were taken from the reaction mixture (10 μL), diluted to 500 μL with 2-propanol and filtered before injection. Data on conversion and enantiomeric composition of the products for the tested lipases are presented in Table 1.

#### **1.2. Enzymatic kinetic resolution of racemic 1-(10-ethyl-10*H*-phenothiazin-2-yl)ethanol *rac*-1 with vinyl acetate in different solvents with PFL**

Into a solution of racemic 1-(10-ethyl-10*H*-phenothiazin-2-yl)ethanol *rac*-1 (27.1 mg, 0.1 mmol) in different solvents (1 mL), vinyl acetate (0.4 mmol, 34.4 mg, 36.8 μL) and PFL (50 mg) were added. The reaction mixtures were shaken at 300 rpm at room temperature. Samples were analyzed by

HPLC as described. Data on conversion and enantiomeric composition of the products for the tested solvents are presented in Table 2.

### 1.3. Analytical scale enzymatic alcoholysis of *rac-2*

Into the mixture of *rac-2* (0.1 mmol, 31.3 mg) in chloroform (1 mL), PFL (50 mg) and the tested alcohol (1 mmol) were added. The reaction mixture was shaken at 300 rpm at room temperature. Samples were analyzed by HPLC. Data on conversion and enantiomeric composition of the products are presented in Table 3.

## 2. The use of immobilized L-AK

### 2.1. Preparation of immobilized L-AK catalysts

PFL powder (150 mg) was dissolved in Tris/HCl-buffer (0.1 M, pH 8, 5 mL). When additives (Celite 50 mg or/and sucrose, 100 mg) were used, they were included in the PFL solution. Into this solution, an aqueous sodium fluoride (50  $\mu$ L of a 1 M solution) was added under vigorous shaking until the mixture turned to homogeneous. After the addition of the gel precursors (MTMS and TMOS, TMOS/MTMS= 1/5, water/gel ratio= 9/1) in one portion, the mixture was vigorously shaken for 10-15 s. The gelation was completed under gentle shaking. For maturation, the sol-gel preparations were kept overnight in a cooled (4 °C) desiccator. The next day, the sol-gel preparations were gently crushed, sequentially washed with 2-propanol, water, 2-propanol and *n*-hexane and finally freeze-dried (12 h, 0.2 mbar).

### 2.2. Acylation of *rac-1* with sol-gel immobilized PFL

The experiment was carried out in the presence of 1.5 mg/mL of protein. The PFL preparation was added into the solution of the substrate *rac-1* in chloroform (1 mL) before vinyl acetate (2 eq.) was added to start the reaction. The reaction mixture was shaken at 160-180 rpm at room temperature (23-24 °C).

### 2.3. Reuse of immobilized enzymes

The immobilized PFL preparation (1.5 mg protein/ mL) was added into the solution of *rac-1* (0.1 M) in chloroform (1 mL) before the addition of vinyl acetate (2 eq.) as described above. Progress and enantioselectivity of reaction were followed by sample analyses with HPLC. The reactions were stopped at 50% by decantation of the liquid phase. The solid lipase preparations were washed with dry chloroform before subjected to a new reaction with a fresh portion of reagents. Reuse was repeated 5 times under identical conditions.

### 3. Preparative scale synthesis of both (*R*)- and (*S*)-1

The optimum conditions determined at analytical scale reactions were successfully applied for the preparative scale synthesis of the highly enantiomerically enriched (*R*)- and (*S*)-1-(10-ethyl-10*H*-phenothiazin-2-yl)ethanol and their acetate ((*R*)- and (*S*)-1 and 2) using in each case 500 mg of the substrate.

Into a solution of racemic 1-(10-ethyl-10*H*-phenothiazin-2-yl)ethanol (*rac*-1, 500 mg) in chloroform (20 mL), vinyl acetate (175  $\mu$ L) and PFL (500 mg) were added. The reaction mixtures were shaken at 300 rpm at room temperature until the conversion reach 50% (approx. 24 h). The enzyme was filtered off and washed with acetone (2 $\times$ 5 mL). Solvents were distilled off from the combined filtrates and the residue was purified by column chromatography (silica gel, CH<sub>2</sub>Cl<sub>2</sub>) resulting in the optically active alcohol [(*S*)-1] and acetate [(*R*)-2] fractions as white semisolids. IR, NMR and MS spectra of the optically active alcohol and acetate were indistinguishable from that of their racemates. Data on yield and enantiomeric excess of the products [(*S*)-1 and (*R*)-2] are shown in Table 5 (entry 1).

Into the mixture of 1-(10-ethyl-10*H*-phenothiazin-2-yl)ethyl acetate *rac*-2 (600 mg) in chloroform (20 mL), PFL (500 mg) and ethanol (1 mL) were added. The reaction mixture was shaken at 300 rpm at room temperature until the conversion reach 50% (approx. 24 h). Further purifications were performed as described above. Data on yield and enantiomeric excess of the products [(*S*)-2 and (*R*)-1] are shown in Table 5 (entry 2).

**Table 5.** Preparative scale enzymatic resolution of *rac*-1,2 with PFL in chloroform

Entry	Substrate	ee (%)		$\eta^*$ (%)	<i>E</i>	ee (%)		$\eta^*$ (%)	<i>E</i>
		( <i>R</i> )-2	( <i>S</i> )-1			( <i>R</i> )-1	( <i>S</i> )-2		
1	<i>rac</i> -1	99	96	47	>>200				
2	<i>rac</i> -2					99	99	48	>>200

\*based on the *rac*-1 or *rac*-2 as starting compound

## CONCLUSIONS

The synthesis of both enantiomers of 1-(10-ethyl-10*H*-phenothiazin-2-yl)ethanol **1** and his acetate **2** has been achieved by enzymatic kinetic resolution with PFL as efficient biocatalyst.

Whereas the enzymatic acetylation of the racemic ethanol **1** afforded the (*R*) enantiomer of acetate [(*R*)-2] and the (*S*) enantiomer of the alcohol [(*S*)-1] in high enantiomeric excess, the ethanolysis of the racemic acetate *rac*-2 yielded the opposite enantiomeric form [(*R*)-1 and (*S*)-2].

The stability, activity and reusability of the sol-gel encapsulated PFL were determined. The immobilized biocatalyst provide to be efficient in both studied resolution processes.

## ACKNOWLEDGEMENT

Anca Munceanu expresses all the gratitude for Professor Florin Irimie for the scientific and logistic help granted during elaborating her PhD thesis, part of which is the actual paper.

## REFERENCES

1. a) Mosnaim, A.D.; Ranade, V.V.; Wolf, M.E.; Puente, J.; Antonieta, V.M. *Am. J. Ther.* **2006**, *13*, 261–273; b) Kaiser, C.; Pavloff, A.M.; Garvey, E.; Fowler, P.J.; Tedeschi, D.H.; Zirkle, C.L.; Nodiff, E.A.; Saggiomo, A. *J. Med. Chem.* **1972**, *15*, 665–673.
2. a) Hull, K.G.; Visnic, M.; Tautz, W.; Sheffron, A. *Tetrahedron* **1997**, *53*, 12405–12414; b) Truppo, M.D.; Pollard, D.; Devine, P. *Org. Lett.* **2006**, *9*, 335–338; c) De Martino, G.; La Regina, G.; Di Pasquali, A.; Ragno, R.; Bergamini, A.; Ciaprini, C.; Sinistro, A.; Maga, G.; Crespan, E.; Artico, M.; Silvestrini, R. *J. Med. Chem.* **2005**, *48*, 4378–4388; d) Tanis, S.P.; Evans, B.R.; Nieman, J.A.; Parker, T.T.; Taylor, W.D.; Heasley, S.E.; Herrington, P.M.; Perrault, W.R.; Hohler, R.A.; Dolak, L.A.; Hester, M.R.; Seest, E.P. *Tetrahedron: Asymmetry* **2006**, *17*, 21–54.
3. a) Tosa, M; Pilbák, S.; Moldovan, P.; Paizs, C.; Szatzker, G.; Szakács, G.; Novák, L.; Irimie, F.D.; Poppe, L. *Tetrahedron: Asymmetry* **2008**, *19*, 1844–1852.
4. a) Ghanem, A.; Aboul-Enein, H.I. *Tetrahedron: Asymmetry* **2004**, *15*, 3331–3351; b) Brem, J.; Paizs, C.; Tosa, M.I.; Vass, E.; Irimie, F.D. *Tetrahedron: Asymmetry* **2009**, *20*, 489–496.
5. a) Bencze, L.C.; Paizs, C.; Toşa, M.I.; Trif, M.; Irimie, F.D. *Tetrahedron: Asymmetry* **2010**, *21*, 1999–2004; b) Paizs, C.; Tosa, M.; Majdik, C.; Tähtinen, P.; Irimie, F.D.; Kanerva, L.T. *Tetrahedron: Asymmetry* **2003**, *14*, 619–627; c) Kirk, O.; Christensen, M.W. *Org. Proc. Res. Dev.* **2002**, *6*, 446–451; d) De Gonzalo, G.; Lavandera, I.; Brieva, R.; Gotor, V. *Tetrahedron* **2004**, *60*, 10525–10532.
6. a) Paizs, C.; Tähtinen, P.; Tosa, M.; Majdik, C.; Irimie, F.D.; Kanerva, L.T. *Tetrahedron* **2004**, *60*(46), 10533–10540; b) Bencze, L.C.; Paizs, C.; Tosa, M. I.; Vass, E.; Irimie, F.D. *Tetrahedron: Asymmetry* **2010**, *21*, 443–450.
7. a) Brem, J.; Toşa, M.I.; Paizs, C.; Vass, E.; Irimie, F.D. *Tetrahedron: Asymmetry* **2010**, *21*(3), 365–373.
8. a) Toşa, M.; Paizs, C.; Majdik, C.; Novák, L.; Kolonits, P.; Irimie, F.D.; Poppe, L. *Tetrahedron: Asymmetry* **2002**, *13*(2), 211–221; b) Toşa, M.; Paizs, C.; Majdik, C.; Moldovan, P.; Novák, L.; Kolonits, P.; Szabó, E.; Poppe, L.; Irimie, F.D. *J. Mol. Catal. B: Enzymatic* **2002**, *17*(6), 241–248.
9. Bansode, T.N.; Shelke, J.V.; Dongre, V.G. *Eur. J. Med. Chem.* **2009**, *44*, 5094–5098.
10. Brem, J.; Tosa, M.I.; Paizs, C.; Munceanu, A.; Matkovic-Calogovic, D.; Irimie, F.D. *Tetrahedron: Asymmetry* **2010**, *21*, 1993–1998.
11. Brem, J., Pilbák, S., Paizs, C., Bánóczy, G., Irimie, F.D, Toşa, M. I., Poppe, L. *Tetrahedron: Asymmetry* **2011**, *22*, 916–923.

12. Vanttinen, E.; Kanerva, L.T. *J. Chem. Soc. Perkin Trans 1* **1994**, *1*, 3459-3463; Långvik, O.; Saloranta, T.; Kirilin, A.; Liljeblad, A.; Mäki-Arvela, P.; Kanerva L.T.; Murzin, D.Y.; Leino, R. *Chem Cat Chem* **2010**, *2*, 1615-1621.
13. Devi, B.L.A.P.; Guo, Z.; Xu, X. *J. Am. Oil. Chem. Soc.* **2009**, *86*, 637-642.
14. a) Zarcula, C.; Corici, L.; Croitoru, R.; Ursoiu, A.; Peter, F. *J. Mol. Catal. B: Enzym.* **2010**, *65*, 79-86; b) Tomin, A.; Weiser, D.; Hellner, G.; Bata, Zs.; Corici, L.; Péter, F.; Koczka, B.; Poppe, L. *Process Biochem.* **2011**, *46*, 52-58.
15. Santos, J.C.; Paula, A.V.; Nunes, G.F.M.; de Castro, H.F. *J. Mol. Catal. B: Enzym.* **2008**, *52-53*, 49-57.
16. a) Gorokhova, I.V.; Ivanov, A.E.; Zubov, V.P. *Russ. J. Bioorg. Chem.* **2002**, *28*, 38-43; b) Mendes, A.A.; Giordano, R.C.; de L.C. Giordano, R.; de Castro, H.F. *J. Mol. Catal. B: Enzym.* **2011**, *68*, 109-115; c) Gorokhova, I.V.; Ivanov, A.E.; Zubov, V.P. *Russ. Chem. B, Int. Ed.* **2001**, *50*, 152-154.
17. a) Stepanenko, V.; De Jesus, M.; Correa, W.; Guzman, I.; Vazquez, C.; Ortiz, L.; Ortiz-Marciales, M. *Tetrahedron: Asymmetry* **2007**, *18*, 2738-2745; b) Cauquil, G.; Casadevall, A. *Bull. Soc. Chim. Fr.* **1955**, 768-783.
18. a) Bornschauer, U. T.; Kazlauskas, R. *J. Hydrolases in Organic Synthesis: Regio- and Stereoselective Biotransformations*; Wiley-VCH: Weinheim-New York, **2006**; b) Gog, A.; Roman, M.; Tosa, M.; Paizs, C.; Irimie, F.D. *Renewable Energy* **2012**, *39*, 10-16.
19. Brem, J.; Turcu, M.C.; Paizs, C.; Lundell, K.; Tosa, M.I.; Irimie, F.D.; Kanerva, L. *Process Biochemistry* **2012**, *47*, 119-126.
20. a) Reetz, M.T.; Zonta, A.; Simpelkamp, J. *Angew. Chem. Int. Ed. Engl.* **1995**, *34*, 301-303; b) Reetz, M.T.; Zonta, A.; Simpelkamp, J. *Biotechnol. Bioeng.* **1996**, *49*, 527-534; Reetz, M.T.; Tielmann, P.; Wiesenhöfer, W.; Könen, W.; Zonta, A. *Adv. Synth. Catal.* **2003**, *345*, 717-728.
21. Chen, C-S.; Fujimoto, Y.; Girdaukas, G.; Sih, C.J. *J. Am. Chem. Soc.* **1982**, *104*, 7294-7299.

## QUANTIFICATION OF NICOTINE AND COTININE IN TEENAGER'S URINE

ALINA BRATAN<sup>a,b</sup>, MANUELA MINCEA<sup>a</sup>, IOANA RODICA LUPSA<sup>b</sup>,  
MARILEN GABRIEL PIRTEA<sup>c</sup> AND VASILE OSTAFE<sup>a,c,\*</sup>

**ABSTRACT.** The aim of the study was to develop an Ultrahigh Performance Liquid Chromatography coupled with Mass Spectrometry (UPLC-MS/MS) method for the simultaneous identification and quantification of nicotine and its principal metabolite cotinine in teenager's urine. Sample preparation was performed by liquid-liquid extraction followed by UPLC-MS/MS operated in electrospray positive ionization (ESI) mode with selective reaction monitoring (SRM) data acquisition. In order to measure the prevalence of tobacco consume in adolescents, 150 samples were collected and analyzed. The experiments realized for method validation revealed a linear range between LOQ ( $2.5 \text{ ng}\cdot\text{mL}^{-1}$ ) and  $1000 \text{ ng}\cdot\text{mL}^{-1}$  for both nicotine and cotinine. The accuracy was less than 9 %. Repeatability and intermediate precision were  $\leq 7.6$  and  $\leq 8.9\%$ , respectively. Concentrations of nicotine and cotinine in smokers adolescents urine were found to range between from 2.5 to  $11.170 \text{ ng}\cdot\text{mL}^{-1}$  for nicotine and 2.5 to  $10.530 \text{ ng}\cdot\text{mL}^{-1}$  for cotinine, respectively. These findings significantly support the likelihood of extensive nicotine consumption through smoking teenagers in Romania.

**Keywords:** teenagers, nicotine, cotinine, urine, UPLC-MS, method validation.

## INTRODUCTION

Tobacco has been smoked for at least the last three thousand years. What at first appeared to be a trend proved to be a nightmare because nowadays even the manufacturers admit that tobacco cigarettes can seriously damage health and they mention this on their cigarette packages. With all the negative advertising done to tobacco, adults and teenagers continue to smoke.

---

<sup>a</sup> West University of Timisoara, Timisoara, Faculty of Chemistry – Biology – Geography, Advanced Environmental Research Laboratories, Oituz 4, Timisoara 300086, Romania

<sup>b</sup> National Institute of Public Health-Regional Center of Public Health Timisoara, Babes Victor 16, Timisoara, 300226, Romania

<sup>c</sup> West University of Timisoara, Multidisciplinary Research Platform "Nicholas Georgescu - Roengen", Oituz 4, Timisoara 300086, Romania

\* Corresponding author: [vostafe@cbg.uvt.ro](mailto:vostafe@cbg.uvt.ro)



Nicotine (Figure 1a) is the most abundant of the volatile alkaloids in the tobacco leaves [1], being responsible for smoking addiction. By weight, nicotine normally represents about 5 % of a tobacco plant [2]. Nicotine acts on nicotinic cholinergic receptors, affecting most organ systems in the body and is a highly addictive drug [3]. Cigarettes contain 8 to 20 mg of nicotine (depending on the brand), but only approximately 1 mg is actually absorbed in the human body [2]. Nicotine presents a relative short half-life ( $t_{1/2} = 1-2$  hours) [4].

An average of 70–80% of the nicotine absorbed by a smoker is metabolized to cotinine [5]. Measurement of cotinine levels provides a sensitive estimate of tobacco smoke exposure. Cotinine (Figure 1b) is the major degradation product of nicotine metabolism in the liver by C-oxidation [6], and can be determined in various biological matrices, including blood, saliva, urine, and semen [5], even after a few days subsequent to individual exposure on tobacco smoke by determining the half-life in the body [7]. Cotinine levels in the blood are not a good markers of nicotine content, whereas urinary excretion of cotinine represents a good indicator being less influenced by the flow of urine and *pH* [8] even after a few days subsequent to individual exposure on tobacco smoke by determining the half-life in the body [7]. Moreover, in a pilot study hair nicotine/cotinine concentrations were determinate for monitoring exposure to tobacco smoke among infants and adults [9].

In human organism, the half-life of cotinine is much higher (10-20 h) than nicotine, being considered as the main biomarker for assessment of environmental exposure to tobacco smoke (passive smoking) [10]. Although there is not a perfect agreement in the scientific literature about the half-life of nicotine and cotinine, all data agreed that the persistence of cotinine in the body is between 10 to 20 times longer than that of nicotine [4, 7, 11, 12]. Even so, it should be noted that cotinine determination enables monitoring of only a relatively short period (3-4 days) of previous exposure to tobacco smoke.

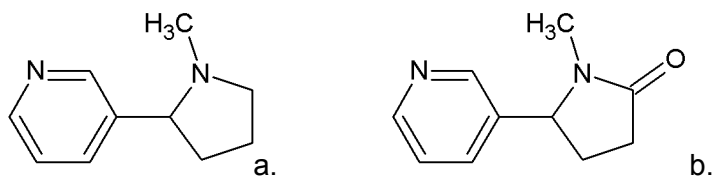


**Figure 1.** Chemical structure of nicotine (a) and cotinine (b).

Exposure to secondhand smoke (SHS) is a significant threat to public health and represents a danger for both the development and health status of children and adolescents[13].

Different analytical methods, including chromatographic techniques interfaced with mass spectrometry, thin layer chromatography, and several immunologically based detection systems [14-19], have been used for determination of nicotine, cotinine and/or other metabolites in urine. Methods combining chromatography and mass spectrometry allow for a Limit of Detection (LOD) of around 1 ng / mL at a cost of approximately \$25 per sample, while the enzyme immunoassay (EIA) tests are less expensive, costing about \$15 per sample, but less precise with a LOD of 10 ng / mL. Also, due to cross-reactivity with other nicotine metabolites EIA may overestimate cotinine concentrations [20]. However, the chromatographic assays can have the capability of being more specific, particularly when they are interfaced with mass spectrometry (MS) or tandem mass spectrometry (MS/MS) [21].

In Romania, tobacco consumption represents an important public health issue, the statistics showing that more than 33000 people die yearly from smoking. One important reason of high rates of tobacco consumption in Romania is explained by high frequency of smoking among women and youth in general. Growth of this percent was constant in women: 11.3% of women aged over 15 years was reported in 1989, 15.2% in 1994 and 25% in 2000. Also, 21% of the population of Romania was already smoking daily at 15 years of age [22]. These studies were performed with epidemiological methods, based on responses to special questionnaires. In this paper we present a study based on a special questionnaire, but also on a chromatographic analysis of urine of the subjects, in this way providing objective results.

This paper presents an analytical method for the simultaneous determination and quantification of nicotine and its main metabolite, cotinine in urine, using liquid-liquid extraction (LLE) followed by ultrahigh performance liquid chromatography coupled with electrospray ionization - mass spectrometry (UPLC – MS). The method was applied to quantify nicotine and cotinine in urine samples of 150 adolescents from western part of Romania. Such study was not performed in Romania until now.

## RESULTS AND DISCUSSION

### Method Development

A complete separation of nicotine and cotinine in urine specimens was achieved by ultra-performance liquid chromatography using a gradient of acetonitrile (between 10 and 100%) having also 0.1% ammonium formate (buffered at pH 5.5), with a flow rate set at 0.4 mL·min<sup>-1</sup>. Although the separation of the two analytes was achieved in less than 0.8 min, the gradient program continued for two min, with the aim to increase the concentration of organic modifier in order to elute from the column the hydrophobic contaminants present in the sample extract.

We successfully isolate each analyte by providing adequate retention of polar compounds and excellent peak shape (Figure 2). Sensitivity was also optimized since using a mobile phase highly enriched in ammonium formate ensured an efficient ionization towards the molecules of interest. Likewise, reduced endogenous matrix interferences resulted in very clean chromatograms and a high throughput was obtained due to the feasibility of using a higher flow rate.

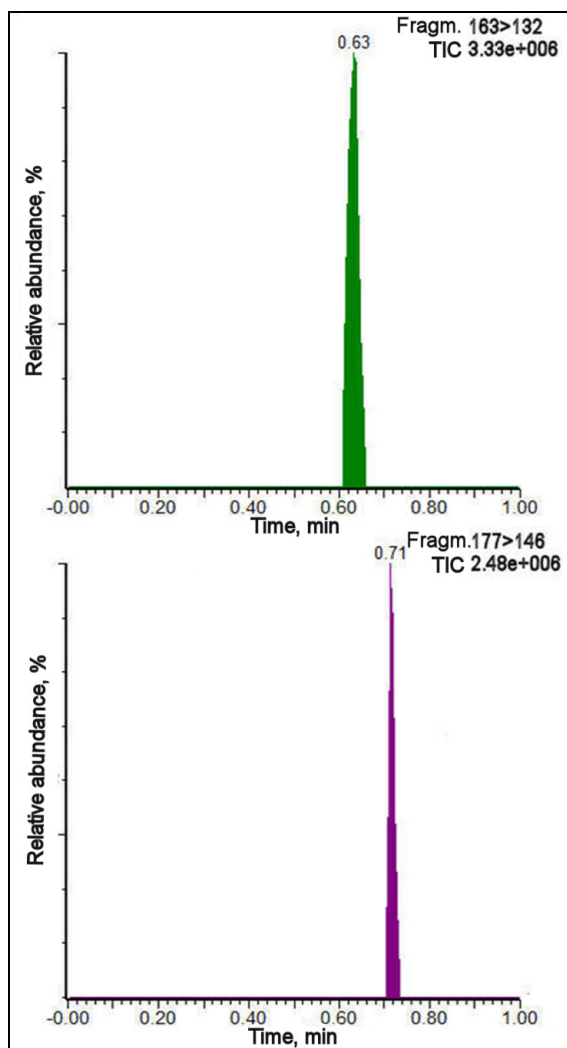


**Figure 2.** Examples of UPLC – MS chromatograms of standard nicotine ( $R_t$  0.63, MRM 163 > 132) and cotinine ( $R_t$  0.71, MRM 177 > 146).

Repeatability of the retention times ( $R_t$ ) was evaluated by calculating mean values variability over the set of three values. The results have proved to be satisfactory for both compounds of interest as repeatability was 0.8% for nicotine and 1.1% for cotinine, respectively. Direct infusion of individual standard solutions, with a flow rate and mobile phase composition corresponding to the elution time from the LC column, allowed optimization of tandem mass spectrometry parameters. Gas streams, spray voltage, heated capillary voltage and temperature and compound specific normalized collision energies were manually tuned, resulting in a high sensitivity fragment spectra with a precursor ion response <10% in abundance.

### Sample Preparation

The selective extraction protocol for urine samples used in this work was performed with a single LLE. Nicotine and cotinine were extracted from urine with chloroform: propan-2-ol (95:5, v/v), after neutralization with phosphate buffer at pH 7.0. Extraction was followed by evaporation of the organic phase and reconstitution in the initial mobile phase mixture. This simple, cost and steps-limited methodology provided very clean extracts of urine samples containing nicotine and cotinine.

### Method Validation

The calibration graph resulted from the analysis of the calibration standard solutions prepared in pooled urine from non-smoking test persons was linear between the quantification limit ( $2.5 \text{ ng}\cdot\text{mL}^{-1}$ ) and  $1000 \text{ ng}\cdot\text{mL}^{-1}$  urine (the highest concentration used for the realization of standard curves) (see Table 1).

**Table 1.** Validation parameters of standard curves for nicotine and cotinine ( $n = 6$ ) realized in negative urines

Analyte	Concentration ( $\text{ng}\cdot\text{mL}^{-1}$ )	Accuracy (%)	Repeatability (%)	Intermediate precision (%)
Nicotine	10	0.91	7.6	8.9
	100	0.93	6.5	7.8
	1000	0.97	6.1	7.1
Cotinine	10	0.92	7.1	8.7
	100	0.95	6.6	8.0
	1000	0.97	6.2	7.4

## Accuracy

The loss due to processing was determined to check the accuracy of the method. For this purpose reference standards prepared in water and urine were processed and analyzed. Standards solution prepared in mobile phase with the same cotinine concentrations as the reference standards in their respective matrix were injected in UPLC-MS system without further treatment (n=6). Mean absolute recovery rates for nicotine and cotinine, respectively, of 96.7% and 97.1% (in water) and 93.6% and 94.6% (in pooled urine) were obtained by comparison the direct injection results. This means that 3.3% of nicotine and 2.9% cotinine are lost during the processing and analysis of aqueous analytes samples. In the case of urine samples, the losses due to processing are about 6.4% and 5.4%, respectively.

## Recovery

Trueness was evaluated through recovery studies, fortifying blank urine samples at three levels (10, 100, and 1000 ng·mL<sup>-1</sup>). Each level was replicated six times and the obtained results can be observed in Table 2. Recoveries were higher than 90% for all the analytes and levels assayed.

**Table 2.** Recoveries of nicotine and cotinine (n = 6)

Analyte	Concentration (ng·mL <sup>-1</sup> )			Recovery (%)			Relative Standard Deviation (%)		
	L	M	H	L	M	H	L	M	H
Nicotine	0	100	1000	91.3	96.8	96.9	7.3	6.2	6.3
Cotinine	0	100	1000	89.6	97.6	95.1	7.9	6.5	6.6

L = low, M = medium, H = high, referring to the level of concentration of the analytes.

## Carry-over

Carry-over was evaluated accordingly, after injection of the highest calibrator (1000 ng·mL<sup>-1</sup> for nicotine and cotinine), followed by the analysis of a blank urine sample. This procedure was repeated three times successively. Due to the fact that the column was systematically cleaned with 100% acetonitrile, as pointed out in the description of the elution gradient program, none of the target compounds were detected, demonstrating the absence of any carry-over effect.

## Determination of Nicotine and Cotinine in Teenager's Urine Sample

Nicotine and cotinine levels have earlier been used to validate the smoking status of an individual [23, 24]. In order to assess the effects of tobacco use on human health [25, 26], these biomarkers have also been used

in epidemiological studies [27-30], to estimate the passive smoking, and for assessment of the efficacy of quit smoking methods [31]. While studies on nicotine and cotinine levels in cigarette smokers as well as those for passive smoking in other ethnic groups are well documented, for Romanian teenagers there are not reliable data issued by high confidence method, as UPLC-MS.

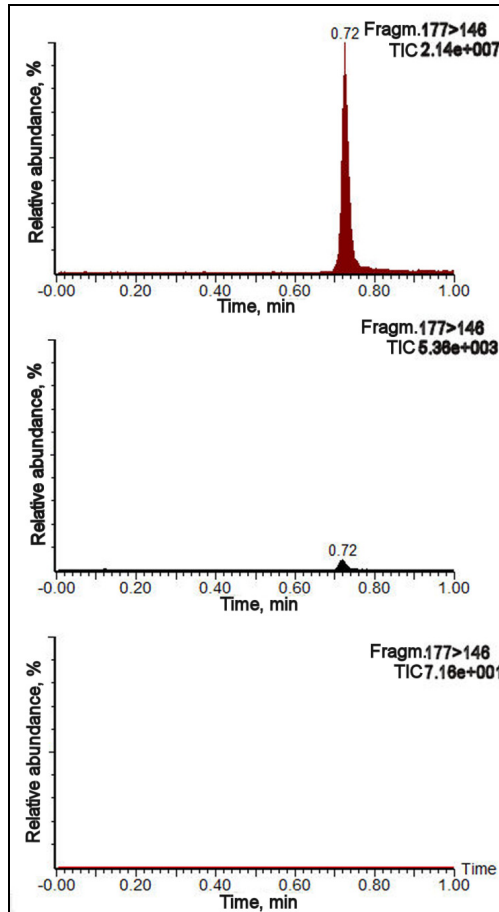


**Figure 3.** Comparison of chromatographic profiles of urine samples collected from a nonsmoker (lower panel), a passive smoker (middle panel) and an active smoker (upper panel). MRM for cotinine 177 >146.

Asking individuals to self-report tobacco use is a cheap method that allowed the collection of detailed information on tobacco use [20]. Self-reports have generally been found to be accurate, but may be prone to recall bias or intentional misreporting [32]. Kandel *et al.* also examined the discrepancies

between self-reported cigarette smoking and salivary cotinine concentration among adolescents. Despite interview procedures designed to emphasize the confidentiality of the interview and to explain to adolescents that they would provide a biological sample to be assayed for the presence of tobacco products, about 42% of the adolescents who reported smoking in the last 3 days had salivary cotinine concentrations below the cut-point, whereas 49% of adolescents with salivary cotinine above the cut-point reported not having smoked within the last 3 days [33]. Among groups for whom smoking is supposed as being undesirable intentional underreporting was observed [34]. In situations where the validity of self-report data is suspect, biomarkers for tobacco exposure provide an objective assess and supply a measure of average or cumulative exposure over a period of time [20].

The concentrations for the urines of the target group ranged from 2.5 (LOQ) to 11.170 ng·mL<sup>-1</sup> for nicotine and 2.5 (LOQ) to 10.530 ng·mL<sup>-1</sup> for cotinine. Some chromatographic profiles are presented in Figure 3, as examples of the urine without cotinine, with low level of cotinine (between 10 and 100 ng·mL<sup>-1</sup>) and with high level (more than 100 ng·mL<sup>-1</sup>), respectively.

As we can see from Table 3 the number of teenagers that have declares themselves as active smokers is lower than the number of adolescents that have urine levels of cotinine higher than 100 ng / mL, and can be considered in this category based on an objective criterion. These results are not surprising as at least some of the tested students tend to lie about their smoking status.

**Table 3.** Classification of the subjects according with the cotinine cut-off level found in urines.

No subjects	AS-d*	AS-a**	PS-d*	PS-a**	NS-d*	NS-a**
150	27	31	76	67	47	52
%	18	20.66	50.67	44.67	31.33	34.67
Cotinine range (ng·mL <sup>-1</sup> )	>100		10-100		<10	

\* d = status declared in the questionnaire,

\*\*a = status assigned after urine analysis

AS = active smokers, PS = passive smokers, NS = non-smokers

Discrepancies were seen also in the situation of passive smokers, as less teenagers were classified in this category based on the UPLC-MS analysis as they have declare in the questionnaires. This lack of concordance can be assigned to the fact that, although these subjects were living in families where the parents are active smokers, the effect of this habit of the adults is not so intense on the state of the children. Quite vice versa was the situation of

non-smokers, where less passive non-smokers than those declared were found by UPLC-MS urine analysis. In this case, we can assume that even these high school students do not live in family with smokers, they spend some time in the presence of smokers.

In all the cases where the UPLC-MS analysis indicated cotinine values higher than  $10 \text{ ng}\cdot\text{mL}^{-1}$ , the urine was fortified with cotinine standard in order to confirm the presence of this analyte by the same retention time. An example is presented in Figure 4.

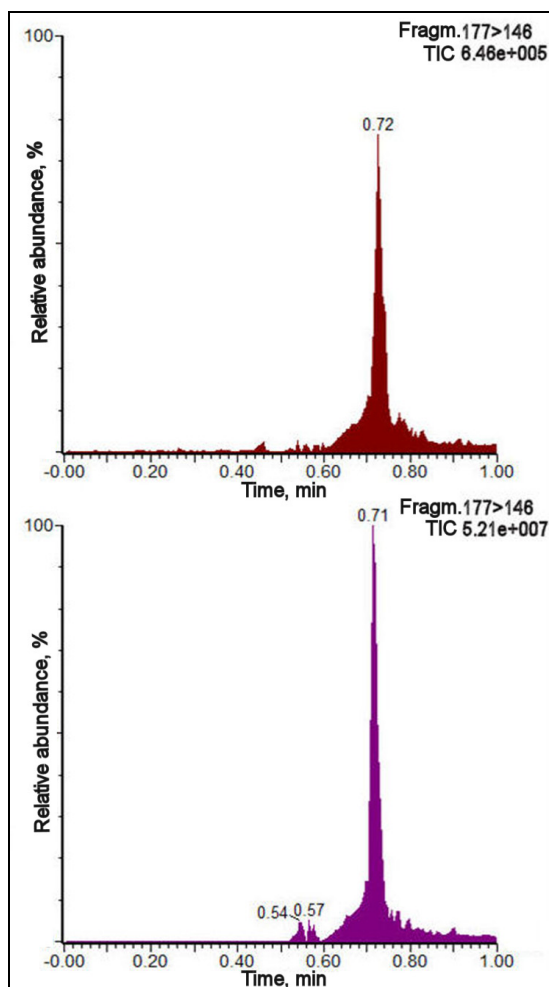


**Figure 4.** Example of chromatographic profiles of a urine sample from an active smoker (upper panel) and the same urine fortified with 100 ng cotinine. MRM for cotinine 177 > 146.



From the 150 samples, 42 have nicotine and cotinine levels below the quantification limit (less than  $2.5 \text{ ng}\cdot\text{mL}^{-1}$  of each compound), *e. g.* 28% of the investigated teenagers were for sure non-smokers. Other 10 adolescents were added to the non-smoker category as the level of cotinine was less than  $10 \text{ ng}\cdot\text{mL}^{-1}$  and they have declared themselves either to be non-smokers living in a non-smokers environment or non-smokers living in smokers families. In total, 34.6% of the subjects were considered as non-smokers, based on the cotinine level in their urine. Based on the UPLC-MS analysis of the urines of the subjects, we have found that 20.6% of the high school students from western part of Romania are active smokers. These results are in a good concordance with other studies [22]. Similar results were obtained when nicotine levels of urine were taken into account. For all the subjects the creatinine levels were in the normal range  $5.5 - 11 \text{ ng}\cdot\text{mL}^{-1}$ . This study is the first report of use of an UPLC-MS analytical method to assess the nicotine and cotinine urinary levels of teenagers in Romania.

## CONCLUSIONS

A sensitive and selective UPLC-ESI-MS/MS method for the simultaneous detection and quantification of nicotine and its principal metabolite, cotinine in urine was developed and validated. The simple and fast sample preparation protocol based on LLE provided a satisfactory matrix clean-up and recovery, while the subsequent use of UPLC chromatography allowed to obtain very good separation and peak shape, enhanced sensitivity and high samples throughput for comprehensive measurement of free nicotine and cotinine.

The total time to complete this assay is substantially shorter than for other methods that require extensive extractions before assay. The simple extraction into chloroform: propanol mixture combined with a 2 min assay time allowed tens of samples to be analyzed in 8 h working time.

This analytical procedure was successfully applied to the urine samples collected in order to investigate the prevalence of smoking amongst teenagers. The findings gathered during this work provided strong evidence that smoking is a very serious trend in adolescents. Indeed, traces of nicotine and cotinine were found in 72% of urine samples. Prevalence of nicotine consumption, in the form of smoke products, suggested that about 20% of the teenagers were active smokers.

The method was validated according to international guidelines and was applied to quantify the amount of nicotine and cotinine in 150 teenagers, being the first report of such a study performed in Romania.

## EXPERIMENTAL SECTION

### Chemicals and Reagents

(S)-Nicotine ((S)-3-(1-Methyl-2-pyrrolidinyl)pyridine, Fluka N5511, 1 mg·mL<sup>-1</sup> in methanol) and (S)-cotinine ((S)-1-Methyl-5-(3-pyridyl)-2-pyrrolidinone, Fluka C0430, 1 mg·mL<sup>-1</sup> in methanol) were purchased from Sigma-Aldrich. All other solvents and reagents were of chromatography quality, purchased also from Sigma – Aldrich: ammonium formate (12466 Fluka), formic acid (06440 Fluka), chloroform (CHROMASOLV, 650438 Sigma), 2-propanol (LC-MS CHROMASOLV, 34965 Fluka), acetonitrile (LC-MS CRHOMASOLV, Fluka 14261). HPLC grade water was prepared by SG Ultra Clear 2001-B Water Deionization System (Cole-Parmer) and additionally filtered through syringe filters PTFE 0.22 μm (Teknokroma, Barcelona, Spain) immediately before use.

The working solutions at concentration level of 1 mg·mL<sup>-1</sup> of each standard were made in 0.1% ammonium formate in 10% acetonitrile (buffered at pH 5.5) and from this, the calibration standards dilutions between 1 mg·mL<sup>-1</sup> till 0.1 ng·mL<sup>-1</sup> were freshly prepared before each analytical series.

### Urine Sample Collection Method

All subjects were high school teenagers, from Timisoara, a major city from western part of Romania. The cohort consisted of 150 subjects with ages between 14 to 19 years, from which 27 subjects has declared to be nonsmokers (NS) and to live in an environment where smoking was not allowed, 76 passive smokers (PS) who declared to not smoke but lived with a smoker and 47 declared themselves to be active smokers (AS) who smoked daily at least three cigarettes. All subjects filled out a questionnaire concerning smoking habits. Subjects were instructed on how to collect urine samples when they arose in the morning. Smokers were asked not to have their first cigarette of the day before the samples were collected. Spontaneous urine samples were collected in sealable polyethylene bottles and stored in the deep-freezer at approx. -18 °C until sample processing for nicotine and cotinine determination was carried out. Urine creatinine was measured using standard methodology [35].

### Sample Preparation

Because urine is relatively protein-free a simple liquid-liquid extraction specimen preparation was preferred. An aliquot of urine (2 mL) was diluted with 1 mL phosphate buffer (0.2 M, pH 7.0) prior to vortex mixing or with 900 μL phosphate buffer and with 100 μL of standards solution (1 μg·mL<sup>-1</sup> of each of the analytes). Liquid-liquid extraction (LLE) was performed with 2.5 mL chloroform:propan-2-ol (95:5, v/v) for 10 min using a rotator unit [36].

After centrifugation for 5 min at 2500 rpm, the organic layer was collected and further evaporated to dryness under a gentle nitrogen stream at 50°C. The extract was reconstituted in 0.5 mL solution of 0.1% ammonium formate in 10% acetonitrile (buffered at pH 5.5) and filtered (0.22  $\mu\text{m}$  PTFE) prior to UPLC – MS injection. For samples having very high concentration of nicotine and cotinine, a dilution of the final extract was performed to fit into the calibration range of the standard curves. Calibration is performed using calibration standards which are prepared in pooled urine and are treated in the same manner as the samples to be analyzed.

### Chromatographic Separation and Detection

Separation was carried out on a Waters Acquity UPLC-MS system (Binary Solvent Manager, Xevo TQD equipped with an electrospray ionization interface). Nicotine and cotinine separation was achieved with a UPLC BEH Phenyl 1.7  $\mu\text{m}$  column (2.1 x 100 mm) using a gradient elution procedure. Mobile phase A consisted in 0.1% ammonium formate in acetonitrile and mobile phase B was 0.1% ammonium formate in 10% acetonitrile. The gradient profile was: 0 – 0.5 min, 100% B; 0.5 – 1 min, 95% B; 1 – 1.5 min, 0% B; 1.5 – 1.9, 0% B; 1.9 – 2 min, 100% B. The column temperature was set at 30°C. The analyses were run at a flow rate of 0.4 mL·min<sup>-1</sup>, and the sample volume injected was 5  $\mu\text{L}$ . The ESI parameters for Xevo TQD MS detector were fixed as follows: capillary voltage at 3 kV, cone voltage at 50 V, source temperature at 120 °C, desolvation temperature at 450 °C, and desolvation gas at 800 L·h<sup>-1</sup>. Nitrogen was used as the desolvation gas, and argon was employed as the collision gas. The detailed MS/MS detection parameters for each analyte are presented in Table 4 and were optimized by direct injection of a 1 ng·mL<sup>-1</sup> standard solution of each analyte into the detector at a flow rate of 10  $\mu\text{L}\cdot\text{min}^{-1}$ .

**Table 4.** Mass spectrometer parameters for nicotine and cotinine detection

Analyte	$R_t$ (min)	Precursor ion (m/z)	Quantification ion (m/z)	Collision potential (V)	Confirmation ion (m/z)	Collision potential (V)
Nicotine	0.63	163	132	25	120	30
Cotinine	0.72	177	146	20	98	35

Analyses were carried out in multiple reaction monitoring modes, using two specific transitions for each analyte and the detector was fixed at maximum Extended Dynamic Range with peak mass widths of 2 and 1.5 a.m.u. for the first and third quadruples, respectively. The dwell time for all transitions was 0.01 seconds.

According to the WADA Technical Document addressing to this particular topic identification criteria were defined [37]. The retention time ( $R_t$ ) tolerance window between the analyte and the Quality Control (QC) of the same batch was within the range  $\pm 2\%$ . For MS/MS experiments, three diagnostic ions are required, including the precursor ion and two fragmentation ions.

### **Method Validation**

Experiments were conducted following the recommendation of the bioanalytical method validation from the US Food and Drug Administration (FDA) and the guidelines on the 3<sup>rd</sup> American Association of Pharmaceutical Scientists (AAPS)/FDA Bioanalytical Workshop from 2006 [38, 39].

A pool of six urine samples from nicotine-abstinent individuals who had not been exposed to environmental smoke within the last 5 days was prepared to obtain negative urine for the validation process.

Accuracy was expressed as the ratio between the theoretical and the average measured concentration.

Repeatability was determined as the relative standard deviation (RSD) of the ratio of the intra-day standard deviation and the theoretical value at each concentration level [40]. Intermediate precision was determined as the RSD of the ratio of the inter-day standard deviation on the theoretical value at each concentration level [41].

The limit of quantification (LOQ) was expressed as the lowest QC sample with a good trueness, repeatability and intermediate precision fitting for purpose.

For recovery experiments of the selected compounds, blank samples ( $n = 6$ ) fortified with a known amount of analytes before the extraction step (10, 100 and 1000  $\text{ng}\cdot\text{mL}^{-1}$ ) were realized.

Carry-over was evaluated correspondingly by injecting a blank urine sample subsequently to the analysis of the highest calibrator. This experiment was conducted in triplicate.

### **ACKNOWLEDGMENTS**

This work was supported by the project 464 RoS-NET financed by the EU Instrument for Pre-Accession (IPA) funds, under the framework of the Romania-Republic of Serbia IPA Cross-border Cooperation Programme.

## REFERENCES

1. A.L. Wilson, L.K. Langley, J. Monley, T. Bauer, S. Rottunda, E. McFalls, C. Kovera, J. R. McCarten, *Pharmacol. Biochem. Behav.*, **1995**, *51*, 509-514.
2. L. Vlase, L. Filip, I. Mîndruțău, S. Leucuța, *Stud. Univ. Babes-Bol. Physica*, **2005**, *L(4B)*, 531-535.
3. N.L. Benowitz, *Annu. Rev. Pharmacol. Toxicol.*, **1996**, *36*, 597-613.
4. N.L. Benowitz, P. Jacob, 3rd, *Clin. Pharmacol. Ther.*, **1994**, *56*, 483-493.
5. S.L. Bramer, B. A. Kallungal, *Biomarkers*, **2003**, *8*, 187-203.
6. D. Yildiz, *Toxicol.*, **2004**, *43*, 619-632.
7. N.L. Benowitz, S.M. Hall, R.I. Herning, P. Jacob, 3rd, R.T. Jones, A.L. Osman, *N. Engl. J. Med.*, **1983**, *309*, 139-142.
8. D. Behera, R. Uppal, S. Majumdar, *Indian J. Med. Res.*, **2003**, *118*, 129-133.
9. M.N. Tzatzarakis, C.I. Vardavas, I. Terzi, M. Kavalakis, M. Kokkinakis, J. Liesivuori, A. M. Tsatsakis, *Hum. Exp. Toxicol.*, **2012**, *31*, 258-265.
10. T. Welerowicz, K. Śliwka, B. Buszewski, *Chromatographia*, **2007**, *66*, 63-70.
11. N.L. Benowitz, P. Jacob, 3rd, *Br. J. Clin. Pharmacol.*, **2001**, *51*, 53-59.
12. A. Pilotti, *Acta Physiol. Scand. Suppl.*, **1980**, *479*, 13-17.
13. C.I. Vardavas, M.N. Tzatzarakis, M. Plada, A. M. Tsatsakis, A. Papadaki, W. H. Saris, L. A. Moreno, A. G. Kafatos, *Hum. Exp. Toxicol.*, **2010**, *29*, 459-466.
14. P. Dhar, *J. Pharm. Biomed. Anal.*, **2004**, *35*, 155-168.
15. P. Gariti, D.I. Rosenthal, K. Lindell, J. Hansen-Flaschen, J. Shrager, C. Lipkin, A.I. Alterman, L.R. Kaiser, *Cancer Epidemiol. Biomarkers Prev.*, **2002**, *11*, 1123-1125.
16. U.E. Ziegler, J. Kauczok, U.A. Dietz, H.B. Reith, K. Schmidt, *Pharmacology*, **2004**, *72*, 254-259.
17. O.A. Ghosheh, D. Browne, T. Rogers, J. de Leon, L.P. Dwoskin, P.A. Crooks, *J. Pharm. Biomed. Anal.*, **2000**, *23*, 543-549.
18. B.H. Jung, B.C. Chung, S.J. Chung, M.H. Lee, C.K. Shim, *J. Pharm. Biomed. Anal.*, **1999**, *20*, 195-202.
19. C.M. López, A.H. Sassone, M.E. Rodriguez Girault, C.S. Lenzken, E.C. Villaamil Lepori, O.E. Roses, *J. Liq. Chromatogr. R. T.*, **2004**, *27*, 2371-2379.
20. R.M. Kauffman, A.K. Ferketich, D.M. Murray, P.E. Bellair, M.E. Wewers, *Nicotine Tob. Res.*, **2010**, *12*, 582-588.
21. A.N. Hoofnagle, T.J. Laha, P.M. Rainey, S.M. Sadrzadeh, *Am. J. Clin. Pathol.*, **2006**, *126*, 880-887.
22. G. Deaconu, "Study on the use of the pharmacologic therapy with bupropion on tobacco abstinence for smokers with high nicotine dependence", PhD thesis, The University of Medicine and Pharmacy of Craiova, Craiova, Romania, **2010**.
23. G.D. Byrd, K.M. Chang, J.M. Greene, J.D. deBethizy, *Drug Metab. Dispos.*, **1992**, *20*, 192-197.

QUANTIFICATION OF NICOTINE AND COTININE IN TEENAGER'S URINE

24. N.T. Lequang, G. Roussel, D. Roche, M.L. Miguères, J. Chretien, O.G. Ekindjian, *Pathol. Biol. (Paris)*, **1994**, *42*, 191-196.
25. I.M. Carey, D.G. Cook, D.P. Strachan, *Epidemiology*, **1999**, *10*, 319-326.
26. F. de Waard, J.M. Kemmeren, L.A. van Ginkel, A.A. Stolker, *Br. J. Cancer*, **1995**, *72*, 784-787.
27. D. Trout, J. Decker, C. Mueller, J.T. Bernert, J. Pirkle, *J. Occup. Environ. Med.*, **1998**, *40*, 270-276.
28. G. Apsehoff, H.M. Ashton, H. Friedman, N. Gerber, *Clin. Pharmacol. Ther.*, **1994**, *56*, 460-462.
29. M. Barrueco, R. Cordovilla, M.A. Hernandez-Mezquita, J. M. Gonzalez, J. de Castro, P. Rivas, J. L. Fernandez, F. Gomez, *Med. Clin. (Barc.)*, **1999**, *112*, 251-254.
30. G. Scherer, E. Richter, *Hum. Exp. Toxicol.*, **1997**, *16*, 449-459.
31. G.M. Lawson, R.D. Hurt, L.C. Dale, K.P. Offord, I.T. Croghan, D.R. Schroeder, N.S. Jiang, *J. Clin. Pharmacol.*, **1998**, *38*, 510-516.
32. S. Connor Gorber, S. Schofield-Hurwitz, J. Hardt, G. Levasseur, M. Tremblay, *Nicotine Tob. Res.*, **2009**, *11*, 12-24.
33. D.B. Kandel, C. Schaffran, P.C. Griesler, M.C. Hu, M. Davies, N. Benowitz, *Nicotine Tob. Res.*, **2006**, *8*, 525-537.
34. R.P. Ford, D.M. Tappin, P.J. Schluter, C.J. Wild, *J. Epidemiol. Community Health*, **1997**, *51*, 246-251.
35. M.A. Wall, J. Johnson, P. Jacob, N.L. Benowitz, *Am. J. Public Health*, **1988**, *78*, 699-701.
36. F. Marclay, M. Saugy, *J. Chromatogr. A*, **2010**, *1217*, 7528-7538.
37. WADA, "WADA Technical Document TD2003IDCR. Identification criteria for qualitative assays incorporating chromatography and mass spectrometry", World Anti-Doping Agency (WADA), Montreal (Canada), **2003**.
38. DHHS, FDA, CDER, CVM, "Guidance for Industry: Bioanalytical Method Validation", U.S. Department of Health and Human Services; Food and Drug Administration; Center for Drug Evaluation and Research (CDER); Center for Veterinary Medicine (CVM), Rockville, MD (USA), **2001**.
39. C.T. Viswanathan, S. Bansal, B. Booth, A.J. DeStefano, M.J. Rose, J. Sailstad, V.P. Shah, J.P. Skelly, P.G. Swann, R. Weiner, *Pharm. Res.*, **2007**, *24*, 1962-1973.
40. E. Rozet, A. Ceccato, C. Hubert, E. Ziemons, R. Oprean, S. Rudaz, B. Boulanger, P. Hubert, *J. Chromatogr. A*, **2007**, *1158*, 111-125.
41. S. Rudaz, S. Souverain, C. Schelling, M. Deleers, A. Klomp, A. Norris, T.L. Vu, B. Ariano, J.L. Veuthey, *Anal. Chim. Acta*, **2003**, *492*, 271-282.



# CORROSION BEHAVIOR OF Zn-Ni COATINGS ELECTRODEPOSITED IN PULSED CURRENT AND MAGNETIC FIELD ON DIFFERENT SUBSTRATES BY ELECTROCHEMICAL IMPEDANCE SPECTROSCOPY TECHNIQUES

MIHAIL CHIRA<sup>a,\*</sup>, HORATIU VERMESAN<sup>a</sup>, VASILE RUS<sup>a</sup>,  
ERNEST GRUNWALD<sup>b</sup>

**ABSTRACT.** The electrodeposition of Zn-Ni alloy was performed on different substrates and by different deposition techniques. The corrosion behavior was investigated in 1% NaCl electrolyte by potentiodynamic and electrochemical impedance spectroscopy. The corrosion resistance of the coatings depends on the deposition technique and substrate used.

**Keywords:** *electrodeposition, pulsed current, magnetic field, boron nitride, zinc-nickel, silicon dioxide*

## INTRODUCTION

Due to the environmental protection regulations and extension of the corrosion-resistance demands for products, the automotive, machine parts, electronic, electrochemical, computers and telecommunications industries have been constrained to invest in research and development of new technologies to improve the physical-mechanical properties and corrosion resistance of iron based products, coated with suitable alloys at low cost. [1]

Zn-Ni deposits in automotive industry, especially on the car body [2], show a good behavior to pitting corrosion caused by salt and dirt that remain for long time in the hidden areas of the profiled parts. Zn-Ni alloys that contain 10-15% Ni have higher corrosion resistance [3] compared to other coatings.

---

<sup>a</sup> *Technical University of Cluj-Napoca, Romania, Departament of Materials Engineering Technical University, 103-105, B.dul Muncii, 400641 Cluj-Napoca, Romania*

<sup>b</sup> *SC BETAK SA Bistrita, Romania*

\* *Corresponding author: mihai2706@yahoo.com*



Zn-Ni alloy coatings can be electroplated on high grade alloyed and unalloyed steels, with mechanical strength up to 2100 Nmm<sup>-2</sup>; however, their corrosion resistance depends on the environment.

Electroplated coatings have a micro and macroscopic structure depending on the electrolyte and the bath operating parameters. Unlike other electroplated metal coatings, Zn-Ni coatings are uniform, elastic, clean, aesthetically pleasant and obtainable at finely adjustable thickness, according to the environment in which they operate [3,4].

Physicochemical properties of Zn-Ni electrodeposited coatings depend mainly on the microstructure, phase composition and structural parameters [3].

Electrodeposition of Zn-Ni alloy is mostly studied for its corrosion protection properties. The study of the magnetic field effects on this electrodeposited alloy is interesting because of the absence of magnetic characteristics, unlike magnetic alloys such as Fe-Ni and Co-Fe [15].

Several phases are identified and from the experimental data it can be concluded that atomic nickel remains in the same ratio, the magnetic field acting as a leveling agent and leading to the formation of a uniform coating by reducing roughness and grain size. XRD diagrams show that the change on magnetic field alters the structure of the Zn deposit and the Zn-Ni alloy [6].

Pulsed current electrodeposition is an alternative technique for obtaining thin films and allows the incorporation of composite particles in high concentration and the control of the deposit (film composition, thickness up to atomic level, deposit uniformity and deposited layer roughness) by adjusting amplitude and pulse width.

Pulsed current electrodeposition influences the structure and morphology of nano-composites, the average size of crystallites due to current density and growth mechanism [7].

Electrochemical impedance spectroscopy (EIS) was used for the study of the corrosion behavior of deposited coatings, as it provides information regarding electrode capacity, charge transfer kinetics and reaction mechanism [16].

The aim of this work is to study the corrosion behavior of Zn-Ni coatings electrodeposited in pulsed current and magnetic field on different substrates and to compare this behavior with that of conventional electrodeposition.

## RESULTS AND DISCUSSIONS

### *Potentiodynamic polarization testing*

Figures 1, 2 and 3 show the potentiodynamic Tafel slopes.

The following notations will be used further on:

**Table 1.** Notations of the samples used in the paper.

Sample notation	Method of obtaining
<b>ZnNi</b>	the sample obtained by conventional electrodeposition of ZnNi alloy on steel substrate
<b>ZnNi + f</b>	the sample obtained by electrodeposition in pulsed current of ZnNi alloy on steel substrate
<b>ZnNi + bp</b>	the sample obtained by electrodeposition in a magnetic field of the ZnNi alloy on steel substrate
<b>ZnNi + bp + f</b>	the sample obtained by electrodeposition in pulsed current and in magnetic field of the ZnNi alloy on steel substrate
<b>Si + ZnNi</b>	the sample obtained by conventional electrodeposition of the ZnNi alloy on steel substrate / silicon dioxide
<b>Si + ZnNi + f</b>	the sample obtained by electrodeposition in pulsed current of ZnNi alloy on steel substrate / silicon dioxide
<b>Si + ZnNi + bp</b>	the sample obtained by electrodeposition in a magnetic field of the ZnNi alloy on steel substrate / silicon dioxide
<b>Si + ZnNi + bp + f</b>	the sample obtained by electrodeposition in pulsed current and in magnetic field of the ZnNi alloy on steel substrate / silicon dioxide
<b>Si + B + ZnNi</b>	the sample obtained by conventional electrodeposition of the ZnNi alloy on steel substrate / silicon dioxide / boron nitride
<b>Si + B + ZnNi + f</b>	the sample obtained by electrodeposition in pulsed current of ZnNi alloy on steel substrate / silicon dioxide / boron nitride
<b>Si + B + ZnNi + bp</b>	the sample obtained by electrodeposition in a magnetic field of the ZnNi alloy on steel substrate / silicon dioxide / boron nitride
<b>Si + B + ZnNi + bp + f</b>	the sample obtained by electrodeposition in pulsed current and in magnetic field of the ZnNi alloy on steel substrate / silicon dioxide / boron nitride

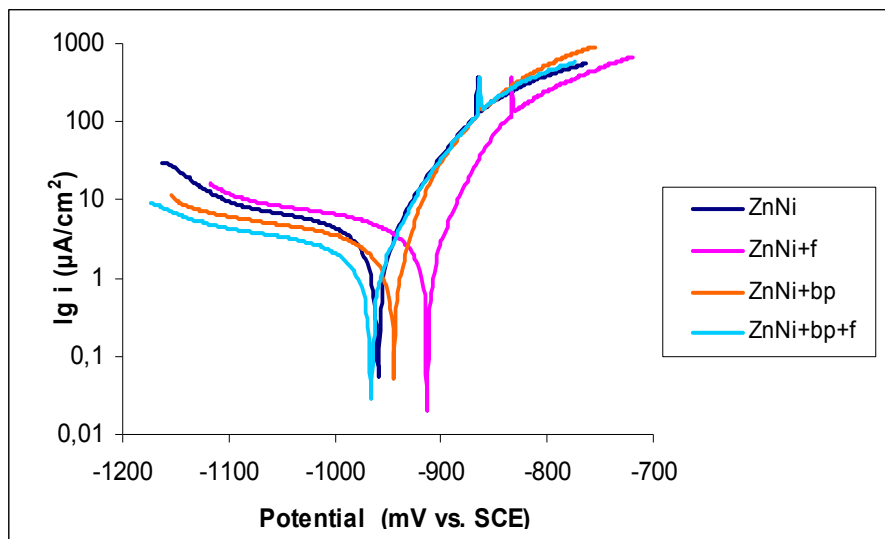


**Figure 1.** Polarization slopes for Zn-Ni coatings (steel substrate electroplated by the four methods) in 1% NaCl electrolyte.

Electrochemical parameters corresponding to Figure 1 are given in Table 2.

Due to the fact that the Zn-Ni alloy tends to passivate the cathodic slopes obtained in all experiments do not present a valid Tafel slope. As a result, the corrosion current density was determined using only the anodic slopes. This may generate a degree of imprecision vis-à-vis corrosion rate estimated in these conditions. However, it could perform a comparison between the behaviors of various layers. Parameters obtained as a result of the investigation of the corrosion tests are presented in Table 2.

**Table 2.** Corrosion rate of Zn-Ni coatings (steel substrate electroplated by the four methods) in 1% NaCl electrolyte at  $25 \pm 1^\circ\text{C}$ .

SAMPLE	$\beta_a$ [mV/decade]	$\beta_c$ [mV/decade]	$R_p$ [ $\text{k}\Omega\text{cm}^2$ ]	$E(i=0)$ [mV]	$I_{cor}$ [ $\mu\text{A}/\text{cm}^2$ ]
Zn-Ni	61.7	-416.9	5.60	-960	3.951
Zn-Ni + f	43.5	-192.3	5.97	-917.7	2.743
Zn-Ni + bp	44.0	-430.1	8.17	-950.2	2.504
Zn-Ni +bp+f	54.0	-385.2	11.24	-970.9	2.027

It was observed that Zn-Ni coatings electrodeposited in pulsed current and those in pulsed current combined with magnetic field, show lower current densities compared to the other samples. Also the anodic and cathodic Tafel slopes for the sample obtained by electrodeposition in pulsed current is lower than that of other samples. This finding indicates that the Zn-Ni coating electrodeposited in pulsed current has a higher activation energy corresponding to dissolution than that of other samples. In other words, it can be seen that the corrosion current density is two times lower compared to the one of the sample obtained by conventional electrodeposition.

The diagram and quantitative data for the samples obtained by electrodeposition of Zn-Ni coating on steel substrate / SiO<sub>2</sub> using the four coating techniques are shown in Figure 2 respectively Table 3.

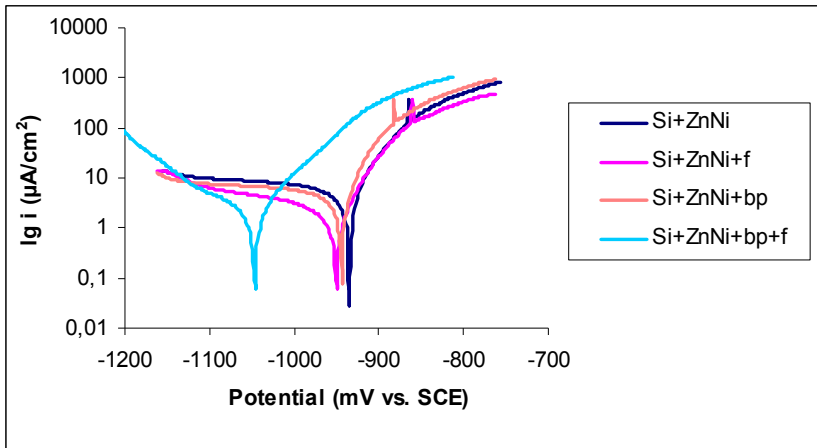


**Figure 2.** Polarization curves for Zn-Ni coatings (electroplated on steel substrate / SiO<sub>2</sub> using the four coating techniques) in 1% NaCl electrolyte.

**Table 3.** Corrosion rate of Zn-Ni coatings (electroplated on steel substrate / SiO<sub>2</sub> using the four coating techniques) in 1% NaCl electrolyte at 25 ± 1°C

SAMPLE	$\beta_a$ [mV/decade]	$\beta_c$ [mV/decade]	$R_p$ [kΩcm <sup>2</sup> ]	$E(i=0)$ [mV]	$I_{cor}$ [μA/cm <sup>2</sup> ]
Si+ Zn-Ni	51.5	-681.7	3.75	-940.8	5.971
Si+ Zn-Ni +f	41.1	-175.1	7.03	-955.7	1.625
Si+ Zn-Ni + bp	39.2	-556.6	4.25	-950	4.601
Si+ZnNi+bp+f	48.1	-105.8	7.78	-1051.6	1.501

Analyzing the Tafel slopes (figure 2) and data shown in Table 3 it can be seen that the current densities for the samples obtained by electrodeposition of Zn-Ni coatings in pulsed current and magnetic field, were lower compared to those obtained for other samples. Also the anodic and cathodic Tafel slopes

are lower than those of other samples. This finding shows that the Zn-Ni coating electrodeposited in pulsed current and magnetic field has a higher activation energy corresponding to the dissolution compared to the other samples. The corrosion current density of sample obtained in pulsed current and magnetic field is approximately seven times lower than that of the sample obtained by conventional electrodeposition, although corrosion potential has more negative values (thermodynamic corrosion possibility) yet the kinetic factors of the developing oxide film reduce the corrosion rate and  $i_{cor} = 1.501 \mu A/cm^2$ .

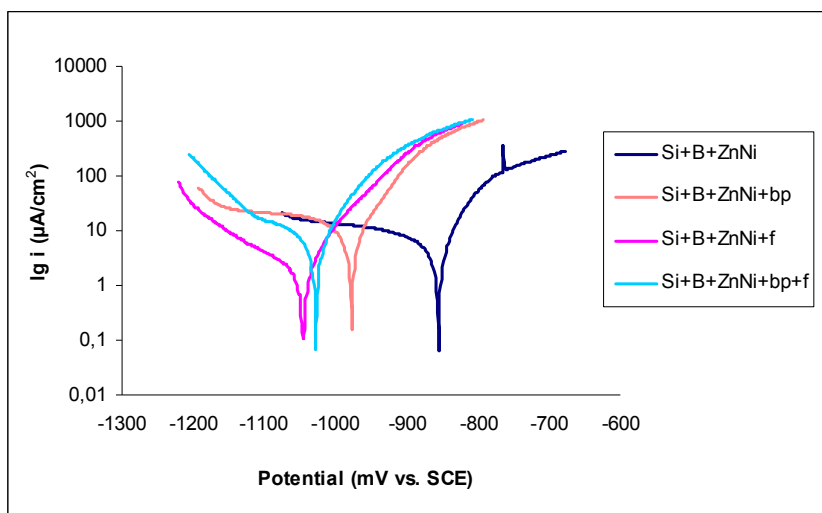


**Figure 3.** Polarization curves for Zn-Ni coatings (electrodeposited on steel substrate / SiO<sub>2</sub> / BN using the four coating techniques) in 1% NaCl electrolyte.

The diagram and quantitative data for the samples obtained by electrodeposition of Zn-Ni on steel substrate/SiO<sub>2</sub>/BN using the four coating techniques are shown in Figure 3 and Table 4, respectively.

**Table 4.** Corrosion rate of Zn-Ni coatings (electroplated on steel substrate / SiO<sub>2</sub> / BN using the four coating techniques) in 1% NaCl electrolyte at 25 ± 1°C

SAMPLE	$\beta_a$ [mV/decade]	$\beta_c$ [mV/decade]	$R_p$ [kΩcm <sup>2</sup> ]	$E(i=0)$ [mV]	$I_{cor}$ [μA/cm <sup>2</sup> ]
Si+B+Zn-Ni	62.3	-427.8	3.42	-860.7	6.749
Si+B+Zn-Ni+f	56.3	-157.8	8.04	-1050.7	1.886
Si+B+Zn-Ni+bp	54.2	-117.7	1.94	-982.2	6.313
Si+B+Zn-Ni+bp+f	52.2	-114.0	2.58	-1032.5	4.940

As seen in Table 4, the sample obtained by electrodeposition of Zn-Ni in pulsed current (Si + B + Zn-Ni + f) shows a lower current density compared to the other samples, and the anodic and cathode Tafel slopes are lower compared to the samples obtained by conventional electrodeposition. This finding indicates that Zn-Ni coating electrodeposited in pulsed current shows a higher activation energy corresponding to dissolution compared to that of the other samples. Corrosion current density for the sample obtained in pulsed current is about 2.6 times smaller than that of the sample obtained by conventional electrodeposition.

By grouping in Table 5 the best data results in terms of corrosion resistance for the three sets of samples, certain conclusions can be drawn.

**Table 5.** Corrosion rate of Zn-Ni coatings (electroplated on steel / SiO<sub>2</sub> and on steel / SiO<sub>2</sub> / BN substrates using the four coating techniques) in 1% NaCl electrolyte at 25 ± 1°C

SAMPLE	$\beta_a$ [mV/decade]	$\beta_c$ [mV/decade]	$R_p$ [kΩcm <sup>2</sup> ]	E(i=0) [mV]	$I_{cor}$ [μA/cm <sup>2</sup> ]
Zn-Ni	61.7	-416.9	5.60	-964.5	3.951
Si+ ZnNi+bp+f	48.1	-105.8	7.78	-1051.6	1.501
Si+B+Zn-Ni+f	56.3	-157.8	8.04	-1050.7	1.886

The data in Table 5 show that the corrosion current density of the (Si + Zn-Ni + bp + f) sample is lower compared to the (Si + B + Zn-Ni + f) sample, which in turn is lower compared to the Zn-Ni sample. Also the anodic and cathodic Tafel slopes for the (Si + Zn-Ni + bp + f) sample are smaller compared to the other samples, which indicates that the (Si + Zn-Ni + bp + f) sample has higher zinc dissolution activation energy, and thus has a better corrosion resistance. Although the polarization resistances for the three samples have similar value, the corrosion rates are different. It can be concluded that the corrosion resistance of the Zn-Ni coatings studied depend on the electrodeposition technique used, and on the substrate composition, the sample obtained by electrodeposition of Zn-Ni alloy on the steel substrate/SiO<sub>2</sub> in pulsed current and magnetic field showing the best corrosion resistance.

#### *Electrochemical impedance spectroscopy testing*

Nyquist diagrams for the samples obtained by electrodeposition of Zn-Ni alloy on steel substrate, on steel/SiO<sub>2</sub>, and on steel/SiO<sub>2</sub>/BN are shown in Figure 4, 5 and 6.

The shapes of the Nyquist impedance spectra for the three samples are similar and are characterized by a loop at high frequencies, followed by an ascending line at low frequencies. This shows that the corrosion process is controlled by both the charge transfer and the diffusion; the semicircular loops indicating the charge transfer.

The semicircles diameter is associated with the coating polarization resistance  $R_p$  and corresponds with the corrosion rate.

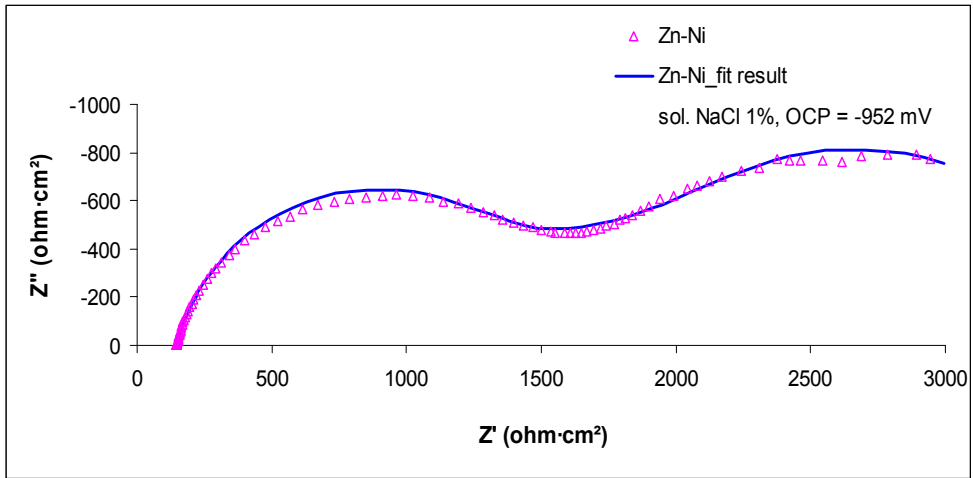


**Figure 4.** Nyquist diagrams for Zn-Ni alloy.

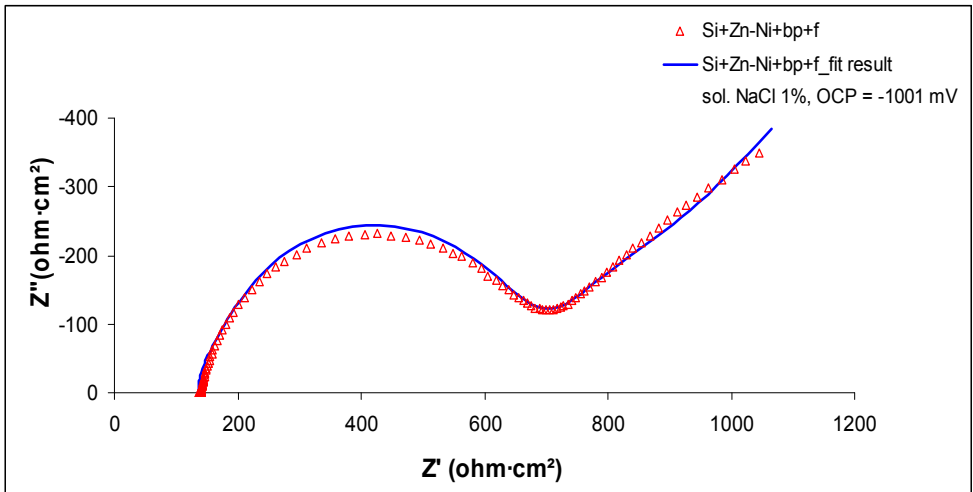


**Figure 5.** Nyquist diagrams for Zn-Ni alloy on steel/SiO<sub>2</sub>.

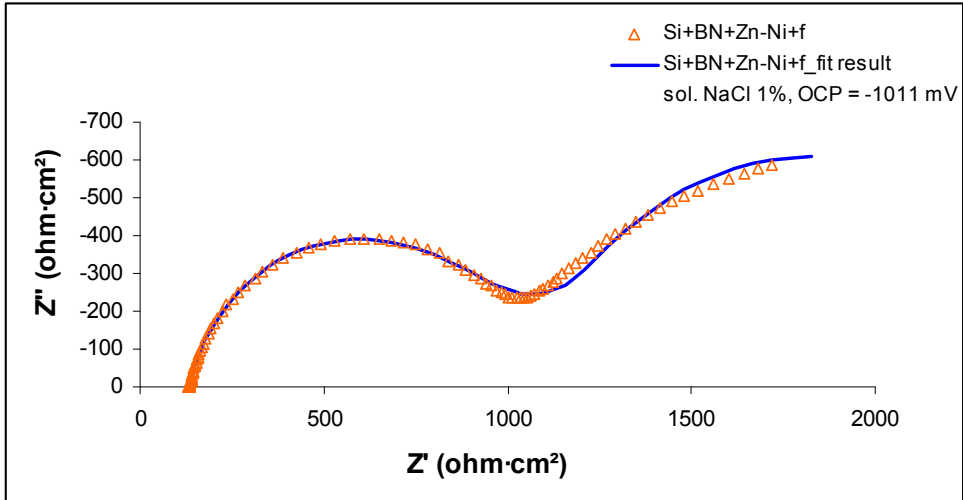
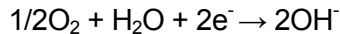


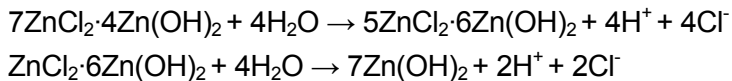
**Figure 6.** Nyquist diagrams for Zn-Ni alloy on steel/SiO<sub>2</sub>/BN.

The correct interpretation of the electrochemical impedance spectra and the finding of a satisfactory equivalent circuit depend on a better understanding of corrosion phenomena at the sample surface. According to Suzuki [9] and Chung et al. [10], one of the cathode reactions on the zinc deposited sample surface in chloride ions environment, at intervals higher than -1.3 V (SCE) is the reduction of dissolved oxygen:



This reaction increases the local pH at the surface of the zinc coating. The hydroxide film is the basis for further growth of corrosion products [10]. Corrosion products may consist of compounds such as ZnO, Zn(OH)<sub>2</sub>, ZnCO<sub>3</sub>, Zn<sub>5</sub>(OH)<sub>6</sub>(CO<sub>3</sub>)<sub>2</sub> and Zn<sub>5</sub>(OH)<sub>8</sub>Cl<sub>2</sub> • H<sub>2</sub>O and perhaps a mixture of these compounds [11]. Branco et al. [11] stated that due to their low solubility, the zinc corrosion products precipitate on the surface exposed to the action of sodium chloride solution. The film formed on the surface is not ideal and is not a completely compact layer, because the compactness of the film and the protective properties depend on the composition and formation conditions [9]. The pores in the corrosion products have influence on the electrochemical response of the system at low frequencies [9]. According to Yadav et al. [13] the stability of zinc corrosion products in chloride solutions depends on the concentration of Cl<sup>-</sup> and H<sup>+</sup> ions as well as on the corrosion products, such as: Zn(OH)<sub>2</sub>, ZnCl<sub>2</sub> • 6Zn(OH)<sub>2</sub> and ZnCl<sub>2</sub> • 4Zn(OH)<sub>2</sub> formed in chloride solutions [9,13]. The chemical reactions of this product are:





These two reactions indicate that the chemical stability of corrosion products becomes larger with increasing concentrations of  $\text{Cl}^-$  and  $\text{H}^+$  ions. According to Yadav et al. [13] the corrosion product  $\text{ZnCl}_2 \cdot 4\text{Zn(OH)}_2$  formed at low pH has a porous structure. This porous corrosion product appears not to act as a barrier layer for  $\text{O}_2$  and  $\text{Zn}^{2+}$  transport; thus corrosion continues. On the other hand, according to Giridhar and van Ooij [14] the increasing of the pH determines the passivation of the surface.

The equivalent circuit for the electrochemical impedance spectra corresponding to the samples steel/Zn-Ni, steel/ $\text{SiO}_2$ /Zn-Ni obtained in pulsed current and in magnetic field, as well as for steel/ $\text{SiO}_2$ /BN/Zn-Ni sample obtained in pulsed current, are shown in Figure 7. The equivalent circuit was mapped using ZView program.

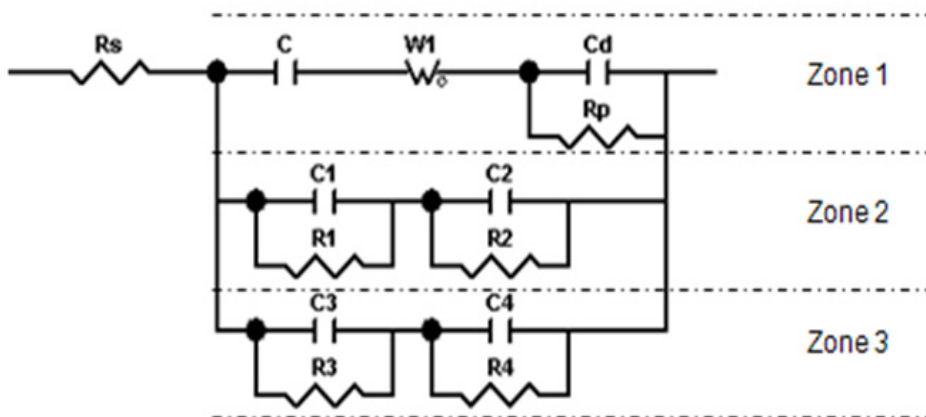


**Figure 7.** Equivalent circuit for Nyquist diagrams interpretation

On the surface of the studied sample there are three zones corresponding to the three levels (randomly distributed on the surface of the sample), showing different behaviors (figure 7).

Using the relation for the capacity of the plan capacitor ( $C = \epsilon_0 \epsilon_r S/d$ ) and the corresponding Warburg impedance relations ( $W-T = L^2/D$ ) the thickness of the double electric layer ( $d_d$ ), the thickness of the oxide layer ( $d_1 + d_2$  and  $d_3 + d_4$ ) and the length of diffusion ( $L_1$ ) were determined as shown in Table 6.

**Table 6.** The double electric layer ( $d_d$ ) diffusion length ( $L_1$ ), the oxide layer formed in the second zone ( $d_1$ ) thickness, the distance between the "fittings" of the capacitor formed by water molecules on oxide in the second zone ( $d_2$ ), the oxide layer thickness formed in the third zone ( $d_3$ ) and the distance between the "fittings" of the capacitor formed by the water molecules on oxide in the third zone ( $d_4$ ).

Sample	$d_d$ [Å]	$L_1$ [Å]	$d_1$ [Å]	$d_2$ [Å]	$d_3$ [Å]	$d_4$ [Å]
Zn-Ni	39.93	206	3	0.82	9.2	0.19
Si+ZnNi+bp+f	21.77	150	1.32	0.82	9.2	7.3
Si+B+ZnNi+f	41.12	651	3	0.82	9.2	0.19

From Table 6 it is observed that the thickness of the oxide layer ( $d_3 + d_4$ ) formed on the sample Si + ZnNi + bp + f is approximately two times higher than the thickness of the oxide layer formed on the other samples.

**Table 7.** The values for the equivalent circuit elements (figure 7).

Equivalent circuit elements	Sample		
	Zn-Ni	Si+ZnNi+bp+f	Si+B+ZnNi+f
$R_s$ [ $\Omega\text{cm}^2$ ]	39.33	35.41	35.83
$R_p$ [ $\Omega\text{cm}^2$ ]	461.97	104.4	208.8
$C_d$ [ $\mu\text{F}/\text{cm}^2$ ]	17.88	32.79	17.36
$R_1$ [ $\Omega\text{cm}^2$ ]	991.8	652.5	730.8
$C_1$ [ $\mu\text{F}/\text{cm}^2$ ]	8.81	20	8.81
$R_2$ [ $\Omega\text{cm}^2$ ]	1174.5	783	1174.5
$C_2$ [ $\mu\text{F}/\text{cm}^2$ ]	862.4	862.4	862.4
$R_3$ [ $\Omega\text{cm}^2$ ]	1174.5	913.5	704.7
$C_3$ [ $\mu\text{F}/\text{cm}^2$ ]	2.87	2.87	2.87
$R_4$ [ $\Omega\text{cm}^2$ ]	313.2	208.8	261
$C_4$ [ $\mu\text{F}/\text{cm}^2$ ]	3620.6	3.62	3620.6

In Figure 8 is shown the schematic representation of the formations of the various oxide layers according to equivalent circuits presented in Figure 7.

From the data shown in tables 6 and 7 it can be assumed that for the sample obtained by conventional electrodeposition of Zn-Ni alloy on steel substrate, water molecules are adsorbed in the first zone on the surface (figure 8 a)) between the surface of the metal and the Helmholtz plane, which determines (from an electric point of view) the presence of a capacitance C. In the same zone, the diffusion of  $\text{Zn}^{2+}$  ions in the electrolyte is characterized (from electric point of view) by Warburg impedance ( $W_1$ ). The presence of  $\text{Zn}^{2+}$

ions in the electrolyte, near the surface, at a ( $d_d$ ) distance, causes the formation of a capacitance ( $C_d$ ) of the double electric layer and a polarization resistance ( $R_p$ ). In the second zone (Figure 8 a) a thin oxide layer is formed, with a ( $d_1$ ) thickness, a ( $C_1$ ) capacitance and a ( $R_1$ ) resistance, and on this oxide layer a large numbers of water molecules are present (electric dipoles) that cause a ( $C_2$ ) capacitance and a ( $R_2$ ) polarization resistance. It was assumed that the dipoles concentration is high due to the high value of the ( $R_2$ ) resistance. In the third zone (Figure 8) an oxide layer ( $d_3$ ) is formed, thicker than in zone 2, having a ( $C_3$ ) capacitance and a ( $R_3$ ) resistance, followed by a dipolar layer of water molecules of ( $C_4$ ) capacitance that causes a ( $R_4$ ) polarization resistance.

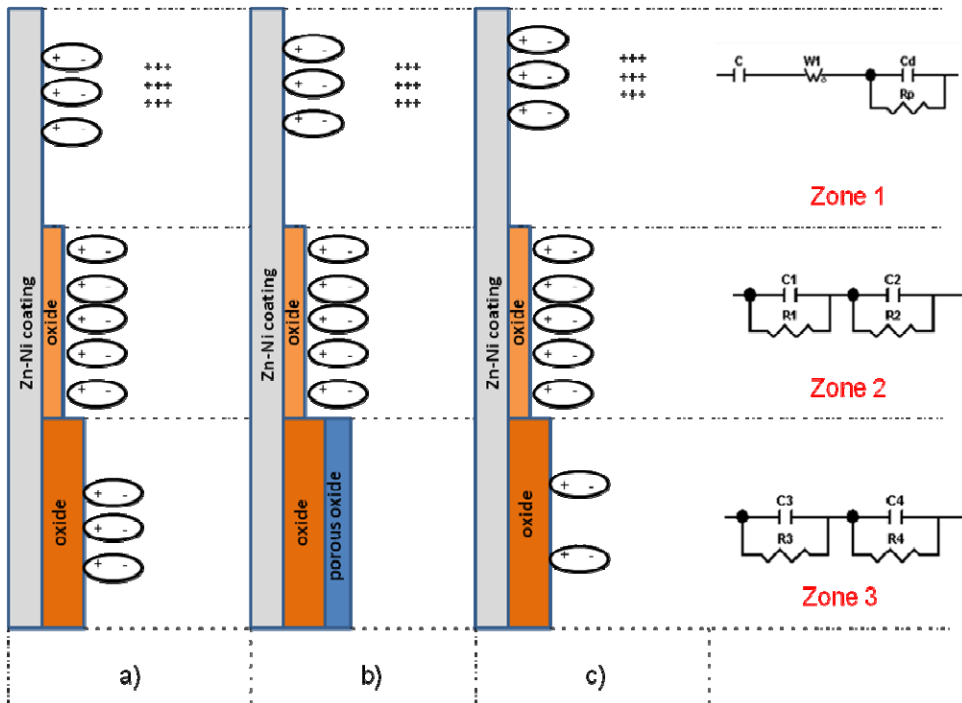


**Figure 8.** Schematic representation of the three zones and of the corresponding equivalent circuit for: a) the sample obtained by conventional electrodeposition of Zn-Ni alloy on steel substrate, b) the sample obtained by electrodeposition of Zn-Ni alloy in pulsed current and magnetic field on steel / silicon dioxide substrate (sample noted with Si + Zn-Ni + bp + f ), c) the sample obtained by electrodeposition of Zn-Ni alloy in pulsed current on steel / silicon dioxide / boron nitride substrate (sample noted Si + B + Zn-Ni + f ).

By analyzing the data for the sample obtained by electrodeposition of Zn-Ni alloy in pulsed current and magnetic field on steel / silicon dioxide substrate, shown in Tables 6 and 7, we can observe that the polarization resistance is lower than the polarization resistance of the sample obtained by conventional electrodeposition, and the thickness of the oxide layer formed in the second zone is lower (Figure 8 b)). In the third zone (Figure 8 b)) a ( $d_3$ ) thickness oxide layer is formed on the surface, with a ( $R_3$ ) resistance, and on this layer, a ( $d_4$ ) thickness oxide layer is formed with a resistance three times lower than that of the base layer, which lead us to assume that this ( $d_4$ ) thickness layer is porous.

From the data shown in tables 6 and 7, it can be observed that for the sample obtained by electrodeposition of Zn-Ni alloy in pulsed current on steel / silicon dioxide / boron nitride substrate, the polarization resistance is higher than that of the (Si + Zn-Ni + bp + f) sample, but is lower compared to that of the conventional electrodeposition. Generally, the sample obtained by electrodeposition of Zn-Ni alloy in pulsed current on steel / silicon dioxide / boron nitride substrate has a similar behavior with that of the sample obtained by conventional electrodeposition, but in the third zone (Figure 8 c)) it is observed that the ( $R_3$ ) and ( $R_4$ ) resistances are lower, which lead us to assume that the oxide layer formed is porous and the density of the dipoles on the surface is smaller.

The circuit formed by the C,  $W_1$ ,  $C_d$ ,  $R_p$  circuit elements, characterizes the corrosion active zones, the capacitance of the double electric layer, the polarization resistance and the diffusion. The circuit formed by the  $C_1$ ,  $R_1$ ,  $C_2$ ,  $R_2$  circuit elements, characterizes the zones where an oxide film is formed, followed by corrosion products zone. The circuit formed by the  $C_3$ ,  $R_3$ ,  $C_4$ ,  $R_4$  circuit elements characterizes the zones where an oxide layer is formed, followed by the formation of a porous oxide layer. The  $C_1$ ,  $R_1$ ,  $C_3$ ,  $R_3$  circuit elements are modeling the systems response at high frequencies, and the  $C_2$ ,  $R_2$ ,  $C_4$ ,  $R_4$  circuit elements are modeling the systems response at low frequencies

## CONCLUSIONS

1. By comparing the results of potentiodynamic measurements and interpretation of Nyquist diagrams it can be concluded that the Zn-Ni alloy electrodeposited on steel / silicon dioxide ( $\text{SiO}_2$ ) substrate in pulsed current and magnetic field and on steel / silicon dioxide ( $\text{SiO}_2$ ) / boron nitride (BN) substrate in pulsed current show a better corrosion resistance compared to that of conventional electrodeposition on steel substrate.

2. According to the experimental data obtained for the three sets of samples it was found that for the same substrate, the samples corrosion resistance depends on the coating technique used. Also, for the same electrodeposition technique used, but for different substrates, the corrosion resistance is different. Thus, the corrosion resistance depends on the substrate and the coating technique used.

3. By comparing the results of potentiodynamic measurements and interpretation of Nyquist diagrams it can be concluded that the electrodeposited Zn-Ni alloy on steel / silicon dioxide ( $\text{SiO}_2$ ) substrate in pulsed current and magnetic field shows the best protection against corrosion .

## EXPERIMENTAL SECTION

### *Obtaining the samples*

Experiments were carried out in the Corrosion and Corrosion Protection Laboratory of Technical University of Cluj-Napoca, Romania.

Substrate used for electrochemical deposition was commercially available rolled carbon steel sheet from which  $16 \text{ cm}^2$  square samples were cut. All parts have been grinded with 1500 grit sandpaper. After grinding the pieces were degreased in 10% NaOH solution, washed, pickled in HCl solution (15%) and washed again.

To improve corrosion resistance, an intermediate layer was attempted which would have similar behavior with a diode so that the corrosion current would be as close to zero as possible.

For this purpose eight samples were immersed in sodium silicate ( $\text{Na}_2\text{SiO}_3$ ) for 2 minutes, then 3 minutes in hydrochloric acid HCl (15%) solution in order to obtain a silicon dioxide ( $\text{SiO}_2$ ) layer on the steel surface.

After being washed, four of the eight samples were covered with a boron nitride (BN) layer by electrodeposition, in order to obtain trivalent boron doped silicon. Electrochemical deposition of boron nitride was done with the sample mounted as anode and stainless steel was used as cathode [8].

In the end, the following substrates were obtained: steel (S235JR) steel / silicon dioxide ( $\text{SiO}_2$ ) and steel / silicon dioxide ( $\text{SiO}_2$ ) / boron nitride (BN). On these substrates a coating of ZnNi was electrodeposited by four methods: 1) conventional electrodeposition (Zn-Ni), 2) pulsed current electrodeposition (Zn-Ni + f), 3) electrodeposition in magnetic field with field lines parallel with the sample surface (Zn-Ni + bp), and 4) electrodeposition in pulsed current and magnetic field with field lines parallel with the sample surface (Zn-Ni + bp + f).

Electrolyte composition for Zn-Ni electrodeposition and for boron nitride (BN) is given in Tables 8 and 9.

**Table 8.** Bath composition for the Zn-Ni electrodeposition

Zincat	135,2 ml/l
NaOH	98 g/l
Performa Ni	12 ml/l
Performa BASE	6 ml/l
Performa BASE	94 ml/l
Performa BRI	2 ml/l
Performa ADD	0,7 ml/l
Current density	1,5 A/dm <sup>2</sup>
Temperature	20-25 °C
Anodes	Nickel
Linear stirring of the cathode rod	10 oscillations/min

**Table 9.** Bath composition for the electrodeposition of boron nitride (BN)

H <sub>3</sub> BO <sub>3</sub>	100 g/l
HCON(CH <sub>2</sub> ) <sub>2</sub>	100 g/l
Current density	1,5 mA/cm <sup>2</sup>
Temperature	20-25 °C
Cathode	Stainless Steel
Distance anode - cathode	10 mm

Chemicals: Performa Ni, Performa BASE, Performa BRI and Performa ADD were purchased from the company COVENTYA S.A.S, France.

The electrodeposition in pulsed current was performed using a rectangular pulse generator with 25 ms pulse duration.

The magnetic field in which the samples were placed has a value of 70 mT and has the field lines parallel to the sample surface.

### *Corrosion testing*

#### *Potentiodynamic polarization testing*

Potentiodynamic polarization tests were performed in order to determine the corrosion rate of Zn-Ni coatings. Corrosion tests were carried out using a Voltalab 10 potentiostat. The electrochemical cell consists of reference electrode (saturated calomel) platinum auxiliary electrode and work electrode which is the tested sample that has an area of 0.785 cm<sup>2</sup>. The anode Tafel slope ( $\beta_a$ ), cathode slope ( $\beta_c$ ) and current density were determined at a potential scan rate of 10 mV/min, from +200 mV to -200 mV, against the open circuit potential.

#### *Electrochemical impedance spectroscopy testing*

The samples were placed in 1% NaCl solution during the electrochemical impedance spectroscopy (EIS) testing. The electrochemical cell consists of reference electrode (saturated calomel), platinum auxiliary electrode and the work electrode which is the tested

sample that has an area of 0.785 cm<sup>2</sup>. Impedance data were obtained at open circuit potential using a Voltalab 10 potentiostat equipped with a frequency response analyzer. Impedance measurements were performed in a frequency range between 100 kHz and 1 mHz using a sinusoidal voltage with amplitude of 10 mV. Impedance spectra were analyzed using the attached software of the potentiostat.

## ACKNOWLEDGMENT

This paper was supported by the project "Improvement of the doctoral studies quality in engineering science for development of the knowledge based society-QDOC" contract no. POSDRU/107/1.5/S/78534, project co-funded by the European Social Fund through the Sectorial Operational Program Human Resources 2007-2013.

## REFERENCES

1. E. Popesco, R. Tournier, *Zincarea electrolitică practică*, Editura MEDRO, București, **1998**.
2. Hwa Young Lee, Sung Gyu Kim, *Surface and Coatings Technology*, **2000**, 135, 69.
3. G. Barcelo, *Journal of Applied Electrochemistry*, **1998**, 28,1113.
4. Brenner, *Electrodeposition of Alloys: Principles and Practice*, Vols. I and II, Academic Press, New York, **1963**.
5. E. Gomez, *Metal Finishing*, **1991**, 6, 44.
6. S. Couchane, J. Douglade, J. Amblard, R. Rehamnia, J.-P. Chopart, Metal field effects on Zn-Ni electrodeposition, the 15<sup>th</sup>Riga and 6<sup>th</sup> PAMIR Conference on Fundamental and Applied MHD. **2005**.
7. T. Frade, V. Bouzon, A. Gomes, M.I. Pereira da Silva, *Surface and Coatings Technology*, **2010**, 204, 3592.
8. M. Pal Chowdhurya, B.R. Chakraborty, A.K. Pal, *Materials Letters*, **2004**, 58, 3362 Suzuki, *Corrosion Science*, **1985**, 25, 1029.
9. S.C. Chunga, J.R. Chengb, S.D. Chioub, H.C. Shiha, *Corrosion Science*, **2000**, 42, 1249.
10. V. Barranco, S. Feliu Jr., S. Feliu, *Corrosion Science*, **2004**, 46, 2203.
11. R.G. Kelly, J.R. Scully, D.W. Shoesmith, R.G. Buchheit, *Electrochemical Techniques in Corrosion Science and Engineering*, first ed., Marcel Dekker, Inc., New York, **2003**, pp. 205–255.
12. A.P. Yadav, A. Nishikata, T. Tsuru, *Corrosion Science*, **2004**, 46, 361.
13. Giridhar, W.J. van Ooij, *Surface & Coatings Technology*, **1992**, 53, 35.
14. V.R. Rao, V. Kasturi, H. Chitharanjan, *Journal of Magnetism and Magnetic Materials*, **2013**, 345, 48.
15. K.R. Sriraman, S. Brahimi, J.A. Szpunar, J.H. Osborne, S. Yue, *Electrochimica Acta*, **2013**, 105, 314.

## EXPERIMENTAL AND THEORETICAL INVESTIGATIONS ON COORDINATION COMPOUNDS OF ACETAZOLAMIDE

EDIT FORIZS<sup>a,\*</sup>, ATTILA-ZSOLT KUN<sup>a</sup>, EMESE-ZSUZSÁNNA BOD<sup>a</sup>,  
FIRUȚA GOGA<sup>a</sup>, JENŐ BÓDIS<sup>a</sup>

**ABSTRACT.** Syntheses, characterization and molecular modeling of mixed-ligand complexes of copper(II) and cobalt(II) with monodeprotonated acetazolamide, N-(5-sulfamoyl-1,3,4-thiadiazol-2-yl)acetamide and N,N-chelating ligands (1,2-propanediamine and 1,2-ethanediamine) are described. The structures of the complexes were optimized by PM6, PM6-DH+ and PM7 semiempirical calculations.

**Keywords:** Acetazolamide, Cu(II) and Co(II) complexes, N,N-chelating ligands, PM6, PM6-DH+, PM7

### INTRODUCTION

Transition metal complexes of sulfonamide derivatives with 1,3,4-thiadiazole ring have attracted considerable attention due to their pharmacological and biological activity [1,2]. According to previous investigations, copper complexes of sulfonamide derivatives are more active than their free ligands [3]. Acetazolamide, N-(5-sulfamoyl-1,3,4-thiadiazol-2-yl)acetamide (H<sub>2</sub>acm) is an inhibitor of carbonic anhydrase, an important diuretic drug and is also used for the treatment of glaucoma, epilepsy and to prevent altitude sickness [4].

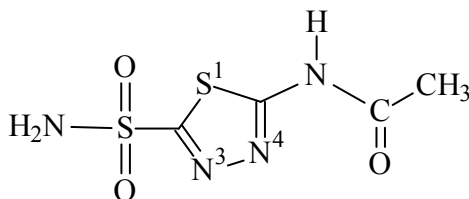


**Figure 1.** Acetazolamide.

<sup>a</sup> Faculty of Chemistry and Chemical Engineering, Babeş-Bolyai University, RO-400028 Cluj-Napoca, Romania, \* eforizs@chem.ubbcluj.ro



Acetazolamide contains several potential binding sites [3-9]. According to previous studies, acetazolamide ligand can act in monodeprotonated form [7] or in twice deprotonated form as dianionic ligand [8].

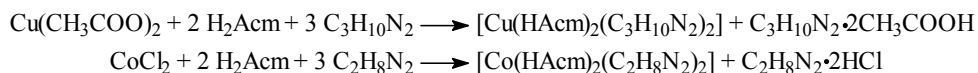
In monoanionic form acetazolamide can coordinate as monodentate ligand either by the N(4) atom of the 1,3,4-thiadiazole ring [7] or through the sulfonamido N atom [4, 5], depending where the deprotonation occurred, but can coordinate also through one of the O atoms of sulfonamido group [7]. However, according to other authors [9] can behave as bidentate ligand coordinating through the N(3) atom of thiadiazole ring and the N atom of sulfonamide group forming a chelate with the metal ion.

Deprotonation of both acetamido and sulfonamido groups leads to a dianion ( $\text{acm}^{2-}$ ). The twice deprotonated acetazolamide can coordinate the metal involving both the bridging and the chelating binding mode observed in a dinuclear copper(II) complex [8].

Continuing our studies on coordination behavior of biological active ligands [10,11], we synthesized two new mixed-ligand complexes containing acetazolamide  $[\text{Cu}(\text{Hacm})_2(\text{pda})_2] \cdot 2\text{H}_2\text{O}$  (**1**) and  $[\text{Co}(\text{Hacm})_2(\text{en})_2] \cdot 4\text{H}_2\text{O}$  (**2**) where pda: 1,2-propanediamine and en: 1,2-ethanediamine are commonly used as bidentate ligands. The complexes were investigated by elemental analyses, FTIR spectroscopy, thermal analysis and by molecular modeling using semiempirical calculations.

## RESULTS AND DISCUSSION

The mixed-ligand complexes of Cu(II) and Co(II) with N,N-chelating diamines were prepared by mixing diamine containing aqueous solutions of metal salt and acetazolamide:



**FTIR spectra.** The FTIR spectra of the complexes (Figure 2) indicate strong bands at 3347 and 3268  $\text{cm}^{-1}$  for **1** and 3288 and 3221  $\text{cm}^{-1}$  for **2**, which can be assigned to  $\nu(\text{NH}_2)$  stretching vibrations. In both spectra of the complexes the symmetric and antisymmetric stretching vibration bands of the  $\text{NH}_2$  groups of the diamine ligands and the sulfonamide moiety of the acetazolamide are overlapped. The strong  $\nu(\text{C}=\text{N})$  band of the thiadiazole ring observed at 1547  $\text{cm}^{-1}$  in case of the free ligand is shifted toward lower wave numbers in the complexes (1517  $\text{cm}^{-1}$  for **1** and 1431  $\text{cm}^{-1}$  for **2**). The  $\nu(\text{NH})$  bands at 3092  $\text{cm}^{-1}$  of the free ligand disappear in the complexes

due to the deprotonation of the acetamido nitrogen. The shift of  $\nu(\text{C}=\text{O})$  stretching vibration band ( $1680\text{ cm}^{-1}$  in free ligand) to lower values ( $1603\text{ cm}^{-1}$  for both complexes) also is an evidence for the deprotonation of acetamide nitrogen atoms. The stretching vibration bands of  $\text{SO}_2$  group ( $1369$  and  $1174\text{ cm}^{-1}$  assigned to  $\nu_{\text{as}}(\text{SO}_2)$  and  $\nu_{\text{s}}(\text{SO}_2)$  in the free acetazolamide ligand) are shifted to lower wave numbers in both IR spectra ( $1333$  and  $1164\text{ cm}^{-1}$  for **1**;  $1329$  and  $1148\text{ cm}^{-1}$  for **2**). The  $\nu(\text{CH}_2)$  bands of 1,2-propanediamine are observed at  $2975\text{ cm}^{-1}$ . The aliphatic  $\nu(\text{CH}_2)$  band of the diamine is shown at  $2942\text{ cm}^{-1}$  for complex **2**.

The broad bands of complexes recorded at  $3600\text{--}3400\text{ cm}^{-1}$  may be assigned to different hydrogen bonds (Fig. 2).

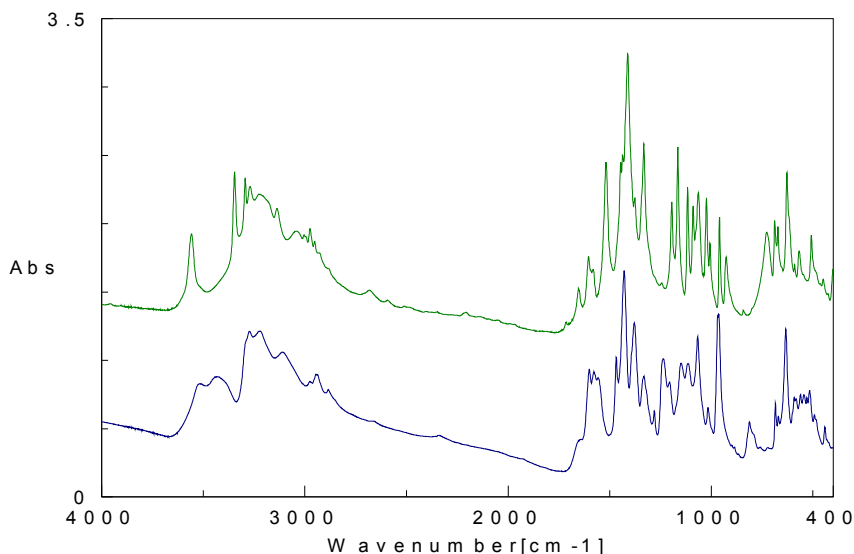


**Figure 2.** FTIR spectra of  $[\text{Cu}(\text{Hacm})_2(\text{pda})_2]\cdot 2\text{H}_2\text{O}$  (upper spectrum, shifted with +1) and  $[\text{Co}(\text{Hacm})_2(\text{en})_2]\cdot 4\text{H}_2\text{O}$  (lower spectrum).

**Thermal analysis.** The thermogravimetric curve of complex **1** indicates a stepwise decomposition. In the first well defined endothermic step, two molecules of water are eliminated in the temperature range of  $100\text{--}153\text{ }^\circ\text{C}$  (experimental weight loss 6.2%, calculated 5.2%). The second step, which occurs between  $153\text{--}388\text{ }^\circ\text{C}$ , corresponds to the elimination of two molecules of 1,2-propanediamine and a molecule of acetazolamide (experimental weight loss 40.2%, calculated 41.1%). The last decomposition step is exothermic due to the pyrolysis of organic moieties, the final residue is  $\text{CuO}$  (Fig.3, **1**).

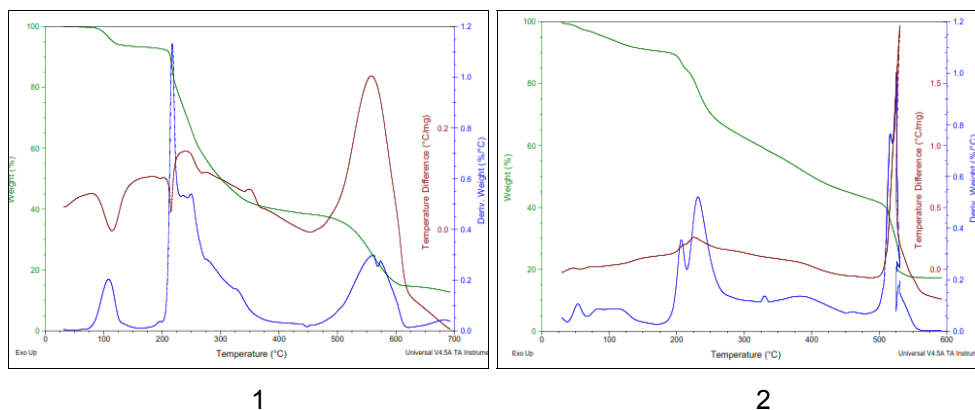


**Figure 3.** Thermal analysis of  $[\text{Cu}(\text{Hacm})_2(\text{pda})_2] \cdot 2\text{H}_2\text{O}$  (1) and  $[\text{Co}(\text{Hacm})_2(\text{en})_2] \cdot 4\text{H}_2\text{O}$  (2).

Complex **2** undergo a similar decomposition (Fig.3, **2**). The first decomposition step corresponds to the elimination of four water molecules (experimental weight loss 9.7%, calculated 10,3%). Above 200°C, two 1,2-ethanediamine molecules are evolved in the range 200–250°C. The high decomposition temperatures suggest a bidentate binding mode of 1,2-ethanediamine. Further weight loss corresponds to the pyrolysis of acetazolamide moieties. The final decomposition product in air is  $\text{Co}_3\text{O}_4$ .

**Optimized geometries.** The proposed starting structures for complexes are containing two N,N-chelating 1,2-ethanediamine and two deprotonated acetazolamide units. We considered 9 possible coordination modes of the deprotonated acetazolamide illustrated in Figure 4: deprotonation at the NH group and coordination to O (1), deprotonation at the NH and coordination at  $\text{NH}_2$  (2), deprotonation at NH and coordination to N(3) (3), deprotonation at NH and coordination to N(4) (4), deprotonation at NH and coordination at NH (5), deprotonation at  $\text{NH}_2$  group and coordination to O (6), deprotonation at  $\text{NH}_2$  and coordination to  $\text{NH}_2$  (7), deprotonation at  $\text{NH}_2$  and coordination to N(3) (8) and deprotonation at  $\text{NH}_2$  and coordination to N(4) (9).

Table 1 contains energy data of the optimized  $[\text{Cu}(\text{Hacm})_2(\text{pda})_2]$  structures while Figure 5 illustrates the most stable coordination mode. In case of this Cu(II) complex all calculations indicate that the deprotonated N atom of the acetamide NH group is energetically preferred with coordination of the metal to N(4) atom.

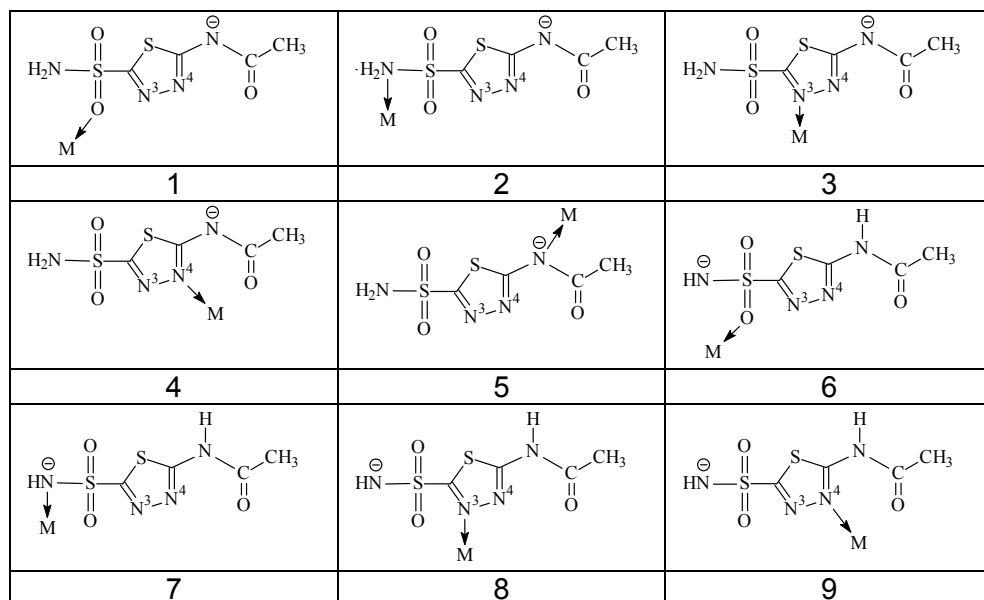


**Figure 4.** Considered coordination modes of acetazolamide ligand.

**Table 1.** Relative energy data of  $[\text{Cu}(\text{Hacn})_2(\text{pda})_2]$  optimized with PM6, PM6-DH+ and PM7 methods

Structure	PM6 (kJ/mol) (relative to -673.0470)	PM6-DH+ (kJ/mol) (relative to -761.036)	PM7 (kJ/mol) (relative to -1123.22)
1	95.8282	85.00261	171.1344
2	59.5591	98.6455	185.5776
3	0.0634	18.5449	13.2774
4	0	0	0
5	78.6089	69.2834	45.4121
6	312.6957	297.0887	231.0034
7	347.2449	336.2183	189.4263
8	249.4513	250.6127	200.6197
9	249.5219	250.8633	200.4163

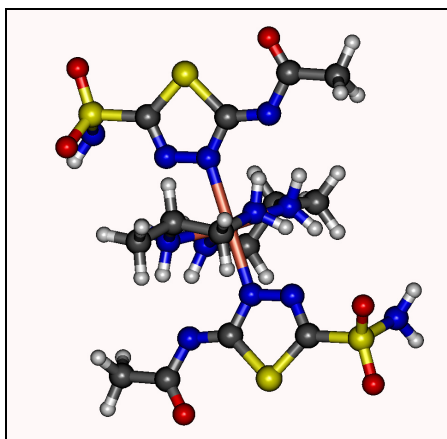


**Figure 5.** Optimized structure of  $[\text{Cu}(\text{Hacm})_2(\text{pda})_2]$  with PM7.

The calculations for the Co(II) complex at both PM6 and PM6-DH+ level indicate that the deprotonated N atom of the acetamide NH group is the energetically preferred site for coordination, while calculations at PM7 level indicate metal binding at the N(4) atom, and support the coordination mode assumed according to the IR data.

**Table 2.** Relative energy data of  $[\text{Co}(\text{Hacm})_2(\text{en})_2]$  with PM6, PM6-DH+ and PM7

Structure	PM6 Relative energy (kJ/mol) - 608.93	PM6-DH+ Relative energy (kJ/mol) -715.741	PM7 Relative energy (kJ/mol) - 672.328
1	194.9547	206.8164	126.8139
2	110.1785	107.021	234.2346
3	29.0250	37.8642	10.1508
4	82.3057	94.7958	0
5	0	0	54.8586
6	61.2224	196.7384	17.2664
7	126.5402	135.3369	21.0143
8	212.4348	185.2092	173.1728
9	103.6749	148.3999	293.5534

The optimized structure of Co(II) complex is displayed on Figure 6.

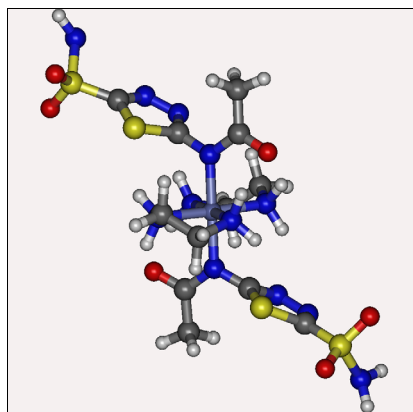


**Figure 6.** Optimized structure of  $[\text{Co}(\text{Hacm})_2(\text{en})_2]$  with PM6.

## CONCLUSIONS

FTIR spectra and thermal data of complexes suggest octahedral coordination of the metal ions with bidentate bonding of diamine ligands. According to PM7 calculations, the deprotonated acetazolamide coordinates *via* the N(4) atom. The obtained theoretical results are compatible with experimental ones.

## EXPERIMENTAL SECTION

The acetazolamide complexes were prepared in basic aqueous solution. FTIR spectra were recorded on a Jasco FTIR 600 spectrophotometer in the  $4000\text{--}400\text{ cm}^{-1}$  range, using KBr pellets. Thermal decomposition was investigated with a Universal V2.3C TA Instruments, by using samples of 7–12 mg, at a heating rate of  $10^\circ\text{C min}^{-1}$ . The composition of complexes was determined by elemental analysis (C, H, N).

**Synthesis of  $[\text{Cu}(\text{Hacm})_2(\text{pda})_2]\cdot 2\text{H}_2\text{O}$  (1).** To a suspension of acetazolamide (0.45 g, 2 mmol) in water ( $10\text{ cm}^3$ ), 1,2-propanediamine ( $0.5\text{ cm}^3$ ) was added resulting a clear solution. To this solution,  $\text{Cu}(\text{CH}_3\text{COO})_2\cdot\text{H}_2\text{O}$  (0.2 g, 1 mmol) in 1,2-propanediamine–water mixture ( $0.4\text{ cm}^3$  of 1,2-propanediamine in  $10\text{ cm}^3$  of water) was added dropwise. The dark blue reaction mixture was stirred at room temperature for 30 minutes, and then was left at room temperature. After two weeks appeared blue microcrystals. The resulted product was separated by filtration, washed with acetone and dried. Analysis: found (calc. for  $\text{CuC}_{14}\text{H}_{34}\text{N}_{12}\text{O}_8\text{S}_4$  MW 689.70) C 24.30 (24.36), N 23.77 (24.36), H 5.07 (4.97), Yield: 35 %, M.P.:  $190^\circ\text{C}$  (dec.).

IR (KBr pellet),  $\text{cm}^{-1}$ :  $\nu(\text{NH}_2)$  3346s, 3294s, 3268s;  $\nu(\text{CH}_2)$  2975m,  $\nu(\text{C}=\text{O})$  1603s;  $\nu(\text{C}=\text{N})$  1517s, 1412vs,  $\nu_{\text{as}}(\text{SO}_2)$  1333s,  $\nu_{\text{s}}(\text{SO}_2)$  1164s.

**Synthesis of  $[\text{Co}(\text{Hacm})_2(\text{en})_2]\cdot 4\text{H}_2\text{O}$  (2).** Complex (2) was prepared similarly to (1) using  $\text{CoCl}_2\cdot 6\text{H}_2\text{O}$  (0.24g, 1 mmol) and 1,2-ethanediamine instead of 1,2-propanediamine. The reaction mixture was allowed to stay 3 days at room temperature and the resulted red-brown crystals were separated by filtration, washed with acetone and dried. Analysis: found (calc. for  $\text{CoC}_{12}\text{H}_{34}\text{N}_{12}\text{O}_{10}\text{S}_4$  MW 693.07) C 21.09 (20.78), N 23.97 (24.25), H 5.09 (4.94), Yield: 20 %, M.P.:  $>290^\circ\text{C}$  (dec.).

IR (KBr pellet),  $\text{cm}^{-1}$ :  $\nu(\text{NH}_2)$  3288s, 3221s;  $\nu(\text{CH}_2)$  2942m, 2883w;  $\nu(\text{C}=\text{O})$  1603s;  $\nu(\text{C}=\text{N})$  1431vs, 1380vs,  $\nu_{\text{as}}(\text{SO}_2)$  1329s,  $\nu_{\text{s}}(\text{SO}_2)$  1148s. Abbreviations: m - medium, s – strong, vs – very strong, w – weak.

**Computational details.** Mopac 2012 program [12] was used for geometry optimizations in gas phase at the PM6, PM6-DH+ and PM7 semiempirical levels of theory [13]. The proposed starting structures for the program were generated in Spartan'06 [14]. Frequency calculations have been carried out at the same computational level to confirm that the optimized molecular structures of the complexes correspond to energetic minima. The results of experimental data and the calculated frequencies show a good agreement.

## REFERENCES

1. G. Mincione, A. Scozzafava, C.T. Supuran, *Met.-Based Drugs*, **1997**, 4, 27.
2. C.T. Supuran, A. Scozzafava, *J. Enzyme Inhib.*, **1997**, 12, 37.
3. G. Alzuet, S. Ferrer, J. Borrás, J.R.J. Sorenson, *J. Inorg. Biochem.*, **1994**, 55, 147.
4. F. Öztürk, A. Bulut, H. Paşaoğlu, I. Bulut, O. Büyükgüngör, *Spectrochim. Acta Part A: Molecular and Biomolecular Spectroscopy*, **2012**, A 97, 24.
5. G. Alzuet, L. Casella, A. Perotti, J. Borrás, *J. Chem. Soc. Dalton Trans.*, **1994**, 2347.
6. G. Alzuet, S. Ferrer, J. Borrás, *J. Inorg. Biochem.*, **1991**, 42, 79.
7. S. Ferrer, J.G. Haasnoot, R.A.G. de Graaff, J. Reedijk, J. Borrás, *Inorg. Chim. Acta*, **1992**, 192, 129.
8. E.E. Chufán, J.C. Pedregosa, S. Ferrer, J. Borrás, *Vibrational Spectroscopy*, **1999**, 20, 35.
9. U. Hartmann, H. Vahrenkamp, *Chem. Ber.*, **1994**, 127, 2381.
10. L. David, O. Cozar, E. Forizs, C. Craciun, D. Ristoiu, C. Balan, *Spectrochim. Acta Part A*, **1999**, 55, 2559.
11. P. Bombicz, J. Madarász, E. Forizs, M. Czugler, G. Pokol, S. Gál, A. Kálmán, Z. *Kristallogr.*, **2000**, 215, 317.
12. MOPAC2012, J.J.P. Stewart, Stewart Computational Chemistry, Colorado Springs, CO, USA, <http://openmopac.net> (2012).
13. J.J.P. Stewart, *J. Mol. Modeling* **2007**, 13, 1173.
14. Spartan'06 Wavefunction Inc. Irvine CA **2006**.

## MINERALOGICAL CHARACTERISATION AND HEAVY METALS ASSESSMENT OF SOILS FROM URBAN RECREATIONAL AREAS IN CENTRAL TRANSYLVANIA

ANDRA CRISTINA GAGIU<sup>a\*</sup>, ELENA MARIA PICA<sup>a</sup>,  
GHEORGHE BLAGA<sup>b</sup>, PETRU PASCUTA<sup>a</sup>, KERI AGNES<sup>a</sup>

**ABSTRACT.** Forty-five soil samples collected from fifteen intensively visited recreational areas in four different sized urban settlements in central Transylvania, Romania were investigated through X-ray powder diffraction for mineralogical characterization and analyzed using atomic absorption spectrometry in order to identify Cd, Cu, Co, Pb, Zn, Mn and Ni contamination. Pollution indexes were calculated and revealed that one-third of the recreational areas studied requires immediate remediation measures in order to reduce potential risks for human health.

**Keywords:** *urban soil, recreational areas, mineralogy, heavy metals*

### INTRODUCTION

In urban settlements a particular type of soil can be found that differs fundamentally from soil normally encountered in natural ecosystems, due to the fact that its properties are strongly influenced by anthropogenic activities [1]. The most common places where urban inhabitants come in contact with soils are recreational areas. Therefore soils in parks and playgrounds proved to be able to influence public health by transferring pollutants that tend to accumulate and persist over time endangering children or vulnerable persons [2]. In recreational areas residents can easily get in contact with contaminates through inhalation or ingestion of soil particles when outdoor activities are conducted.

---

<sup>a</sup> *Technical University of Cluj-Napoca, Faculty of Materials Science and Engineering.*

\* *e-mail andra\_gagiu@yahoo.com*

<sup>b</sup> *The University of Agricultural Sciences and Veterinary Medicine of Cluj-Napoca*



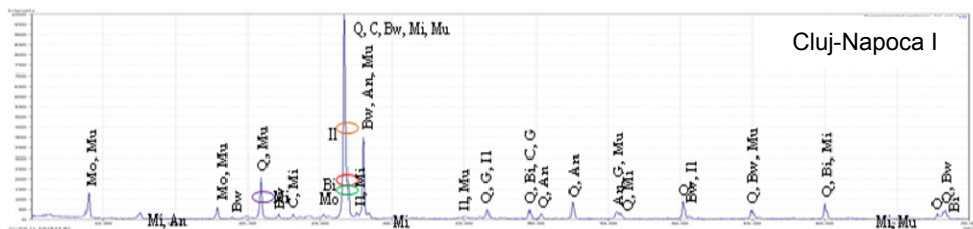
Heavy metals represent a particular class of contaminants, harmful to human health. In urban soils they have been identified as important markers of pollution [3] and therefore captured researchers' attention worldwide. A consistent number of studies related to metal contamination in recreational areas have been conducted in China, Brazil, Chile, Australia, Sweden, Lithuania, Spain, England, Italy and Serbia [4].

There is little research available on soils of recreational areas in urban settlements in Romania and therefore people are not aware of the potential risks that they impose. The aim of this study is to properly characterize soil mineralogy and to assess heavy metal contamination in this type of locations in central Transylvania.

Transylvania is the region in the centre of Romania bounded by the Carpathian Mountains. Numerous cities, communes and villages developed here over time. The current study focused on four cities located in the centre of the region, respectively Cluj-Napoca, Turda, Câmpia Turzii and Târgu Mureş. Even though these cities have different surfaces they are densely inhabited and host various anthropogenic activities. This study will examine soils from recreational areas (parks and playgrounds) within these cities and will highlight potential environmental problems caused by soil contamination with heavy metals.

## RESULTS AND DISCUSSION

Characterizing the mineralogical composition of soil represents an important part in heavy metals contamination studies due to the fact that minerals may considerably influence the toxicity, bioavailability and leaching for this type of contaminates [5]. Using X-ray powder diffraction (XRPD), the mineralogical composition of recreational area soils samples can be identified and interpreted.





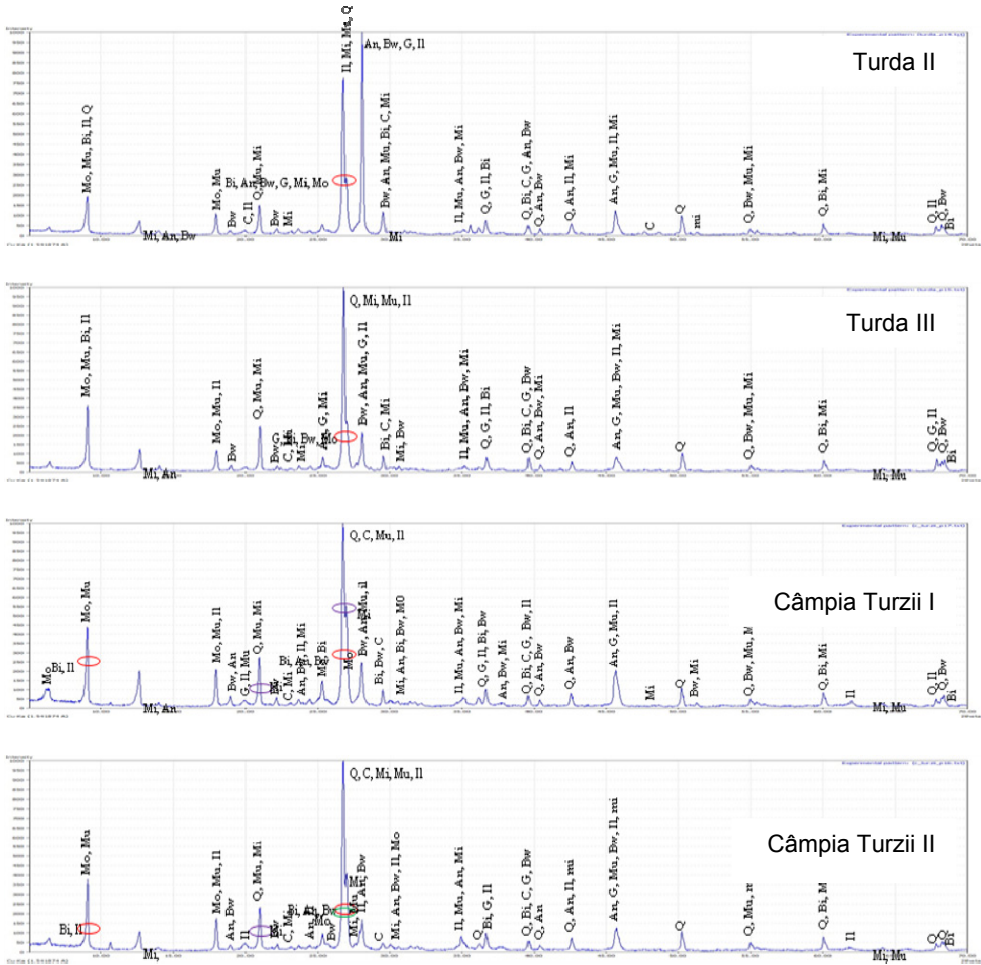


**Figure 1.** Mineralogical composition obtained by X-ray diffraction for all 15 locations analysed (Legend: An - anorthite, Bi - biotite, Bw - bytownite, C - calcite, G - gibbsite, Il - illite, Mi - microcline, Mo - montmorillonite, Mu - muscovite and Q – quartz)

Based on recorded changes in diffracted X-ray intensities the mineralogical composition of the soil samples was detected [6]. As a result, each of the diagrams included in Figure 1 expresses a sequence of diffraction peaks generated by recorded photon intensity versus a detector angle 2θ and generates information about the mineralogical composition that exists within a soil sample.

In the first diagram of figure 1 the mineralogical composition of the Cluj-Napoca I location is represented and the minerals contained were identified. Therefore it can be stated that the analyzed soil is a polymineral sample and contains a various type of minerals: anorthite biotite, bytownite, calcite, gibbsite, illite, microcline, montmorillonite, muscovite and quartz. Similar identifications were conducted for all the other fourteen locations analyzed. The results reveal that Cluj-Napoca II, Cluj-Napoca III, Cluj-Napoca IV, Cluj-Napoca V, Turda I, Turda II, Turda III, Câmpia Turzii I, Câmpia Turzii II and Târgu Mureş I present similar mineralogical compositions when being compared to sample Cluj-Napoca I. From a qualitative point of view, they all contain quartz, feldspars, clay minerals, carbonate minerals and hydroxides in various proportions. Samples collected from the locations referred to as Târgu Mureş II, Târgu Mureş III, Târgu Mureş IV, and Târgu Mureş V lack calcite and gibbsite. For better visualization qualitative mineralogical data was structured in Table 1.

**Table 1.** Mineralogical composition of recreational area soil samples

Recreational area	Mineralogical composition									
Cluj-Napoca I	Anorthite	Biotite	Bytownite	Calcite	Gibbsite	Illite	Microcline	Montmorillonite	Muscovite	Quartz
Cluj-Napoca II	Anorthite	Biotite	Bytownite	Calcite	Gibbsite	Illite	Microcline	Montmorillonite	Muscovite	Quartz
Cluj-Napoca III	Anorthite	Biotite	Bytownite	Calcite	Gibbsite	Illite	Microcline	Montmorillonite	Muscovite	Quartz
Cluj-Napoca IV	Anorthite	Biotite	Bytownite	Calcite	Gibbsite	Illite	Microcline	Montmorillonite	Muscovite	Quartz
Cluj-Napoca V	Anorthite	Biotite	Bytownite	Calcite	Gibbsite	Illite	Microcline	Montmorillonite	Muscovite	Quartz
Turda I	Anorthite	Biotite	Bytownite	Calcite	Gibbsite	Illite	Microcline	Montmorillonite	Muscovite	Quartz
Turda II	Anorthite	Biotite	Bytownite	Calcite	Gibbsite	Illite	Microcline	Montmorillonite	Muscovite	Quartz
Turda III	Anorthite	Biotite	Bytownite	Calcite	Gibbsite	Illite	Microcline	Montmorillonite	Muscovite	Quartz
Campia Turzii I	Anorthite	Biotite	Bytownite	Calcite	Gibbsite	Illite	Microcline	Montmorillonite	Muscovite	Quartz
Campia Turzii II	Anorthite	Biotite	Bytownite	Calcite	Gibbsite	Illite	Microcline	Montmorillonite	Muscovite	Quartz
Targul Mures I	Anorthite	Biotite	Bytownite	Calcite	Gibbsite	Illite	Microcline	Montmorillonite	Muscovite	Quartz
Targul Mures II	Anorthite	Biotite	Bytownite	/	/	Illite	Microcline	Montmorillonite	Muscovite	Quartz
Targul Mures III	Anorthite	Biotite	Bytownite	/	/	Illite	Microcline	Montmorillonite	Muscovite	Quartz
Targul Mures IV	Anorthite	Biotite	Bytownite	/	/	Illite	Microcline	Montmorillonite	Muscovite	Quartz
Targul Mures V	Anorthite	Biotite	Bytownite	/	/	Illite	Microcline	Montmorillonite	Muscovite	Quartz

The mineralogical composition plays an important role in adsorbing, oxidizing, reducing and precipitating chemicals such as heavy metals into pure or mixed solids. Clay minerals are the most responsible for restraining such contaminants, and can be divided into two major types: nonexpanding (1:1) and expanding (2:1). The major difference between the two types is that the nonexpanding clay minerals have one silica tetrahedral sheet bonded

to one aluminum octahedral sheet while the expanding clay minerals have two silica tetrahedral sheets surrounding an aluminum octahedral sheet. The 2:1 type is attributed to minerals such as montmorillonite and illite [6] both contained in all soil samples collected for this study. Montmorillonite defines a class of soft clayey water-absorbent minerals. The water content in montmorillonite can vary so that the chemical formula is written as  $(\text{Na,Ca})_{0.3}(\text{Al,Mg})_2\text{Si}_4\text{O}_{10}(\text{OH})_2 \cdot n\text{H}_2\text{O}$ .

Due to the fact that only weak van der Waals type forces exist among the layers of expanding clay minerals the chemicals such as heavy metals often enter between them, where they remain immobilized [7]. Illite is a common phyllosilicate or layered alumino-silicate clay mineral. The general chemical formula for illite is given as  $(\text{K,H}_3\text{O})(\text{Al,Mg,Fe})_2(\text{Si,Al})_4\text{O}_{10}[(\text{OH})_2,(\text{H}_2\text{O})]$  but there is considerable ion substitution. The presence of montmorillonite and illite in the analyzed soil samples can be interpreted in two ways. On one hand the immobilization of metals in the upper soil layer limits vertical migration and reduces the threat of ground water contamination, but on the other hand it increases risks for human health due to the fact that in urban recreational areas children come in contact with top soil particles. Montmorillonite and illite were identified in all 15 locations analyzed.

Carbonate minerals such as calcite are widely available in soil and have considerable influence in the accumulation of various metals in the environment [8]. Calcite is the most stable polymorph of calcium carbonate ( $\text{CaCO}_3$ ), has a rhombohedral crystal system and has been identified through experimental observation as being an absorption substrate with affinity for Zn and Cd [9]. Calcite is present in 11 of the 15 locations analyzed.

Aluminum hydroxides such as gibbsite often designed as  $\gamma\text{-Al}(\text{OH})_3$  are also important adsorbents of heavy metals in soils, making this mineral's presence in the upper layer of urban recreational areas noticeable [10]. As in the case of calcite, gibbsite was identified in 11 out of the 15 locations.

Quartz is also an important mineral present in all recreational area samples analyzed. It is also known for its ability to absorb trace metals from solutions. Experimental studies show that the reactive ability of metals on quartz follows the order  $\text{Cd} > \text{Pb} > \text{Zn} > \text{Ni} > \text{Cu}$  [11]. Taking this into account it can be affirmed that quartz also plays a key role in the accumulation of metal contaminants in soils.

Anorthite, biotite, bytownite, microcline and muscovite have limited or moderated influence on heavy metal retention in soil. Nevertheless, despite the mineralogical composition of soil, the fact should be taken into account, that metal adsorption and retention processes are strongly influenced by a series of chemical and physical parameters such as water or substrate pH that can vary substantially from one location to another. Also metals can be found in a pure form unattached to minerals.

In order to assess heavy metal contamination Cd, Cu, Co, Pb, Zn, Mn and Ni concentrations in the urban recreational area soil samples were determined using atomic absorption spectrometry. Due to the fact that in each recreational area under discussion three samples were analyzed average values were calculated. For better visualization heavy metal concentrations were structured into Table 2 that also included guideline values considered normal in Romania. For each location a general pollution index (PI) was calculated as the ratio between the heavy metal concentrations identified in the study and the normal reference value attributed for Romania. Each PI calculated was classified as low if ( $PI \leq 1$ ), moderate if ( $1 < PI \leq 3$ ) or high if ( $PI > 3$ ) and highlighted in Table 3 [12].

**Table 2.** Heavy metal concentrations and Romanian guidelines for normal values

Identification	Cd (mg/kg)	Cu (mg/kg)	Co (mg/kg)	Pb (mg/kg)	Zn (mg/kg)	Mn (mg/kg)	Ni (mg/kg)
Cluj-Napoca I	0.17	87.9	10.7	11.9	80	496	40.9
Cluj-Napoca II	0.61	83.2	8.5	143.7	219	378	21.7
Cluj-Napoca III	0.82	115.4	13.3	73.9	262	576	47.7
Cluj-Napoca IV	0.24	36.9	8	72.1	319	607	21.1
Cluj-Napoca V	0.40	40.7	16.9	39.9	116	778	35.4
Turda I	0.16	141.2	15.2	172.4	343	1069	47.9
Turda II	0.46	39.5	13.4	55.1	140	826	30.4
Turda III	0.80	41.1	10.1	67.2	171	779	27
Campia Turzii I	0.38	50.3	12.5	93.4	205	1194	41.9
Campia Turzii II	0.49	39.8	14.4	44.7	140	825	33.8
Tg. Mures I	0.15	32.1	13.4	28.6	102	729	29.4
Tg. Mures II	0.17	28.7	13.3	26.3	98	725	24.3
Tg. Mures III	0.34	29.6	12.4	16.4	86	873	35.8
Tg. Mures IV	0.13	19.2	7.6	38.3	60	419	16.5
Tg. Mures V	0.14	22.2	13.4	19.4	73	659	27
Romanian Guideline Values [13]	1	20	15	20	100	900	20

The results presented in Table 2 demonstrate a general tendency to exceed normal values especially for Cu, Pb and Zn, heavy metals that are usually associated with anthropogenic pollution sources. Samples collected from recreational areas in Cluj-Napoca, Turda and Câmpia Turzii reveal higher metal levels than samples collected from Târgu Mureş.

Co, Mn and Ni concentrations exhibit levels comparable to the guideline values established as normal for Romanian soils. Cd concentration values are well maintained under the Romanian guideline values suggesting that in the Transylvanian cities investigated there is no sign of possible cadmium contamination.

Heavy metal concentrations identified in Târgu Mureş are homogeneously distributed for all locations investigated suggesting healthy environments that pose limited threats for recreational area users [14].

The recreational areas referred to as Cluj Napoca II, Cluj Napoca III, Turda I and Câmpia Turzii I reveal alarmingly high Pb concentrations indicating poor soil quality and a considerable threat for human health.

**Table 3.** Pollution Indexes (PI) calculated for heavy metal concentrations identified

Identification	PI - Cd	PI - Cu	PI - Co	PI - Pb	PI - Zn	PI - Mn	PI - Ni
Cluj-Napoca I	0.17	4.40	0.71	0.60	0.80	0.55	2.05
Cluj-Napoca II	0.61	4.16	0.57	7.19	2.19	0.42	1.09
Cluj-Napoca III	0.82	5.77	0.89	3.70	2.62	0.64	2.39
Cluj-Napoca IV	0.24	1.85	0.53	3.61	3.19	0.67	1.06
Cluj-Napoca V	0.40	2.04	1.13	2.00	1.16	0.86	1.77
Turda I	0.16	7.06	1.01	8.62	3.43	1.19	2.40
Turda II	0.46	1.98	0.89	2.76	1.40	0.92	1.52
Turda III	0.80	2.06	0.67	3.36	1.71	0.87	1.35
Campia Turzii I	0.38	2.52	0.83	4.67	2.05	1.33	2.10
Campia Turzii II	0.49	1.99	0.96	2.24	1.40	0.92	1.69
Tg. Mures I	0.15	1.61	0.89	1.43	1.02	0.81	1.47
Tg. Mures II	0.17	1.44	0.89	1.32	0.98	0.81	1.22
Tg. Mures III	0.34	1.48	0.83	0.82	0.86	0.97	1.79
Tg. Mures IV	0.13	0.96	0.51	1.92	0.60	0.47	0.83
Tg. Mures V	0.14	1.11	0.89	0.97	0.73	0.73	1.35

As it can be seen from Table 3 the pollution indexes differ considerably from one metal to another. For Cd, Co, and Mn low pollution indexes were calculated indicating that metal concentrations resemble values considered normal for soils in Romania and that there are no pollution problems that need to be further discussed.

Ni pollution indexes can be characterized as being medium in 14 out of the 15 locations analyzed. There is no alarming Ni contamination that has been identified in recreational area soils of centre Transylvanian cities since there are no locations where high values were recorded.

Zn pollution registered high values in 2 locations, medium in 7 and low in 6. These values reveal punctual Zn pollution directly linked to anthropogenic activities.

Cu and Pb contamination prove to be more serious since in the majority of locations studied pollution indexes are medium and high. For Cu there are 4 locations with high pollution indexes and 10 with medium while for Pb 6 locations have high pollution indexes and another 6 medium. These data highlight widespread Cu and Pb contamination in recreational areas within cities of central Transylvania. Therefore, it can be concluded that due to the fact that one-third of the locations analysed reveal significant Cu and Pb pollution problems, there is a great possibility that numerous parks and playgrounds within cities of Transylvania pose risks for human health and wellbeing due to heavy metal contamination.

Heavy metal pollution indexes were represented in Figure 3 for better visualisation for all locations investigated. Cu and Pb contaminations seem to have similar compositional patterns. Hotspots have been evidenced in Cluj - Napoca II, Cluj-Napoca III, Turda I and Câmpia Turzii I. Cluj-Napoca II is a middle size park in the former industrial area of Cluj-Napoca and Cluj-Napoca III is a small playground located near an intensively used roadway with great amounts of traffic. Turda I is the biggest park in the centre of the city Turda and Câmpia Turzii I is a medium sized playground near the steel plant. All four recreational areas are relatively old, and have a strong connection to anthropogenic activities.

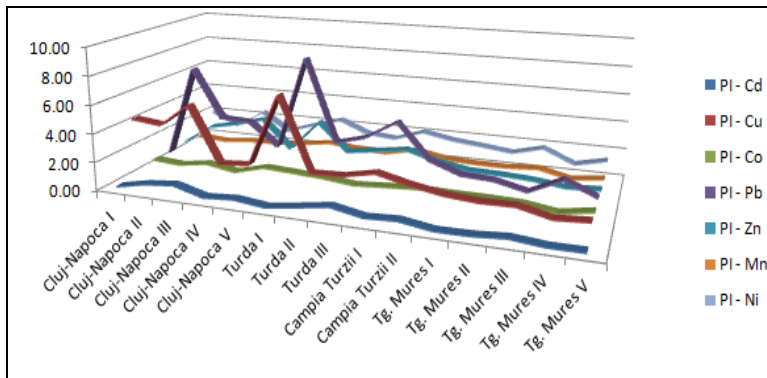


**Figure 2.** Heavy metal pollution in the investigated recreational areas

The Integrated Pollution Index (IPI) calculates the average of pollution indexes established for all seven metals in each recreational area [12]. Integrated pollution indexes vary between 0.77 and 3.41 and have been classified as low ( $IPI \leq 1$ ), middle ( $1 < IPI \leq 2$ ) or high ( $IPI > 2$ ). The lowest values are recorded in Târgu Mureş II, Târgu Mureş III, Târgu Mureş IV, and Târgu Mureş V. These are the same locations that lack calcite and



gibbsite, minerals known to have considerable influence in the accumulation of various metals in the environment. The integrated pollution index identified in the recreational areas named Turda I was the highest, followed by Cluj-Napoca III, Cluj-Napoca II and Câmpia Turzii I. Remediation measures need to be taken for these parks and playgrounds in order to reduce potential risks posed for human health.

## CONCLUSIONS

The results obtained in this study characterise soils in recreational areas of 4 different cities in central Transylvania from a mineralogical point of view and assess heavy metal contamination.

All topsoil samples (0-15 cm) from parks and playgrounds in Cluj-Napoca, Turda, Câmpia Turzii and Târgu Mureş contain anorthite, biotite, bytownite, illite, microcline, montmorillonite, muscovite and quartz, in various proportions. In 11 out of the 15 locations analyzed calcite, gibbsite, two minerals known to have considerable influence in the accumulation of various metals in the environment have been identified.

Heavy metal assessment reveals high concentrations especially for Cu, Pb and Zn in some locations associating contamination with anthropogenic pollution sources. Co, Mn and Ni concentrations exhibit levels comparable to the guideline values established as normal for Romanian soils. Cd concentration values are well maintained under the Romanian guideline values suggesting that in Cluj-Napoca, Turda, Câmpia Turzii and Târgu Mureş there is no sign of possible cadmium contamination.

Calculating pollution indexes for metals in all locations analyzed links Zn contamination directly to anthropogenic activities and highlights that one-third of the locations analysed reveal significant Cu and Pb pollution problems.

The integrated pollution index determined for all locations underlines the fact that in Târgu Mureş heavy metals are homogeneously distributed and values do not exceed national guidelines. Therefore it can be stated that these parks and playgrounds represent healthy environments that pose no threats to for recreational area users. In contrast, in Cluj-Napoca, Turda and Câmpia Turzii there are some locations that require immediate remediation measures in order to reduce potential risks posed for human health. In order to minimize exposure to the contaminated topsoil, contaminated areas should be restricted and soil quality annually controlled [15].

The data presented within this study represents a starting point for recreational areas quality assessments and clearly indicates that in urban settlements in Romania more attention should be paid to heavy metal contamination of parks and playgrounds.

## EXPERIMENTAL SECTION

The study area comprises 15 diverse, intensively visited locations described as follows. Cluj-Napoca I is a frequently used playground located near a highly circulated street in Manastur neighborhood, Cluj-Napoca II is an old park known as known as “The railway park”, Cluj-Napoca III is a playground on Muncii street, situated in the industrial area, Cluj-Napoca IV is the Central Park, the biggest park in the city and Cluj-Napoca V is a playground in Gheorgheni neighborhood. Turda I is the oldest and biggest park in Turda City, Turda II is a newly renovated park and Turda III is a recreational area located near the river bank. Câmpia Turzii I is a playground located near the former steel plant and Câmpia Turzii II is an old park in the center. Târgu Mureş I, II, III and V are playground located in different neighbourhoods of the city while Târgu Mureş IV is an extended recreational area with a big adventure park and a zoological garden.

In order to identify the mineral compositions and Cd, Cu, Co, Pb, Zn, Mn and Ni concentrations of soils from recreational areas mentioned above, 45 topsoil samples, were collected. Each sample is consisted of a number of sub samples mixed together and was collected from the depth interval of 0-15 cm. Soil samples were air dried for 24 hours, sieved [16] and then redried using a drying stove at 110 °C [17] in order to eliminate physically bound water.

The mineralogical composition was identified through X-Ray diffraction using a Shimadzu XRD-6000 X-ray diffractometer. When analyzing soil samples, the diffraction phenomenon occurs when x-rays are scattered by a periodical array of atoms as the ones that can be found within the crystalline structure of a mineral. The scattering of X-rays from differently arranged atoms produces a unique diffraction pattern which contains information about the atomic arrangement within a crystal. The difference among crystalline structure of minerals determines the position and intensity of peaks in a diffraction pattern [6]. A qualitative computer analysis of the peak positions and intensities associated with each sample was conducted. Mineralogical composition and its influence on heavy metal adsorption and retention were highlighted and explained using scientific literature examples.

Heavy metal concentrations from soil samples digested in aqua regia were analysed through atomic absorption spectrometry using a Solaar S4 Atomic Absorption spectrometer. This is an extremely accurate technique for metal determinations in solutions, with a wide range of detection that allows the identification of a spectrum of 70 metallic elements. Data obtained was structured into tables and for each location a general pollution index (PI) was calculated as the ratio between the heavy metal concentrations identified in the study and the normal reference value attributed for Romania. Each PI calculated

was classified as low if ( $PI \leq 1$ ), moderate if ( $1 \leq PI \leq 3$ ) or high if ( $PI > 3$ ). The arithmetical mean of the pollution indexes calculated for each location generated the integrated pollution index (IPI) which was classified as low ( $IPI \leq 1$ ), middle ( $1 < IPI \leq 2$ ) or high ( $IPI > 2$ ). Using the pollution index and the integrated pollution index, conclusions could be drawn in terms of heavy metal soil contamination.

## ACKNOWLEDGMENTS

This paper has been completed with the support of the Doctoral School within the Technical University of Cluj-Napoca, Romania.

## REFERENCES

1. S. Norra, D. Stuben, *Jurnal of Soils and Sediments*, **2003**, 4, 230.
2. A.M.G. Figueriedo, M. Tocchini, T.F.S dos Santos, *Procedia Environmental Sciences*, **2011**, 4, 303.
3. D.S. Manta, M. Angelone, A. Bellanca, R. Neri, M. Sprovieri, *The Science of the Total Environment*, **2002**, 300, 229.
4. A.C. Gagi, E.M. Pica, *Annals of the Constantin Brancusi University of Targu Jiu*, Engineering Series, **2012**, 3, 221.
5. A. Violante, V. Cozzolino, L. Perelomov, A.G. Caporale, M. Pigna, *Jurnal of Soil Science and Plant Nutrition*, **2010**, 10, 268.
6. S.A. Speakman, Basics of X-ray Powder Diffraction, Massachusetts Institute of Technology available at <http://prism.mit.edu/xray/Basics%20of%20X-Ray%20Powder%20Diffraction.pdf>
7. A. Dube, R. Zbytniewski, T. Kowalkowski, E. Cukrowska, B. Buszewski, *Polish Journal of Environmental Studies*, **2001**, 10, 1.
8. O. Tunusoglu, T. Shahwan, A. E. Eroglu, *Geochemical Journal*, **2007**, 41, 379.
9. L. Lassabatere, L. Spadini, C. Delolme, L. Fevrier, R. G. Cloutier, T. Winiarski, *Chemosphere*, **2007**, 69, 1499.
10. J. Frenzel, A.F. Oliveira, H.A. Duarte, T. Heine, G. Seifert, *Journal of Inorganic and General Chemistry*, **2005**, 631, 1267.
11. W. Honghai, W. Daqing, P. Jinlian, *Chinese Journal of Geochemistry*, **1999**, 18, 201.
12. T.B. Chen, Y.M. Zheng, M. Lei, Z.C. Huang, H.T. Wu, H. Chen, K.K. Fan, K.Yu, X. Wu, Q.Z. Tian, *Chemosphere*, **2005**, 60, 542.
13. \* \* \*, 756 Governments Order from 3<sup>rd</sup> November **1997** for approving regulations for environmental pollution.
14. E. Miguel, I. Iribarren, E. Chacon, A. Ordonez, S. Charlesworth, S., *Chemosphere*, **2007**, 66, 505.
15. J. Kumpiene, E. Branvall, R. Taraskevicius, C. Aksamitauskas, R. Zinkute, *Jurnal of Geochemical Exploration*, **2011**, 108, 15.
16. K. Ljung, O. Selinus, E. Otabbong, *Science of the Total Environment*, **2006**, 366, 749.
17. A.C. Gagi, E.M. Pica, GRA - Global Research Analysis, **2013**, 2, 8, 66, available at <http://theglobaljournals.com/gra/file.php?val=MTAzMQ>

## QSAR STUDY ON NITROGEN-CONTAINING FLAVONOIDS BY SIMILARITY CLUSTER PREDICTION

TEODORA ELENA HARSA<sup>a</sup>

**ABSTRACT.** A set of 40 flavonoids, downloaded from the PubChem database, was submitted to a qsar study by using an alignment procedure of the molecules over the hypermolecule, that mimics the investigated correlational space, within the correlation weighting analysis. The best models have been validated in the external test set and in a new version of validation/prediction by using similarity clusters.

**Key-words:** QSAR, log P, flavonoids, correlation weighting, similarity.

### 1. INTRODUCTION

Flavonoids are phenolic substances with a low molecular weight and they are abundant in plant tissues, fruits (particularly in the skin) [1,2]. In the human body they manifest a lot of biological properties, such as antioxidants, antiallergenic, antibacterial, antifungal, antiviral and anticarcinogenic agents. These characteristics confer to flavonoids pharmacological properties useful in the treatment of diseases, ranging from allergies, bacterial and viral infectious processes to those of greater risk like the coronary diseases, cancer and HIV [3-4].

In the past half century, the use of QSAR (quantitative-structure-activity-relationship, one of the well-developed areas in computational chemistry) [5] has become increasingly helpful in understanding many aspects of chemical-biological interactions in drug and pesticide research, particularly enzyme functions, as well as in the areas of toxicology [6-8].

The parameter correlated in this paper is logP, the (calculated) partition coefficient in octanol/water, a measure of hydrophobicity that gives information about the transport of a drug through the cell membranes to the biological receptor [9].

---

<sup>a</sup> Babes-Bolyai University, Department of Chemistry Faculty of Chemistry and Chemical Engineering, Arany Janos 11, 400028, Cluj, Romania, harsa.teodoraelena@yahoo.com

Any similarity measure has three principal components: (i) the representation that is used to describe each of the structures taken in the work; (ii) the weighting scheme, used to assign weights to different parts of the structure representation that reflect their relative degrees of importance; and (iii) the similarity coefficient, used to quantify the degree of resemblance between two suitably weighted representations [10]. There is a variety of ways for computing the similarity score; it is recognized that there is no a single similarity measure that will provide optimal screening in all circumstances [11–13].

2D similarity approaches can be defined as simple methods since they employ topological measurements derived from molecular graphs, but many times they show inconsistencies for the appropriate representation of QSAR/QSPR predictive spaces [14].

Correlation weighting was previously discussed by Toropov and Toropova [15,16]

Graph theoretical descriptors, invariants up to isomorphism, also called topological indices [17-19] are used as predictor variables in qsar studies. Within this paper we used the indices generated by the TopoCluj software [20].

## 2. DATA SET

A set of 40 molecular structures, belonging to the class of flavonoids, have been downloaded from the database Pubchem [21] (Table 1), together with their log P. The set was split in the training set and test set (25 and 15 molecules, respectively). The structures have been optimized by HyperChem software, at molecular mechanics MM+ and semi-empirical PM3 levels of theory.

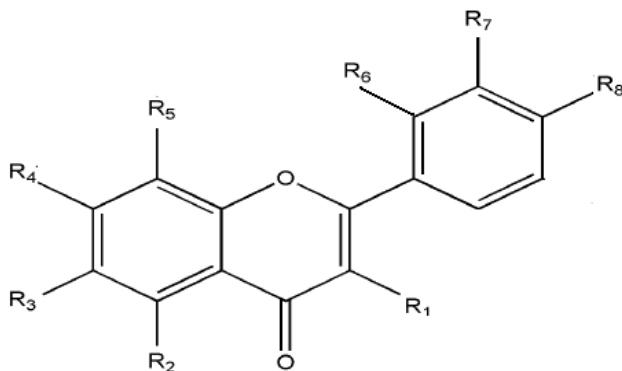


**Table 1.** The set of flavonoids, taken from PubChem database [21].

	Substituents	log P		Substituents	log P
1	R <sub>2</sub> -NH <sub>2</sub>	3.4	2	R <sub>1</sub> -H <sub>2</sub> , R <sub>3</sub> -OH, R <sub>8</sub> -NH <sub>2</sub>	2.9
3	R <sub>1</sub> -H <sub>2</sub> , R <sub>8</sub> -NH <sub>2</sub>	2.5	4	R <sub>2</sub> -NH <sub>2</sub> , R <sub>6</sub> -NH <sub>2</sub>	2.4
5	R <sub>2</sub> -NH <sub>2</sub> , R <sub>8</sub> -N(Me) <sub>2</sub>	2.2	6	R <sub>2</sub> -NH <sub>2</sub> , R <sub>8</sub> -N(Et) <sub>2</sub>	3
7	R <sub>3</sub> -NH <sub>2</sub>	3.3	8	R <sub>2</sub> -NH <sub>2</sub> , R <sub>8</sub> -NH(Et)	2.5
9	R <sub>4</sub> -NH <sub>2</sub>	3.3	10	R <sub>1</sub> -NH <sub>2</sub>	3.1
11	R <sub>1</sub> -NH <sub>2</sub> , R <sub>3</sub> -NH <sub>2</sub>	2.4	12	R <sub>2</sub> -OH, R <sub>5</sub> -NH <sub>2</sub>	2.7
13	R <sub>3</sub> -NH <sub>2</sub> , R <sub>4</sub> -OH, R <sub>5</sub> -NH <sub>2</sub>	1.5	14	R <sub>1</sub> -NH <sub>2</sub> , R <sub>6</sub> -NH <sub>2</sub>	2.4
15	R <sub>6</sub> -NH <sub>2</sub> , R <sub>7</sub> -Me	3.2	16	R <sub>2</sub> -OH, R <sub>4</sub> -OH, R <sub>7</sub> -NH <sub>2</sub> , R <sub>7</sub> -OMe	1.4
17	R <sub>2</sub> -OH, R <sub>3</sub> -NH <sub>2</sub> , R <sub>4</sub> -OH	1.4	18	R <sub>2</sub> -OH, R <sub>5</sub> -NH <sub>2</sub> , R <sub>8</sub> -NH <sub>2</sub>	1.1
19	R <sub>2</sub> -OH, R <sub>4</sub> -OH, R <sub>7</sub> -NH <sub>2</sub> , R <sub>8</sub> -OH	1.1	20	R <sub>4</sub> -OH, R <sub>5</sub> -NH <sub>2</sub> , R <sub>8</sub> -NH <sub>2</sub>	1.8
21	R <sub>3</sub> -OH, R <sub>8</sub> -NH <sub>2</sub>	2.9	22	R <sub>3</sub> -NH <sub>2</sub> , R <sub>8</sub> -N(Me) <sub>2</sub>	3
23	R <sub>3</sub> -OMe, R <sub>8</sub> -NH <sub>2</sub>	2.8	24	R <sub>7</sub> -OMe, R <sub>8</sub> -NH <sub>2</sub>	2.8
25	R <sub>3</sub> -Me, R <sub>4</sub> -Me, R <sub>8</sub> -N(Me) <sub>2</sub>	4.4	26	R <sub>2</sub> -NH <sub>2</sub> , R <sub>8</sub> -OH	1.8
27	R <sub>7</sub> -NH <sub>2</sub> , R <sub>8</sub> -NH <sub>2</sub>	2.2	28	R <sub>2</sub> -NH <sub>2</sub> , R <sub>8</sub> -NH(Me)	2.1
29	R <sub>2</sub> -NH <sub>2</sub> , R <sub>6</sub> -OH, R <sub>8</sub> -OH	2.3	30	R <sub>3</sub> -Me, R <sub>8</sub> -N(Me) <sub>2</sub>	4
31	R <sub>2</sub> -NH <sub>2</sub> , R <sub>6</sub> -N(Me) <sub>2</sub>	3.2	32	R <sub>2</sub> -NH <sub>2</sub> , R <sub>6</sub> -NH(Me)	3
33	R <sub>2</sub> -NH <sub>2</sub> , R <sub>6</sub> -OH	2.7	34	R <sub>2</sub> -NH <sub>2</sub> , R <sub>6</sub> -OMe	3
35	R <sub>2</sub> -NH <sub>2</sub> , R <sub>5</sub> -OH, R <sub>6</sub> -NH <sub>2</sub>	2	36	R <sub>2</sub> -NH(Me), R <sub>6</sub> -N(Me) <sub>2</sub>	3.8
37	R <sub>2</sub> -NH(Me), R <sub>8</sub> -N(Me) <sub>2</sub>	2.9	38	R <sub>2</sub> -NH <sub>2</sub> , R <sub>8</sub> -NH <sub>2</sub>	1.4
39	R <sub>2</sub> -NH <sub>2</sub> , R <sub>7</sub> -OH	2.7	40	R <sub>2</sub> -NH <sub>2</sub> , R <sub>6</sub> -OH, R <sub>8</sub> -NH <sub>2</sub>	2

### 3. METHOD

In performing the QSAR, we followed an algorithm based on the alignment of molecules over a hypermolecule [22] and correlation weighting analysis [15,16]. This algorithm includes the main steps: (a) download from PubChem (or other public domain) a dataset of molecules and optimize them at a choice level of theory; (b) compute global and local quantum and/or topological descriptors; (c) build up the hypermolecule of the set by superimposing the common and distinct features of all the molecules; (d) split the set of molecules in the learning and test sets, respectively; (e) write the binary vectors, with 1 if there exists a fragment in the current molecule in a given position of the hypermolecule and 0 otherwise; (f) weight the binary vectors by various physico-chemical or mathematical local properties; (g) data reduction: discard the non-variant descriptors and (statistically) non-significant descriptors  $X_j$  over the  $j^{\text{th}}$  position of the hypermolecule; (h) make correlation weighting (including all significant positions  $j$  of the hypermolecule) and generate correlation weights  $CD_{ij}$  (as product of local descriptors – e.g. charge, mass, etc. with the regression coefficients for the significant positions of the hypermolecule), next sum them to give a global descriptor  $SD_i = \sum_j CD_{ij}$ ; (i) models generation (i.e. QSPR/QSAR equations) by using various global descriptors; (j) validation of the model, either by the leave-one-out LOO (or similar procedures) or by the (external) test set; (k) validation by clusters of similarity.

### 3.1. Alignment over the hypermolecule

On the set of 40 flavonoids, a Hypermolecule [22] was built up, as a union of the common and distinct substructures over all the molecules in the set (Figure 1). Molecules were aligned over the hypermolecule positions and binary vectors were constructed (see Table 2, some significant positions), with 1 when in the current molecule there exists a corresponding atom and zero, otherwise. Next, the values 1 are replaced with local characteristics: partial charges, mass fragments or local topological descriptors. We used here the mass fragments in building the weighted vector for every molecule.

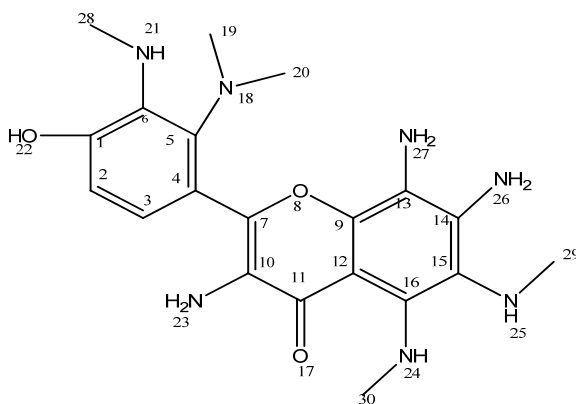


**Table 2.** Binary vectors of the hypermolecule, for the 40 flavonoids.

Molecule	17	18	19	20	21	22	23	24	25	26	27	28	29	30
1	1	0	0	0	0	0	0	1	0	0	0	0	0	0
2	1	0	0	0	0	0	0	0	0	0	0	0	0	0
3	1	0	0	0	0	0	0	0	0	0	0	0	0	0
4	1	1	0	0	0	0	0	1	0	0	0	0	0	0
5	1	0	0	0	0	0	0	1	0	0	0	0	0	0
6	1	0	0	0	0	0	0	1	0	0	0	0	0	0
7	1	0	0	0	0	0	0	0	1	0	0	0	0	0
8	1	0	0	0	0	0	0	1	0	0	0	0	0	0
9	1	0	0	0	0	0	0	0	0	1	0	0	0	0
10	1	0	0	0	0	0	1	0	0	0	0	0	0	0
11	1	0	0	0	0	0	1	0	1	0	0	0	0	0
12	1	0	0	0	0	0	0	0	0	0	1	0	0	0
13	1	0	0	0	0	0	0	0	1	0	1	0	0	0
14	1	0	0	0	0	0	1	0	0	0	0	0	0	0
15	1	1	0	0	0	0	0	0	0	0	0	0	0	0
16	1	0	0	0	0	1	0	0	0	0	0	0	0	0
17	1	0	0	0	0	0	0	0	1	0	0	0	0	0
18	1	0	0	0	0	0	0	0	0	0	1	0	0	0

Molecule	17	18	19	20	21	22	23	24	25	26	27	28	29	30
19	1	0	0	0	1	1	0	0	0	0	0	0	0	0
20	1	0	0	0	0	0	0	0	0	0	1	0	0	0
21	1	0	0	0	0	0	0	0	0	0	0	0	0	0
22	1	0	0	0	0	0	0	0	1	0	0	0	0	0
23	1	0	0	0	0	0	0	0	0	0	0	0	1	0
24	1	0	0	0	0	0	0	0	0	0	0	1	0	0
25	1	0	0	0	0	0	0	0	0	0	0	0	0	0
26	1	0	0	0	0	1	0	1	0	0	0	0	0	0
27	1	0	0	0	1	0	0	0	0	0	0	0	0	0
28	1	0	0	0	0	0	0	1	0	0	0	0	0	0
29	1	0	0	0	0	1	0	1	0	0	0	0	0	0
30	1	0	0	0	0	0	0	0	0	0	0	0	0	0
31	1	1	1	1	0	0	0	1	0	0	0	0	0	0
32	1	1	1	0	0	0	0	1	0	0	0	0	0	0
33	1	0	0	0	0	0	0	1	0	0	0	0	0	0
34	1	0	1	0	0	0	0	1	0	0	0	0	0	0
35	1	1	0	0	0	0	0	1	0	0	0	0	0	0
36	1	1	1	0	0	0	0	1	0	0	0	0	0	1
37	1	0	0	0	0	0	0	1	0	0	0	0	0	1
38	1	0	0	0	0	0	0	1	0	0	0	0	0	0
39	1	0	0	0	0	0	0	1	0	0	0	0	0	0
40	1	0	0	0	0	0	0	1	0	0	0	0	0	0

For all the structures, topological indices (including distance, detour and Cluj indices) have been computed (Table 3) by using TOPOCLUJ software [20].

**Table 3.** Global descriptors and log P for the set of flavonoids in Table 1

Structure	IE max	IP max	HOMO	SD	log P
1	99	606.5	-8.584	0.708	3.4
2	119	712.5	-8.761	0.226	2.9
3	103.5	627	-8.743	-0.160	2.5
4	125	769.5	16.020	-0.257	2.4
5	179	1063	-5.395	-0.450	2.2
6	263	1524	-4.962	0.322	3
7	99	594.5	-9.527	0.611	3.3
8	188	1119	-5.426	-0.160	2.5
9	99	591	-9.464	0.612	3.3
10	107	617.5	-9.687	0.419	3.1
11	122	696.5	-7.067	-0.257	2.4
12	114	693	-6.823	0.028	2.7
13	131	766.5	-9.584	-1.151	1.5
14	134	783	-7.762	-0.257	2.4
15	129	799.5	-9.175	0.515	3.2



Structure	IE max	IP max	HOMO	SD	log P
16	192	1159	-7.423	-0.319	1.4
17	135.5	783	-7.809	-1.411	1.4
18	135.5	823.5	-6.096	-1.313	1.1
19	158.5	972	-9.275	-0.572	1.1
20	136	807	-8.829	-0.855	1.8
21	119	712.5	-8.753	0.226	2.9
22	179	1044	-8.978	0.322	3
23	149	856.5	-6.833	0.129	2.8
24	153	946	-6.756	0.129	2.8
25	200	1154.5	-7.090	1.932	4.4
26	119	726.5	-8.270	0.147	1.8
27	123.5	760.5	-9.031	-0.450	2.2
28	148.5	894	-5.375	-0.546	2.1
29	146	887	-7.361	0.603	2.3
30	179	1044	-7.644	1.287	4
31	197	1216	-7.864	0.648	3.2
32	160.5	992	-8.134	0.405	3
33	125	769.5	-8.194	0.033	2.7
34	160.5	992	-8.244	0.405	3
35	142	871	-8.075	-0.494	2
36	234.5	1447.5	-7.262	1.283	3.8
37	215	1273	-5.723	0.206	2.9
38	119	726.5	-8.302	-1.222	1.4
39	119	750	-9.419	0.033	2.7
40	146	887	-7.380	-0.643	2

### 3.2. Data reduction and correlation weighting

In the step of data reduction, all the descriptors with the variance  $Var < 30\%$  and those with intercorrelation larger than 0.80 have been discarded. Correlation weighting was performed on all the positions in the hypermolecule, next the statistically non-significant positions were discarded. In case of the significant positions, the correlating coefficients are used to compose new local descriptors, by multiplying with the local weighted vectors (thus resulting new weighted vectors). Next, the local correlating descriptors are summed to give a global descriptor, denoted SD. This new descriptor, that is a linear combination of the local correlating descriptors for the significant positions in the hypermolecule (i.e. H13, H14, H19, H22, H27, H30 – Table 4), will be used as the basis of modeling log P (see below).

**Table 4.** Correlation weighting descriptors (see text)

<b>M<sub>i</sub></b>	<b>H13</b>	<b>H14</b>	<b>H19</b>	<b>H22</b>	<b>H27</b>	<b>H30</b>	<b>SD<sub>i</sub></b>
1	2.119	-1.411	0	0	0	0	0.708
2	0.675	-0.449	0	0	0	0	0.226
3	-0.479	0.319	0	0	0	0	-0.160
4	-0.769	0.512	0	0	0	0	-0.257
5	-1.346	0.896	0	0	0	0	-0.450
6	0.964	-0.642	0	0	0	0	0.322
7	1.830	-1.218	0	0	0	0	0.612
8	-0.480	0.319	0	0	0	0	-0.160
9	1.830	-1.218	0	0	0	0	0.612
10	1.253	-0.834	0	0	0	0	0.419
11	-0.769	0.512	0	0	0	0	-0.257
12	0.090	-0.065	0	0	0.003	0	0.028
13	-3.107	2.068	0	0	-0.113	0	-1.151
14	-0.769	0.512	0	0	0	0	-0.257
15	1.541	-1.026	0	0	0	0	0.515
16	-0.866	0.532	0	0.015	0	0	-0.319
17	-3.656	2.245	0	0	0	0	-1.411
18	-4.172	3.011	0	0	-0.151	0	-1.313
19	-1.557	0.956	0	0.028	0	0	-0.572
20	-2.307	1.536	0	0	-0.084	0	-0.855
21	0.675	-0.449	0	0	0	0	0.226
22	0.964	-0.642	0	0	0	0	0.322
23	0.386	-0.257	0	0	0	0	0.129
24	0.386	-0.257	0	0	0	0	0.129
25	5.006	-3.075	0	0	0	0	1.932
26	0.464	-0.309	0	-0.008	0	0	0.147
27	-1.346	0.896	0	0	0	0	-0.450
28	-1.635	1.088	0	0	0	0	-0.546
29	1.908	-1.270	0	-0.035	0	0	0.603
30	3.851	-2.564	0	0	0	0	1.287
31	1.541	-1.026	0.133	0	0	0	0.648
32	0.964	-0.642	0.083	0	0	0	0.405
33	0.098	-0.065	0	0	0	0	0.033
34	0.964	-0.642	0.083	0	0	0	0.405
35	-1.775	1.281	0	0	0	0	-0.494
36	3.274	-2.179	0.282	0	0	-0.094	1.283
37	0.675	-0.449	0	0	0	-0.019	0.206
38	-3.656	2.434	0	0	0	0	-1.222
39	0.098	-0.065	0	0	0	0	0.033
40	-1.924	1.281	0	0	0	0	-0.643

## 4. RESULTS AND DISCUSSION

### 4.1. QSAR models

The models were performed on the training set (the first 25 structures in Table 1) and the best results are listed below and in Table 5. The number of descriptors was limited to four, to fulfill the considerations of Topliss and Costello [23].

(i) Monovariate regression

$$\log P = 2.581 + 1.052 \times SD$$

(ii) Bivariate regression

$$\log P = 3.266 + 1.069 \times SD - 0.001 \times D3D$$

(iii) Three-variate regression

$$\log P = 5.099 + 0.934 \times SD - 0.003 \times Detour + 0.017 \times IE_{\max}$$

(iv) Four-variate regression

$$\log P = 4.995 + 0.932 \times SD + 0.042 \times Detour - 0.002 \times IE_{\max} - 0.005 \times IP_{\max}$$

**Table 5.** Best models for log P in the training set of flavonoids in Table 1.

	Descriptors	R <sup>2</sup>	Adjust. R <sup>2</sup>	St. Error	F
1	SD	<b>0.884</b>	0.879	0.279	176.25
2	N (no. heavy atoms)	0.041	0.001	0.804	0.991
3	Detour	0.034	0.008	0.807	0.809
4	IE max	0.001	0.043	0.821	0.018
5	SD, D3D	<b>0.914</b>	0.906	0.246	116.691
6	SD, Detour	0.906	0.897	0.258	105.648
7	SD, Distance	0.901	0.892	0.263	100.461
8	SD, IP max	0.898	0.889	0.268	96.983
9	SD, IE max	0.895	0.886	0.272	94.014
10	SD, Detour, IE max	<b>0.937</b>	0.929	0.215	105.092
11	SD, IE max, D3D	0.932	0.923	0.223	96.497
12	SD, Detour, D3D	0.920	0.909	0.242	80.897
13	SD, IE max, IP max	0.918	0.906	0.245	78.592
14	SD, Distance, IE max	0.914	0.902	0.252	74.255
15	SD, Detour, HOMO	0.907	0.894	0.262	68.326
16	SD, Distance, HOMO	0.902	0.888	0.268	64.692
17	SD, Detour, IE max, IP max	<b>0.950</b>	0.941	0.195	96.555
18	SD, D3D, Detour, IE max	0.939	0.927	0.217	77.033
19	SD, IE max, IP max, HOMO	0.923	0.908	0.243	60.388

One can see that, in monivariate regression, the usual alignment free descriptors, i.e. topological indices (Table 5, entries 2 to 4) correlate badly with  $\log P$ ; the only suitable descriptor is SD, that fits in the statistical hyperspace by an alignment procedure on the hypermolecule.

## 4.2. Model Validation

### (a) External Validation

The values  $\log P$  for the test set of flavonoids (Table 1, last 15 structures) were calculated by using the best equation in Table 5, entry 17. Data are listed in Table 6 and the monivariate correlation:

$$\log P = 0.054 + 1.004 \times \log P_{calc.}; n=15; R^2=0.768; s=0.366; F=42.956$$

is plotted in Figure 2.

**Table 6.** Calculated values of  $\log P$  for the molecules in the test set (Table 1)

Molecules	$\log P$ calc.	$\log P$
26	2.671	1.8
27	2.164	2.2
28	1.987	2.1
29	2.959	2.3
30	3.807	4
31	2.947	3.2
32	2.796	3
33	2.554	2.7
34	2.796	3
35	1.817	2
36	3.410	3.8
37	2.604	2.9
38	1.395	1.4
39	2.425	2.7
40	1.798	2

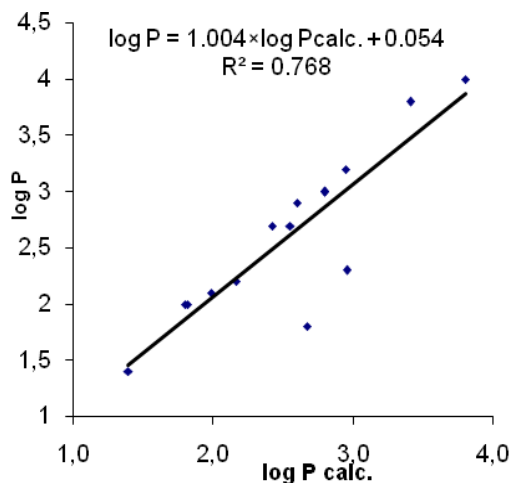


**Figure 2.** The plot  $\log P$  vs.  $\log P$  calc. for the test set (external validation)

### Similarity Cluster Validation

Validation can be performed by calculating  $\log P$  for the molecules in the test set with equations learned on clusters of similarity: each of the 15 molecules is the leader in its own cluster, selected by (2D) similarity among the 25 structures of the initial learning set. The values  $\log P$  calc. for each of the 15 molecules in the test set were computed by 15 new equations (the leader being left out) with the same descriptors as in eq. 17, Table 5. Data are listed in Table 7 and the monivariate correlation:  $\log P = -0.005 + 0.98 \times \log P_{calc.}$ ;  $n=15$ ;  $R^2=0.951$ ;  $s=0.168$ ;  $F= 252.005$  is plotted in Figure 3.

One can see that the prediction of  $\log P$  by the similarity clusters is far better than that obtained in the external validation, even in the learning set ( $R^2=0.951$  vs 0.950;  $s=0.168$  vs 0.195 and  $F=252.005$  vs 96.555).

**Table 7.** Calculated values of  $\log P$  by similarity clusters, for the molecules in the test set

Molecules	$\log P_{calc.}$	$\log P$
26	2.246	1.8
27	2.212	2.2
28	2.037	2.1
29	2.614	2.3
30	3.902	4
31	3.325	3.2
32	3.086	3
33	2.701	2.7
34	2.957	3
35	2.157	2
36	3.995	3.8
37	2.801	2.9
38	1.319	1.4
39	2.702	2.7
40	1.923	2

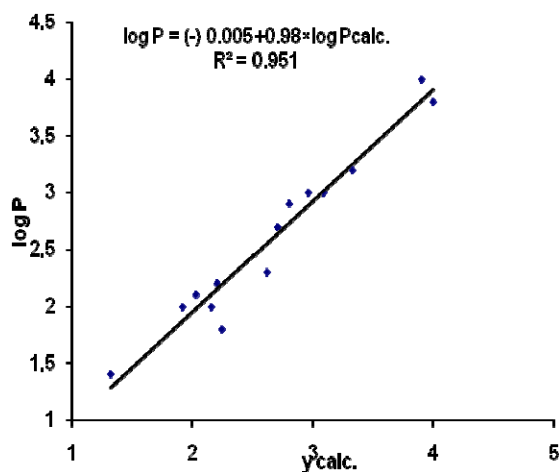


**Figure 3.** The plot  $\log P$  vs.  $\log P$  calc. by similarity clusters

The explication of this exceptional result is that, by clustering, one obtains a set of quasi-congeners, thus making possible the basic paradigm of QSAR: similar structures show similar properties. The cluster populations can be varied to obtain the best estimation within each cluster and thus a best prediction. This represents a new correlating procedure, we call "direct prediction" and it can be performed even without previous learning steps.

## CONCLUSIONS

A set of 40 flavonoids, downloaded from the PubChem database, was submitted to a qsar study by using the hypermolecule concept, in a procedure similar to that of the „alignment" of drug molecules to the biological receptors. In fact, the hypermolecule mimics the investigated correlational space, within the correlation weighting analysis. The best models have been validated in the external test set and in a new version of validation/prediction by using clusters of similarity, that favorise apparition of „quasi-congeneric" state, mandatory for a best correlation.

## ACKNOWLEDGEMENTS

I am thankful fo Professor Mircea V. Diudea for helpful discussion.

## REFERENCES

1. P.G. Pietta, *J Nat Prod*, **2000**, 63, 1025.
2. K. Wolfe, X. Wu, R.H. Liu, *J Agric Food Chem*, **2003**, 51,609.
3. A. Scalbert, G. Williamson, *J Nutr*, **2000**, 130, 2073.
4. S.A. Payán-Gómez, N. Flores-Holguín, A. Pérez-Hernández, M. Piñón-Miramontes and D. Glossman-Mitnik, *Chemistry Central Journal*, **2010**, 4, 12, 1.
5. C. Hansch, P.P. Maloney, T. Fujita, R.M. Muir, *Nature*, **1962**, 194, 178.
6. C. Hansch, D. Hoekman, A. Leo, D. Weininger, C.D. Selassie, *Chem. Rev.*, **2002**, 102, 783.
7. C.D. Selassie, R. Garg, S. Kapur, A. Kurup, R.P. Verma, S.B. Mekapati, C. Hansch, *Chem. Rev.* **2002**, 102, 2585.
8. R.P. Verma, A. Kurup, S.B. Mekapati, C. Hansch, *Bioorg. Med. Chem.* **2005b** 13, 933.
9. C. Hansch, A. Leo, *American Chemical Society: Washington, DC*, **1995**.
10. P. Willet, *J. Chem. Inf. Model.*, **2013**, 53, 1.

11. G.B. McGaughey, R.P. Sheridan, C.I. Bayly, J.C. Culberson, C. Kretsoulas, S. Lindsley, V. Maiorov, J.-F. Truchon, W.D. Cornell, *J. Chem. Inf. Model.*, **2007**, 47, 1504.
12. R.P. Sheridan, *Drug Discovery*, **2007**, 2, 423.
13. R.P. Sheridan, S.K. Kearsley, *Drug Discovery Today*, **2002**, 7, 903.
14. P. Willett, *J. Chem. Inf. Comput. Sci.* **1998**, 38, 983.
15. A.A. Toropov, A.P. Toropova, *Internet El. J. Molec. Design*, **2002**, 1, 108.
16. A.A. Toropov, A.P. Toropova, *J. Mol. Struct. (Theochem)* **2001**, 538, 287.
17. M. Randić, *J. Chem. Inf. Comput. Sci.* **1995**, 35, 373.
18. M. Randić, *New J. Chem.* **1995**, 196, 781.
19. L.B. Kier, L.H. Hall, *J. Pharm. Sci.* **1981**, 70, 583.
20. O. Ursu, M. V. Diudea, TopoCluj software program. Babes-Bolyai University, Cluj, 2005.
21. PubChem database, accessed 23.05. 2013.
22. A.T. Balaban, A. Chiriac, I. Motoc and Z. Simon, *Steric Fit in QSAR (Lectures Notes in Chemistry*, Vol. 15), Springer, Berlin, **1980**, Chap. 6.21.
23. J.G. Topliss and R.J. Costello, *J. Med. Chem.* **1972**, 15, 1066.

## A NOVEL QSAR APPROACH IN MODELING HYDROPHOBICITY OF A SET OF FLAVONOIDS

ALEXANDRA MARIA HARSA<sup>a</sup>

**ABSTRACT.** A novel QSAR approach, based on correlation weighting and alignment over a hypermolecule, that mimics the investigated correlational space, was performed on a set of 40 flavonoids, downloaded from the PubChem database. The best models describing log P of this set of flavonoids were validated in the external test set and in a new version of prediction by using similarity clusters.

**Key-words:** QSAR, log P, flavonoids, correlation weighting, similarity clustering.

### 1. INTRODUCTION

Quantitative structure-activity relationships (QSAR) mathematically relate descriptors of a molecular structure to a biological activity (or a physico-chemical property involved in that activity). A structure-activity relationship can indicate which features of a given molecule are responsible for its activity, thus making possible to synthesize new and more potent compounds with enhanced biological activity [1,2]. QSAR analysis is based on the assumption that the activity of compounds is a function of their structural characteristics [3].

Molecular similarity was extensively and successfully used in drug discovery, often to compare molecules in the absence of other mechanistic information [4-6]. Reasons for the increasing popularity of similarity based methods include technological advances in high throughput screening and synthesis in the last decade and the need of applications of computer based methods in compound selection and activity evaluation [7]. Similarity search [8,9] and clustering methods [9,10] can be used to classify compounds into structural groups [11] and in prediction of biological activities as well [12]. The paradigm of similarity-based QSAR approaches was explicitly enounced by Johnson and Maggiora [13,14]: "*molecules that are structurally similar likely will have similar properties*". Thus, when the activity of a set of molecules is

---

<sup>a</sup> Babes-Bolyai University, Department of Chemistry, Faculty of Chemistry and Chemical Engineering, Arany Janos 11, 400028, Cluj, Romania, maria\_sanda\_13@yahoo.com



unknown, one can predict that activity by taking into account the similarity values between the molecules under study and the molecules of a data set whose activities are known.

Studies of similarity [15] in chemical structures can be overtaken by using topological indices [16]. Among thousands of such topological descriptors, the Cluj indices have been defined by Diudea [17,18], as follows.

A Cluj fragment  $CJ_{i,j,p}$  collects vertices  $v$  lying closer to  $i$  than to  $j$ , the endpoints of a path  $p(i,j)$ . Such a fragment collects the vertex proximities of  $i$  against any vertex  $j$ , joined by the path  $p$ , with the distances measured in the subgraph  $D_{(G-p)}$ , as shown in the following equation:

$$CJ_{i,j,p} = \left\{ v \mid v \in V(G); D_{(G-p)}(i, v) < D_{(G-p)}(j, v) \right\}$$

In graphs containing rings, more than one path could join the pair  $(i, j)$ , thus resulting more than one fragment related to  $i$  (with respect to  $j$  and a given path  $p$ ). The entries in the Cluj matrix are taken, by definition, as the maximum cardinality among all such fragments:

$$[UCJ]_{i,j} = \max_p |CJ_{i,j,p}|$$

Indices  $I_e$  and  $I_p$  are calculated, from the Cluj topological matrices  $UCJ_e$ , and  $UCJ_p$ , respectively (see above), as half sum of matrix entries. In the above symbols,  $e$  refers to edge-calculated matrix while  $p$  refers to the path-calculated ones.

Correlation weighting [19] was used as a weighting scheme applied to local descriptors. Within this paper, we used the correlation weighting in the frame of a hypermolecule built on the overall set of structures taken in study (see below).

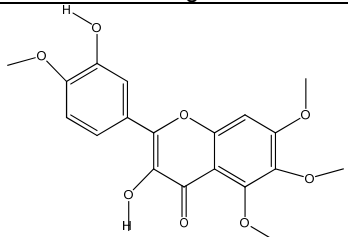
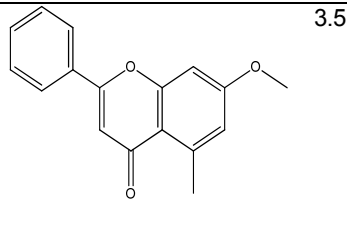
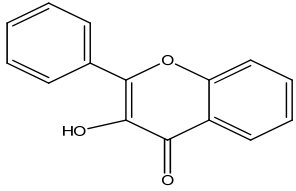
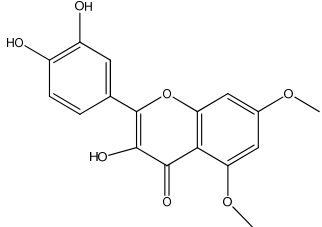
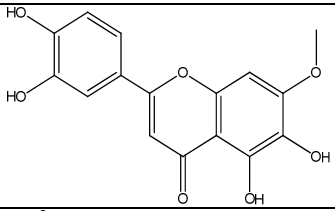
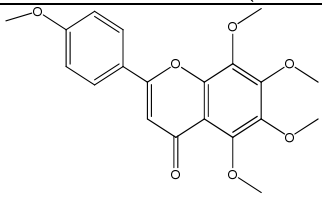
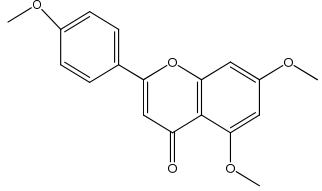
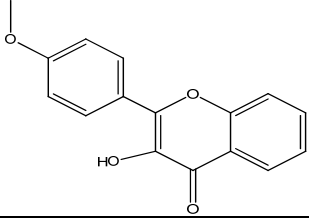
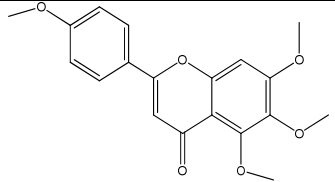
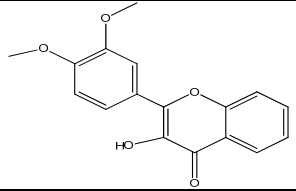
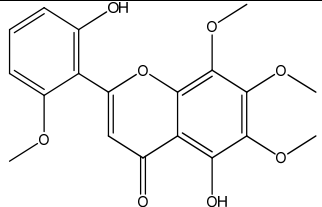
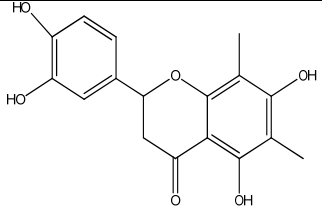
The article proposes a new approach called "direct prediction" which develops clusters of similar structures aimed to be quasi-congeneric subsets in predicting of a biological activity.

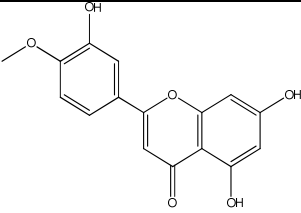
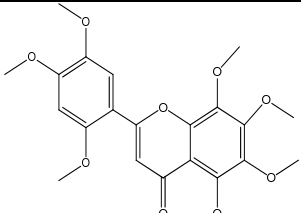
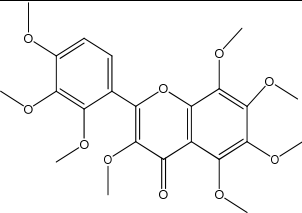
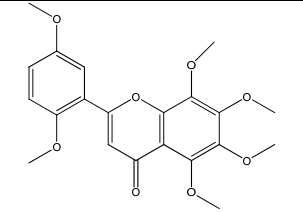
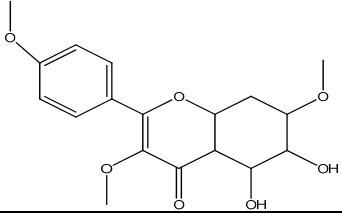
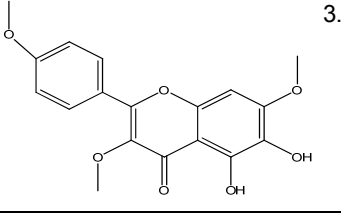
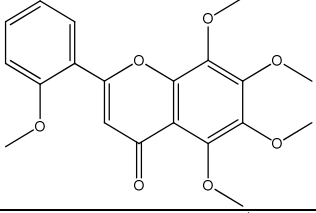
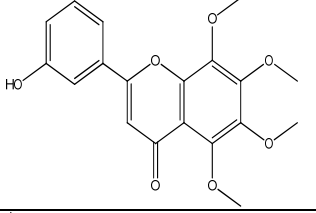
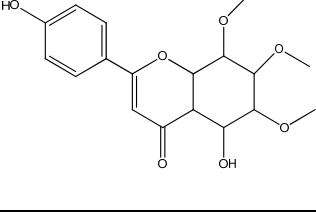
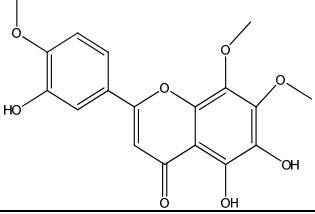
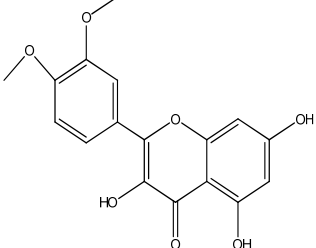
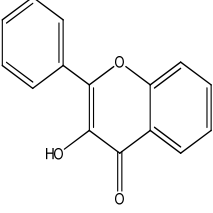
## 2. STRUCTURAL DATA

A set of 40 flavonoids were taken from PubChem Database (Table 1) and were divided into a training set (30 molecules) and a test set (ten molecules), taken randomly. The property chosen for modeling was  $\log P$  (see Table 1), the (calculated) partition coefficient between n-octanol and water, a measure of hydrophobicity, involved in the passive transport of a drug molecule through cell membrane.

A hypermolecule (Figure 1) was built up as the union of all structural features in all 40 molecules under study. The hypermolecule is considered to mimics the investigated statistical hyperspace [20].

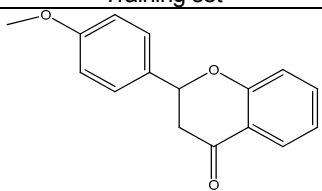
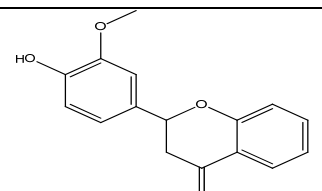
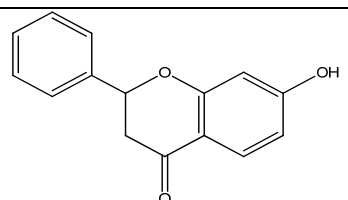
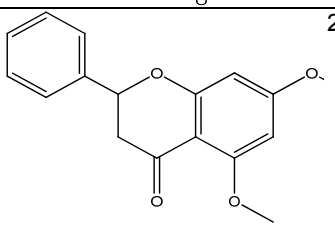
**Table 1.** Flavonoid molecular structures and their log P (from PubChem)

Structures		log P	Structures		log P
Training set					
1		2.8	2		3.5
3		3.4	4		1.6
5		2.3	6		3
7		2.2	8		3.4
9		3.1	10		3.3
11		2.9	12		2.8

Structures		log P	Structures		log P
Training set					
13		1.7	14		3
15		3.2	16		3
17		2.9	18		3.1
19		3	20		2.7
21		3.1	22		2.6
23		2.2	24		2.6

A NOVEL QSAR APPROACH IN MODELING HYDROPHOBICITY OF A SET OF FLAVONOIDS

Structures		log P	Structures		log P
Training set					
25		2.6	26		3.8
27		1.5	28		2.3
29		1.8	30		3.1
Test set					
31		2.6	32		1.5
33		1.7	34		3.2
35		2.1	36		2.8

	Structures	log P		Structures	log P
	Training set				
37		3.1	38		2.5
39		2.7	40		2.8

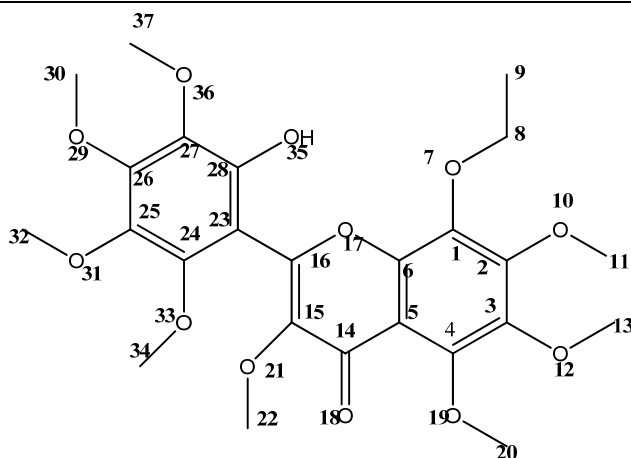


**Figure 1.** The hypermolecule comprising the common features of the dataset

### 3. METHOD

The structures have been optimized in Hyperchem, at PM3 level of theory. Topological indices implemented in TOPOCLUJ software [21] have been computed for all the structures. A selection of these indices is listed in Table 2.

#### 3.1. Alignment over the hypermolecule

By aligning all the molecular structures over the hypermolecule, a binary vector (Table 3) was assigned to each molecule: 1-for a common feature in a given position of the hypermolecule and 0- for an empty position.

Next, the binary vector was weighted by the mass of “hydride” fragments composing each molecule. The weighted vector was used in the data-reduction step and correlation weighting procedure [22].

**Table 2.** Topological descriptors computed for the flavonoids in Table 1.

Structure	logP	SD	Detour	IEmax.
1	2.8	0.167	3197	325
2	3.5	0.462	1781	138.5
3	3.4	0.244	1431	107
4	1.6	-0.907	2690	249.5
5	2.3	-0.109	2424	214.5
6	3	0.204	3480	369.5
7	2.2	-0.326	2444	232.5
8	3.4	0.244	1800	158.5
9	3.1	0.323	3203	334
10	3.3	0.157	2225	218
11	2.9	0.170	3564	386
12	2.8	0.399	2422	204.5
13	1.7	-1.117	2200	192
14	3	0.204	4802	570.5
15	3.2	0.292	5546	672.5
16	3	0.204	4180	475.5
17	2.9	0.245	2936	294.5
18	3.1	0.327	2936	294.5
19	3	0.204	3556	388.5
20	2.7	0.072	3205	322.5
21	2.8	0.148	3170	309
22	2.6	0.041	3191	314.5
23	2.2	-0.419	2695	263
24	2.6	-0.457	1431	107
25	2.6	0.095	1986	164
26	3.8	0.846	2966	308.5
27	1.5	-1.396	2212	187.5
28	2.3	-0.279	1789	138
29	1.8	-0.977	1990	162
30	3.1	0.492	3522	367
31	2.6	-0.429	2420	222
32	1.5	-1.396	2225	194
33	1.7	-0.791	1779	135.5
34	3.2	0.069	1254	85
35	2.1	-0.429	1602	114
36	2.8	-0.281	1414	103.5
37	3.1	-0.018	1592	131
38	2.5	-0.544	1789	153
39	2.7	0.279	1594	114
40	2.8	0.267	1994	169.5

**Table 3.** The binary vectors, cf. hypermolecule, for the 40 flavonoids.

	1	2	3	4	5	6	7	8	9	10	11	12	13	14	15	16	17	18	19	20	
1	1	1	1	1	1	1	0	0	0	1	1	1	1	1	1	1	1	1	1	1	0
2	1	1	1	1	1	1	0	0	0	1	1	0	0	1	1	1	1	1	1	0	0
3	1	1	1	1	1	1	0	0	0	0	0	0	0	1	1	1	1	1	1	0	0
4	1	1	1	1	1	1	0	0	0	1	1	0	0	1	1	1	1	1	1	1	1
5	1	1	1	1	1	1	0	0	0	1	1	1	0	1	1	1	1	1	1	1	0
6	1	1	1	1	1	1	1	1	1	1	1	1	1	1	1	1	1	1	1	1	1
7	1	1	1	1	1	1	0	0	0	1	1	0	0	1	1	1	1	1	1	1	1
8	1	1	1	1	1	1	0	0	0	0	0	0	0	1	1	1	1	1	1	0	0
9	1	1	1	1	1	1	0	0	0	1	1	1	1	1	1	1	1	1	1	1	1
10	1	1	1	1	1	1	0	0	0	0	0	0	0	1	1	1	1	1	1	0	0
11	1	1	1	1	1	1	1	1	1	1	1	1	1	1	1	1	1	1	1	1	0
12	1	1	1	1	1	1	0	0	0	1	0	0	0	1	1	1	1	1	1	1	0
13	1	1	1	1	1	1	0	0	0	1	0	0	0	1	1	1	1	1	1	1	0
14	1	1	1	1	1	1	1	1	0	1	1	1	1	1	1	1	1	1	1	1	1
15	1	1	1	1	1	1	1	1	0	1	1	1	1	1	1	1	1	1	1	1	1
16	1	1	1	1	1	1	1	1	0	1	1	1	1	1	1	1	1	1	1	1	1
17	1	1	1	1	1	1	0	0	0	1	1	1	0	1	1	1	1	1	1	1	0
18	1	1	1	1	1	1	0	0	0	1	1	1	0	1	1	1	1	1	1	1	0
19	1	1	1	1	1	1	1	1	0	1	1	1	1	1	1	1	1	1	1	1	1
20	1	1	1	1	1	1	1	1	0	1	1	1	1	1	1	1	1	1	1	1	1
21	1	1	1	1	1	1	1	1	0	1	1	1	1	1	1	1	1	1	1	1	0
22	1	1	1	1	1	1	1	1	0	1	1	1	0	1	1	1	1	1	1	1	0
23	1	1	1	1	1	1	0	0	0	1	0	0	0	1	1	1	1	1	1	1	0
24	1	1	1	1	1	1	0	0	0	0	0	0	0	1	1	1	1	1	1	0	0
25	1	1	1	1	1	1	0	0	0	1	1	0	0	1	1	1	1	1	1	1	0
26	1	1	1	1	1	1	0	1	1	1	0	0	0	1	1	1	1	1	1	0	0
27	1	1	1	1	1	1	0	0	0	1	0	0	0	1	1	1	1	1	1	1	0
28	1	1	1	1	1	1	0	0	0	1	0	0	0	1	1	1	1	1	1	1	0
29	1	1	1	1	1	1	0	0	0	1	0	0	0	1	1	1	1	1	1	1	0
30	1	1	1	1	1	1	1	1	0	1	1	0	0	1	1	1	1	1	1	1	0
31	1	1	1	1	1	1	0	0	0	1	1	1	1	1	1	1	1	1	1	0	0
32	1	1	1	1	1	1	0	0	0	1	0	0	0	1	1	1	1	1	1	1	0
33	1	1	1	1	1	1	0	0	0	1	0	1	0	1	1	1	1	1	1	1	0
34	1	1	1	1	1	1	0	0	0	0	0	0	0	1	1	1	1	1	1	0	0
35	1	1	1	1	1	1	1	0	0	0	0	0	0	1	1	1	1	1	1	1	0
36	1	1	1	1	1	1	0	0	0	0	0	0	0	1	1	1	1	1	1	0	0
37	1	1	1	1	1	1	0	0	0	0	0	0	0	1	1	1	1	1	1	0	0
38	1	1	1	1	1	1	0	0	0	0	0	0	0	1	1	1	1	1	1	0	0
39	1	1	1	1	1	1	0	0	0	1	0	0	0	1	1	1	1	1	1	1	0
40	1	1	1	1	1	1	0	0	0	1	1	0	0	1	1	1	1	1	1	1	1

### 3.2. Data reduction and correlation weighting

In the step of data reduction, all the descriptors with the variance  $\text{Var} < 30\%$  and those with intercorrelation larger than 0.80 have been discarded.

Correlation weighting was performed on all the positions in the hypermolecule: the correlating coefficients of the statistically significant positions of the hypermolecule were used to multiply the local descriptors, actually the mass fragments, thus resulting new weighted vectors  $CD_{ij}$ . Next,

the local correlating descriptors are summed to give a global descriptor,  $SD_i = \sum_j CD_{ij}$ . This new descriptor is a linear combination of the local correlating descriptors for the significant positions in the hypermolecule (i.e. H1, H3, H7, H8, H10, H11, H12, H19 – Table 4). It correlates with log P as below:

$$\log P = 2.783 + 0.999 \times SD$$

$$N=40; R^2=0.845; s=0.230; F = 206.616$$

The summative descriptor SD will be used as the basis for modeling log P.

**Table 4.** Correlation weighted descriptors (see text)

Structure	SD	H1	H3	H7	H8	H10	H11	H12	H19
1	0.167	-0.464	0.671	0	0	0.222	-0.119	-0.062	-0.080
2	0.462	-0.586	0.918	0	0	0.280	-0.151	0	0
3	0.244	-0.431	0.676	0	0	0	0	0	0
4	-0.907	1.449	-2.270	0	0	-0.693	0.372	0	0.234
5	-0.109	0.309	-0.447	0	0	-0.148	0.080	0.044	0.053
6	0.204	-0.661	1.036	0.149	-0.266	0.342	-0.184	-0.096	-0.116
7	-0.326	0.521	-0.816	0	0	-0.249	0.134	0	0.084
8	0.244	-0.431	0.676	0	0	0.000	0	0	0
9	0.323	-0.871	1.259	0	0	0.416	-0.224	-0.117	-0.141
10	0.157	-0.277	0.434	0	0	0	0	0	0
11	0.170	-0.571	0.894	0.129	-0.230	0.296	-0.159	-0.083	-0.106
12	0.399	-0.428	0.671	0	0	0.236	0	0	-0.080
13	-1.117	1.238	-1.939	0	0	-0.629	0	0	0.213
14	0.204	-0.661	1.036	0.149	-0.266	0.342	-0.184	-0.096	-0.116
15	0.293	-0.946	1.483	0.214	-0.381	0.490	-0.264	-0.138	-0.166
16	0.204	-0.661	1.036	0.149	-0.266	0.342	-0.184	-0.096	-0.116
17	0.245	-0.667	0.969	0	0	0.296	-0.159	-0.088	-0.106
18	0.327	-0.928	1.342	0	0	0.444	-0.239	-0.132	-0.160
19	0.204	-0.661	1.036	0.149	-0.266	0.342	-0.184	-0.096	-0.116
20	0.072	-0.233	0.365	0.053	-0.094	0.121	-0.065	-0.034	-0.041
21	0.148	-0.464	0.727	0.097	-0.172	0.222	-0.119	-0.062	-0.080
22	0.041	-0.143	0.224	0.032	-0.057	0.074	-0.040	-0.022	-0.027
23	-0.419	0.464	-0.727	0	0	-0.236	0	0	0.080
24	-0.457	0.806	-1.263	0	0	0	0	0	0
25	0.095	-0.155	0.242	0	0	0.074	-0.039	0	-0.027
26	0.846	-0.969	1.645	0	-0.364	0.534	0	0	0
27	-1.396	1.547	-2.423	0	0	-0.786	0	0	0.266
28	-0.279	0.309	-0.485	0	0	-0.157	0	0	0.053
29	-0.977	1.083	-1.696	0	0	-0.550	0	0	0.186
30	0.492	-0.856	1.454	0.193	-0.345	0.444	-0.239	0	-0.160
31	-0.429	0.806	-1.165	0	0	-0.385	0.207	0.108	0
32	-1.396	1.547	-2.423	0	0	-0.786	0	0	0.266
33	-0.791	1.238	-1.789	0	0	-0.629	0	0.176	0.213
34	0.069	-0.122	0.191	0	0	0	0	0	0
35	-0.429	0.571	-0.969	-0.137	0	0	0	0	0.106
36	-0.281	0.497	-0.778	0	0	0	0	0	0
37	-0.019	0.033	-0.051	0	0	0	0	0	0
38	-0.544	0.961	-1.505	0	0	0	0	0	0
39	0.279	-0.309	0.485	0	0	0.157	0	0	-0.053
40	0.267	-0.407	0.638	0	0	0.207	-0.105	0	-0.066



## 4. RESULTS AND DISCUSSION

### 4.1. QSAR models

The models were performed on the training set (the first 30 structures in Table 1) and the best results (in decreasing order of  $R^2$ ) are listed below and in Table 5.

(i) Monivariate regression

$$\log P = 2.739 + 1.028 \times SD$$

(ii) Bivariate regression

$$\log P = 3.011 + 0.995 \times SD + 0.033 \times HOMO$$

(iii) Three-variate regression

$$\log P = 4.153 + 0.970 \times SD - 0.002 \times Detour + 0.013 \times IE_{max}$$

(iv) Four-variate regression

$$\log P = 4.149 + 0.969 \times SD - 0.00001 \times D3D - 0.002 \times Detour + 0.013 \times IE_{max}$$

**Table 5.** Best models in describing log P in the training set of flavonoids in Table 1

	Descriptors	$R^2$	Adjust. $R^2$	St. Error	F
1	SD	<b>0.882</b>	<b>0.878</b>	<b>0.200</b>	<b>209.213</b>
2	IE max	0.240	0.213	0.508	8.863
3	Detour	0.213	0.185	0.517	7.592
4	SD, HOMO	0.885	0.877	0.201	104.767
5	SD, IP max	0.882	0.874	0.203	101.818
6	SD, D3D	0.882	0.873	0.204	100.883
7	SD, Distance	0.882	0.873	0.204	100.930
8	SD, Detour	0.882	0.873	0.204	100.908
9	SD, IE max	0.882	0.873	0.203	101.567
10	SD, Detour, IE max	<b>0.934</b>	<b>0.926</b>	<b>0.156</b>	<b>122.133</b>
11	SD, Distance, IE max	0.906	0.895	0.185	83.746
12	SD, IE max, D3D	0.904	0.893	0.188	81.449
13	SD, C, HOMO	0.888	0.875	0.203	68.442
14	SD, IE max, IP max	0.887	0.873	0.204	67.791
15	SD, IP max, HOMO	0.886	0.873	0.205	67.317
16	SD, Distance, HOMO	0.886	0.873	0.204	67.417
17	SD, Detour, D3D	0.885	0.872	0.205	67.046
18	SD, IE max, HOMO	0.885	0.872	0.204	67.267
19	SD, D3D, Detour, IE max	<b>0.933</b>	<b>0.923</b>	<b>0.159</b>	<b>88.080</b>
20	SD, IE max, IP max, HOMO	0.892	0.874	0.203	51.509

## 4.2. Model Validation

An essential factor related to QSAR development is represented by the model validation. In this respect, Y-randomization and external validation Golbraikh-Tropsha procedure are required in order to confirm the statistical significance and predictive abilities of the obtained QSAR models [23].

### (a) External Validation

The values  $\log P$  for the test set of flavonoids were calculated by using equation cf. entry 10, Table 5. Data are listed in Table 6 and the monivariate correlation:  $\log P = 0.125 + 0.976 \times \log P_{calc.}$ ;  $n=10$ ;  $R^2=0.887$ ;  $s=0.217$ ;  $F=62.525$  is plotted in Figure 2. One can see that Golbraikh-Tropsha criteria are fulfilled ( $R^2_{pred}>0.8$ ) [23].

**Table 6.** Calculated values of  $\log P$  for themolecules in the test set (Table 1)

Molecules	$\log P_{calc.}$	$\log P$
2	3.195	3.5
3	3.204	3.4
12	2.840	2.8
24	2.524	2.6
27	1.255	1.5
34	3.066	3.2
35	2.333	2.1
36	2.679	2.8
37	2.973	3.1
39	3.035	2.7

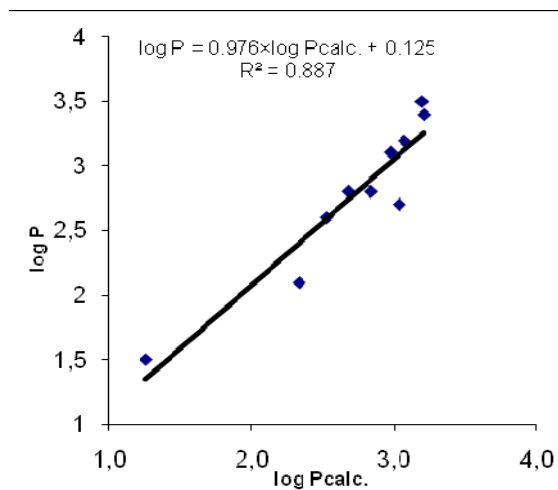


**Figure 2.** The plot  $\log P$  vs.  $\log P_{calc.}$  for the test set (external validation)

### (b) Similarity Cluster Validation

Validation can also be performed by calculating  $\log P$  for the molecules in the test set by using clusters of similarity: each of the 10 molecules is the leader of its own cluster, selected by 2D similarity among the 30 structures of the initial learning set. The values  $\log P_{calc.}$  were computed by 10 new equations (the leader being left out) with the same descriptors as in eq. 10, Table5. Data are listed in Table 7 and the monivariate correlation:

$$\log P = -0.002 + 1.028 \times \log P_{calc.}; n=10; R^2=0.909; s=0.194; F= 80.033$$

is plotted in Figure 3.

One can see that the prediction of log P by the similarity clusters is better than that obtained in the external validation. This is because the similarity procedure provides a set of quasi-congeners, thus making possible the basic paradigm of QSAR: similar structures show similar properties.

**Table 7.** Calculated values of log P by similarity clusters, for the molecules in the test set

Molecules	log P calc.	log P
2	3.132	3.5
3	3.169	3.4
12	2.772	2.8
24	2.585	2.6
27	1.305	1.5
34	3.057	3.2
35	2.268	2.1
36	2.693	2.8
37	3.023	3.1
39	2.955	2.7

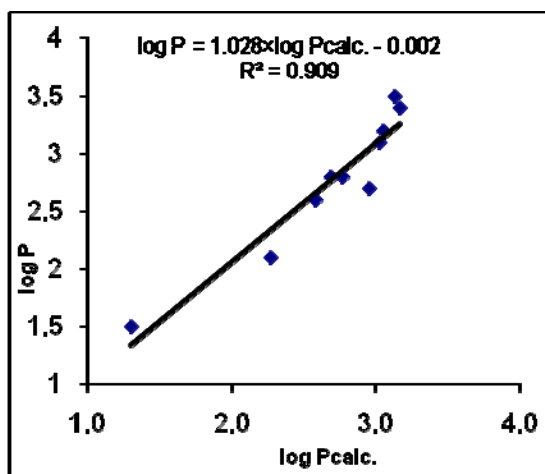


**Figure 3.** The plot log P vs. log P calc. by similarity clusters

## CONCLUSIONS

A novel QSAR approach, based on correlation weighting within the hypermolecule, considered to mimic the investigated correlational space, was performed on a set of 40 flavonoids, downloaded from the PubChem database. The set was split into a learning set and a test set, the last one being used for the validation of the models, in the so-called „external set validation”. Also, the validation was made by a new version of prediction by using similarity clusters. The similarity clustering permitted realization of „quasi-congeneric” set of structures, thus providing a better prediction than the classical external validation procedure.

## ACKNOWLEDGEMENTS

I am thankful fo Professor Mircea V. Diudea for helpful discussion.

## REFERENCES

1. W.E. Dismukes, *Clinical Infectious Diseases*, **2000**, 30, 653.
2. T.A. Özlem, *Turk J Med Sci*, **2001**, 31, 493.
3. D. Rogers, and A.J. Hopfinger, *J. Chem. Inf. Comput. Sci.*, **1994**, 34, 854.
4. R.P. Sheridan, S.K. Kearsley, *Drug Discov. Today*, **2002**, 7, 903.
5. H.J. Bohm, G. Schneider, *Wiley-VCH*, Weinheim, **2000**.
6. G. Schneider, H.J. Bohm, *Drug Discov. Today* **2002**, 7, 64.
7. J.A. DiMasi, R.W. Hansen, H.G. Grabowski, *J. Health Econ.*, **2003**, 22, 151.
8. P.M. Dean, *Blackie Academic*, London, **1995**.
9. P. Willet, *Research Studies Press Ltd*: Letchworth, U.K., **1987**.
10. J.M. Barnard, G.M. Downs, *J. Chem. Inf. Comput. Sci.*, **1992**, 32, 644.
11. D.J. Wild, C.J. Blankey, *J. Chem. Inf. Comput. Sci.*, **2000**, 40(1), 155.
12. R.D. Brown, Y.C. Martin, *J. Chem. Inf. Comput. Sci.*, **1996**, 36, 572.
13. M.A. Johnson, G.M. Maggiora, Eds., John Wiley & Sons, New York, **1990**.
14. C.D. Moldovan, A. Costescu, G. Katona and M.V. Diudea, *MATCH Commun. Math. Comput. Chem.*, **2008**, 60, 977.
15. P. Willett, *J. Chem. Inf. Comput. Sci.*, **1998**, 38, 983.
16. M. Randić, *J. Chem. Inf. Comput. Sci.* **1995**, 35, 373.
17. M.V. Diudea, *MATCH Commun. Math. Comput. Chem.* **1997**, 35, 169.
18. M.V. Diudea, *J. Chem. Inf. Comput. Sci.*, 1997, 37, 300.
19. A.A. Toropov, and A.P. Toropova, *Internet El. J. Molec. Design*, **2002**, 1, 108.
20. A.T. Balaban, A. Chiriac, I. Motoc, and Z. Simon, *Steric Fit in QSAR (Lectures Notes in Chemistry*, Vol. 15), Springer, Berlin, **1980**, Chap. 6.21.
21. O. Ursu, M.V. Diudea, "TOPOCLUJ software program", Babes-Bolyai University, Cluj, **2005**.
22. A. A. Toropov, A. P. Toropova, *J. Mol. Struct. (Theochem)* **2001**, 538, 287.
23. A. Golbraikh, A. Tropsha, *J Comp Aided Mol Des*, **2002**, 16, 357.



## INFLUENCE OF MICROWAVE FIELD ON THE ASCORBIC ACID CONTENT IN LEAVES OF SOME COMMON AROMATIC PLANTS IN ROMANIA

MANUELA STAN<sup>a</sup>, MARIA LOREDANA SORAN<sup>a\*</sup>,  
CODRUȚA VARODI<sup>a</sup>, ILDIKO LUNG<sup>a</sup>

**ABSTRACT.** The present work reports the variation of the ascorbic acid content in leaves of parsley, dill and celery plants grown in microwave fields of two microwave frequency domains: GSM (mobile communication) and WLAN (wireless internet connection). The percentage increase in ascorbic acid content of irradiated plants reported to control plants was calculated. The ascorbic acid was identified and quantified by high-performance liquid chromatography (HPLC) and electrochemical methods. The experiments were performed on Grace Alltima C18 column (100 x 3 mm, 3  $\mu$ m) thermostated at 30°C with gradient elution. The mobile phase used for chromatographic separation consists of 15 mM potassium phosphate buffer at pH 2.7 and methanol. Electrochemical experiments employed chronoamperometry using a typical three-electrode electrochemical cell. Amperometric measurements were carried out under magnetic stirring using 0.1 M phosphate buffer solution (pH 6.8) as supporting electrolyte. Our study showed different percentage increases in ascorbic acid content of microwave irradiated plants determined by HPLC and electrochemical method, respectively, with lowest values (6.8%, 11%) in parsley irradiated with WLAN frequency microwaves, and highest values (more than 200%) in celery irradiated with GSM frequency microwaves.

**Keywords:** *ascorbic acid, HPLC, chronoamperometry, microwave effects on plant growth, aromatic plants*

### INTRODUCTION

Within the last years, there was an exponential increase in the use of mobile phones and wireless devices, causing an increased level of electromagnetic radiation that can potentially affect all living organisms [1; 2]. Consequently, many scientific reports are focused on the germination process

---

<sup>a</sup> National Institute for Research and Development of Isotopic and Molecular Technologies, 65-103 Donath, 400293 Cluj-Napoca. Romania, \* loredana.soran@itim-cj.ro

as well as the development stages of the plants after their exposure to various magnetic fields [3-6]. As a result of their studies, authors concluded that seeds germinate quickly under magnetic field influence, and the plant roots are thicker, longer and exhibit a larger area depending on the exposure time and magnetic field strength [4]. Parsley (*Petroselinum crispum*), dill (*Anethum graveolens*) and celery (*Apium graveolens*), leafy vegetables belonging to the Umbelliferae (Apiaceae) family and among the most frequently used culinary plants growing in Romania, are important sources of minerals, vitamins (e.g. vitamins B, C, E), and other components such as carotenoids, chlorophylls and polyphenols [7, 8].

Vitamin C, also known as ascorbic acid (AA), L-ascorbic acid or L-ascorbate, is a valuable vitamin for human organism. Ascorbic acid is easily oxidized to form dehydroascorbic acid (DHAA), oxidation being reversible [9]. Besides its role to prevent scurvy, many other health benefits have been attributed to ascorbic acid such as antioxidant, anti-carcinogenic, immunomodulator and cold prevention [10]. Experimental studies have shown that ascorbic acid has an essential role in plant growth [11, 12].

Ascorbic acid (vitamin C) is an essential vitamin for human nutrition, thus knowing its content in diverse food sources and how it is affected by external factors has become an important research topic. Different studies reported the change in the ascorbic acid content in plants under the influence of various factors such as genotypic differences, preharvest and postharvest factors [13], drought stress [14, 15], temperature increase [16], ozone stress [17, 18], electromagnetic radiations [19, 20]. It was shown that stress factors affect different physiological and biochemical parameters of plants and activate plant defense mechanisms through their antioxidant defense systems [17].

The aim of the present study was to investigate the effect of microwaves in the GSM (mobile communication) and WLAN (wireless internet connection) frequency domains, on the ascorbic acid content in leaves of parsley, dill and celery. Our study consists of a comparative evaluation of the experimental results obtained for irradiated and control (non-irradiated) plants by HPLC and electrochemical methods, respectively.

## RESULTS AND DISCUSSION

### HPLC method

The HPLC method coupled with diode array detection (HPLC-DAD) was developed for identification and quantification of ascorbic acid in parsley, dill and celery leaf extracts. The ascorbic acid was quantified by external standard method following the validation protocol described in a previous work

[21]. The HPLC detection was carried out at 243 nm. In a previous work [21], the retention time of ascorbic acid in plant extracts was found to be 1.85 min. The regression equation was expressed as  $y = 6E+07x - 9E+06$  (where  $x$ –concentration,  $y$ –area), and the coefficient of correlation ( $R^2$ ) was 0.9986. The limit of detection (0.2  $\mu\text{g/mL}$ ) and the limit of quantification (0.22  $\mu\text{g/mL}$ ) were determined by a method previously described [22]. Working ascorbic acid standard solutions in the concentration range 0.3 – 1  $\mu\text{g/mL}$  were prepared by successive dilutions with ultrapure water from a stock solution of ascorbic acid (1  $\mu\text{g/mL}$ ).

Overlay of HPLC chromatograms of the extracts (the peaks corresponding to ascorbic acid) registered for irradiated and non-irradiated plants have shown an increase in the ascorbic acid content of plants grown in microwave fields (Fig. 1).

Quantitative determinations were performed in order to establish the percentage increase (%). The amount of ascorbic acid per 100 g of fresh plant was determined for both irradiated and non-irradiated plants (Table 1).

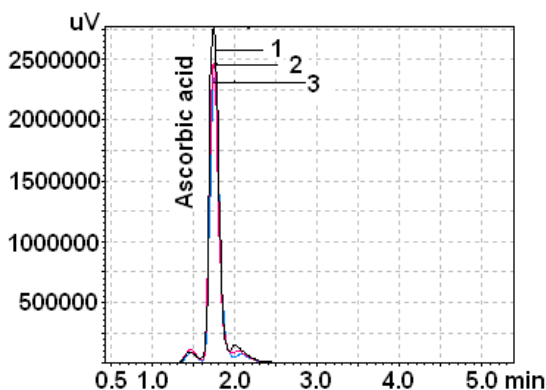


**Figure 1.** HPLC chromatograms of celery extracts. GSM-irradiated (1), WLAN-irradiated (2), and non-irradiated (3).

**Table 1.** The amount of ascorbic acid (AA) and the percentage increase (+%) reported to control plants determined by HPLC method.

Plant lot	Ascorbic acid content (mg AA/100 g plant) $\pm$ RSD (%)		
	Parsley	Dill	Celery
M1 <sup>a</sup>	285 $\pm$ 0.78 (+8%)	201 $\pm$ 0.63 (+66%)	320 $\pm$ 0.56 (+211%)
M2 <sup>b</sup>	282 $\pm$ 0.50 (+6.8%)	180 $\pm$ 0.95 (+49%)	290 $\pm$ 1.03 (+181%)
R <sup>c</sup>	264 $\pm$ 1.32	121 $\pm$ 1.41	103 $\pm$ 1.51

<sup>a</sup> plants irradiated with GSM frequency microwaves; <sup>b</sup> plants irradiated with WLAN frequency microwaves; <sup>c</sup> control plants.



For non-irradiated (control) plants, the comparative evaluation of experimental data showed the highest amount of ascorbic acid in parsley.

In irradiated plants, a greater increase in levels of ascorbic acid was determined in plants irradiated with GSM microwaves compared to WLAN irradiated plants. The highest quantity of ascorbic acid was found in celery plants irradiated with GSM microwaves. Ascorbic acid concentration in celery leaves increased 3.1 times after three weeks of GSM microwave treatment.

### Electrochemical method

Analysis of the extracts of control and irradiated plants were also performed by electrochemical method. For this purpose, a new calibration curve was drawn ( $y = 1.88E-08x + 1.04E-4$ ) with a good correlation factor ( $R^2 = 0.9987$ ) using ascorbic acid standards (between 1  $\mu\text{g/mL}$  - 1800  $\mu\text{g/mL}$ ) prepared in ultrapure water by successive dilutions. The limit of detection (1.29  $\mu\text{g/mL}$ ) and the limit of quantification (2.57  $\mu\text{g/mL}$ ) were calculated [22]. For determination of precision were selected two standard solutions (8.80 and 17.60 mg/L) with concentration in the calibration range and were added to the extracts. The precision was expressed as RSD (%) and calculated as (standard deviation / mean)  $\times$  100. The precision for intra- and inter-day values was less than 5%. The precision and accuracy are in good agreement because low values of RSD (%) and high values for recovery (Table 2) were obtained.

**Table 2.** Intra- and inter-day precisions and accuracies for determination of ascorbic acid by electrochemical method.

Concentration of ascorbic acid (mg/L)	Intra-day (n = 3)		Inter-day (n = 3)	
	Precision (RSD, %)	Recovery (%)	Precision (RSD, %)	Recovery (%)
8.80	1.34	105.20	4.10	107.10
17.60	3.47	97.60	2.76	93.31

In order to evaluate the matrix effect on analysis, a recovery test was performed. Standard AA solution was added to all three plant extracts at two different levels of concentration (88.0 and 176.0 mg AA/L) and analyzed in triplicate. The mean recovery ranged from 93.9% to 107.6%, with higher variation in the case of parsley (Table 3).

**Table 3.** Ascorbic acid (AA) recovery in aromatic plants studied determined by electrochemical method.

Plant	Initial amount of AA (mg/L)	Added amount of AA (mg/L)	Mean of found amount of AA (mg/L)	Recovery (%)
Parsley	70.4	88.0	170.0	107.6
		176.0	231.0	93.9
Dill	35.2	88.0	130.0	105.7
		176.0	210.0	99.5
Celery	21.1	88.0	95.6	106.1
		176.0	196.0	99.4

The results obtained for control and irradiated plants using electrochemical method were in good agreement with the results obtained by HPLC technique (Table 4). The quantitative differences between the two analysis methods may be due to matrix effects occurring in electrochemical determinations due to acetic acid solution used to prepare the plant extracts.

**Table 4.** The amount of ascorbic acid (AA) and the percentage increase (+%) reported to control plants determined by electrochemical method.

Plant lot	Ascorbic acid content (mg AA/100 g plant) ± RSD (%)		
	Parsley	Dill	Celery
M1 <sup>a</sup>	215 ± 1.47 (+36%)	149 ± 1.50 (+70%)	235 ± 1.35 (+280%)
M2 <sup>b</sup>	176 ± 1.27 (+11%)	106 ± 1.49 (+20%)	109 ± 1.45 (+76%)
R <sup>c</sup>	158 ± 1.42	88 ± 1.80	62 ± 1.54

<sup>a</sup> plants irradiated with GSM frequency microwaves; <sup>b</sup> plants irradiated with WLAN frequency microwaves; <sup>c</sup> control plants.

Chen and co-workers suggest that efficient antioxidant defense plays an important role in microwave treated *Nannochloropsis oculata* algae, the algal cells could improve their antioxidant ability through the enhancement of enzymatic and non-enzymatic preventive substances and cause resistance to environmental stresses like microwave irradiation [23].

As an antioxidant, ascorbic acid has an important role in protecting against oxidative stress [24]. As previously shown by literature reports, plants react differently under the influence of similar stress factors. It was shown that

water deficit induced oxidative stress and significantly increased the ascorbic acid content in leaves of Jonagold wilmuta apple tree compared to control Jonagold wilmuta apple tree, while the content of ascorbic acid did not indicate oxidative stress in Elstar apple tree [14]. Similar trends were obtained by Lee, whose experimental results indicated that superior ozone tolerance in the Hood soybean cultivar (compared with Hark) was associated with a greater increase in endogenous levels of ascorbic acid [17]. Likewise, other studies related to the effect of drought stress on plants showed that ascorbic acid content was higher in tolerant genotypes [15].

As result of our studies, celery was less affected by microwaves than parsley and dill. Elevated ascorbic acid under microwave stress could be related to higher protection against microwaves in irradiated plants.

## CONCLUSIONS

On the basis of the results obtained, according to our studies plants respond differently to microwave stress. Our experimental results show an increase in the content of ascorbic acid in the stressed leaves of celery and dill subjected to microwave fields, while the ascorbic acid content was not significantly different in control and stressed leaves of parsley. Overall, GSM frequency microwaves showed more significant influence on the ascorbic acid levels of studied plants than WLAN frequency microwaves. The lowest percent increase in the amount of ascorbic acid was detected, by HPLC and electrochemical method, respectively, in parsley grown in WLAN microwave field (6.8%, 11%), while the highest percent increase was determined in celery grown in GSM microwave field (211%, 280%).

## EXPERIMENTAL SECTION

### Plant material

The plant seedlings (parsley, dill and celery) were grown in laboratory from Agrosel seeds (Câmpia Turzii, Romania). Quantities of 10 seeds were planted in each of the 150 mL identical plastic pots filled with equal quantities of commercial garden soil. Three weeks after seeding the plant vessels were placed in three identical anechoic chambers [25], a reference chamber (R) and two microwave irradiation chambers for plant irradiation on two microwave domains, namely GSM (mobile communication), using a generator with 860 – 910 MHz frequency range (M1) and WLAN (wireless internet connection), using a 802.11 g router generator with operating frequency ranging between 2.412 – 2.48 GHz and main operating channel at 2.42 GHz (M2). A number

of 50 plants per chamber were considered for the study. Plants inside the chambers were illuminated at an intensity of 700 lux and the internal temperature of chambers was maintained at room temperature (25°C). Both control and irradiated plants were watered daily with 10 mL distilled water. After exposure to microwaves during three weeks, the plants were removed from the chambers and the fresh leaf material was analyzed.

### **Reagents and standards**

L(+)-ascorbic acid was purchased from J.T. Baker (Holland), potassium phosphates, phosphoric acid, acetic acid and methanol of HPLC grade were purchased from Merck (Germany). All chemicals were analytical reagent grade. Standard L(+)-ascorbic acid stock solutions in the concentration range 0.3 – 1 µg/mL were prepared in ultrapure water.

### **Extraction procedure**

The sonication method using an ultrasonic bath (Elmasonic S 15H, 37 kHz) was employed for extraction of ascorbic acid, and a modified version of the procedure presented by Yıldız and co-workers was followed [8]. The fresh leaf material of control and irradiated plants was finely chopped, weighed in portions of 1 g and after 10 minutes soaking with 8% (v/v) aqueous acetic acid was extracted two times by sonication with 5 mL extraction agent for 30 min at room temperature, thus the whole ultrasound extraction process taking 1 h. The supernatants were decanted and the combined extracts were rapidly filtered through a Buchner funnel using filter paper, then through nylon syringe filters (0.45 µm) and the total volume was adjusted to 10 mL. All extractions were carried out in triplicate. The plant extracts were stored at 2-4°C in tightly stoppered dark glass vials. It was previously shown that the role of the acid used in extraction of vitamin C is to protect against rapid oxidative reactions which could occur due to active enzymes released from cells during the extraction process [26]. The ascorbic acid from parsley, celery and dill was identified and quantified by HPLC and electrochemical methods, using the same plant extracts.

### **HPLC analysis**

The analyses were carried out on a Shimadzu HPLC model LC-2010 with PDA detector. The chromatographic separation was performed using a Grace Alltima C18 column (100 x 3 mm, 3 µm) thermostated at 30°C. As eluent A, 15 mM phosphate buffer at pH 2.7 and eluent B, methanol, were used. The gradient elution program was as follows: 10% B (min 0), 20% B (min 5), 10% B (min 10). The injection volume was 20 µL and the flow rate of mobile phase was set to 0.4 mL/min. The injection of the plant extracts into HPLC system was performed three times. The HPLC detection was carried out at 243 nm, the maximum absorption wavelength of ascorbic acid.

### Electrochemical analysis

The chronoamperometric measurements were performed with an Autolab Potentiostat 302N (EcoChemie, Netherlands) connected with a traditional three-electrode system. A platinum electrode was used as the auxiliary electrode, carbon paste electrode (CPE) and Ag|AgCl/KCl sat were used as the working and reference electrodes, respectively. Batch amperometric measurements were carried out under magnetic stirring, using 0.1 M phosphate buffer solution (pH 6.8) as supporting electrolyte and +600 mV as working potential. The pH of the buffer solution was measured with the digital Hanna Instruments HI 255 Combined Meter.

The traditional CPE was prepared by hand-mixing of graphite powder with silicon oil in 70:30 ratio using an agate mortar. The homogeneous carbon paste electrode was packed into a cavity of a homemade carbon paste electrode (3.0 mm in diameter).

### ACKNOWLEDGMENTS

The authors would like to express their appreciation for the support of the Romanian National Authority for Scientific Research, CNCS-UEFISCDI, project number PN-II-RU-TE-2011-3-0283.

### REFERENCES

1. W. Stankiewicz, M. P. Dabrowski, R. Kubacki, E. Sobicyewska, S. Szmigielski, *Electromagn. Biol. Med.*, **2006**, 25, 45.
2. I. Lung, M.L. Soran, C. Tudoran, C. Măruțoiu, *Cent. Eur. J. Chem.*, **2013**, 11, 535.
3. Y.P. Chen, *Photochem. Photobiol.*, **2006**, 82, 503.
4. A. Vashisth, S. Nagarajan, *Bioelectromag.*, **2008**, 29, 571.
5. Y.P. Chen, J.F. Jia, X.L. Han, *Planta*, **2009**, 229, 291.
6. T. Cakmak, R. Dumlupinar, S. Erdal, *Bioelectromag.*, **2010**, 31, 120.
7. Z. Lisiewska, W. Kmiecik, A. Korus, *J. Food Compos. Anal.* **2006**, 19, 134.
8. L. Yıldız, K.S. Başkan, E. Tütem, R. Apak, *Talanta*, **2008**, 77, 304.
9. S. Nojavan, F. Khalilian, F.M. Kiaie, A. Rahimi, A. Arabanian, S. Chalavi, *J. Food Comp. Anal.*, **2008**, 21, 300.
10. N. Matei, V. Magearu, *An. Univ. București Chimie*, **2004**, I-II, 65.
11. D.R. Gallie, *Scientifica*, **2013**, 2013, article ID 795964, 24 pages.
12. T.A. Khan, M. Mazid, F. Mohammad, *J. Agrobiol.*, **2011**, 28, 97.
13. K.L. Seung, A.A. Kader, *Postharvest Biol. Technol.*, **2000**, 20, 207.
14. H. Šircelj, F. Batič, F. Štampar, *Phyton-Ann. Rei. Bot. A.*, **1999**, 39, 97.

15. V. Chugh, N. Kaur, A.K. Gupta, *Indian J. Biochem. Biophys.*, **2011**, *48*, 47.
16. I. Schonhof, H.P. Kläring, A. Krumbein, W. Claußen, M. Schreiner, *Agr. Ecosyst. Environ.*, **2007**, *119*, 103.
17. E.H. Lee, *Chronobiol. Int.*, **1991**, *8*, 93.
18. K.O. Burkey, G. Eason, E.L. Fiscus, *Physiol. Plant.*, **2003**, *117*, 51.
19. Y. Yinan, L. Yuan, Y. Yongqing, L. Chunyang, *Environ. Exp. Bot.*, **2005**, *54*, 286.
20. A. Vian, C. Faure, S. Girard, E. Davies, F. Hallé, P. Bonnet, G. Ledoigt, F. Paladian, *Plant Signal. Behav.*, **2007**, *2*, 522.
21. M. Stan, M.L. Soran, C. Măruțoiu, *J. Anal. Chem.*, **2014**, (in press).
22. P.C. Meier, R.E. Zünd, *Statistical Methods in Analytical Chemistry*. John Wiley and Sons, New York, USA, **1993**, 103.
23. B. Chen, Y.Yu, J. Huang, Effect of microwave radiation on the antioxidant responses of *Nannochloropsis oculata*. *4-th International Conference on Bioinformatics and Biomedical Engineering (ICBBE)*, Chengdu, China, 18-20 June, **2010**, 1.
24. W. Zhang, Z. Tian, X. Pan, X. Zhao, F. Wang, *Hort. Environ. Biotechnol.*, **2013**, *54*, 1.
25. E. Surducun, V. Surducun, A. Halmagyi, Plant growth stimulation in microwave field. Romanian Patent RO-125068B1, **2012**.
26. O.A. Bessey, C.G. King, *J. Biol. Chem.*, **1933**, *103*, 687.



## COMPARATIVE STUDY OF GREEN FLUORESCENT PROTEIN MUTANTS

SZABÓ (PÁLFI) MÁRIA<sup>a,b</sup>, BÁLINT EMESE-ÉVA<sup>a,b</sup>,  
SZILÁGYI LÁSZLÓ<sup>b,c</sup>, ÁBRAHÁM BEÁTA<sup>b</sup>

**ABSTRACT.** Two histidine - substituted mutants of Enhanced Green Fluorescent Protein (S202H-EGFP and S202H/Q204H-EGFP) was realized and the effect of mutation on the spectral properties of mutant proteins was examined. The denaturation of the wild type and mutant proteins in guanidine hydrochloride solution was also studied. The structural stability analysis revealed that the global structure of the protein is partially destabilized due to the performed mutations. Meanwhile the sensitivity of mutant proteins to the solvent acidity increased. It was found that with increase of proton concentration in the solvent the absorbance and the fluorescence intensity of proteins decreased.

**Keywords:** *green fluorescent protein, histidine, fluorescence, absorbance, chromophore*

### INTRODUCTION

The green fluorescent protein is an autofluorescent protein that emits green light, upon exciting with ultraviolet light, without the addition of any exogenous substrate [1]. This protein has a characteristic structure that consists of a small, compact  $\beta$ -barrel. The beta-barrel is constructed of eleven beta-strands and an alpha-helix runs through the centre of the barrel. The protein's chromophore is located in the centre of the barrel structure. The compact "beta-can" structure assures high level of stability to the protein and also protects the chromophore group from the destructive effects of the bulk solvent [2].

---

<sup>a</sup> "Politehnica" University of Bucharest, Department of Analytical Chemistry and Environment Engineering, Polizu street No. 1-7, 011061, Bucharest, Romania, palfimaria2004@yahoo.com

<sup>b</sup> Sapientia Hungarian University of Transylvania, Department of Bioengineering, Libertatii square No.1, 530104, Miercurea Ciuc, Romania, e-mail: albertbeata@sapientia.siculatorum.ro

<sup>c</sup> Eötvös Lóránd University, Department of Biochemistry, Pázmány Péter street 1/C,1117, Budapest, Hungary, szilagyl@elte.hu



It is shown that proteins with beta barrel structure are more stable than globular or other proteins; also the energy barrier of unfolding is higher at this type of proteins [14]. Although GFP, its mutants and some other fluorescent protein (DsRed, zFP506) have very similar structure, still it was shown that their structural stability may differ significantly [18]. Several studies exist in which the structural stability of GFP and its mutant forms were investigated. These proteins proved to be more resistant against the denaturing effects of chaotropic agents (GuHCl, SDS) and also had higher thermal stability like other proteins [14,15,16, 17].

The protein's color originates from a conjugated pi electron system that belongs to the chromophore group. The chromophore group is generated in the protein's interior by cyclization of three consecutive amino-acid residues (Ser65, Tyr66 and Gly67) in a self-catalyzed intramolecular rearrangement of this tripeptide sequence [3]. Fluorescence emission occurs when the chromophore group of the protein is raised to an excited state as a result of electron transfer from a ground state to a higher energy level, as the electrons drop back to the ground state, the chromophore group emits energy in the form of green light [4].

The native green fluorescent protein's fluorophore exists in two conformations in ground state. A protonated form, the predominant state, which has an excitation maximum at 395 nanometers and a less prevalent, unprotonated form that absorbs at approximately 475 nanometers [5]. The relative quantity of these two forms is affected by the proton concentration of the environment. Protons from the solvent could enter into the protein's interior and alter the ionization state of the chromophore [9]. The pH sensitivity of the chromophore is determined by the proton transfer from the protein surface to the interior of the protein. The crystal structure studies at different pH revealed that some of the side chains of the beta barrel could change their orientation in the function of medium's pH [10]. The amino acid residues in the proximity of the chromophore group and its hydrogen bond network, through their orientation could promote either the protonation or deprotonation of the hydroxyl group of Tyr66, but both forms are always present [9]. At wtGFP the phenol group of tyrosine 66 is predominantly uncharged, while at EGFP the charged Tyr is the dominant form [9]. The emission wavelengths of these forms of the chromophore are similar, but their fluorescence lifetimes differ. [13]

The wild type GFP was subjected to several mutations to improve one or more characteristics of the protein [6]. The mutational investigations have revealed that the protein's fluorescence is linked to its structural integrity [7, 23]. As the protein is denaturated, the protection of the chromophore is loosed and it is turned to a nonfluorescent state [8]. The EGFP (Enhanced

Green Fluorescent Protein) is a mutant form of GFP with two mutations (F64L, S65T) in the chromophore region and have a single excitation peak at 488 nm. These modifications resulted in a protein with greater fluorescence intensity [3].

GFP and its mutant forms are widely used as fluorescent markers in cell biology and biotechnology. By modification of fluorescent proteins many research groups tried to develop biosensors like pH sensors, metal sensors, chloride ion sensors or intracellular red-ox sensors [6].

Two histidine-substituted mutants of EGFP were created, namely the S202H-EGFP and the S202H/Q204H-EGFP mutant protein, as described in a previous study. This work's aim was to obtain metal binding mutants of EGFP, which can be further used as metal sensor [12]. In the present study the effect of mutation was examined on the spectral properties and structural stability of mutant proteins. The structural model of mutant proteins was prepared *in silico*. The results of the spectral studies and the structural stability analysis show that these modifications did not have significant effect on the global structure of the protein.

## RESULTS AND DISCUSSION

### Absorption spectra analysis

EGFP has an excitation maximum at 487 nm. The absorption spectrum of the wild type EGFP and its mutants was determined in mediums with different pH values (pH 4.6-8), to investigate the effect of mutations to the spectral properties of the proteins.

The phenol group of Tyr66, which is part of the protein's chromophore group, has pH dependent ionization states, a phenolate form and an uncharged phenol form [10]. The absorption characteristics of the two forms of the chromophore are different, the protonated form has an absorption maximum at 395 nm, while the unprotonated form absorbs at 485 nm, as shown in the Figure 1.

At neutral pH the absorption spectra of mutant proteins were similar with the spectrum of the wild type protein (WT-EGFP). Differences appear only in the minor peaks sizes. At 395 nm the S202H-EGFP and the WT-EGFP show greater absorption than the S202H/Q204H-EGFP mutant protein. So at these two proteins (S202H-EGFP and the WT-EGFP) the ratio of the protonated and unprotonated form of the chromophore is bigger than at the S202H/Q204H-EGFP mutant protein.

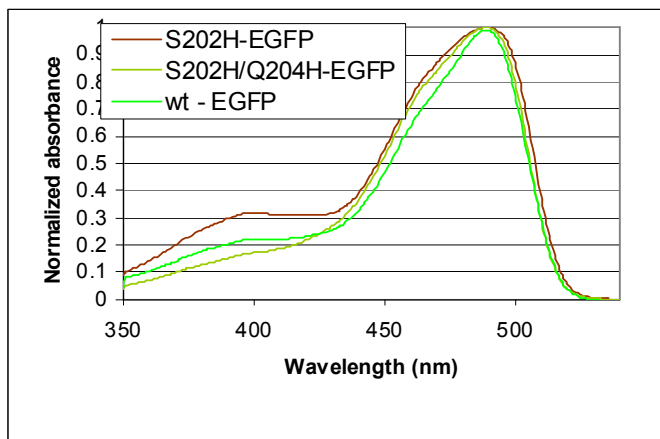


**Figure 1.** Normalized absorption spectrums of EGFP and its mutants

On the obtained spectrums it can be observed two absorption peaks, a minor peak at 395 nm and a major peak at 478 nm. These two absorption maximums can be explained with the simultaneous presence of the protein's chromophore in two ionization forms (protonated and unprotonated).

As can be observed on Figure 2. at EGFP the protonation of hydroxyl group of Tyr-66, which is part of the chromophore, induces a decrease of absorption at 488 nm while the absorption at 390 nm increases. By reducing the pH from 8 to 4.6 the protein's absorption decreased at 488 nm and in the same time an increase of absorption at 390 nm was observed. U. Haupts *et al.* also investigated the effect of medium's pH to the absorbance of EGFP, they obtained similar results [9].

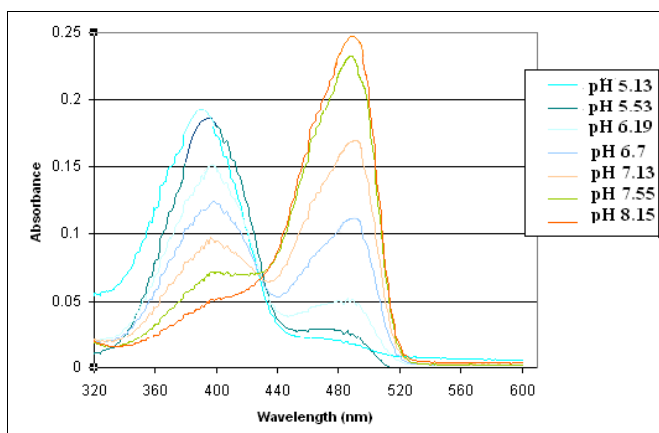


**Figure 2.** Normalized absorption spectrums of WT-EGFP at different pH

The equilibrium between the two ground state conformations of the GFP is controlled by the proton concentration of the medium [11]. At low proton concentration the conditions favor the formation of the phenolate form of tyrosine, so the majority of the chromophore is unprotonated. At high proton concentration a proton from the bulk solvent protonates the phenol group of chromophore. In this protonated form the protein's chromophore is nonfluorescent [10].

Although a compact beta can structure surrounds the chromophore, it is proposed that the Tyr66 is in direct contact with a buried water molecule. Through this water the molecules of solvent can affect the chromophore's protonation state [5]. These two forms of chromophore can transform to each other in a reversible manner, the process is controlled by the proton concentration of the medium. [10]

#### *Emission spectra analysis*

The effect of the medium's pH to the emission spectrums of the wild type EGFP and its mutants has been studied. The emission spectra of proteins in solutions with different pH values was measured. In solutions with neutral pH the emission spectrums of investigated proteins are practically identical. Deviations in the proteins emission spectrums appear in acidic environment.

The investigated three proteins showed different sensitivity towards environmental pH.

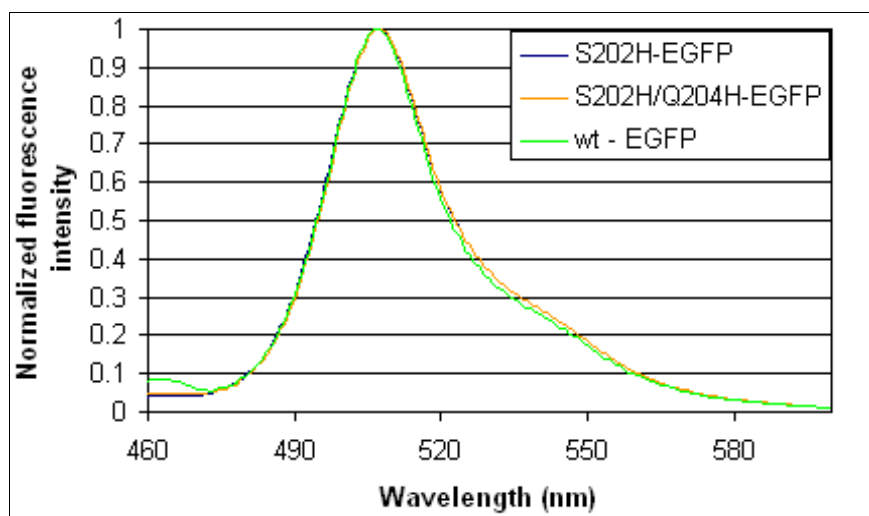


**Figure 3.** Emission spectra of WT- EGFP and its mutants (Excitation: 400 nm)

It was observed that fluorescence intensity decreased with decreasing of the pH value, on the other hand the positions of the emission maxima of investigated proteins are independent of the environmental pH. Effect of pH on the fluorescence intensity of the S202H/Q204H mutant protein is illustrated in Figure 4.

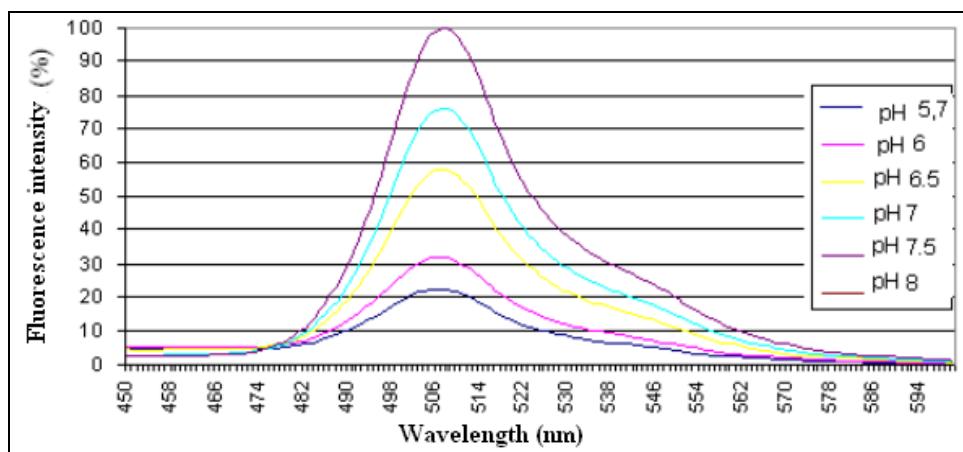


**Figure 4.** Normalized emission spectrums of S202H/Q204H mutant of EGFP at different pH (Excitation: 400 nm)

All the three investigated proteins showed similar changes in the emission spectra. The lower emissions at lower pH values correlate with the reduced absorption at 488 nm in similar conditions, as described earlier [5]. The obtained fluorescence intensities in the function of the environmental pH are illustrated in Figure 5.

At Figure 5. in acidic medium the chromophore is fully protonated and the protonated form is nonfluorescent. It may be noted that in mediums with low pH values (pH  $\leq$  4) the investigated proteins lose their fluorescence. The wild type protein proved to be the most sensitive to the pH of the environment, its fluorescence intensity decreased faster than the mutant protein's. The mutant proteins' pH sensitivity also differs, the S202H mutant protein proved to be more sensitive than S202H/Q204H mutant.

It has been shown that the pH induced changes in fluorescence intensity are completely reversible, in the range of 5-8 pH. In this pH range by using CD spectrometry couldn't be detected any conformational changes in the global structure of the protein. Despite this, it was proposed that some slight structural changes near the chromophore occur that allow the proton transfer from the bulk solvent to the interior of the protein [9].

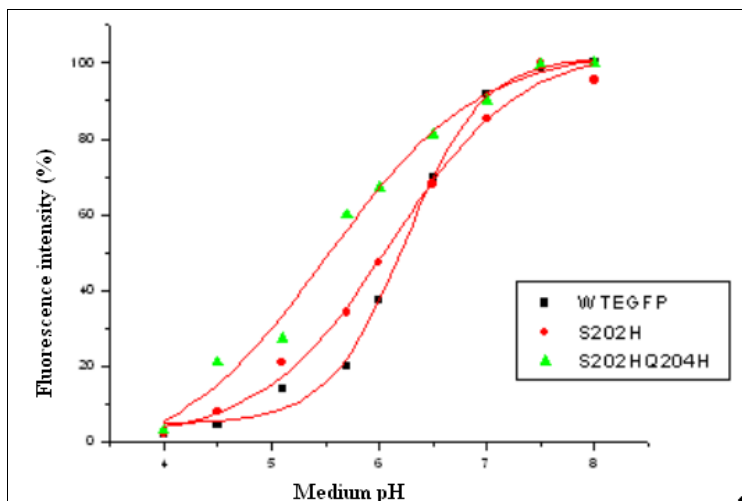


**Figure 5.** pH sensitivity of EGFP and its mutants

### ***Structural stability analysis of mutant proteins***

It is known that the fluorescence of these proteins is closely related to their structural integrity. These proteins can emit fluorescence only in native form, their chromophore group must be protected. The beta can structure assure a high level stability to the protein and at the same time protect the chromophore from the molecule of the solvent [6]. So the unfolding of these proteins results in the loss of their fluorescence. Due to the extremely compact structure of the fluorescent protein, the unfolding is a very slow process [14].

The structural stability of three green fluorescent proteins (EGFP, S202H-EGFP, S202H/Q204H-EGFP) was analysed.

By measuring the fluorescence intensity in the presence of chaotropic agents one can obtain information about the structure destabilization, the protein unfolding. Denaturation of the wild type EGFP and its mutants in guanidine hydrochloride solutions has been studied by measuring the decrease of fluorescence intensity. This type of monitoring of the fluorescent protein's unfolding has been used in several studies [8, 14, 16, 18, 19].

During denaturation the protein's structure is destabilized, beta strands are shifted. This shift generates a gap between the beta strands, thus decreases the protection of chromophore group and it becomes accessible for small molecules. The water molecules get inside the protein and protonate the chromophore. Protonated form of chromophore is non-fluorescent [8]. So the fluorescence intensity of EGFP decreases during protein denaturation.

Denaturation of the proteins was studied in solutions that contained guanidine hydrochloride in different concentration. Figure 6. shows the remaining fluorescence intensity of wt-EGFP and its mutants in denaturing medium, after incubation for 20 hours at room temperature (298 K).

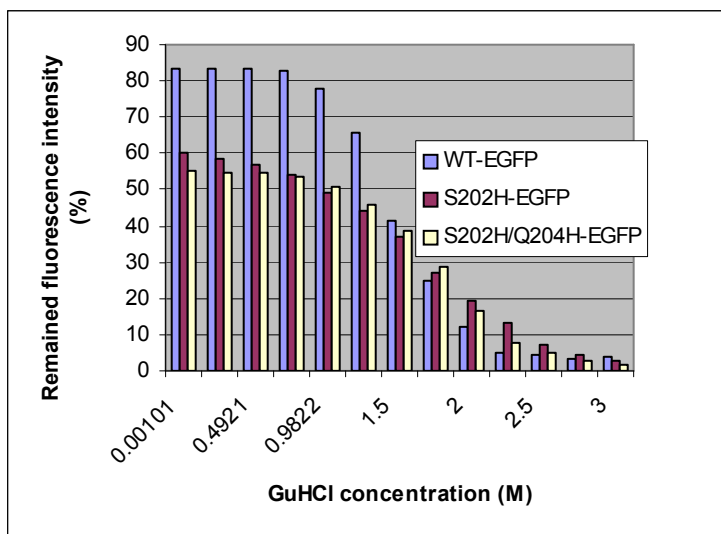
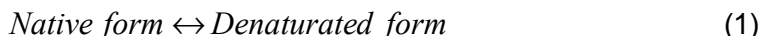


**Figure 6.** Decrease of fluorescence intensity during denaturation of the proteins

Fluorescence intensity of EGFP increased with 15-20% in the presence of 0.1-0.2 M GuHCl, referred to the initial intensity [14, 18, 19]. In this study it was also observed a similar effect of GuHCl in small concentrations. This increased fluorescence intensity could be due to the altered spatial arrangement of the chromophore [17].

It was proposed that after 20h incubation of the proteins in the presence of GuHCl, its denaturation became into an equilibrium state, where the protein is also present in native and in denaturated forms. The ratio between these two states is the function of GuHCl concentration. This equilibrium is described in the equation 1.



The equilibrium constant of the process can be described by the equation 2.

$$K_d = \frac{F_{\text{denaturated}}}{F_{\text{native}}} \quad (2)$$

The measure of the native state stability is the difference between the standard free energy ( $\Delta G$ ) of the native state and denatured state of the protein, and can be described by the equation 3.

$$\Delta G^0 = -RT * \ln(K_d), \text{ where } R = 1.987 \text{ cal / mol} * K \quad (3)$$

Denaturation of the wild type and their mutants is shown in Figure 6. Illustrating the variation of free energy in the function of guanidine concentration can determine the value of free energy of the protein in water. Free energy of the protein in guanidine hydrochloride solutions can be described by the equation 4.

$$\Delta G^{\circ}_{GuHCl} = \Delta G^{\circ}_{H_2O} + m * [GuHCl] \quad (4)$$

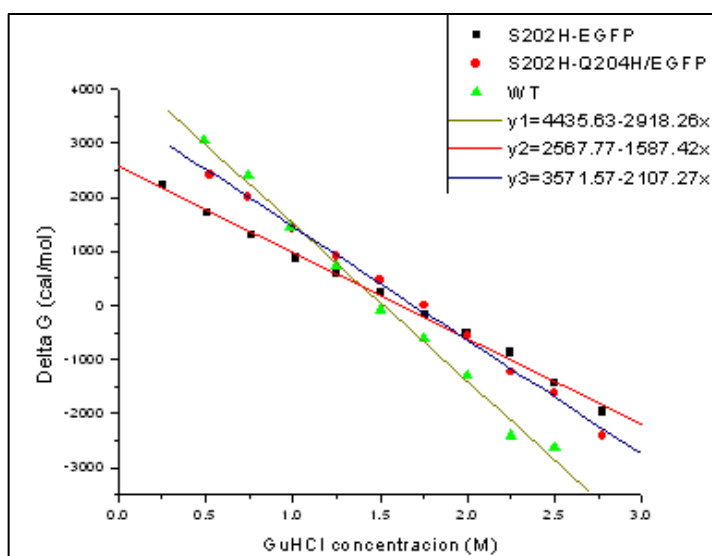


**Figure 7.** The free energy of proteins in different guanidine hydrochloride solutions

In this study the same method described in [18] was used for determination of the standard free energy of denaturation.

Comparing the values obtained for the free energies of the proteins, as shown in figure 8, it can be observed that wild type protein proved to be the most stable in guanidine solutions. Its free energy in water is 4435.6 cal/mol, Olesia V. Stepanenko et al. obtained similar magnitude for conformational stability of wt EGFP [18]. As it is shown on the Figure 8., the S202H / Q204H mutant is more stable than the S202H mutant. These results suggest that the effectuated substitutions in the protein's beta barrel slightly altered the compact structure of EGFP, causing a partial destabilization in it.



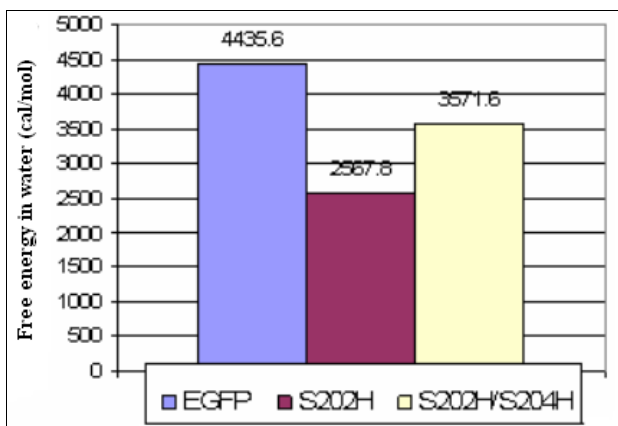


**Figure 8.** Free energy of proteins in water

## CONCLUSIONS

Spectral characteristics of the original protein and their mutants at neutral pH are similar. Spectroscopic studies have shown that both fluorescence and absorption of proteins is influenced by environmental acidity, as described in [7], [11]. In the case of all the three investigated proteins two absorption maximums can be observed in the absorption spectra, one is at 395 nm and another at 485 nm, that corresponds to the two ionization forms of the chromophore.

It was observed that the fluorescence intensity decreased with the decreasing of the medium's pH. At high proton concentration (pH<4) the proteins do not emit fluorescence. It was observed that mutant proteins (S202H/EGFP and S202H/Q204H/EGFP) are less sensitive to environmental acidity than the original protein (WT-EGFP). This unexpected behaviour of mutant proteins apparently contradicts with our results obtained from structural stability analysis, where the original protein proved to be the most stable, and the global structure of mutants is partially destabilized. This anomaly can be explained by the appearance of a local buffer effect due to the imidazole groups of histidines introduced in mutant proteins by directed mutagenesis.

It is known that histidines are potential proton acceptors and, due this fact, it can be proposed that through the protonation of these groups the proton concentration is reduced in the proximity of the chromophore group. It seems that the newly introduced histidine residues (Hys202 and Hys 204) protects the chromophore group from protonation. This effect is pronounced in the range of pH 5-6, where a relatively big difference between fluorescence intensity decrease of mutant proteins and wild type protein can be seen.

Finally, summarizing all results, it can be concluded that the presence of histidine residue in the proximity of the chromophore reduces protein's sensitivity to environmental acidity. This hypothesis is confirmed by the most reduced sensitivity towards the environmental pH of the S202H/Q204H/EGFP mutant, where two histidines were introduced. But this local buffering effect is limited to a relatively small pH range, it emerges between 5-6.5 pH values.

## **EXPERIMENTAL SECTION**

### ***Protein expression***

The mutations were carried out by using the QuikChange Site-Directed Mutagenesis Kit (Stratagene), as described in earlier work [12]. The wild type EGFP and its two histidine substituted mutants (S202H/S204H and S202H) were expressed in *E. coli* strain BL21 Star (DE3) cells, by using the pET15b expression vector. The recombinant proteins contained an N-terminal hexahistidine tag, so the proteins were purified by immobilized metal ( $\text{Ni}^{2+}$ ) affinity chromatography. Purified proteins were dialyzed against 25 mM sodium phosphate buffer, with pH 7.

### ***Absorption spectra measurements***

Absorption spectra measurements were made in 2ml quartz cuvettes at room temperature (293K). 1 ml of the purified protein solution (protein dissolved in 20 mM sodium phosphate, 100 mM NaCl, pH = 7) was used to the measurements. Measurements were performed in solutions with different pH values (pH = 4.6 - 8.1), in phosphate buffer. The concentration of proteins was different so to compare the obtained spectrums, the spectrum of the most concentrated protein was normalized.

### ***Emission spectra measurements***

Fluorescence intensity measurements were made in 3ml quartz cuvette. The fluorescence spectra of EGFP and its mutants was carried out by a Fluoro Max Spex 320 spectro-fluorimeter, at 298 K. Excitation wavelengths were assayed at 400 and 450 respectively. The emission was detected in the range of 460-600 nm. 2ml samples were used for measurements. The samples containing the protein (His6EGFP) in low  $\mu\text{M}$  range in 20 mM  $\text{Na}_2\text{HPO}_4$ , with different pH (pH= 4, 4.5, 5, 5.5, 6, 6.5, 7, 7.5, 8). The concentration of proteins was different so to compare the obtained spectrums, the spectrum of the most concentrated protein was normalized.

### ***Analysis of protein denaturation in guanidine solution***

Protein denaturation in guanidine solution was analysed. In these experiments different concentrations of guanidine hydrochloride solution was used (0.5-5M). The protein concentration in the denaturing solutions was in low micromolar range. After 16 hours of incubation at room temperature, the fluorescence intensity of denatured EGFP was measured by a FluoStar OPTIMA fluorimeter, excitation wavelength was 485 nm and emission wavelength was 520 nm.

### **ACKNOWLEDGMENTS**

The work has been funded by the Sectoral Operational Programme Human Resources Development 2007-2013 of the Romanian Ministry of Labour, Family and Social Protection through the Financial Agreement POSDRU/6/1.5/S/16.

This study was supported by the Department of Bioengineering of Sapientia Hungarian University of Transylvania.

### **REFERENCES**

1. M. Chalfie, S.R. Kain, "Green fluorescent protein. Properties, applications, and protocols", John Wiley and Sons Inc., New Jersey, **2006**, chapter 4.
2. F. Yang, L.G. Moss, G.N. Phillips, *Nature biotechnology*, **1996**, *14*, 1247.
3. R.M. Wachter, *Photochemistry and Photobiology*, **2006**, *82*, 339.
4. J.R. Lakowicz, "Principles of fluorescence spectroscopy", Business Media LLC, New York, **2006**, chapter 1.
5. M. Chatroraj, A.K. Brett, U.B. Gerold, G.B. Steven, *Proc. Natl. Acad. Sci., Biophysics*, **1996**, *93*, 8365.
6. A. Cubitt, R. Heim, S. Adams, A. Boyd, L. Gross, R.Y. Tsien, *Trends in biochemical sciences*, **1995**, *20*, 449.
7. S.G. Olenych, N.S. Claxton, G.K. Ottenberg, M.W. Davidson, *National High Magnetic Field Laboratory*, The Florida State University, Tallahassee, Florida.
8. K. Jung, J. Park, P.J. Maeng, H. Kim, *Bull. Korean Chem. Soc.*, **2005**, *26/3*, 415.
9. U. Haupts, S. Maiti, P. Schwill, W.W. Webb, *Proc. Natl. Acad. Sci. Biophysics*, **1998**, *95*, 13575.
10. M.S. Anoop, B.U. Jayant, K. Guruswamy, *Protein Science*, **2005**, *14*, 1794.
11. C. Scharnagl, K.R. Raupp, S.F. Fischer, *Biophysical Journal*, **1999**, *77*, 1854.
12. M. Pálfi, E. Kovács, L. Szilágyi, I. Miklóssy, B. Ábrahám, Sz. Lányi, *Studia UBB Chemia*, **2009**, *2*, 41-42.

13. A.W. Scruggs, C.L. Flores, R. Wachter, N.W. Woodbury, *Biochemistry*, **2005**, *44*, 13377-13384.
14. V. Stepanenko, I. Kuznetsova, V. Verkhusha, M. Staiano, S. D'Auria, K. Turoverov, *Spectroscopy*, **2010**, 24367–373.
15. A. Nagy, A. Málnási-Csizmadia, B. Somogyi, D. Lőrinczy, *Thermochemica Acta*, **2004**, 410161–163.
16. K.M. Alkaabi, A. Yafea, S. Ashraf, *Applied Biochemistry and Biotechnology*, **2005**, Vol. 126.
17. M. Pálfi, E. Kovács, L. Szilágyi, I. Miklóssy, B. Ábrahám, Sz. Lányi, *Scientific Bulletin Series B: Chemistry And Materials Science*, **2010**, Vol. 72, Iss.2.
18. O.V. Stepanenko, V.V. Verkhusha, V.I. Kazakov, M.M. Shavlovsky, I.M. Kuznetsova, V.N. Uversky, K.K. Turoverov, *Biochemistry*, **2004**, *43*, 14913-14923.
19. V.V. Verkhusha, I.M. Kuznetsova, O.V. Stepanenko, A.G. Zaraisky, M.M. Shavlovsky, K.K. Turoverov, V.N. Uversky, *Biochemistry*, **2003**, *42*, 7879-7884
20. Y. Liu, H.R. Kim, A.A. Heikal, *Journal of Physical Chemistry B*, **2006**, *110*, 24138-24146.
21. K.M. Alkaabi, A. Yafea, S.S. Ashraf, *Applied biochemistry and biotechnology*, **2005**, *125*,149-156.
22. T.N. Campbell, F.Y.M. Choy, *Molecular Biology Today*, **2001**, *2(1)*, 1-4.
23. E.É. Bálint, J. Petres, M. Szabó, Cs. Orbán, L. Szilágyi, B. Ábrahám, *Journal of Fluorescence*, **2013**, *23*, 273-281.



## EXTRACTION IN CCL<sub>4</sub> OF IONIC ASSOCIATES OF IODINE- IODIDE COMPLEXES WITH THE CATIONIC DYE BRILLIANT GREEN

TATYANA S. TISHAKOVA<sup>a</sup>

**ABSTRACT.** Investigation and efficiency increase for extraction procedure of ionic associates of iodine-iodide complexes with cationic dye brilliant green have been performed by the determination of iodide. Extraction constant of ionic associate of iodine-iodide complexes with brilliant green in CCl<sub>4</sub> has been estimated ( $K_{extr} 115 \pm 5$ ).

**Keywords:** *ionic associates, iodine-iodide complexes, extraction constant, brilliant green*

### INTRODUCTION

Iodide-ion is a main component among iodine-containing ions. Voltammetry and ionic chromatography with inductively coupled plasma mass spectrometry were more often used for the determination of iodine and iodine-containing ions [1-6]. These methods are highly-sensitive but they are characterized by high prices of the analyses due to usage of expensive equipment, reagents and outsourcing of qualified personnel.

Electrochemical [7, 8] and spectrophotometric methods [9-12] are more accessible. It has been reported that these methods were used jointly for the determination of iodide and bromide [13]. Therefore development of new, or updating the already existing procedures of analysis which are based on the combination of electrochemical and spectrophotometric methods for monitoring the iodine, iodide, iodate in different samples is an actual task of modern analytical chemistry.

The problem in the development of methods for determination of iodide-ions is related to the increasing of sensitivity and selectivity of determination. Spectrophotometric methods for determination of trace amounts of iodide using extraction of ionic associates of iodide-ions with

---

<sup>a</sup> *Kharkiv National Medical University, Department of bioorganic and medical chemistry, 4 Lenin Avenue, Kharkiv, Ukraine, ttishakova@yahoo.com*

triphenylmethane dyes have been reported [14]. Spectrophotometric method reported in the work [15] ranks below in sensitivity (by 100 times) as compared with methods based on the measurement of absorbance of iodine-iodide complexes. The determination of iodide-ions in form of ionic associates with brilliant green after electrochemical oxidation to iodate and interaction with excess of iodide has been reported in [16]. Under these conditions the sensitivity of the determination in the form of iodine-derivatives of organic dyes yields to the methods in the base of which there is a formation of ionic associates of cationic dyes with iodine-iodide complexes.

*Tris*-phenyl-methane dyes have an important place in analytical practice due to their high sensitivity and selectivity. Inconsistency in literature about extraction ability of these dyes and absence of uniform criteria for estimation of reagents does not allow an objective comparison and the choice of the best fitted dye. From this perspective the range of acidity of aqueous phase, concentration of dye at which absorbance of extracts is constant, extraction coefficient, molar absorptivity, time of extraction etc. are the main criteria.

The aim of this work is to establish optimal conditions of extraction in carbon tetrachloride of ionic associates of iodine-iodide complexes with cationic dye brilliant green and to estimate the extraction constant. The procedure of extraction is one of the step of methods for determination of trace amounts of iodide in form of ionic associate (IA) with brilliant green using electrochemical oxidation which has already been reported in the literature [16].

## RESULTS AND DISCUSSION

Increased demands to the blank solution for which signal should be minimal and reproducible appear under the work near the limit of quantification. It was noticed that long-term storage of brilliant green solution elevates absorbance in blank solution. This effect is connected with temperature aggregation of cations of brilliant green; under the heating aggregates destruct.

Before the test, required quantity of sulfuric acid was added to the aliquot of working solution of dye and this mixture was heated to boil. This procedure results in decreased aggregation of dye and thereby, decreased absorbance value of the blank solution.

The performance of the extraction in the air results in the sufficient decreasing of absorbance value of blank solution. Because of this increasing carrying of further analysis is complicated. It is known that potassium iodide contains iodine and it is oxidized with air. During the extraction in  $\text{CCl}_4$  the

quantity of iodine which forms ionic associates with brilliant green, increases. Consistent extractions from blank solution allow excluding contaminations but not decreasing the value of absorbance essentially. That's why necessity to carry out investigation in inert medium has appeared.

Inert medium was created in two ways:

The oxygen of air was displaced from the funnel using carbon dioxide obtained in Kipp's apparatus. Desired decreasing in values of absorbance did not occur in the medium of carbon dioxide. Dependence is given on the Figure 1:

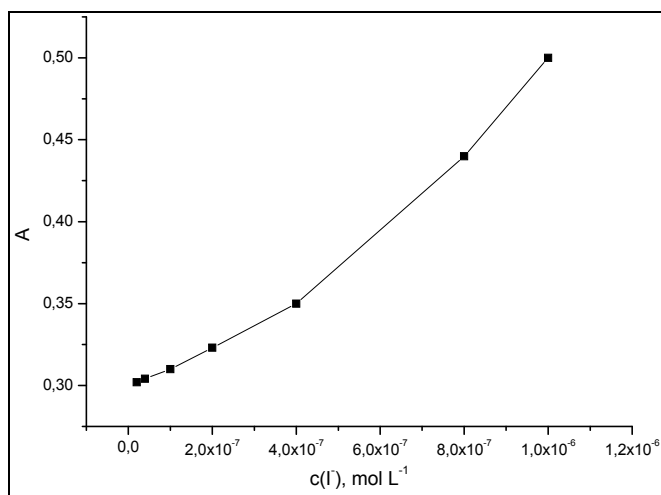


**Figure 1.** Dependence of absorbance of IA of iodine-iodide complexes with brilliant green on concentration of iodide-ion (in the medium of carbon dioxide).

Another way of extraction in inert medium is displacement of oxygen of air from funnel with gaseous nitrogen. Procedure of displacement of oxygen using gaseous nitrogen was used for solutions preparation, using double-distilled water saturated with gaseous nitrogen.

Saturation procedure of double-distilled water with gaseous nitrogen and passing of gaseous nitrogen through the solution in the funnel before extraction provide substantial decrease of absorbance of blank solution and allows the recording of reproducible and stable values of absorbance [17, 18].

The absorbance of extracts from the blank solution when performing the extraction without passing gaseous nitrogen through the solution in the funnel and using solution prepared with double-distilled water were recorded and they are the following (after three parallel measurements):  $A_{01} = 0.250$ ,



$A_{02} = 0.230$ ,  $A_{03} = 0.220$ . Absorbance of extracts from the blank solution when using of double-distilled water saturated with nitrogen were determined as follows:  $A_{01} = 0.068$ ,  $A_{02} = 0.070$ ,  $A_{03} = 0.073$ . From the foregoing it is evident that gaseous nitrogen passed through the double-distilled water employed in the solution preparation decreases the value of absorbance of the blank solution.

### Determination of extraction constant of ionic associates of iodine-iodide complexes with cationic dye brilliant green carbon tetrachloride

Under the extraction of ionic associates of cation ( $R^+$ ) of brilliant green and anions ( $I_3^-$ ) of iodine-iodide complexes the whole process can be resolved on three components:

- equilibrium of formation of complex anion,  $I^- + I_2 \rightleftharpoons I_3^-$
- equilibrium of formation of ionic associates in aqueous phase,  $R^+ + I_3^- \rightleftharpoons R^+I_3^-$
- equilibrium of distribution of ionic associate between aqueous phase and organic solvent  $(R^+I_3^-)_{aq.ph.} \rightleftharpoons (R^+I_3^-)_{org.ph.}$

Equilibrium constant of formation of complex anion ( $\lg K(I^- + I_2 \rightleftharpoons I_3^-) = 2.9$ ) is known [19]. As to measure equilibrium constant of formation of ionic associate separately using spectrophotometric method is not possible (absorbance spectrum of cation of dye in the associate and out of it does not differ significantly), only equilibrium constant of extraction can be determined:

$$K_{extr}(R^+ + I_3^- \rightleftharpoons (R^+I_3^-)_{org.ph.}) = \beta(R^+ + I_3^-)_{org.ph.} = \beta(R^+ + I_3^-) \times K_D((R^+I_3^-)_{aq.ph.} \rightleftharpoons (R^+I_3^-)_{org.ph.}) \quad (1)$$

Under the determination of extraction constant it is convenient to change degree of extraction of ionic associate at the change in concentration of iodide-ion in aqueous phase. In this case general reaction equation is following:

$$\begin{aligned} K(I^- + I_2 \rightleftharpoons (R^+I_3^-)_{org.ph.}) &= K(I^- + I_2 \rightleftharpoons I_3^-)_{org.ph.} \\ &= K(I^- + I_2 \rightleftharpoons I_3^-) \times K_{extr}(R^+ + I_3^- \rightleftharpoons (R^+I_3^-)_{org.ph.}) \end{aligned} \quad (2)$$

$$K \times K_{extr} = \frac{[R^+I_3^-]}{[I_2] \times [I^-]}$$

$$K_{extr} = \frac{\overline{[R^+I_3^-]}}{[I_2] \times [I^-] \times K} \quad (3)$$

where,  $\overline{[R^+I_3^-]}$  – equilibrium concentration of ionic associate in the phase of organic solvent;

$$\overline{[R^+I_3^-]} = A/\epsilon l;$$

$A$  – absorbance of ionic associate in the phase of CCl<sub>4</sub>;

$\epsilon$  – molar extinction coefficient of ionic associate in CCl<sub>4</sub>,  $\epsilon = 65000$  L mol<sup>-1</sup> cm<sup>-1</sup>;

$l$  – working size of quartz cell;

$[I_2] = c(I_2) - \overline{[R^+I_3^-]} \times V(CCl_4)/V(H_2O) - [I_3^-]$  is an equilibrium concentration of iodine in aqueous phase;

$c(I_2)$  – total concentration of iodine in aqueous phase before extraction;

$V(CCl_4), V(H_2O)$  – volumes of phases under the extraction;

$[I_3^-] = [I^-] \times [I_2] \times 10^{2.9}$  – concentration of iodide-iodide anions in aqueous phase;

$[I^-]$  – equilibrium concentration of iodide in aqueous phase.

Measured data of absorbance of extracts of ionic associates of brilliant green and anions of iodine-iodide complexes in CCl<sub>4</sub> at the different concentrations of iodide-ions in aqueous phase are given in the table 1.  $c(I_2) = 5 \times 10^{-6}$  mol L<sup>-1</sup>. Volumes of phases are the same:  $V(CCl_4) = V(H_2O) = 50$  mL.

**Table 1.** Absorbances of extracts of ionic associates of brilliant green and anions of iodine-iodide complexes in CCl<sub>4</sub> at the different concentrations of iodide-ions in aqueous phase

$c(I^-), \text{mol L}^{-1}$	$A_{extr}, n = 3$		
$1 \times 10^{-2}$	0.260	0.258	0.261
$1 \times 10^{-3}$	0.257	0.256	0.258
$1 \times 10^{-4}$	0.233	0.234	0.232
$5 \times 10^{-5}$	0.210	0.208	0.212

Concentration ratio  $[I_3^-]/[I_2]$  depends on the concentration of iodide in water:

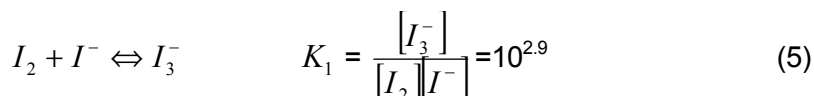
$$1/[I_2] = [I^-] \times 10^{2.9} \quad (4)$$

At the  $c(I^-) = 1 \times 10^{-4}$ ,  $5 \times 10^{-5}$  mol L<sup>-1</sup> anionic complexes are only  $10^{-1.1} = 0.068$  and  $10^{-1.4} = 0.040$ .

Extraction constant value has been estimated using measurement at the  $c(I^-) = 1 \times 10^{-4}$ ,  $5 \times 10^{-5}$  mol L<sup>-1</sup> by the equation (3). After the averaging out the value of extraction constant ( $K_{extr}$ ) was  $115 \pm 5$ .

### Determination of iodine in form of ionic associate of iodine-iodide complexes with brilliant green

It appears that ionic associates extract only at sufficiently high concentration of iodide-ion, if to perform determination of iodine in iodide in the solution without addition of excess of iodide using spectrophotometric method with brilliant green. Equilibrium of formation of complex  $I_3^-$  from  $I_2$  and  $I^-$  is characterized with constant  $\lg K_1 = 2.9$  [19]. From the expression of law of mass action follows that yield of form of  $I_3^-$  depends from concentration of  $I^-$ :



At the equilibrium concentration of iodide ( $[I^-] = 1$  mol L<sup>-1</sup>), equilibrium concentration of complex ( $[I_3^-]$ ) is  $10^{2.9} [I_2]$  that is part of iodine in iodine-iodide complexes is  $\sim 0.999$ , but when  $[I^-] = 10^{-6}$  mol L<sup>-1</sup> equilibrium concentration of complex ( $[I_3^-]$ ) is  $10^{-2.9} [I_2]$ , that is part of iodine in complex form is  $\sim 0.001$ .

Dependence of extraction degree (R) of iodine in form of ionic associate on logarithm of iodide-ion concentration in the solution is given at the figure 2.

If we assume that practically complete extraction of component in organic phase is possible at the  $R > 0.9$  after two consistent extraction, then total value of extraction degree exceeds the value  $R_{\Sigma} \geq 0.99$ .  $R_{\Sigma} = R_1 + R_2 = R + R \times (1 - R) = 0.9 + 0.9 \cdot 0.1 = 0.99$ .

According to the figure 2 such completeness of the extraction of iodine in carbon tetrachloride in form of ionic associates of iodine-iodide complexes with cationic dye brilliant green is possible at the  $c(KI) > 10^{-4}$  mol L<sup>-1</sup>.

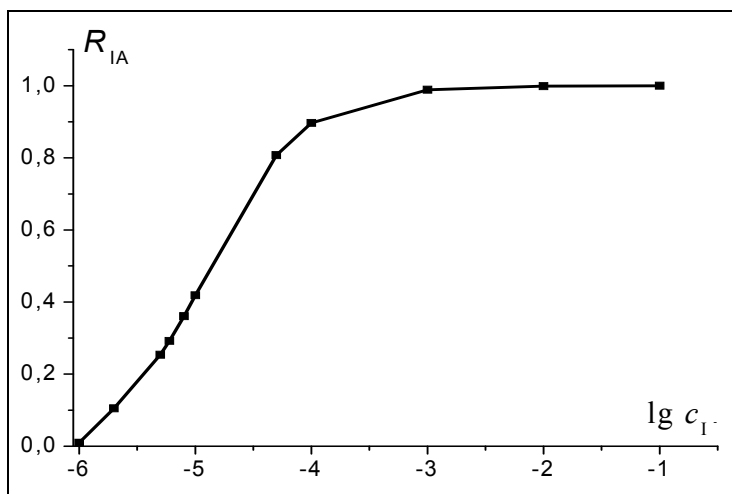


**Figure 2.** Dependence of extraction degree of iodine in CCl<sub>4</sub> in form of ionic associate of iodine-iodide complexes with cationic dye brilliant green on logarithm of iodide-ion concentration in the solution at the same volumes of phases.

Sensitivity of spectrophotometric determination of iodine in the presence of iodide by the procedure with brilliant green is much less than sensitivity of iodide determination. Iodide is determined using electrochemical oxidation [16]; under this condition sensitivity is increased 3 times.

## CONCLUSIONS

1. Investigation and efficiency increase of extraction procedure of ionic associates of iodine-iodide complexes with cationic dye brilliant green have been performed at the determination of iodide:

- heating of aliquot of working solution of brilliant green in the sulfuric acid, saturation of double-distilled water with nitrogen and passing nitrogen through the funnel before extraction provide significant decreasing of absorbance of "blank test" and obtaining of reproducible and stable value of absorbance.

2. Extraction constant of ionic associate of iodine-iodide complexes with brilliant green in CCl<sub>4</sub> has been estimated,  $K_{extr}$  is  $115 \pm 5$ .

3. It is necessary to create  $c(\text{KI}) \geq 10^{-4}$  mol L<sup>-1</sup> for quantitative extraction of iodine-iodide anions in aqueous phase.

## EXPERIMENTAL SECTION

### Apparatus

Absorbance was measured using UV/Vis spectrophotometer SF – 46 (LOMO, Russia), equipped with 10 mm quartz cells.

Carbon tetrachloride (Reachim, pure for analysis) was purified by distillation with activated carbon.

Extraction was carried out using separating funnel (type VD -1 250 GOST 25336-82).

### Reagents

All reagents used were of analytical and all solutions were prepared saturated with gaseous nitrogen.

### Preparation of the solutions

A standard solution of potassium iodide was prepared by dissolving 0.166 g potassium iodide (Reachim, chemically pure) in double-distilled water and diluting to the mark in 100 mL volumetric flask. Solutions with less concentration are prepared with diluting of this solution.

A 1 mol L<sup>-1</sup> sulfuric acid solution was prepared by dilution of concentrated sulfuric acid (Reachim, chemically pure) with double-distilled water.

Saturated solution of brilliant green was prepared by dissolving 5 g of C<sub>27</sub>H<sub>33</sub>N<sub>2</sub>C<sub>2</sub>O<sub>4</sub>H•H<sub>2</sub>O (Reachim, pure for analysis) in 100 mL of double-distilled water, at which point undissolved residue was filtered out. Filtered saturated solution of brilliant green was further twice diluted with double-distilled water. Solution is kept in dark place. Solutions with less concentration are prepared with diluting of this solution.

### Procedure

10 mL of brilliant green solution ( $5 \times 10^{-3}$  mol L<sup>-1</sup>) and 2 mL of H<sub>2</sub>SO<sub>4</sub> (c = 1 mol L<sup>-1</sup>) were mixed in beaker and warmed before extraction, then this mixture was used in extraction-photometric determination. This procedure results in decreased aggregation of dye and, thereby, decreased absorbance value of the blank solution. Warmed mixture of brilliant green and sulfuric acid, 10 mL of potassium iodide solution (c =  $2 \times 10^{-3}$  mol L<sup>-1</sup>) and 20 mL of organic solvent were added to the separating funnel and saturated with nitrogen. Extraction was carried out for 3 min, periodically passing nitrogen through solution in funnel. Organic phase was discarded after first extraction. Extraction was repeated once more. Absorbance of second extract was

measured at absorption maximum band ( $\lambda = 645$  nm) with path length of 1 cm. Absorbance value of second extract is absorbance of blank sample. After second extraction, test solution was added to separating funnel, and then extracted with 20 mL of carbon tetrachloride. Extraction was carried out for 3 min, periodically passing nitrogen through solution in funnel. Organic phase was transferred into 50-mL volumetric flask. Extraction was repeated with new portion of solvent and extracts were combined. Volume of solution was diluted to the mark with extract after third extraction. This procedure is needed to ensure recovery rate 99%. Obtained solution was mixed and absorbance of combined extract was measured at absorption maximum band ( $\lambda = 645$  nm) with path length of 1 cm. To determine iodide different concentration of iodide are inserted in the funnel after the blank solution.

## REFERENCES

1. Qiong He, Junjie Fei, Shengshui Hu, *Analytical Sciences*, **2003**, 19 (5), 681-6.
2. Ahmad H. Alghamdi, *Arabian Journal of Chemistry*, **2010**, 3 (1), 1–7.
3. ZuLiang Chen, Mallavarapu Megharaj, Ravendra Naidu, *Talanta*, **2007**, 72 (5), 1842–1846.
4. Kai-en Wang, Shhiuh-Jen Jiang, *Analytical sciences*, **2008**, 24, 509–514.
5. Bruggink, C.; van Rossum, W.J.M.; Spijkerman, E.; van Beelen, E.S.E.; *J. Chromatogr., A*, **2007**, 1144,170.
6. Rebarry, B.; Paul, P.; Ghosh, P. K.; *Food Chem.*, **2010**, 123, 529.
7. N. Choengchan, K. Uraisin, K. Choden [etc.], *Talanta*, **2002**, 58(6), 1195–1201.
8. Xue Huang, Yongxin Li, Yuanli Chen, Lun Wang, *Sensors and actuators B : Chemical*, **2008**, 134 (2), 780–786.
9. Reyhanem Rahnama Kozani, Ferydoun Ashrafi, Masuod Khalilnezhad, Mohammad Reza Jamali, *E-journal of Chemistry*, **2009**, 6 (4), 1267–1273.
10. Mary George, K.S Nagaraja, Natesan Balasubramanian, *Eurasian J Anal. Chem.*, **2011**, 6 (2), 129–139.
11. T. Cherian, B. Narayana, *South African Journal of Chemistry*, **2007**, 60, 8–10.
12. M.A. El-Ries, Elmorsy Khaled, F.I. Zidane, S.A. Ibrahim, M.S. Abd-Elmonem, *Drug Testing and Analysis*, **2012**, 4(2), 129–135.
13. V.M. Biluk, "Determination of iodide- and bromide-ions with spectrophotometric and spectrofluorometric methods using electrochemical oxidation", Author's abstract, Kharkiv, **2008**, 20 (in Ukrainian).

14. S.B. Niazi, M. Mozammil, *Analytica Chimica Acta*, **1991**, *115*, 252.
15. Krishna K. Verma, Dayashanker Gupte, Sunil K. Sanghi, Archana Jain, *Analyst*, **1987**, *112 (11)*, 1519–1522.
16. A.V. Drozd, T.S. Tishakova, *Central European Journal of Chemistry*, **2011**, *9 (3)*, 432–436.
17. A.V. Drozd, V.M. Loboichenko, T.S. Tishakova, *Journal of Analytical Chemistry*, **2011**, *66 (2)*, 135–138.
18. T.S. Tishakova, A.V. Drozd, *Scientific conference abstracts*, Gurzuf, **2010**, 53.
19. Stability Constants. Part 2. *Inorganic ligands*, London, **1958**, 105.

## ORGANIC POLYMER-MODIFIED CEMENT CONCRETET

MARIN AMĂREANU<sup>a</sup>, LARISA MELIȚĂ<sup>a,\*</sup>

**ABSTRACT.** The present paper presents the research results about the organic and inorganic additions influence, in different percentages in the lab-processed cement concretes, on their mechanical strengths. The cement CEM I 52.5 was used as mineral binder, an epoxy resin was used as polymer and silica fume (SF) as addition. Experiments were performed regarding on availability of the complex binder (organic-inorganic) - water system, in order to assess its ability to develop resistant strengthened structures. These are exemplified by the compression and tensile strengths of obtained concretes, by the developed forces (F) in avulsion tests of the concrete reinforcement, as well as the organic solvent extractions (toluene and ethanol) of polymer from the strengthened cement matrix. It was highlighted the positive role of additions in preparation of those concretes.

**Keywords:** *concrete, polymers, hydraulically active additives, mechanical strengths*

### INTRODUCTION

The flexural and tensile strengths of the cement stone is five times and ten times, respectively, smaller than the compression strength; the deformation extent under load is limited, while it becomes brittle when it breaks. When the applied load increases a largely elastic deformation takes place, followed by a sudden break [1].

When metal components are used for reinforcement, the elastic properties of the construction elements are improved. However, the mechanical performances of the reinforced concrete it's only about 10% of the tensile strength of the metal reinforcement, because the theoretical, intrinsic strength of the cement stone cannot be reached in practice due to its important high porosity.

---

<sup>a</sup> *Technical University of Civil Engineering of Bucharest, Bdul. Lacul Tei nr: 122-124, Sector 2, cod 020396, Bucharest, Romania, \* larisamelita@gmail.com*



The porosity of the cement stone can be reduced by diminishing the water/binder ratio (W/B) when super-plasticizers are used, and by addition of water soluble polymers which can form stable colloidal aqueous emulsions; thus, the pores are filled with polymers and the latter have a plasticizing effect which allows lowering of W/B ratio.

Polymer-modified concrete cements are obtained if, during preparation, a macro-molecular component is added; thereby turning them into a type of concrete with modified properties in comparison to common concretes [2-4]. The **cement** is the predominant component of the complex binder system of cement - organic polymer. **The organic binder**, in small amounts, helps to improve the adhesion between cement stone and aggregate and also between the cement particles [1]. The polymer-modified concrete cements have significantly improved mechanical properties, such as the tensile and bending strength and are more compact, as well as more chemically stable [5-13].

The specialty literature [1, 6] mentions the vinyl poly-acetate, hydroxymethyl-propyl cellulose, polyacrylamide and the epoxy resin as being the polymers used for obtaining cement concrete types. The polymer may account for up to 20% of the complex binder. When choosing the inorganic binder-polymer system attention must be paid to the degree of compatibility between the components, by correlating their properties and the way in which they influence each other during hardening.

For example, the viscosity of the polymer dispersions influences the diffusion processes taking place during the hydration – hydrolysis of the Portland or aluminous cement [1]. In the case of epoxy resins, the presence of a basic environment resulting from hydration – hydrolysis can ensure the monomer cross-binding, thus rendering unnecessary the use of a special hardening component (amines) and thereby simplifying the concrete processing technology. Moreover, using the epoxy resin – cement mixture, the maximal mechanical properties obtained for the polymer/cement ratio are significantly lower than when a binder is added: approximately 0.1 as compared to 0.5 [14].

In this paper the experimental research, performed on organic polymer-modified cement concrete, obtained with river siliceous aggregates mixed with epoxy resin and silica fume are presented. Thus, the dosage effects of resin with / without hardener and silica fume respectively are analyzed, on the physical-mechanical properties of the polymer cement concrete obtained. The effect of calcium ions from the cement on the reinforce resin has been shown through the extraction tests of the epoxy resin from concrete.

## RESULTS AND DISCUSSION

### *Experimental results*

The obtained results, following the physical and mechanical tests, are presented in tables 1 to 3.

### *Assessment of results*

#### *Compression strength*

Figure 1 shows the variation of the compression strengths for concrete types B1, BH1, BH2 and B3 depending on the introduced amount of modified concrete B3, against to the concrete B1, with the resulting values.

An increase of the compression strength values was noted following the improvement of the blank concrete composition if during the process an amount of modified concrete B3 was added; this was placed starting with the basic layer of cubic test specimens, in the amount of 33.33% (for BH1 concrete), 66.66% (for BH2 concrete) and 100% (for B3 concrete) respectively.

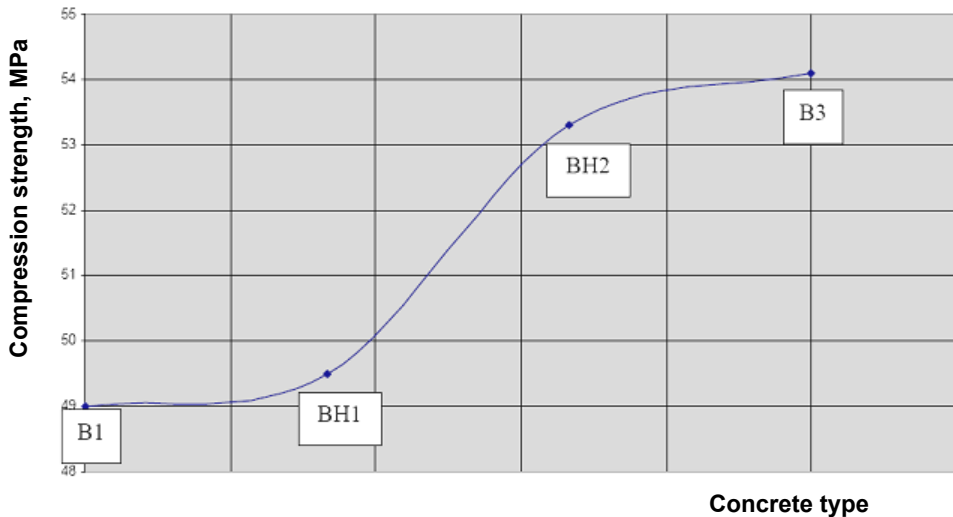


**Figure 1.** Variation of the compression strengths for concrete types B1, BH1, BH2 and B3 depending by the amount of SF, resin and hardener in the mixture; B1 – blank concrete; BH1 – concrete with 33.33% mixture corresponding to B3, in the cube basis layer, and 66.67% blank concrete B1; BH2 – concrete with 66.66% mixture corresponding to B3 in the cube basis layer, and 33.34% blank concrete B1; B3 – concrete with resin, hardener and ultrafine silica (100%).

**Table 1.** The concretes compression strength at 28 days

Type of concrete	$f_c$ (MPa)
Blank concrete (B1)	49.0
Concrete with resin and hardener (B2)	48.8
Concrete with resin, hardener and SF (B3)	54.1
Concrete with resin (B2')	35.6
Concrete with resin and SF (B3')	36.7
Concrete with 1/3 resin, hardener and SF (BH1)	49.5
Concrete with 2/3 resin, hardener and SF (BH2)	53.3

It can be noted in table 1 that B2 modified concrete does not differ, as value, from the point of view of the compression strength from the concrete B1. Concrete types B2' and B3' do not reach the compression strength values of the blank concrete, as they are used in significantly smaller amounts, because the presence of the resin without hardener hinder carrying on the polycondensation-crystallization phase of the cement hydrocompounds; this phase completes the resistance structure of the concrete [15].

### **Flexural tensile strength**

Figure 2 shows the variation of the flexural tensile strength values for concrete types B1, BH1, BH2 and B3, depending on the amount of modified concrete, in comparison to the blank concrete B1, with the resulting values.

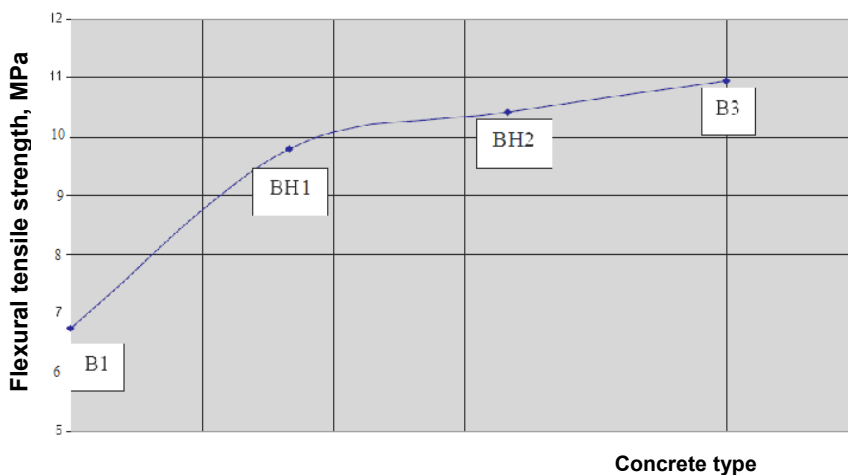


**Figure 2.** Variation of the flexural tensile strength values for concrete types B1, BH1, BH2 and B3 depending by the amount of SF, resin and hardener in the mixture; B1 – blank concrete; BH1 – concrete with 33.33% mixture corresponding to B3, in the stretch load layer, and 66.67% blank concrete B1; BH2 – concrete with 66.66% mixture corresponding to B3 in the stretch load layer, and 33.34% blank concrete B1; B3 – concrete with resin, hardener and ultrafine silica (100%).

The flexural tensile strength tests also resulted in an enhancement of concrete values if the blank concrete was improved by adding the corresponding mixture of concrete composition B3, placed starting with the basic layer (the layer submitted to the tensile strength) of prismatic samples, in amounts of 33.34% (BH1), 66.67% (BH2) and 100% (B3) respectively.

**Table 2.** The concretes flexural tensile strength at 28 days

<i>Type of concrete</i>	$f_{tt}$ (MPa)
<i>Blank concrete (B1)</i>	6.75
<i>Concrete with resin and hardener (B2)</i>	8.55
<i>Concrete with resin, hardener and SF (B3)</i>	10.95
<i>Concrete with resin (B2')</i>	6.98
<i>Concrete with resin and SF (B3')</i>	7.65
<i>Concrete with 1/3 resin, hardener and SF (BH1)</i>	9.79
<i>Concrete with 2/3 resin, hardener and SF (BH2)</i>	10.41

It can be noted, in table 2 that all the other systems under focus, having a polymer-modified structure, account for an obvious enhancement of the flexural tensile strength values in comparison with the blank cement (including the concrete types improved only by adding resin, without hardener).

It is important to underline that all these polymer-modified concrete types showed a ductile break under stress, unlike the blank concrete which became brittle.

Tables 1 and 2 also account for the decisive role played by the SF in modifying the physical and mechanical properties of concrete types under focus, a fact which is also proven by the higher values of the mechanical strengths of concrete types having SF in their composition, in comparison to those which do not (the concrete with resin without hardener with lesser compression strength make exception).

Table 2 also shows the role of the epoxy resin on the flexural tensile strength values, but also the fact that, even if the resin is added without a hardener, it favours a slight increase of the flexural tensile strength of the resin-modified concrete. The resulting concrete types are ductile, unlike the blank concrete, evidenced also in the reference [4].

The importance of the mineral adding (SF) and of the organic polymer (epoxy resin) is therefore confirmed, both of them having a significant role in enhancing the mechanical strength values.

This can be explained by the fact that the mixture of the inorganic binder with the polymer emulsion determines two concurring effects resulting in a higher density of the system: a dispersion effect of the inorganic binder particles – with the advantage of a more uniform texture – and a lubricating effect which allows for reducing the distance between solid particles to a

minimum, thus favouring rapid coagulation. All these effects have a positive influence on the strength structure.

The hardening structure is processed along several stages [14, 16] as follows:

- immediately after mixing the components, the non-hydrated cement particles, the polymer and aggregate particles are surrounded by water and small air bubbles formed during mixing. In the first stage of the interaction process, gelling water particles are formed. At the same time, the polymer particles migrate towards the cement grains and set on them;

- in a more advanced stage, these processes develop and high density, continuous layers of polymer are set on the surface of solid particles (cement covered with water components, or aggregate particles). Finally a continuous binding matrix is formed by water components covered with polymer membranes, which include the remaining non-hydrated cement grains, aggregate particles and small air bubbles. The organic continuous binder matrix influences the nucleation and crystal forming processes, but also their morphology.

The tests focusing on polymer extraction from the hardened polymer - cement matrix showed that the polymer sets on the surface of an anhydride grain or on a cement-hydrated grain, through a series of chemical bonds, with the  $\text{Ca}^{2+}$  ions. The amount of extracted polymer was significantly smaller than the initially introduced amount (with 22%, mass percent, as follows: from 100 g of binder matrix with 3 g of polymer initial content, has been extracted, in used solvent, 2.34 g of polymer) which shows that part of the polymer was set on insoluble components, as a result of chain reticulation through bivalent  $\text{Ca}^{2+}$  basic ions. It can be deduced that the presence of  $\text{Ca}^{2+}$  basic ions determines polymer reticulation, as confirmed by test results presented by other authors [17].

Due to the fact that the polymer binds the calcium ions from the surface of anhydrous or hydrated cement grains, a continuous binding matrix that tightly links these particles is formed; as a result the mechanic strength values are enhanced.

Apart from these chemical interactions, the presence of polymers in the inorganic binder-water system also leads to significant physical effects.

Physical interaction is emphasized by the surface active character of the polymer, resulting from  $\text{HO}^-$  clusters' adsorption on the surface of anhydrous or hydrated particles, thereby modifying the pace of physical and chemical processes taking place in the system, such as the hydration of anhydrous particles or changes undergone by hydrous components. The presence of adsorbed layers on the particle surface changes the conditions for the formation of new components; it also influences the contact between newly formed layers and their structure [15].

In case of systems with a high interaction rate (with a high content of  $C_3A$ ) where strong internal stresses usually take place, the presence of polymers reduces such negative phenomena; due to its elastic properties the polymer absorbs the internal structure stresses and partially leisure the process, with the help of sub-microscopic contacts formed between the hydrous component particles. The lubricating and dispersion processes favour the primary close congealing, thus enhancing mechanical strengths [17, 18].

### ***Avulsion test***

The criterion for assessing the level of adherence of the binding matrix to the reinforcement is given by the result of avulsion tests performed on the concrete-embedded rods.

For the concrete types used in the experiment the resulting strength values are presented in table 3.

**Table 3.** The forces values after applying the avulsion load and break-up characteristic of concrete

<i>Type of concrete</i>	Force F, (daN)	Break-up characteristics
<i>Blank concrete (B1)</i>	4100	Bar breaks
<i>Concrete with resin and hardener (B2)</i>	4000	Concrete fails
<i>Concrete with resin, hardener and SF (B3)</i>	4300	Bar breaks
<i>Concrete with resin (B2')</i>	3400	Concrete fails (easy slip)
<i>Concrete with resin and SF (B3')</i>	3700	Concrete fails

A higher value of force can be noted for the avulsion test performed on concrete with SF, resin and hardener but, the same like in blank concrete case, the metallic rod embedded was broken. A high value of the force was obtained for the concrete type modified with an amount of resin and hardener; in this case the concrete broken.

When preparing the concrete, the use of resin (combined or not with SF) does not increase the avulsion force. It can be noted the decisive role, in concrete preparation, of the hardener with epoxy resin in their structural strength development.

## CONCLUSIONS

The present paper points out the role of SF and of the organic polymer (epoxy resin with a binder) in the hardening of the concrete types under focus, through an enhancement of mechanical strength values. The continuous binder matrix made by the hydrocompounds, covered with polymer membranes which include the un-hydrated cement remains, the aggregate particles and the bubbles, influence the nucleation process and crystal growth so that, positively influencing the hardening [15]. Thus, a densification of the system takes place due to the two combined effects: an effect of dispersion involving the inorganic binder particles, leading to the formation of a more uniform texture, and a lubrication effect allowing the convergence of solid particles to a minimum distance, thus favouring close range coagulation; both effects have a positive influence on the formation of a strong structure.

By including the organic polymer in the binding matrix structure of the concrete the number of structural macro-flaws decreases and the adherence coefficient of the binding matrix-aggregate increases, thereby offering a potential explanation for strength enhancement [1]. At the same time, the organic polymer, through the above-mentioned effects, can improve the viability of these concrete types, making them safer in various aggressive environments; concrete types with a ductile behaviour during breaking are obtained and evidenced during the mechanical strengths.

Through the original methods of concrete moulding (combining, in various ratio, a standard concrete with an improved composition concrete – set on the stretched side of the hardened mixture, between the two concretes, during their tensile strength) have been obtained better results of its mechanical strengths.

The strengths enhancement in case of the concrete types obtained with a complex binder type: cement-polymer or cement-polymer-SF, against to the blank concrete, corroborated with the reduced energy consumption during compaction (due to the use of fluidizing additives) result in an enhanced concrete viability and construction lifespan, important technical and economic advantages.

The high performance concrete types obtained through experiments can be improved in view of producing high durability concrete (specific for road concretes). They can also be used for bridges, with the following advantages:

- increased bridge span; by using high strength concrete an electro-chemical cell, thereby enlarging the central opening of the bridge and allowing for more passage space under the bridge;
- a reduced number of beams for a given span;
- beams could be lower, thus permitting a higher opening;
- the use of SF determines a lowering of the heat produced during cement hydration, thus reducing the risk of cracks.

## EXPERIMENTAL SECTION

### *Materials and reagents*

The organic polymer-modified concrete components are: the mineral binder, the organic binder (polymer), the mixing water, the aggregates and, in certain cases, the additions.

The used mineral binder is cement CEM I 52.5 (Carpatcement) having the physical and chemical characteristics presented in table 4, while the polymer is an epoxy resin (Policolor S.A. Bucharest) with next characteristics: the molecular weight  $M = 370$ , the dynamic viscosity, at 25°C, 10 Pa·s, the epoxy equivalent of 0.51 equiv./100 g and 15% max volatile substances. The used hardener, 30% by the resin, is polyamidoamine type.

**Table 4.** Physical and chemical characteristics of cement CEM I 52.5

		<i>Chemical composition (%)</i>										
		CaO	SiO <sub>2</sub>	SO <sub>3</sub>	Al <sub>2</sub> O <sub>3</sub>	Fe <sub>2</sub> O <sub>3</sub>	MgO	Na <sub>2</sub> O	K <sub>2</sub> O	R <sub>ins</sub> <sup>x</sup>	LOI <sup>xx</sup>	Free CaO
		63.72	20.13	3.09	4.49	3.28	2.35	0.30	0.91	0.20	2.11	0.90
		<i>Mineralogical composition (%)</i>										
		C <sub>3</sub> S	C <sub>2</sub> S		C <sub>3</sub> A		C <sub>4</sub> AF					
		67.18	11.768		6.355		9.97					
CEM I 52.5	<i>Physical characteristics</i>											
	<i>Specific surface</i> (cm <sup>2</sup> /g)			<i>Stability</i> (mm)			<i>Setting time</i> (minutes)					
	4198			0.0			initial		final			
							165		230			
		<i>Mechanical characteristics</i>										
		<i>Compression strength at</i> 2 days (MPa)					<i>Compression strength at</i> 28 days (MPa)					
		36.8					57.8					

<sup>x)</sup> insoluble residuum; <sup>xx)</sup> loss on ignition

The existing research and data in the field have suggested the potentially decisive role of hydraulically active additions (silica fume-SF) and macro-molecular components on the hardening behaviour, as well as on the properties of cements processed with these complex systems. Starting from this premise, the research results for various types of concrete are synthetically presented in table 5.



The utilized aggregates, in the concretes preparation, are river siliceous aggregates with continuous granularity (0-16 mm) and the required amount is also presented in table 5. The granularity limit in which were chosen the granularity curves are presented in table 6.

**Table 5.** Types of concrete taken into account

<i>Concrete notation</i>	B1	B2	B3	B2'	B3'
<i>Characteristic</i>					
<i>Class</i>	C 50/60	C 50/60	C 50/60	C 50/60	C 50/60
<i>Consistency</i>	T2	T2	T2	T2	T2
<i>Cement type</i>	CEM I 52.5	CEM I 52.5	CEM I 52.5	CEM I 52.5	CEM I 52.5
<i>Aggregate type and, quantity (kg) for 1m<sup>3</sup> concrete</i>	(0-16) 1730.8	(0-16) 1606.9	(0-16) 1545.56	(0-16) 1606.9	(0-16) 1545.56
<i>Water/ cement ratio</i>	0.4	0.4	0.4	0.4	0.4
<i>Water quantity (L) for 1m<sup>3</sup> concrete</i>	185	185	185	185	185
<i>Cement quantity (kg) for 1m<sup>3</sup> concrete</i>	462.5	462.5	462.5	462.5	462.5
<i>Resin quantity (kg) for 1m<sup>3</sup> concrete</i>	-	48.6	48.6	69.4	69.4
<i>Hardener quantity (kg) for 1m<sup>3</sup> concrete</i>	-	20.8	20.8	-	-
<i>SF quantity (kg) for 1m<sup>3</sup> concrete</i>	-	-	46.2	-	46.2

**Table 6.** Limit of granulate areas for aggregates (0-16) and the granularity used

<i>Sieve diameter (mm)</i>	0.5	1	2	4	8	16
<i>Min.</i>	8	12	21	36	60	100
<i>Passages (%)</i>						
<i>Max.</i>	20	32	42	56	76	100
<i>Used</i>	18	25	33	45	70	100

Table 7 shows the chemical composition of the used addition: the silica fume (SF).

**Table 7.** Chemical characteristics of SF

<i>Component</i>	SiO <sub>2</sub>	Fe <sub>2</sub> O <sub>3</sub>	Al <sub>2</sub> O <sub>3</sub>	CaO	MgO	Na <sub>2</sub> O	K <sub>2</sub> O	MnO	LOI	<i>Reactive silica</i>
<i>U.M. (%)</i>	84.1	8.0	0.8	1.0	0.8	-	-	-	3.9	82.37

The amount of aggregates on various types needed for each type of resulting concrete is presented in table 8.

**Table 8.** Amount of aggregate sorts for each type of concrete

Sort	B1 (kg)	B2 (kg)	B3 (kg)	B2' (kg)	B3' (kg)
(0-1)	432.7	401.8	386.67	401.8	386.67
(1-2)	138.5	128.5	123.33	128.5	123.33
(2-4)	207.7	192.8	185.56	192.8	185.56
(4-8)	432.7	401.8	386.67	401.8	386.67
(8-16)	519.2	482	463.33	482	463.33

The used reinforcement on avulsion test of concrete reinforcement is PC 52 concrete-steel with 12 mm diameter.

### ***Experimental methods***

Experimental studies was performed on the above mentioned systems, with reference to the behaviour of the complex binder-water system, as well as to its ability to develop strong hardening structures which can be verified by determining their strength. In order to achieve the proposed objectives, when concretes were prepared the macro-molecular component accounted for 15% (gravimetric percentage) of the cement amount and the SF addition was 10% (gravimetric percentage) toward the cement amount. The water/cement ratio (W/B) for all types of the obtained cement remained constant and equal to 0.4; the vibration compaction was the procedure used in this case. The experiments have been carried out on the concrete types presented in table 5.

To highlight the influence of the polymer on the stretched part of the samples, used to tensile strength, two other concrete specimens, marked BH1 and BH2 were also prepared by combining BH3 concrete with B1 concrete, in the following proportions:

- 1/3 of the concrete amount required to fill a mould (prism or cube), to be poured at the mould basis, is represented by B3 and the rest being B1;
- 2/3 of the concrete amount required to fill a mould (prism or cube), to be poured at the mould basis, is represented by B3 and the rest being B1.

The levels of compression strength were determined on cubes with a 15 cm side, while the flexural and tensile strength levels on prisms of a 10x10x55 cm size, by applying a concentrated force in the middle of the prism opening being used.

Five of the resulting concrete types (B1, B2, B3, B2' and B3') – cubes with a 15 cm side – were submitted to a reinforcement avulsion test, using a 12 mm diameter embedded rod mounted during casting (on the principle of the chemical anchor).

In order to check the polymer setting, using  $\text{Ca}^{2+}$  ions, a number of tests were aimed at extracting the polymer from the hardened cement and polymer matrix. For this purpose, the composite cement stone was broken into small pieces and placed in organic solvents (toluene, ethanol) in which the polymer itself was soluble. After drying, the test pointed out the mass loss of the sample immersed in organic solvents.

## REFERENCES

1. M. Amăreanu, „Materiale de construcție. Aspecte de rezistență și durabilitate pentru betoane și metale”, Editura Conspress, București, **2013**.
2. M. Harja, M Bărbuță, L. Rusu, *Journal of Applied Sciences*, **2009**, 9(1), 88.
3. M. Bărbuță, M. Harja, I. Baran, *Journal of Materials in Civil Engineering*, **2010**, 22(7), 696.
4. H. Abdel-Fattah, M. El. Hawary, *Construction and Building Materials*, **1999**, 13, 253.
5. M. Bărbuță, M. Harja, D. Babor, *Romanian Journals of Materials*, **2010**, 40(1), 3.
6. M. Mohammadian, A. K. Haghi, *Romanian Journals of Materials*, **2013**, 43(3), 276.
7. B. Wang, H. Al, K. Song, Y. Han, T. Zhang, *Romanian Journals of Materials*, **2013**, 43(1), 14.
8. D.A. Silva, V.M. John, J.L.D. Ribeiro, H.R. Roman, *Cement and Concrete Research*, **2001**, 31(8), 1177.
9. A.M. Olaru, O. Withhold, A. Adams, *Cement and Concrete Research*, **2011**, 41(11), 1123.
10. J.M. Gao, C.X. Qian, B. Wang, K. Morino, *Cement and Concrete Research*, **2002**, 32(1), 41.
11. N. Shirshova, A. Menner, Gary P. Funkhouser, A. Bismarck, *Cement and Concrete Research*, **2011**, 41(4), 443.
12. J. Rottstegge, M. Wilhelm, H.W. Spiess, *Cement and Concrete Research*, **2006**, 28(5), 417.
13. D. Van Gemert, L. Czarniecki, M. Maultzsch, H. Schorn, A. Beeldens, P. Łukowski, E. Knapen, *Cement and Concrete Research*, **2005**, 27(9-10), 926.
14. Annemarie Puri, Special binder buildings – Graduals studies (VI) UPB, **1997-1998**.
15. I. Teoreanu, V. Moldovan, M. Georgescu, M. Muntean, A. Puri, „Bazele fizico-chimice ale întăririi lianților anorganici”, Ed. Didactică și Pedagogică, R.A. București, **1972**.
16. I. Teoreanu, „Bazele tehnologiei lianților anorganici”, Ed. Didactică și Pedagogică, R. A. București, **1993**.
17. T. Chaowasakoo, N. Sombatsompop, *Composites Science and Technology*, **2007**, 67(11-12), 2282.
18. M. Amăreanu, *Romanian Journals of Materials*, **2010**, 40, 203.

## THE EFFECT OF ZINC FROM THE SEED ON ANTIOXIDANT DEFENSE SYSTEM IN WINTER WHEAT (*Triticale aestivum* L.) SEEDLINGS

DEJAN PRVULOVIĆ<sup>a,\*</sup>, RUDOLF KASTORI<sup>a</sup>, IMRE KÁDÁR<sup>b</sup>

**ABSTRACT.** Accumulation of zinc in seeds of winter wheat plants grown at four different levels of zinc (Zn) in soil ranging from 0 to 810 kg/ha of added Zn and remobilization of Zn from seeds to seedlings leaves were examined. Lipid peroxidation, soluble protein content and activity of enzymes of antioxidant defense were also studied in seedling leaves. The accumulation of Zn in seeds and its remobilization from seeds into primary leaves was proportional to Zn supply. Inducible effect of Zn was found on activity of most enzymes of antioxidative defense (superoxid dismutase, catalase and peroxidase). Activity of glutathione peroxidase was decreased. Although Zn is essential micronutrient for plants and could act as an antioxidant at lower doses, at high applied concentrations act as a prooxidant evoking oxidative stress.

**Keywords:** *antioxidative enzymes, lipid peroxidation, oxidative stress, Triticale aestivum L., winter wheat, zinc.*

### INTRODUCTION

Zinc (Zn) is needed as micronutrient by all living organisms and is essential for normal growth and development of plants, as it is known to be required in several aspects of metabolism and reproductive development [1]. The critical soil Zn toxicity level for plants varies as a function of various soil and climatic factors as well as plant species and genotype [2]. Although Zn is an essential micronutrient, it become phytotoxic and inhibits cell growth in plants at excessive concentrations [3]. Leaf epinasty and chlorosis are easy visible symptoms of strong Zn phytotoxicity [4].

---

<sup>a</sup> *University of Novi Sad, Faculty of Agriculture, Trg Dositeja Obradovića, Nr. 8, 21000 Novi Sad, Serbia, \* dprvulovic@yahoo.com*

<sup>b</sup> *Research Institute for Soil Science and Agricultural Chemistry of Hungarian Academy of Sciences, Budapest, Hungary*

Reactive oxygen species (ROS), which includes superoxide ( $O_2^{\cdot-}$ ), hydroxyl radicals ( $OH^{\cdot}$ ) and hydrogen peroxide ( $H_2O_2$ ), the ubiquitous products of single electron reductions of molecular oxygen are among the most reactive compounds known to be produced during and early metals stress. ROS are responsible for the majority of biological oxidative damage associated with oxidative stress, such as DNA, protein and the cell membrane damage [5]. The accumulation of ROS is limited by the action of various enzymatic and non-enzymatic mechanisms. These protective mechanisms include antioxidant enzymes such as superoxide dismutase (SOD), catalase (CAT), various peroxidases and other enzymes [6].

## RESULTS AND DISCUSSION

When applying increasing quantity of  $ZnSO_4$  to the soil, the Zn contents of the seeds of winter wheat plants increased (Table 1). The remobilization of Zn from seed tissues during germination and early growth in seedlings was intensive. In response to an altered Zn content in the seeds, the Zn content of seedlings with highest amount of Zn in seeds reached a value almost double higher than the control. The accumulation of Zn in root and leaves of barley seedlings was proportional to metal concentration in culture medium [1, 7, 8]. Greater Zn concentration in nutrient solution significantly depressed the fresh and dry mass of leaves of different plant species [8, 9, 10]. Dry matter production of shoots was not altered by zinc content in shoot tissues. Only the highest Zn accumulation in shoots resulted in lower dry matter of shoots at early stage of growth. One of the first responses of plants to heavy metal stress is reduction of biomass, which can be considered as an index of plant tolerance [10].

**Table 1.** Dry matter content in shoots, and Zn concentrations in seeds and shoots of winter wheat plants at various Zn addition.

	Zn added (kg/ha)			
	0	90	270	810
Dry matter of shoots [mg/plant]	6.90 ± 0.63 <sup>a</sup>	7.05 ± 0.66 <sup>a</sup>	6.80 ± 0.61 <sup>a</sup>	5.50 ± 0.50 <sup>b</sup>
Zn content in seed [mg/kg]	12.56 ± 1.11 <sup>a</sup>	49.00 ± 0.42 <sup>b</sup>	56.28 ± 0.56 <sup>c</sup>	65.37 ± 0.60 <sup>d</sup>
Zn content in shoots [mg/kg dry matter]	43.58 ± 8.76 <sup>a</sup>	71.87 ± 3.96 <sup>b</sup>	73.45 ± 7.45 <sup>b</sup>	81.90 ± 10.10 <sup>c</sup>
<sup>a, b, c, d</sup> Values within columns without common superscript are significantly different ( $P < 0.05$ ). Values represent the mean ± SD				

Zinc stimulates the production of ROS (Table 2). Lipid peroxidation, which is measured as MDA content, showed no significant alteration in the shoots of seedlings with lower content of Zn in tissues. However, the presence of Zn at higher amount in tissues of shoots expressed slightly enhanced MDA levels in comparison with that in control seedlings. As reported earlier, excess of Zn promoted MDA production in plants due to increased lipid peroxidation through excessive generation of free radicals [6, 7, 8]. Zn content in shoots did not affect level of soluble protein in tissues. Khudsar et al. [11] found that leaves of *Artemisia annua* had significantly lower protein content throughout the plant life in the Zn treated plants.

**Table 2.** Soluble protein content, lipid peroxidation, hydroxyl and superoxide radical accumulation, activities of enzymes of antioxidative response: superoxide dismutase (SOD), catalase (CAT), peroxidase (POD) and glutathione peroxidase (GSH-Px) in shoots of winter wheat at various Zn addition.

	Zn added (kg/ha)			
	0	90	270	810
Soluble protein content [g/kg]	25.99 ± 3.07 <sup>a</sup>	22.84 ± 2.13 <sup>a</sup>	23.24 ± 1.05 <sup>a</sup>	22.91 ± 3.32 <sup>a</sup>
Lipid peroxidation [nmol MDA/g]	60.41 ± 0.23 <sup>a</sup>	60.72 ± 3.73 <sup>a</sup>	66.21 ± 4.16 <sup>b</sup>	67.40 ± 2.84 <sup>b</sup>
Hydroxyl radical [nmol/g]	121.60 ± 11.61 <sup>a</sup>	122.21 ± 9.09 <sup>a</sup>	136.81 ± 6.24 <sup>b</sup>	158.71 ± 13.20 <sup>c</sup>
Superoxide radical [mmol/g]	4.25 ± 0.30 <sup>a</sup>	4.77 ± 0.41 <sup>a</sup>	51.52 ± 0.36 <sup>b</sup>	56.14 ± 0.51 <sup>b</sup>
SOD [U/g]	67.70 ± 6.04 <sup>a</sup>	82.32 ± 7.69 <sup>b</sup>	90.10 ± 8.52 <sup>b</sup>	121.37 ± 8.17 <sup>c</sup>
CAT [U/g]	145.03 ± 10.43 <sup>a</sup>	148.27 ± 9.95 <sup>a</sup>	164.63 ± 11.45 <sup>b</sup>	198.87 ± 13.77 <sup>c</sup>
POD [U/g]	9.77 ± 0.93 <sup>a</sup>	12.23 ± 1.49 <sup>b</sup>	12.41 ± 1.03 <sup>b</sup>	19.71 ± 2.13 <sup>c</sup>
GSH-Px [U/g]	116.03 ± 2.00 <sup>a</sup>	75.20 ± 11.91 <sup>b</sup>	60.52 ± 5.87 <sup>c</sup>	56.34 ± 10.22 <sup>c</sup>
a, b, c Values within columns without common superscript are significantly different ( $P < 0.05$ ). Values represent the mean ± SD				

The changes in the antioxidant enzyme activities, CAT, SOD, POD and GSH-Px, in shoots of winter wheat seedlings are shown in Table 2. Activities of CAT, SOD and POD displayed a progressive increase in response to Zn in dose-response manner, and the peak activity was found at highest Zn content. More than 2-fold increase in activity of these enzymes was

observed in seedlings with highest Zn content. Unlike others, the activity of GSH-Px declined as Zn content increase. To mitigate and repair damage initiated by ROS a significant enhancement in SOD activity was observed in seedlings with higher content of Zn. There are also reports of high SOD activity in different plant species [6, 8, 9].

The role of POD for scavenging different peroxides is generally recognized [12]. Significant increases in the activities of CAT and POD in the present investigation suggest their role in constant detoxification of H<sub>2</sub>O<sub>2</sub> in seedlings under Zn toxicity [6, 7]. However, Hegedűs et al. [1] did not observe any change in CAT activity in Zn stressed barley seedlings. Cuypers et al. [13] and Hegedűs et al. [1] observed that a treatment with Zn resulted in an increase of the POD capacity.

## CONCLUSIONS

Although Zn is not a redox active metal, it was shown that Zn toxicity could lead to oxidative damage as well as to induce antioxidative defense mechanisms against it.

In this study, Zn toxicity induces intracellular oxidizing conditions leading to the production of ROS, this was deduced from the stimulation of SOD, CAT and POD capacities in shoots of the seedlings.

## EXPERIMENTAL SECTION

### *Plant material*

A small-plot long-term field experiment was set up at the Nagyhörösök Experimental Station of the Research Institute for Soil Science and Agricultural Chemistry of the Hungarian Academy of Sciences, Budapest, to investigate the effect of high trace element rates. Winter wheat (*Triticale aestivum* L. cv. Kitarò) was sown on the loamy textured calcareous soil formed on loess. Zn was applied at levels of 0, 90, 270 and 810 kg/ha. At harvest, seed were analysed for Zn content by inductive coupled plasma emission spectrometer (ICP) after digestion in cHNO<sub>3</sub> and cH<sub>2</sub>O<sub>2</sub>. Before sowing, seeds were surface sterilised by soaking in 70% (v/v) ethanol for 1 min, followed by 10% (v/v) sodium hypochlorite solution for 30 s, and rinsing in deionised water. Seed were placed in Petri dishes and germinated in a growth chamber. The seed were half submerged by periodically adding deionised water. Each treatment included five replicates with 35 seedlings per replicate. Samples were harvested on 23 day from the onset of imbibitions. Shoot

samples were analysed for Zn content by ICP. Leaf tissue homogenate were used for biochemical determinations and enzyme activity. All spectrophotometric analysis was conducted on a UV/visible light spectrophotometer (Jenway, 6505, UK).

#### *Measurement of antioxidant activity*

Lipid peroxidation was assayed by measuring malonyl dialdehyde (MDA) production [14]. Superoxide radical production was determined by the adrenaline autooxidation [15] and hydroxyl radical production by the inhibition of deoxyribose degradation [16]. The total protein content in extracts was determined by a method described by Lowry et al. [17]. Total SOD activity was measured by the method of Mandal et al. (2008). CAT was assayed by monitoring the consumption of H<sub>2</sub>O<sub>2</sub> [18]. Peroxidase (POD) was determined by measuring the oxidation of guaiacol [19]. Glutathione peroxidase (GSH-Px) activity was assayed according to the method of Upadhyaya et al. [20].

#### *Statistical analysis*

Results are expressed as mean of determinations of 3 independent samples made in triplicates. Statistical significance was tested by analysis of variance followed by comparison by Duncan's multiple range test ( $P < 0.05$ ) calculated using STATISTICA for Windows version 9.0 (StatSoft, Tulsa, OK, USA). Stepwise multiple regression analyses were used to determine correlation among variables.

## REFERENCES

1. A. Hegedűs, B.D.Harrach, G. Bárdos, S. Erdei, *Acta Biologica Szegediensis*, **2005**, 49, 55.
2. M.M. Lasat, N.S. Pence, D.F. Garvin, S.D. Ebbs, L.V. Kochian, *Journal of Experimental Botany*, **2000**, 51, 71.
3. A. Muschitz, C. Faugeron, H. Morvan, *Acta Physiologiae Plantarum*, **2009**, 31, 1197.
4. A. Bittsánszky, T. Kömives, G. Gullner, G. Gyulai, J. Kiss, L. Heszky, L. Radimszky, H. Rennenberg, *Environment International*, **2005**, 31, 251.
5. R. Mittler, S. Vanderauwera, M. Gollery, F. Van Breusegem, *Trends in Plant Science*, **2004**, 3, 490.
6. K.V.S.K. Prasad, P. Pardha Sardhi, P. Sharmila, *Environmental and Experimental Botany*, **1999**, 42, 1.



7. B. Gupta, G.C. Pathak, N. Pandey, *Russian Journal of Plant Physiology*, **2011**, 58, 85.
8. P.I. Michael, M. Krishnaswamy, *Environmental and Experimental Botany*, **2011**, 74, 171.
9. M. Bonnet, O. Camares, P. Veisseire, *Journal of Experimental Botany*, **2000**, 51, 945.
10. D. Di Baccio, S. Kopriva, L. Sebastiani, H. Rennenberg, *New Phytologist*, **2005**, 167, 73.
11. T. Khudsar, Mahmooduzzafar, M. Iqbal, R.K. Sairam, *Biologia Plantarum*, **2004**, 48, 255.
12. O. Blokhina, E. Virolainen, K.V. Fagerstedt, *Annals of Botany*, **2003**, 91, 179.
13. A. Cuypers, J. Vangronsveld, H. Clijsters, *Journal of Plant Physiology*, **2002**, 159, 869.
14. Z.A. Placer, L.L. Cushman, B.C. Johnson, *Analytical Biochemistry*, **1968**, 16, 359.
15. H.P. Misra, I. Fridovich, *Journal of Biological Chemistry*, **1972**, 247, 3170.
16. K.H. Cheesman, A. Beavis, H. Esterbauer, *Biochemistry Journal*, **1988**, 252, 649.
17. O.H. Lowry, N.J. Rosenbrough, A.L. Farr, R.J. Randall, *Journal of Biological Chemistry*, **1951**, 193, 265.
18. B. Chance, H. Sies, A. Boveris, *Physiological Reviews*, **1979**, 59, 527.
19. Y. Nakano, K. Asada, *Plant and Cell Physiology*, **1981**, 22, 867.
20. A. Upadhyaya, D.M. Sankhla, T.D. Davis, N. Sankhla, B.N. Smith, *Journal of Plant Physiology*, **1985**, 121, 453.

## ISOLATION OF SUCCINIC ACID-PRODUCING *ESCHERICHIA COLI* FROM ANIMAL FAECES

ANDREA (IUHASZ) FAZAKAS<sup>a,\*</sup>, ZSOLT BODOR<sup>a</sup>, ERIKA KOVÁCS<sup>b</sup>,  
ÉVA LASLO<sup>b</sup>, SZABOLCS LÁNYI<sup>a,b\*</sup>, BEÁTA ÁBRAHÁM<sup>b</sup>

**ABSTRACT.** Succinic acid is currently used in the agricultural, food and pharmaceutical industries, is one of the key basic chemicals used in the preparation of biodegradable polymers. The first step in the fermentative production of succinic acid is the screening of bacterial strains. Therefore we were isolated a number of 65 *E. coli* strains from different animal faeces. Out of these strains, we identified a number of six strains by sequencing, and we examined their ability to produce succinic acid with chromatography. Based on the resulting chromatograms, 38 strains of the all *E. coli* strains produced succinic acid.

**Keywords:** *Escherichia coli*, succinic acid, isolation, identification, ARDRA, chromatography

### INTRODUCTION

Succinic acid is a dicarboxylic acid containing four carbon atoms with chemical formula  $C_4H_6O_4$  and it was first prepared from amber by Georgius Agricola in 1546 [1]. Succinic acid has a wide variety of applications and can be used as a starting material for many chemical products, such as biodegradable polymers and solvents [2], adipic acid, 1,4-butanediol and  $\gamma$ -butyrolactone [1]. Currently, succinic acid is produced on industrial scale by catalytic hydrogenation of petrochemically derived maleic anhydride [3]. However, in recent times, has received much attention the bio-based production of succinic acid by bacterial fermentation from renewable resources, because the petroleum is a finite resource and the price of oil is increasing [1, 4]. The US Department of Energy listed succinic acid in the top 12 chemical building blocks, which can be used for the production of various high value-added derivatives from renewable resources by microorganisms [5].

---

<sup>a</sup> Politehnica University of Bucharest, Faculty of Applied Chemistry and Material Science, Splaiul Independenței Nr. 313, sector 6, RO-060042, Romania, \* iuhaszandrea@sapientia.siculorum.ro

<sup>b</sup> Sapientia Hungarian University of Transylvania, Faculty of Science, Department of Bioengineering, Piața Libertății Nr. 1, Miercurea Ciuc, RO-530104, Romania, lanyiszabolcs@sapientia.siculorum.ro

Succinic acid is an intermediate metabolite, and many bacteria are capable to produce it under different environmental conditions [6]. Three well-known natural succinic acid-overproducing strains have been studied: *Mannheimia succiniproducens* [7, 8], *Anaerobiospirillum succiniproducens* [9] and *Actinobacillus succinogenes* [10, 11]. There are some strains that produce no or only very small amounts of succinic acid, but the genetically modified version of these strains already produce, such as *Escherichia coli* [12-15], *Corynebacterium glutamicum* [16], *Saccharomyces cerevisiae* [17, 18].

*Escherichia coli* is one of the most widely used microorganism in industry and biotechnology [3]. It is a gram-negative, facultative anaerobe bacterium, which has a few advantages over other microorganisms as follows: cultures can be grown faster in minimal media, wide range of substrate utilization, hence it is a strong candidate to be used in different biotechnological processes [6, 19]. The availability of genetic engineering tools for this organism and the well understood methods makes to be widely used in metabolic engineering [20].

The main aim of our study was to isolate *Escherichia coli* strains from different animal faeces, which are able to produce succinic acid. In the present study we discuss the isolation of *E. coli*, biochemical properties of isolated strains and identification of the strains with Amplified Ribosomal DNA Restriction Analysis (ARDRA), as well as which strains produce succinic acid.

## RESULTS AND DISCUSSION

As we know *Escherichia coli* is commonly found in the digestive tracts of the normal intestinal flora of different species of animals including humans too, so the isolation was carried out from animal faeces. The faeces were collected from farms from different animals and birds (dog, cow, horse, sheep, pig, hen and pigeon).

All the *E. coli* isolates, which can ferment lactose appear as colonies with a green metallic sheen or blue-black to brown color on the Eosin Methylene Blue (EMB) agar and as yellow colonies on the Tergitol-7 agar. Bacteria that can utilize acetic acid turn the medium blue on the Acetate Differential Agar (ADA) [21]. Out of total 23 samples, 121 isolates were obtained: 75 isolates from EMB agar, 28 isolates from ADA and 18 isolates from Tergitol-7 agar.

Out of these isolates, 92 isolates gave positive tests for indol production, 100 isolates gave positive results for methyl red test, 112 isolates gave negative results for Voges-Proskauer test and 115 isolates gave negative tests for citrate utilization. Those strains which showing results + + - - during the reactions IMViC were confirmed as *Escherichia coli*. Based on the biochemical tests, 78 isolates showed similarities with biochemical properties of *E. coli*.

These 78 isolates were analyzed by ARDRA, thus, the 16S rDNA characterization was realized for all strains. From the digested products obtained with the two restriction endonucleases, *AluI* and *HaeIII*, 11 isolates are shown in Figure 1. and Figure 2.

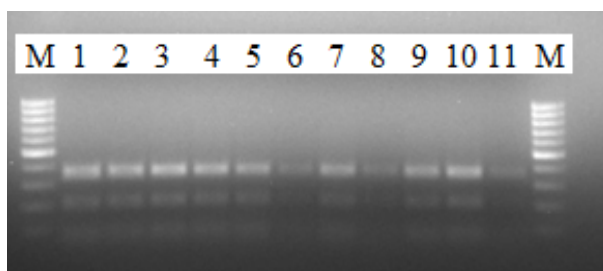


**Figure 1.** Restriction patterns of the 16S rDNA region of strains after digestion with *AluI* (M: 1 kb molecular weight marker, Fermentas, 1: M3/2  $10^{-2}$ , 2: M10/2  $10^{-1}$ , 3: EMB4/3, 4: Ter8/1  $10^{-3}$ , 5: M4/7  $10^{-4}$ , 6: ADA M7  $10^{-2}$ , 7: M8/2  $10^{-2}$ , 8: M3/4  $10^{-1}$ , 9: M3/1, 10: Ter 4  $10^{-3}$ , 11: Ter3/2)

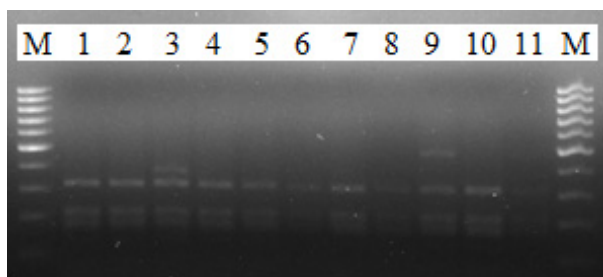


**Figure 2.** Restriction patterns of the 16S rDNA region of strains after digestion with *HaeIII* (M: 1 kb molecular weight marker, Fermentas, 1: M3/2  $10^{-2}$ , 2: M10/2  $10^{-1}$ , 3: EMB4/3, 4: Ter8/1  $10^{-3}$ , 5: M4/7  $10^{-4}$ , 6: ADA M7  $10^{-2}$ , 7: M8/2  $10^{-2}$ , 8: M3/4  $10^{-1}$ , 9: M3/1, 10: Ter 4  $10^{-3}$ , 11: Ter3/2)

On the basis of cluster analysis (Figure 3.), isolated bacterial strains resulted in five different ARDRA groups. The first group includes 65 isolates, including *E. coli* strain ATCC 13706, which was used as a reference strain. The second group includes seven isolates and the remaining three groups each including two strains.

From each group one strain was sequenced, except for the first group, from which six were sequenced. The obtained sequences were compared with sequences found in the NCBI database by the Blast search program. The result of the sequencing are shown in the Figure 3., where instead of the codes of isolates, the name of the strains are listed.

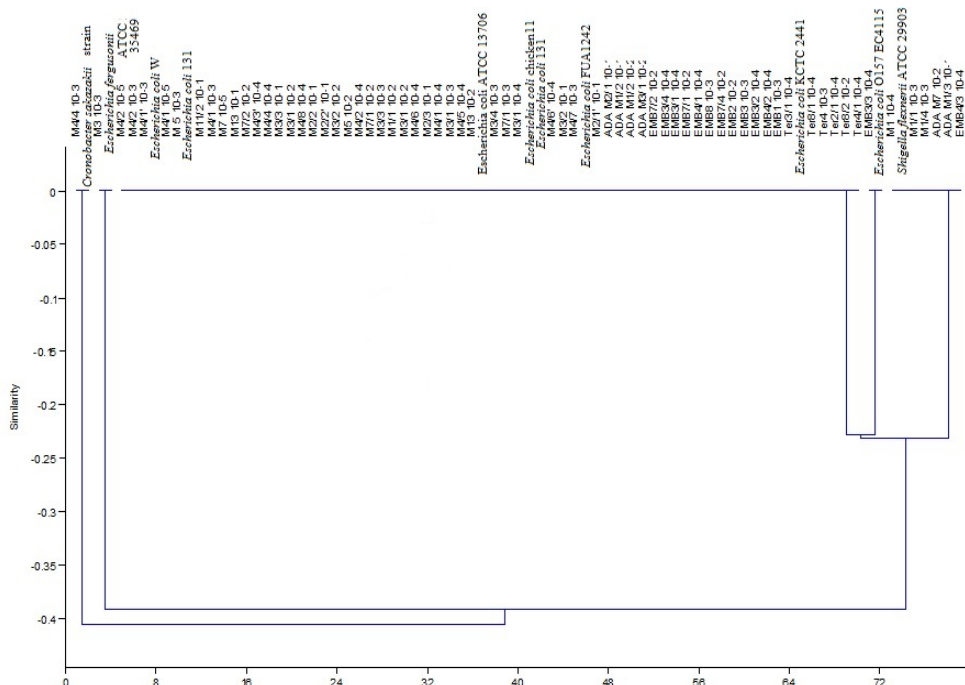


**Figure 3.** Genetic variability of the isolated bacterial strains

The isolated *E. coli* strains were screened based on their abilities to produce succinic acid using glycerol as carbon source under microaerobic conditions as described in Experimental Section. Identification of succinic acid was performed in a gas chromatography–mass spectrometry (GC/MS) experiment. In the fermentation mixtures the succinic acid was identified as trimethylsilylated succinate at 10'71" retention time. A number of 38 *E. coli* isolates from the 65 studied, were able to produce succinic acid. The results of the GC/MS analysis in the case of two strains are presented in Figure 4. The Figure 4A shows that the Ter8/1 10<sup>-3</sup> strain was able to produce succinic acid in minimal medium, but in case of M8/2 10<sup>-2</sup> strain the level of succinic acid is extremely low (B).

ISOLATION OF SUCCINIC ACID-PRODUCING *ESCHERICHIA COLI* FROM ANIMAL FAECES

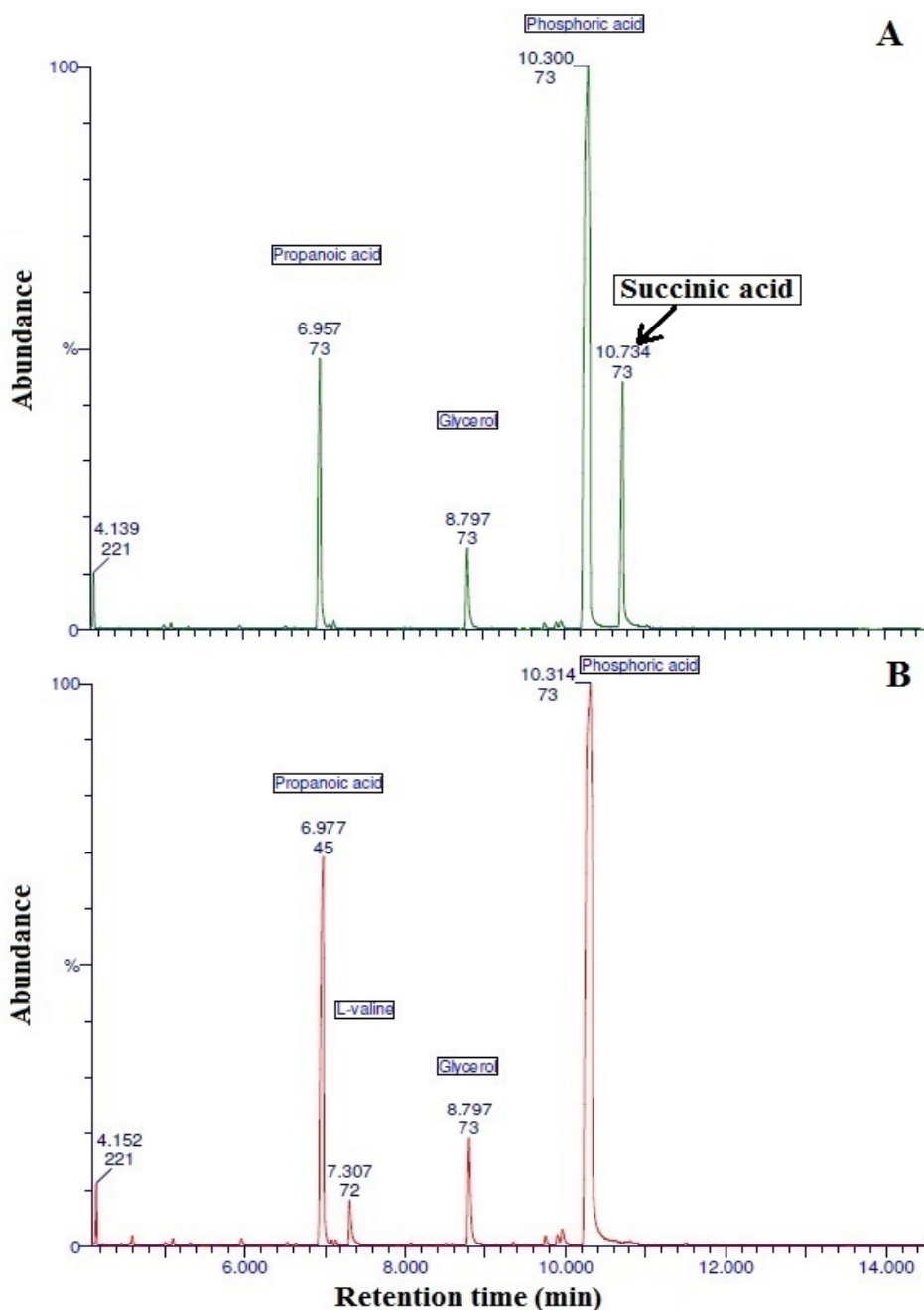


**Figure 4.** GC chromatograms of metabolites in case of *E. coli* KCTC 2441 strain ( $10^{-3}$ ) (A) and *E. coli* W strain ( $10^{-2}$ ) (B)

## CONCLUSIONS

In the industrial production of succinic acid the first important step is the isolation and characterization of possible producing strains. In this study we managed to isolate and characterize different *E. coli* strains from different faeces possible candidates for succinic acid production. Out of total 23 samples, 121 isolates were obtained, from which 78 isolates were confirmed as *Escherichia coli* on the basis of their biochemical properties. All of the isolates were analysed for the differences in the ribosomal DNA with *AluI* and *HaeIII* restriction endonucleases, and five ARDRA groups were obtained. We identified at least one isolate from each group, and six *E. coli* strains were identified by sequencing. After the identification, all of the 65 *E. coli* strains were analyzed according to the ability to produce succinic acid, using GC-MS. Based on the resulting chromatograms, we can conclude that 38 of the 65 *E. coli* strains are able to produce succinic acid.

In the future quantitative analysis will be performed for succinic acid from one of the screened strain. This strain will be genetically modified in order to improve succinic acid production level and create an industrially important strain.

## EXPERIMENTAL SECTION

### Collection and culture of the samples

Samples were collected aseptically and analyzed within 24 hours. From the center of each samples were weighed out 1 g and homogenized with 9 mL physiological solution. From this stock solution 5-fold serial dilutions was prepared and a volume of 1 mL of each solutions was spreaded onto three selective agar: EMB, ADA and Tergitol-7 agar [21] and incubated at 37°C for 24 hours. The organisms showing characteristic colony morphology of *E. coli* were taken onto nutrient agar and repeatedly subcultured onto nutrient agar until the pure cultures with homogenous colonies were obtained. The pure cultures were taken onto nutrient agar slant and used for biochemical assays.

### Biochemical tests

Each pure culture was subjected to four biochemical tests, namely IMViC: indole production, methyl red test, Voges-Proskauer test and citrate utilization.

Glucose-peptone broth (glucose 1 g/L, peptone from casein 20 g/L, peptone from meat 5 g/L, KNO<sub>3</sub> 1 g/L, Na<sub>2</sub>S<sub>2</sub>O<sub>3</sub>·5H<sub>2</sub>O 0.2 g/L, pH=7.3±0.1)

was used for indol test. The strains were cultured in 5 mL of this broth at 37°C for 48 hours. After 48 hours 0.3 mL Kovac's reagent was gently added to the medium and formation of a red colored ring on the top of the medium indicated positive result.

MR-VP broth (glucose 5 g/L, peptone from casein 5 g/L,  $\text{KH}_2\text{PO}_4$  5 g/L,  $\text{pH}=7.5\pm 0.1$ ) was used for methyl red test and Voges-Proskauer test. The strains were cultured in 5 mL MR-VP broth at 37°C. After 48 hours 3-4 drops of methyl red solution was added to the culture to determine the color formation. Formation of red color indicated positive result and yellow color indicated negative result. For the strains which were cultured for the Voges-Proskauer test 5 mL of 10% potassium hydroxide was added and incubated at 37°C for 24 hours. After 24 hours the pink-red color of broth indicated positive result.

Citrate agar ( $\text{NaCl}$  5 g/L,  $\text{MgSO}_4$  0.2 g/L,  $(\text{NH}_4)_2\text{H}_2\text{PO}_4$  1 g/L,  $\text{K}_2\text{HPO}_4$  1 g/L, sodium citrate 2.67 g/L, agar 18 g/L, 4 ml of 1% bromthymol blue,  $\text{pH}=6.8\pm 0.1$ ) was used for the citrate utilization test. A single colony was transferred onto the surface of the agar with a steril needle and incubated at 37°C. After 48 hours, if the color of agar is intense blue, then the test result is positive and if no color change, then the result is negative.

Strains showing results + + - - during the reactions IMViC were confirmed as *E. coli*.

### Identification of the isolated bacterial strains

DNA isolation from 3 mL overnight pure cultures was performed using the Wizard Genomic DNA Isolation Kit (Promega) according to the manufacturer's instructions. The 16S rDNA gene was amplified by PCR using 27F (5'AGAGTTTGATCMTGGCTCAG3') and 1492R (5'TACGGYTACCTTGTTACGACTT3') universal primers. The volume of the reaction mixture was 50  $\mu\text{L}$  and contained 0.1 mM of each deoxynucleoside triphosphate, 1 U of Taq DNA polymerase, 2 mM  $\text{MgCl}_2$ , 0.4  $\mu\text{M}$  of each primer and about 20 ng of genomic DNA template in 1X Taq Buffer with  $(\text{NH}_4)_2\text{SO}_4$  (Fermentas). The amplification reaction was performed in Corbett Palm-Cycler thermocycler (Cornett CG1-96) using the following protocol: an initial denaturation at 94°C for 3 min, followed by 32 cycles of amplification (94°C for 30 sec; 46°C for 30 sec; 72°C for 1 min), a final extension at 72°C for 7 min and a subsequent incubation at 4°C.

The amplified products were checked on a 1% agarose gel stained with ethidium bromide and visualized under UV light by using GelDoc System from BioRad.

Isolates were grouped by ARDRA with two different restriction endonucleases: *HaeIII* and *AluI*. Fragments were separated on 2% agarose gel and ARDRA group representatives were identified by sequencing.



The nucleotide sequence determination was performed with BigDye Terminator v3.1 Cycle Sequencing Kit (Applied Biosystems, USA) and capillary electrophoresis of the samples was performed by Biomi Ltd (Gödöllő, Hungary). The obtained sequences were compared to the GenBank databases by the Blast search program. Sequence similarity over 99% was accepted as species level identification.

### **GC/MS analysis**

The isolated *E. coli* strains were grown in 20 mL minimal medium supplemented with 0.2% (v/v) glycerol under microaerobic condition at 37°C. The cells were incubated in serum bottles (50 mL) with shaking (250 rpm). After 24 h, the cells were harvested by centrifugation (10 minutes at 14000 rpm) and the supernatants were filtered with 0.22 µm Millipore® nitrocellulose membranes. The samples were subjected to trimethylsilyl (TMS) derivatization, and this derivatized sample was used for GC/MS (6890N/5975 Agilent). Compounds were identified by comparing the obtained mass spectra with commercially available NIST 98 spectra library.

### **ACKNOWLEDGMENTS**

The work has been funded by the "Sectoral Operational Programme Human Resources Development 2007-2013 of the Romanian Ministry of Labour, Family and Social Protection through the Financial Agreement POSDRU/6/1.5/S/16" and by "BIOBUILD-Synthesis of some C4, C5 carboxylic acid building block chemicals from renewable biomass resources" PN-II-PCCA-2011-3.2-1367.

### **REFERENCES**

1. H. Song, S.Y. Lee, *Enzyme and Microbial Technology*, **2006**, 39, 352.
2. J.G. Zeikus, M.K. Jain, P. Elankovan, *Applied Microbiology and Biotechnology*, **1999**, 51, 545.
3. J.J. Beauprez, M. De Mey, W.K. Soetaert, *Process Biochemistry*, **2010**, 45, 1103.
4. S.H. Hong, *Biotechnology and Bioprocess Engineering*, **2007**, 12, 73.
5. T. Werpy, G. Petersen, "*Top Value Added Chemicals from Biomass*", Washington DC, **2004**, volume 1.
6. Ch. Thakker, I. Martinez, K.-Y. San, G.N. Bennett, *Biotechnology Journal*, **2012**, 7, 213.

7. P.C. Lee, S.Y. Lee, S.H. Hong, H.N. Chang, *Applied Microbiology and Biotechnology*, **2002**, 58, 663.
8. S.J. Lee, H. Song, S.Y. Lee, *Applied and Environmental Microbiology*, **2006**, 72, 1939.
9. P.C. Lee, W.G.L., S.Y. Lee, H.N. Chang, Y.K. Chang, *Biotechnology and Bioprocess Engineering*, **2000**, 5, 379.
10. R.I. Corona-González, A. Bories, V. González-Álvarez, R. Snell-Castro, G. Toriz-González, C. Pelayo-Ortiz, *Current Microbiology*, **2010**, 60, 71.
11. J.B. McKinlay, C. Vieille, J.G. Zeikus, *Applied Microbiology and Biotechnology*, **2007**, 76, 727.
12. X. Zhang, K.T. Shanmugam, L.O. Ingram, *Applied and Environmental Microbiology*, **2010**, 76, 2397.
13. X. Zhang, K. Jantama, K.T. Shanmugam, L.O. Ingram, *Applied and Environmental Microbiology*, **2009**, 75, 7807.
14. W. Wang, Z. Li, J. Xie, Q. Ye, *Bioprocess and Biosystems Engineering*, **2009**, 32, 737.
15. M.D. Blankschien, J.M. Clomburg, R. Gonzalez, *Metabolic Engineering*, **2010**, 12, 409.
16. S. Okino, R. Noburyu, M. Suda, T. Jojima, M. Inui, H. Yukawa, *Applied Microbiology and Biotechnology*, **2008**, 81, 459.
17. A.M. Raab, G. Gebhardt, N. Bolotina, D. Weuster-Botz, C. Lang, *Metabolic Engineering*, **2010**, 12, 518.
18. Y. Kubo, H. Takagi, S. Nakamori, *Journal of Bioscience and Bioengineering*, **2000**, 90, 619.
19. R. Hatti-Kaul, U. Törnvall, L. Gustafsson, P. Börjesson, *TRENDS in Biotechnology*, **2007**, 25, 119.
20. C. Yu, Y. Cao, H. Zou, M. Xian, *Applied Microbiology and Biotechnology*, **2011**, 89, 573.
21. R.M. Atlas, "*Handbook of Microbiological Media*", CRC Press, New York, **2004**.



## DESIGN, SYNTHESIS AND CHARACTERIZATION OF NEW Cu(II) COMPLEXES WITH *N*-SUBSTITUTED SULFONAMIDE LIGANDS

TAMARA TOPALĂ<sup>a,\*</sup>, ANDREEA BODOKI<sup>a</sup>, ALEJANDRO PASCUAL-  
ÁLVAREZ<sup>b</sup>, LUMINIȚA OPREAN<sup>a</sup>, RADU OPREAN<sup>c</sup>

**ABSTRACT.** Three new Cu(II) complexes with potential biological activity with *N*-substituted sulfonamide-type ligands (one new - HL1 and one - H<sub>2</sub>L2 previously reported by our research group) were synthesized and characterized. The aromatic nucleus and the *N*-heterocyclic nuclei found in the ligands' structures could facilitate an efficient interaction between the complexes and DNA, as a preliminary step in exerting their nuclease activity. The HL1 ligand was characterized by elemental analysis, IR spectroscopy and mass spectrometry. The binary complexes, [Cu(L1)<sub>2</sub>] and [Cu(L2)(H<sub>2</sub>O)<sub>2</sub>] and the ternary Cu(II)-sulfonamide-1,10-phenanthroline complex [Cu(L1)<sub>2</sub>(phen)] were characterized by elemental analysis and spectral methods (IR, UV-Vis, EPR). Complex [Cu(L2)(H<sub>2</sub>O)<sub>2</sub>] was characterized by X-ray diffraction, the data suggesting a severely distorted square-planar geometry.

**Keywords:** *N*-substituted sulfonamides, copper(II) complexes, IR, UV-Vis and EPR spectroscopy, X-ray diffraction

### INTRODUCTION

Sulfonamides were the first effective chemotherapeutic agents employed systematically to treat bacterial infections[1]. Due to the fact that they possess a variety of biological activities, they are widely used in ophthalmic, urinary and gastrointestinal infections [2], but also as anti-hypertensive and diuretic

---

<sup>a</sup> Department of General and Inorganic Chemistry, "Iuliu Hatieganu" University of Medicine and Pharmacy Cluj-Napoca, Faculty of Pharmacy, Str. Ion Creangă, Nr.12, 400010 Cluj-Napoca, Romania, \* topala.liana@umfcluj.ro

<sup>b</sup> Departament of Inorganic Chemistry, Universitat de València, Faculty of Pharmacy, Avda. Vicent Andres Estelles, S/N, Spain

<sup>c</sup> Department of Analytical Chemistry and Instrumental Analysis, "Iuliu Hatieganu" University of Medicine and Pharmacy Cluj-Napoca, Faculty of Pharmacy, Str. Pasteur, Nr. 4, 400349 Cluj-Napoca, Romania

drugs [3]. Many sulfonamide-type compounds with interesting biological activities and promising therapeutic potential have recently been synthesized, such as antitumor agents [4, 5], carbonic anhydrase inhibitors [6, 7], antidiabetics [8] and antiviral drugs [9-11].

Another research direction involving sulfonamides is represented by the use of these structures as ligands in coordination chemistry. N-substituted sulfonamides are suitable candidates for coordination chemistry primarily because of the presence of N and O donor atoms in the sulfonamide moiety. According to specific needs, the functional groups of N-substituted sulfonamides may bear additional donor atoms increasing their potential as ligands for metal ions coordination. Also, the sulfonamide structure may be designed to exhibit particular features that allow for a certain coordination pattern of the metallic center or that are correlated with particular desired functions of the final product [12, 13].

1,10-Phenanthroline (phen) is a well-known motif used to obtain a large range of ligands for various metal ions. Its chelating properties allowed researchers to develop copper(II) complexes with very interesting features, like the capacity to cleave the DNA double helix [14-16].

Transition metal complexes obtained with ligands with therapeutic properties have attracted much attention due to the fact that they show enhanced biological activity compared to the free ligands, including antibacterial and antitumor activity [17-19].

It is well known that DNA is very resistant to spontaneous hydrolysis, due to the negatively charged phosphate backbone that prevents attack by nucleophiles[20]. Nature resolved this matter with the help of hydrolytic enzymes, such as restriction endonucleases and topoisomerases, which reduce the hydrolysis time significantly [21]. Although natural nucleases have been very useful in many applications, they also present disadvantages, such as large size and limited range of sequence selectivity [22], which led scientists to conceive the so-called chemical or artificial nucleases. Chemical nucleases are small molecules that are able to bind to DNA, cleave the nucleic acid and be potentially used as gene regulators, mapping of protein and DNA interactions, probing of DNA specific structures and cancer therapy [23].

Copper ions, constituents of numerous enzymes' active centers are particularly appealing for the design of complexes acting as chemical nucleases, as they possess biologically accessible redox potentials and relatively high nucleobase affinity. Copper ions have been extensively studied as models for generating reactive oxygen species [24]. It has been shown that in the presence of hydrogen peroxide, copper ions produce highly reactive DNA-damaging species and induce more DNA base damage than the iron ions and other biologically relevant transition metal ions [25].

The copper(II) ion coordinates to a large range of organic structures with N, O and S donor atoms.

With this in mind, we designed a new *N*-substituted sulfonamide and synthesized three copper(II) complexes, one of them containing a 1,10-phenanthroline molecule as coligand. The evaluation of the complexes' ability to interact with DNA and their nuclease activity are currently being studied.

## RESULTS AND DISCUSSION

### Crystal structure of complex $[\text{Cu}(\text{L}2)(\text{H}_2\text{O})_2]$

Figure 1 shows the molecular structure of complex  $[\text{Cu}(\text{L}2)(\text{H}_2\text{O})_2]$  as well as the atomic labeling scheme adopted. The structural parameters for the coordination polyhedron are listed in Table 1.

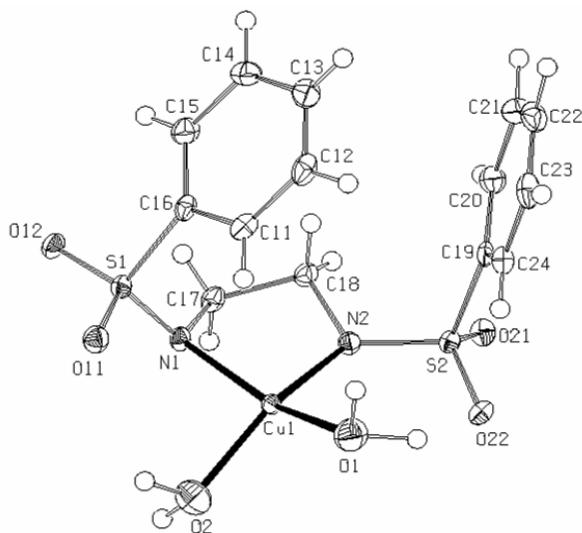


**Figure 1.** Molecular structure of complex  $[\text{Cu}(\text{L}2)(\text{H}_2\text{O})_2]$  showing the atom labeling scheme

**Table 1.** Selected bonds and angles for complex  $[\text{Cu}(\text{L}2)(\text{H}_2\text{O})_2]$

Selected Bond lengths (Å)		Selected Angles (°)	
Cu(1)-N(2)	1.968(2)	N(2)-Cu(1)-N(1)	84.83(10)
Cu(1)-N(1)	1.975(2)	N(2)-Cu(1)-O(2)	151.89(10)
Cu(1)-O(2)	1.991(2)	N(1)-Cu(1)-O(2)	93.00(10)
Cu(1)-O(1)	1.995(2)	N(2)-Cu(1)-O(1)	101.20(10)
		N(1)-Cu(1)-O(1)	154.60(10)
		O(2)-Cu(1)-O(1)	92.73(10)

N,N'-(ethane-1,2-diyl)dibenzenesulfonamide (H<sub>2</sub>L<sub>2</sub>) acts as a bidentate ligand through the two N<sub>sulfonamido</sub> atoms, forming a stable five-member ring with the metal ion. The coordination process is associated with the deprotonation of the two sulfonamide moieties.

Copper(II) is surrounded by two N<sub>sulfonamido</sub> atoms and two O atoms belonging to two water molecules, in a severely distorted square-planar local environment.

The Cu-N<sub>sulfonamido</sub> bond lengths of 1.968(2) Å and 1.975(2) Å are in the range observed for similar reported sulfonamidato complexes [14, 26]. The two Cu-O bond lengths are slightly larger, of 1.991(2) Å and 1.995(2) Å. The angles that describe the coordination polyhedron, in the range 84.83(10) – 101.20(10)°, deviate significantly from 90°. As it is to be expected considering the bidentate nature of the sulfonamide ligand, the angle formed by the central ion and the two N<sub>sulfonamido</sub> atoms is the smallest. The deviations of N(1), N(2), O(1) and O(2) atoms from the mean plane are 0.484, -0.454, 0.404 and -0.454 Å respectively and Cu1 is practically included in the mean plane. These values, together with the bond angles and the tetrahedrality value of 37.75°, are indicative of the severe distortion of the square-planar geometry.

The structure of complex [Cu(L<sub>2</sub>)(H<sub>2</sub>O)<sub>2</sub>] is stabilized by both intra- and inter-molecular hydrogen bonds of moderate strength [27]. The hydrogen bonds involve the hydrogen atoms in the coordinated water molecules and the oxygen atoms of the sulfonamide moieties belonging to the same complex molecule or to adjacent ones. The geometric parameters defining the hydrogen bonds are listed in Table 2.

**Table 2.** Hydrogen bonds for complex [Cu(L<sub>2</sub>)(H<sub>2</sub>O)<sub>2</sub>]

<i>D-H...A</i>	<i>d(D-H) (Å)</i>	<i>d(H...A) (Å)</i>	<i>d(D...A) (Å)</i>	<i>&lt;[9] (°)</i>
O(1)-H(1A)...O(22)	1.07	2.02	2.859(3)	132.9
O(1)-H(1B)...O(12)#1	1.07	1.98	3.035(3)	168.8
O(2)-H(2A)...O(21)#2	1.05	2.00	3.050(3)	175.6
O(2)-H(2B)...O(21)#3	1.06	2.19	2.994(3)	130.4
O(2)-H(2B)...O(11)	1.06	2.44	3.112(3)	119.9

Symmetry transformations used to generate equivalent atoms:

#1 *x*, -*y*+5/2, *z*+1/2 #2 -*x*, -*y*+2, -*z* #3 *x*, *y*+1, *z*

### Infrared spectroscopy

The IR spectra were interpreted according to literature data concerning the absorption bands of the functional groups found in the structure of the sulfonamides. The spectra of the complexes were interpreted by comparison with the IR spectra of the free ligands and according to literature data concerning similar structures [14, 15, 28-30].

The bands assigned to the ligand vibrations are slightly shifted as compared to those that appear in the IR spectra of the uncoordinated sulfonamide, as the electronic structure and the energy of the ligands is modified upon coordination [28].

An important aspect to be noted on the IR spectra of all the Cu(II) complexes is the disappearance of the band assigned to the N-H stretching vibration, indicating the deprotonation of the sulfonamides upon coordination.

In the case of complex  $[\text{Cu}(\text{L}1)_2]$ , the bands characteristic of the antisymmetric and symmetric vibration modes of S=O bonds are  $21\text{ cm}^{-1}$  (for  $[\nu(\text{SO}_2)_{\text{asym}}]$ ),  $11\text{ cm}^{-1}$  (for  $[\nu(\text{SO}_2)_{\text{sym}}]$ ) and  $17\text{ cm}^{-1}$  (for  $[\nu(\text{S-N})]$ ) higher than those corresponding to the free ligands, indicating that the sulfonamide moiety is directly involved in the formation of the complex.

The displacements of the characteristic bands attributed to  $[\nu(\text{SO}_2)_{\text{asym}}]$  and  $[\nu(\text{SO}_2)_{\text{sym}}]$  are slightly shifted towards lower frequencies in complex  $[\text{Cu}(\text{L}1)_2(\text{phen})]$  (from  $1360\text{ cm}^{-1}$  to  $1332\text{ cm}^{-1}$  and from  $1120\text{ cm}^{-1}$  to  $1103\text{ cm}^{-1}$ , respectively), with respect to the uncoordinated ligand, meanwhile the band corresponding to the S-N bond appears at a higher frequency ( $966\text{ cm}^{-1}$ ).

In complex  $[\text{Cu}(\text{L}2)(\text{H}_2\text{O})_2]$ , as a result of the coordination process taking place through the  $\text{N}_{\text{sulfonamido}}$  atoms in both sulfonamide moieties, the bands assigned to  $[\nu(\text{SO}_2)_{\text{asym}}]$  and  $[\nu(\text{SO}_2)_{\text{sym}}]$  are shifted towards lower frequencies of the spectrum, from  $1322\text{ cm}^{-1}$  to  $1266\text{ cm}^{-1}$  and from  $1155\text{ cm}^{-1}$  to  $11133\text{-}1088\text{ cm}^{-1}$ , respectively. The band corresponding to the stretching vibrations of the S-N bond from the same group,  $[\nu(\text{S-N})]$ , is, too, subjected to a rather significant shift towards a lower frequency (from  $1055\text{ cm}^{-1}$  to  $966\text{ cm}^{-1}$ ).

All modifications mentioned above are due to deprotonation of the sulfonamide moiety. The proton loss induces a weak conjugation effect between the N, S and O atoms in the sulfonamide group and an electron transfer to the copper(II) ion via the nitrogen atom [13-15].

The bands corresponding to the characteristic vibrations of 1,10-phenanthroline are rather difficult to assign in the IR spectra of the  $[\text{Cu}(\text{L}1)_2(\text{phen})]$  complex, as they partly overlap the bands characteristic of the bound sulfonamide. However, the high intensity bands at  $1459\text{ cm}^{-1}$  and  $855\text{ cm}^{-1}$  could be assigned to the coordinated 1,10-phenanthroline molecule.

The bands in the range  $1595\text{-}1491\text{ cm}^{-1}$  must include the stretching vibrations of the C=C and C=N bonds in the 1,10-phenanthroline structure but also the similar  $\nu(\text{C}=\text{C})$  vibrations in the aromatic rings present in the structure of the sulfonamide.

### Diffuse reflectance spectroscopy

The diffuse reflectance spectrum of complex  $[\text{Cu}(\text{L}1)_2]$  (Figure 3) shows a broad band at around  $22624\text{ cm}^{-1}$  ( $442\text{ nm}$ ), assigned to a charge-transfer transition, and a wide asymmetric band centered around  $16129\text{ cm}^{-1}$  ( $620\text{ nm}$ ), corresponding to the d-d transitions in the  $\text{CuN}_4$  chromophore [31].



In the diffuse reflectance spectrum of complex  $[\text{Cu}(\text{L}1)_2(\text{phen})]$  (Figure 4) a broad band at around  $22472 \text{ cm}^{-1}$  (445 nm), assigned to a charge-transfer transition is identified, as well as a wide asymmetric band centered around  $15823 \text{ cm}^{-1}$  (632 nm), attributed to the d-d transitions characteristic of a  $\text{CuN}_6$  chromophore with the copper ion in a distorted octahedral environment [31].

The fact that the differences in the diffuse reflectance spectra of the  $[\text{Cu}(\text{L}1)_2]$  and  $[\text{Cu}(\text{L}1)_2(\text{phen})]$  complexes are not significant seem to indicate that the octahedral complex shows an important degree of tetragonal distortion, adopting an elongated tetragonal-octahedral geometry [31].

The d – d transitions in complex  $[\text{Cu}(\text{L}2)(\text{H}_2\text{O})_2]$  generate a wide band with a maximum at  $17241 \text{ cm}^{-1}$  (582nm) (Figure 5), in agreement with the distorted square-planar geometry of a  $\text{CuN}_2\text{O}_2$  chromophore.

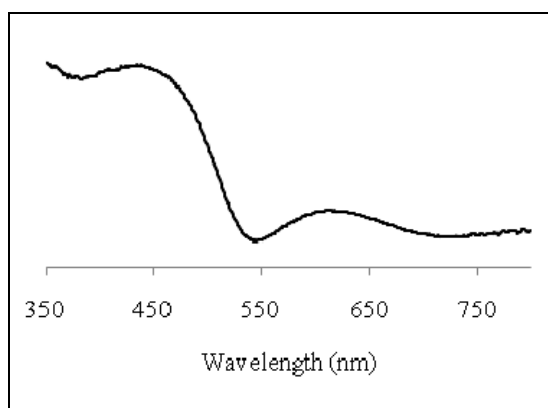


**Figure 3.** Diffuse reflectance spectrum of complex  $[\text{Cu}(\text{L}1)_2]$

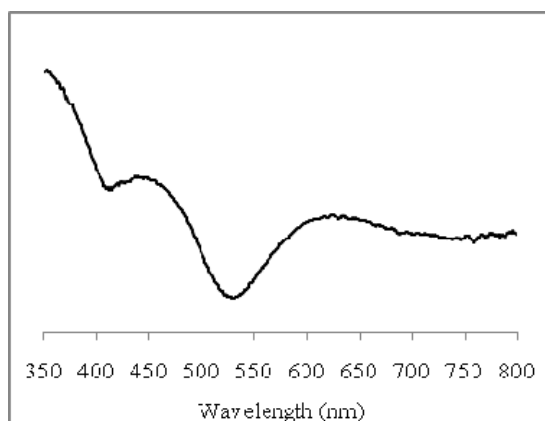


**Figure 4.** Diffuse reflectance spectrum of complex  $[\text{Cu}(\text{L}1)_2(\text{phen})]$

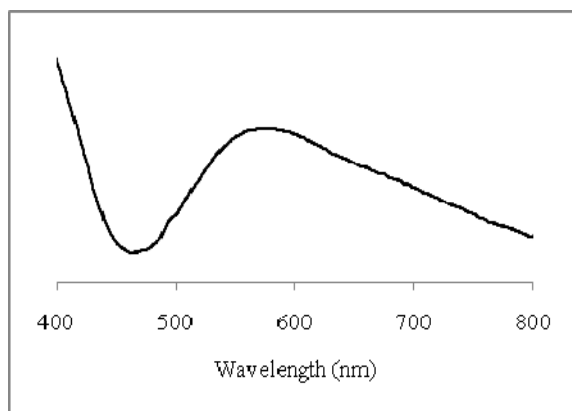


**Figure 5.** Diffuse reflectance spectrum of complex  $[\text{Cu}(\text{L}2)(\text{H}_2\text{O})_2]$

### Electronic paramagnetic resonance spectroscopy

The EPR spectrum of  $[\text{Cu}(\text{L}1)_2(\text{phen})]$  is axial (Figure 6). The EPR parameters obtained by simulation [32] are  $g_{\parallel} = 2.340$  and  $g_{\perp} = 2.063$ . The values  $g_{\parallel} > g_{\perp}$  are indicative of a mainly copper(II)  $d_{x^2-y^2}$  ground state.

The EPR spectrum of  $[\text{Cu}(\text{L}2)(\text{H}_2\text{O})_2]$  is rhombic (Figure 7) with the calculated  $g$  parameters as follows:  $g_x = 2.04$ ,  $g_y = 2.066$  and  $g_z = 2.190$ . The  $R$  value of 0.161 indicates the presence of the unpaired electron of copper(II) in a  $d_{x^2-y^2}$  orbital.

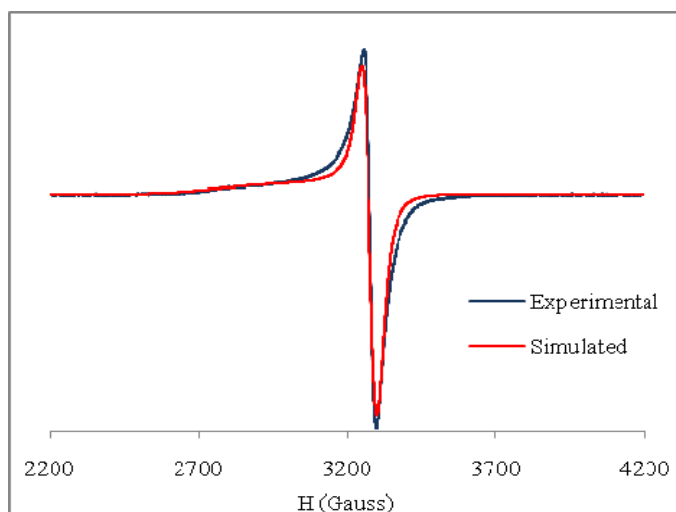


**Figure 6.** EPR spectra (X-band) of complex  $[\text{Cu}(\text{L}1)_2(\text{phen})]$

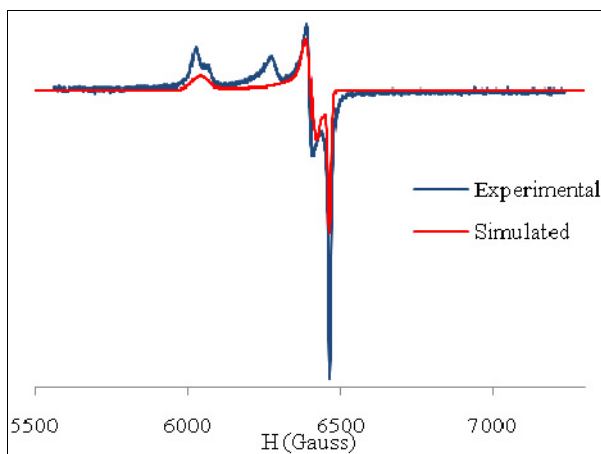


**Figure 7.** EPR spectra (X-band) of complex [Cu(L2)(H<sub>2</sub>O)<sub>2</sub>]

## CONCLUSIONS

A new N-substituted sulfonamide (HL1) was synthesized, as well as three Cu(II) complexes, with different coordination environments and geometries. The obtained compounds were characterized by various physico-chemical methods. The [Cu(L2)(H<sub>2</sub>O)<sub>2</sub>] complex was characterized by X-ray diffraction, while the proposed formulas for the other two Cu(II) complexes are supported by the spectroscopic data.

## EXPERIMENTAL SECTION

### Materials and methods

All chemicals and solvents were commercially available (Sigma, Alfa Aesar, Panreac) and used without further purification.

Elemental analyses (C, H, N, S) were performed on a Carlo Erba AAS instrument. Infrared spectra were recorded with a Thermo Scientific Nicolet iS10 FT-IR spectrophotometer from 4000 to 400 cm<sup>-1</sup> using the Smart iTR ATR accessory. Electrospray ionization-mass spectra (+ mode) analyses were performed on a Bruker Esquire 3000 plus liquid chromatography-mass spectrometry (LC-MS) system. Electronic paramagnetic resonance (EPR) spectra were collected at the X-band frequency at room temperature with a Bruker ELEXSYS spectrometer. The diffuse reflectance spectra of the copper(II) complexes were recorded on an Jasco V-550 instrument, in the interval 300 - 800 nm.

## Synthesis of the ligands

For the synthesis of *N*-(pyridin-2-yl) quinoline-8-sulfonamide, HL1 (see scheme 1), 8.8 mmol (2 g) of solid quinoline-8-sulfonyl chloride were added to a solution containing 8.8 mmol (0.82 g) of pyridin-2-amine in 6 mL of pyridine. The reddish-orange suspension was stirred at 0°C for 1 hour, and then at room temperature for another 2 hours and 30 minutes. 50 mL of cold water were added to the orange suspension and the mixture was stirred for another 2 hours in an ice bath. The resulting light orange solid was filtered and recrystallized with 50 mL of ethanol at 40°C. The purified ligand was a white solid, obtained with a yield of 50%.

Compound *N,N'*-(ethane-1,2-diyl)dibenzenesulfonamide, H<sub>2</sub>L2 (Figure 2), was synthesized and characterized as previously reported by our research group [14].

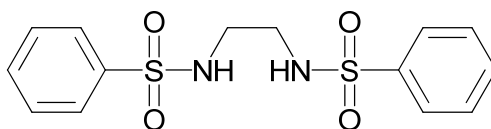


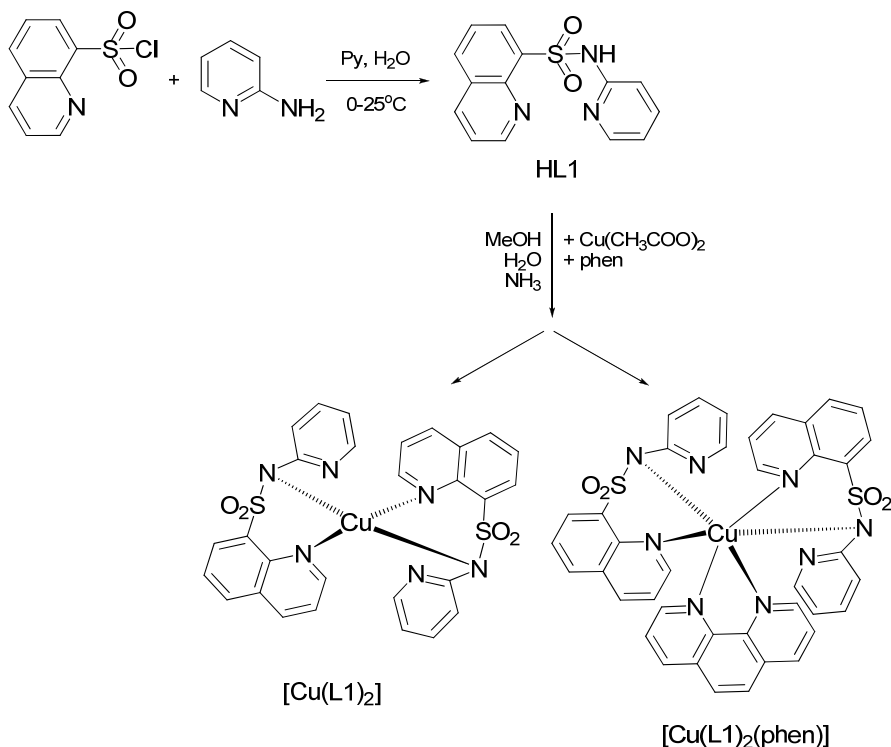
Figure 2. Ligand H<sub>2</sub>L2 structure

## Synthesis of [Cu(L1)<sub>2</sub>] and [Cu(L1)<sub>2</sub>(phen)]

0.25 mmol (0.045 g) of solid 1,10-phenanthroline was added to a solution containing 0.25 mmol (0.05 g) of Cu(CH<sub>3</sub>COO)<sub>2</sub>·H<sub>2</sub>O in 5 mL of H<sub>2</sub>O. The resulting blue mixture was added dropwise to a solution of 0.5 mmol (0.142 g) of HL1 in 30 mL of methanol containing 2 mL of NH<sub>3</sub> 25% and stirred at room temperature for 1 hour. The green solid obtained ([Cu(L1)<sub>2</sub>]) was removed and after a few days, a green microcrystalline deposit ([Cu(L1)<sub>2</sub>(phen)]) formed in the filtrate. The synthetic route used to obtain the [Cu(L1)<sub>2</sub>] and [Cu(L1)<sub>2</sub>(phen)] complexes can be depicted as in Scheme 1.

### Synthesis of [Cu(L2)(H<sub>2</sub>O)<sub>2</sub>]

A ligand solution was prepared by dissolving 1 mmol (0.34 g) of H<sub>2</sub>L2 in 30 mL of methanol containing 2 mL NH<sub>3</sub> 30%. To this solution, a mixture of 1 mmol (0.241 g) Cu(NO<sub>3</sub>)<sub>2</sub>·3H<sub>2</sub>O in 20 mL methanol was added dropwise, under continuous stirring. The resulting blue-purple precipitate, possibly a copper(II) complex with NH<sub>3</sub>, was removed from the reaction mixture. After approximately 48 h, blue plate crystals, suitable for X-ray diffraction, formed in the filtrate.



**Scheme 1.** Synthetic route for the HL1 ligand and its copper(II) complexes

### Elemental analysis

The results of the C, H, N, S elemental analysis of the N-substituted sulfonamide and of the Cu(II) complexes are shown in Table 3.

**Table 3.** Elemental analysis results for the sulfonamide ligand and for the copper(II) complexes

	Molecular formula	Molecular weight (g/mol)	Elemental analysis			
			Experimental % (Calculated %)			
			C	H	N	S
HL1	C <sub>14</sub> H <sub>11</sub> N <sub>3</sub> O <sub>2</sub> S	285.32	58.57 (58.93)	3.76 (3.89)	14.45 (14.73)	11.13 (11.24)
[Cu(L1) <sub>2</sub> ]	C <sub>28</sub> H <sub>20</sub> CuN <sub>6</sub> O <sub>4</sub> S <sub>2</sub>	634.1	53.8 (53.03)	3.37 (3.15)	13.3 (13.25)	10.31 (10.11)
[Cu(L1) <sub>2</sub> (phen)]	C <sub>40</sub> H <sub>28</sub> CuN <sub>8</sub> O <sub>4</sub> S <sub>2</sub>	812.42	59.05 (59.08)	3.39 (3.44)	13.58 (13.78)	7.74 (7.87)
[Cu(L2)(H <sub>2</sub> O) <sub>2</sub> ]	C <sub>14</sub> H <sub>18</sub> CuN <sub>2</sub> O <sub>6</sub> S <sub>2</sub>	437.96	39.19 (38.39)	3.86 (4.14)	5.72 (6.39)	13.12 (14.64)

### Infrared spectroscopy

The bands corresponding to the valence vibrations characteristic to various groups are shown in Table 4.

**Table 4.** Characteristic frequencies ( $\text{cm}^{-1}$ ) of the sulfonamide ligands and of the Cu(II) complexes in the IR spectra

	$\nu(\text{N-H})$	$\nu_{\text{asym}}(\text{SO}_2)$	$\nu_{\text{sym}}(\text{SO}_2)$	$\nu(\text{S-N})$
HL1	3120	1360	1120	958
[Cu(L1) <sub>2</sub> ]	-	1381	1131	975
[Cu(L1) <sub>2</sub> (phen)]	-	1332	1103	966
[Cu(L2)(H <sub>2</sub> O) <sub>2</sub> ] (H <sub>2</sub> L2)	- (3322, 3266d)	1266 (1322)	1133-1088d (1155)	966 (1055)

d - doublet

### Mass spectrum of HL1

Positive mode ionization ESI experiment was run using a DMF ligand solution. In the mass spectrum of the HL1 ligand, the peak at  $m/z$  286.07 corresponds to the pseudomolecular ion  $[\text{HL1} + \text{H}]^+$ .

### X-ray crystallography for complex [Cu(L2)(H<sub>2</sub>O)<sub>2</sub>]

A blue plate crystal of complex  $[\text{Cu}(\text{L2})(\text{H}_2\text{O})_2]$ , measuring 0.15 x 0.08 x 0.04 mm, was mounted on a glass fiber and used for data collection. Crystal data were collected at a temperature of 100.0(2) K, using a Bruker X8 Kappa APEXII diffractometer. Graphite monochromated MoK(alpha) radiation ( $\lambda = 0.71073$  angstrom's) was used throughout. The data were processed with APEX2 [33] and corrected for absorption using SADABS (transmission factors: 1.000 - 0.863) [34]. The structure was solved by direct methods using the program SHELXS-97 [35] and refined by full-matrix least-squares techniques against  $F^2$  using SHELXL-97 [36]. Positional and anisotropic atomic displacement parameters were refined for all nonhydrogen atoms. Hydrogen atoms were located in difference maps and included as fixed contributions riding on attached atoms with isotropic thermal parameters 1.2 times greater than those of their carrier atoms. Criteria of a satisfactory complete analysis were the ratios of "rms" shift to standard deviation less than 0.001 and no significant features in final difference maps. Atomic scattering factors were from "International Tables for Crystallography" [37]. Programs PLATON [38] and SCHAKAL [39] were used to obtain the molecular graphics. A summary of the crystal data, experimental details and refinement results for complex  $[\text{Cu}(\text{L2})(\text{H}_2\text{O})_2]$  are listed in Table 5.

**Table 5.** Crystal and structure refinement for complex [Cu(L2)(H<sub>2</sub>O)<sub>2</sub>]

Empirical formula	C <sub>14</sub> H <sub>18</sub> CuN <sub>2</sub> O <sub>6</sub> S <sub>2</sub>
Formula weight	437.96
Temperature (K)	100(2) K
Wavelength (Å)	0.71073
Crystal system, space group	Monoclinic, P2(1)/c (No. 14)
a [Å]	15.8938(3)
b [Å]	8.7865(2)
c [Å]	13.7732(3)
α [°]	90
β [°]	113.33(10)
γ [°]	90
Volume [Å <sup>3</sup> ]	1766.18(6)
Z, calculated density [Mg m <sup>-3</sup> ]	4, 1.647
Absorption coefficient [mm <sup>-1</sup> ]	1.506
F(000)	900
Crystal size [mm]	0.15 x 0.08 x 0.04
θ range for data collection [°]	1.40 to 26.39
Limiting indices	-19 ≤ h ≤ 18, 0 ≤ k ≤ 10, 0 ≤ l ≤ 17
Reflections collected/unique	20236 / 3609 [R[41] = 0.0408]
Data/restraints/parameters	3609 / 0 / 226
Completeness to θ=26.39 [%]	99.8%
Final R indices [I > 2σ(I)]	R1 = 0.0388, wR2 = 0.0985
R indices (all data)	R1 = 0.0495, wR2 = 0.1039

## ACKNOWLEDGEMENTS

The authors are grateful to Professor Gloria Alzuet Piña (Faculty of Pharmacy, Universidad de València) for the useful discussions and for the help provided in writing this paper.

The present work was supported financially by research Project POSDRU 107/1.5/S/78702.

## REFERENCES

1. T. Nogrady, "Medicinal Chemistry: A biochemical approach", Second edition, Oxford University Press, New York, **1988**, chapter 1.
2. H. Alyar, S. Alyar, A. Unal, N. Ozbek, E. Sahin, N. Karacan, *Journal of Molecular Structure*, **2012**, 1028, 116.

3. F. Abbate, A. Casini, T. Owa, A. Scozzafava, C.T. Supuran, *Bioorganic & Medicinal Chemistry Letters*, **2004**, *14*, 217.
4. N.S. El-Sayed, E.R. El-Bendary, S.M. El-Ashry, M.M. El-Kerdawy, *European Journal of Medicinal Chemistry*, **2011**, *46*, 3714.
5. Z. Huang, Z. Lin, J. Huang, *European Journal of Medicinal Chemistry*, **2001**, *36*, 863.
6. T.H. Maren, C.W. Conroy, *Journal of Biological Chemistry*, **1993**, *268*, 26233.
7. M. Jaiswal, P.V. Khadikar, C.T. Supuran. *Bioorganic & Medicinal Chemistry Letters*, **2004**, *14*, 5661.
8. D. Patel, M. Jain, S.R. Shah, R. Bahekar, P. Jadav, A. Joharapukar, N. Dhanesha, M. Shaikh, K.V.V.M. Sairam, P. Kapadnis, *Bioorganic & Medicinal Chemistry Letters*, **2012**, *22*, 1111.
9. A.K. Ghosh, L.M. Swanson, H. Cho, S. Leschenka, K.A. Hussain, S. Kay, D.E. Walters, Y. Koh, H. Mitsuya, *Journal of Medicinal Chemistry*, **2005**, *48*, 3576.
10. B.R.Stranix, J.F. Lavallee, G. Sevigny, J. Yelle, V. Perron, N. LeBerre, D. Herbart, J.J. Wu, *Bioorganic & Medicinal Chemistry Letters*, **2006**, *16*, 3459.
11. S.L. Bogen, A. Arasappan, F. Velasquez, M. Blackman, R. Huelgas, W. Pan, E. Siegel, L.G. Nair, S. Venkatraman, Z. Guo, R. Doll, N.Y. Shih, F.G. Njoroge, *Bioorganic & Medicinal Chemistry*, **2010**, *18*, 1854.
12. J.L. Garcia-Gimenez, G. Alzuet, M. Gonzalez-Alvarez, A. Castineiras, M. Liu-Gonzalez, J. Borrás, *Inorganic Chemistry*, **2007**, *46*, 7178.
13. J.L. Garcia-Gimenez, M. Gonzalez-Alvarez, M. Liu-Gonzalez, B. Macias, J. Borrás, G. Alzuet, *Journal of Inorganic Biochemistry*, **2009**, *103*, 923.
14. A. Bodoki, A. Hangan, L. Oprean, G. Alzuet, A. Castineiras, J. Borrás, *Polyhedron*, **2009**, *28*, 2537.
15. A. Hangan, A. Bodoki, L. Oprean, G. Alzuet, M. Liu-Gonzalez, J. Borrás, *Polyhedron*, **2010**, *29*, 1305.
16. B. Macías, I. Garcia, M.V. Villa, J. Borrás, M. Gonzalez-Alvarez, A. Castineiras, *Journal of Inorganic Biochemistry*, **2003**, *96*, 367.
17. F. Blasco, L. Perello, J. Latorre, J. Borrás, S. Garcia-Granda, *Journal of Inorganic Biochemistry*, **1996**, *61*, 143.
18. I. Zanellato, J.M. Heldt, A. Vessieres, G. Jaouen, D. Osella, *Inorganica Chimica Acta*, **2009**, *362*, 4037.
19. J.F. Smyth, S. Aamdal, A. Awada, C. Dittrich, F. Caponigro, P. Schoffsky, M. Gore, T. Lesimple, N. Djurasinovic, B. Baron, M. Ravic, P. Fumoleau, C.J.A. Punt, *Annals of Oncology*, **2005**, *16*, 158.
20. M. Roy, S. Dhar, B. maity, A.R. Chakravarty, *Inorganica Chimica Acta*, **2011**, *375*, 173.
21. C. Liu, M. Wang, T. Zhang, H. Sun, *Coordination Chemistry Reviews*, **2004**, *248*, 147.
22. B. Armitage, *Chemical Reviews*, **1998**, *98*: 1171-1200.
23. Q.Jiang, N. Xiao, P. Shi, Y. Zhu, Z. Gio, *Coordination Chemistry Reviews*, **2007**, *251*, 1951.
24. S. Bellú, E. Hure, M. trape, C. Trossero, G. Molina, C. Drogo, P.A.M. Williams, A.M. Atria, J.C. Munoz Acevedo, S. Zacchino, M. Sortino, D. Campagnoli, M. Rizzotto, *Polyhedron*, **2005**, *24*, 501.



25. M. Dizdaroglu, G. Rao, B. Halliwell, E. Gajewski, *Archives of Biochemistry and Biophysics*, **1991**, 285, 317.
26. J. Sanchez-Piso, J.A. Garcia-Vasquez, J. Romero, M.L. Duran, A. Sousa - Pedrares, E. Labisbal, O. R. Nascimento, *Inorganica Chimica Acta*, **2002**, 328, 111.
27. G.A. Jeffrey, "Introduction to hydrogen bonding", Oxford University Press, Oxford, **1997**, chapter 2.
28. R.M. Silverstein, F.X. Webster, "Spectrometric identification of Organic Compounds", Wiley, New York, **1998**, chapter 2.
29. K. Nakamoto, "Infrared and Raman Spectra of inorganic and coordination compounds", Wiley, New York, **1986**, chapter 3.
30. J.L. Garcia-Gimenez, J. Hernandez-Gil, A. Martinez-Ruiz, A. Castineiras, M. Liu-Gonzalez, F.V. Pallardo, J. Borrás, G. Alzuet, *Journal of Inorganic Biochemistry*, **2013**, 121, 167.
31. B.J. Hataway, D.E. Billing, *Coordination Chemistry Reviews*, **1970**, 5, 143.
32. Bruker Analytic, WINEPRSimphonia 1.25, 1994, Karlsruhe.
33. Bruker, APEX2 Software, **2005**, BrukerAXS Inc. Vs.0-1: Madison, Wisconsin, USA.
34. G.M. Sheldrick, SADABS, Program for Empirical Absorption Correction of Area Detector Data, **2007**, University of Goettingen, Germany.
35. G.M. Sheldrick, *Acta Crystallographica*, **1990**, A46, 467.
36. G.M. Sheldrick, SHELXL-97, Program for the Refinement of Crystal Structures, **1997**, University of Goettingen, Germany.
37. A.J.C. Wilson, "International Tables for Crystallography", Kluwer Academic Publishers, Dordrecht, **1995**, Vol. C.
38. A.L. Spek, PLATON, A Multipurpose Crystallographic Tool, **2003**, Utrecht University, Utrecht, The Netherlands.
39. E. Keller, SCHAKAL-97, A computer program for the graphic representation of molecular and crystallographic models, **1997**, University of Freiburg, Germany.

## COMPUTING THE HARARY INDEX OF A CLASS OF NANOSTAR DENDRIMERS

NAHID YAVARI<sup>a</sup>, HOSSEIN SHABANI<sup>a,\*</sup>, HAMID REZA FAZLOLLAHI<sup>a</sup>,  
MIRCEA V. DIUDEA<sup>b</sup>

**ABSTRACT.** The Harary index of a molecular graph  $G$  is defined as the summation of the terms  $1/d_G(u,v)$  where  $d_G(u,v)$  is the topological distance between  $u$  and  $v$  of  $G$ . The aim of this paper is to compute Harary index of a class of nanostar dendrimers by using a group theoretical method.

**Keywords:** *Graph automorphism, Harary index, dendrimer.*

### INTRODUCTION

Dendrimers are hyper-branched synthetic polymers (i.e. macromolecules) with a well-defined molecular topology [1-6]. Dendrimer chemistry was first introduced in 1978 by Vogtle [1]. He synthesized the first “cascade molecule”. In 1985, Tomalia synthesized the first family of dendrimers [3]. Diudea and Katona have characterized the topology of dendrimers [7]. The topological study of these macromolecules is the aim of this article.

Let  $G$  be a molecular graph with the vertex set  $V(G)$  representing atoms and the edge set  $E(G)$  collecting the chemical bonds ( $uv$ ) that join the atoms  $u$  and  $v$  in the molecular graph. The length of the shortest path between two vertices is called the topological distance and is denoted by  $d(u,v)$ ; the maximum distance between the vertex  $u$  and any vertex  $v$  in  $G$  is named the eccentricity of  $u$  and is denoted  $e(u)$ .

Denote by  $Aut(G)$  the automorphism group of  $G$ . A topological index  $TI$  is a number that is invariant under the  $Aut(G)$ . A variety of  $TIs$  have been proposed for the characterization of chemical structures and used for structure-property correlations in QSPR models [8-10].

---

<sup>a</sup> *Institute of Nanoscience and Nanotechnology, University of Kashan, Kashan 87317-51167, I. R. Iran. \* Corresponding Author: shabai@grad.kashanu.ac.ir*

<sup>b</sup> *Faculty of Chemistry and Chemical Engineering, Babes-Bolyai University, 400028 Cluj-Napoca, Romania*

In particular, the Harary index of a graph,  $H(G)$ , has been introduced in 1993, independently by Ivanciuc *et al.* [11] and by Plavšić *et al.* [12]. Even earlier, the QSAR group in Timisoara, Romania, particularly Ciubotariu [13], have used this index to express the decay of interaction between pairs of atoms in molecules as the distance between them increases. It has been named in the honor of Frank Harary, on the occasion of his 70<sup>th</sup> birthday. The Harary index is defined as follows:

$$H(G) = \sum_{u,v \in V(G)} \frac{1}{d_G(u,v)}$$

where the summation runs over all unordered pairs of vertices of the graph  $G$  and  $d_G(u,v)$  denotes the topological distance between any two vertices  $u$  and  $v$  of  $G$  (i.e., the number of edges in a shortest path connecting  $u$  and  $v$ ). Mathematical properties and some applications of  $H$ , the reader can find in refs [14-21].

In this paper, we use a group theoretical method [22-26] for computing the Harary index of the nanostar dendrimer in Figure 1.

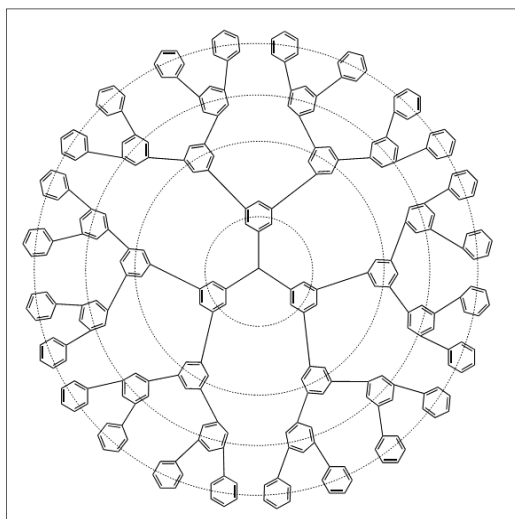


**Figure 1.** Molecular nanostar dendrimer  $D[4]$ .

Throughout this paper, our notation is standard and taken mainly from the standard books of graph theory as like as [27].

### MAIN RESULTS AND DISCUSSION

In this section we compute the Harary index of the dendrimer  $D[n]$  (Figure 1). This dendrimer has a central vertex (denoted  $x_0$ ) of degree 3 and the number of vertices and edges of  $D[n]$  is equal to  $|V(D[n])| = 1 + 18 \times (2^n - 1)$  and  $|E(D[n])| = 21 \times (2^n - 1)$ .

For a vertex  $v$  of the graph  $G$ , let  $N_i(v)$  be the set of vertices at distance  $i$  (of which maximum equals  $e(v)$ ) from  $v$ . There is a partition of the vertex set of  $G$  as  $V(G) = N_0(v) \cup N_1(v) \cup \dots \cup N_{e(v)}(v)$ ; it is named a *representation* of  $G$  with respect to  $v$ . Let  $Rd(v) = \sum_{i=1}^{e(v)} \frac{n_i(v)}{i}$  and then rewrite the Harary index as  $H(G) = \sum_{v \in V(G)} Rd(v)$ .

**Theorem.** If the action of automorphism group of  $G$  on  $V(G)$  contains the orbits  $V_1, V_2, \dots, V_k$ , then  $H(G) = \sum_{i=1}^k |V_i| Rd(v_i)$ , where  $v_i$  is a vertex of the  $i$ -th orbit. In particular, if the action is transitive and  $v$  is a vertex of  $G$  then  $H(G) = |V(G)|Rd(v)$ .

We apply this theorem to compute the Harary index of  $D[n]$ . In each stage  $n$  we have 4 steps  $n_1$  to  $n_4$ . Therefore  $D[n]$  has  $4n + 1$  steps and core is in step 0 ( $m = 0$ ) of this molecule. The automorphism group of  $D[n]$  is isomorphic to the wreath product  $Z_2 \sim S_3$ , where  $S_3$  acts on  $\Omega = \{1, 2, \dots, 3 \times (2^n - 1)\}$ . Choose the node  $x_0$  of  $D[n]$ , with minimum eccentricity, as the root and suppose  $x_{0,0} = x_0$ . Set in the following

$$V(D[n]) = \{x_{0,0}, x_{1,1}, \dots, x_{1,6}, \dots, x_{3(2^n-1),1}, \dots, x_{3(2^n-1),6}\}.$$

If automorphism group of  $D[m]$  acts on  $D[m]$  then the orbits are  $V_0 = \{x_{0,0}\}, V_1 = \{x_{1,1}, x_{2,1}, x_{3,1}\}, \dots, V_{4n} = \{x_{3(2^{n-1}-1)+1,4}, \dots, x_{3(2^n-1),4}\}.$

Let  $m$  be the number of steps in  $D[n]$  and therefore  $n = 4m + 1$ . Suppose  $b$  is the residue  $m$  module 4 and  $d$  is equal to  $b$  except  $d = 4$  where  $b = 0$ . Denote by  $\delta_{i,j}$ , the Kronecker delta and define the bellow notations:

$$\Delta_d = \delta_{2,d} + \delta_{3,d}, \eta(y+t) = \frac{2^{\Delta_d}}{y+t},$$

$$\mu(x,t) = 2^{(x-1)} \left( \frac{1}{3 \cdot (x-1) + t + 1} + \frac{2}{3 \cdot (x-1) + t + 2} + \frac{2}{3 \cdot (x-1) + t + 3} + \frac{1}{3 \cdot (x-1) + t + 4} \right),$$

$$f(t, p) = \sum_{x=1}^p \mu(x, t) + 2^p \sum_{y=1}^b \eta(y + t),$$

$$p = \left\lfloor \frac{k}{4} \right\rfloor - \left( \left\lfloor \frac{m}{4} \right\rfloor - \delta_{4,d} \right) - 1 \text{ and } q = \left\lfloor \frac{m}{4} \right\rfloor - \delta_{4,d}.$$

Therefore for the vertex in  $n = 0$  we have:

$$Rd(x_0) = \frac{3}{2} f(0, \left\lfloor \frac{k}{4} \right\rfloor)$$

and if  $n \neq 0$  then, for any vertex in row  $n$ ,  $Rd$  is equals to:

$$\frac{1}{2} \sum_{m=1}^k 3 \cdot 2^q [2 \cdot \{f(|3-d|, p) + \Delta_d f(|3-d|+2, p) + (\sum_{y=1}^{\delta_{p,-1}(k+d-2)} \frac{\eta(y)}{2^{\Delta_d}} + \delta_{2,d}(k-d))\} +$$

$$2^{\Delta_d} \{ \sum_{z=1}^q f(d+3z-1, p+z) + 2f(3q+d, \left\lfloor \frac{k}{4} \right\rfloor) + \frac{1}{3q+d} + \sum_{x=1}^q \frac{\mu(x, d-1)}{2^{(x-1)}} + \frac{10}{3} (2^{\lfloor \frac{m}{4} \rfloor} - 1) \} ]$$

so, the Harary index of  $D[n]$  is equal to:

$$H(D[n]) =$$

$$\frac{1}{2} \{ 3f(0, \left\lfloor \frac{k}{4} \right\rfloor) + \sum_{m=1}^k 3 \cdot 2^q [2 \cdot \{f(|3-d|, p) + \Delta_d f(|3-d|+2, p) + (\sum_{y=1}^{\delta_{p,-1}(k+d-2)} \frac{\eta(y)}{2^{\Delta_d}} + \delta_{2,d}(k-d))\} +$$

$$2^{\Delta_d} \{ \sum_{z=1}^q f(d+3z-1, p+z) + 2f(3q+d, \left\lfloor \frac{k}{4} \right\rfloor) + \frac{1}{3q+d} + \sum_{x=1}^q \frac{\mu(x, d-1)}{2^{(x-1)}} + \frac{10}{3} (2^{\lfloor \frac{m}{4} \rfloor} - 1) \} ] \}$$

In Table 1, the Harary index of  $D[n]$  for some  $n$  is computed.

**Table 1. Values of Harary index in dendrimers  $D[n]$**

$n$	$H(D[n])$	$k$	$H(D[n])$	$k$	$H(D[n])$	$n$	$H(D[n])$
1	4.5	6	163.775	11	1131.262	16	9403.148
2	19.5	7	258.443	12	1352.133	17	11508.093
3	38.9	8	291.608	13	1890.838	18	11593.067
4	56.589	9	449.681	14	3126.270	19	15747.269
5	78.168	10	788.397	15	4365.852	20	29038.085

## CONCLUSIONS

The Harary index of a molecular graph  $G$ , defined as the summation of the reciprocal of topological distance between  $u$  and  $v$  of  $G$ , can be important in describing the decay of interaction between pairs of atoms in molecules as the distance between them increases. In this paper, a group theoretical method was applied to compute Harary index of a class of nanostar dendrimers.

## ACKNOWLEDGEMENT

This work was partially supported by Institute of NanoSciTech of the University of Kashan.

## REFERENCES

1. E. Buhleier, W. Wehner, F. Vogtle, *Synthesis*, **1978**, 2, 155.
2. G.R. Newkombe, Z.-Q.Yao, H. Baker, V.K. Gupta, *J. Org. Chem.*, **1985**, 50, 2003.
3. D.A. Tomalia, H. Baker, J.R. Dewald, M. Hall, G. Kallos, S. Martin, J. Roeck, J. Ryder, P.A. Smith, *Polym. J. (Tokyo)*, **1985**, 17, 117.
4. D.A. Tomalia, A.M. Naylor, W.A.I. Goddard, *Angew. Chem. Int. Ed.*, **1990**, 29, 138.
5. C.J. Hawker, J.M.J. Frechet, *J. Am. Chem. Soc.*, **1990**, 112, 7638.
6. E.R. Gilles, J.M.J. Frechet, *Drug Discovery Today*, **2005**, 10, 35.
7. M.V. Diudea, G. Katona, in: G.A. Newkome, Ed., *Advan. Dendritic Macromol.*, **1999**, 4, 135.
8. I. Lukovits, *Int. J. Quantum.Chem.: Quantum Biology Symp.*, **1992**, 19, 217.
9. M.V. Diudea, Ed., *QSPR/QSAR Studies by Molecular Descriptors*, Nova, Huntington, N.Y., **2001**.
10. E. Estrada and E. Molina, in: M.V. Diudea, Ed., *QSPR/QSAR Studies by Molecular Descriptors*, Nova Science, Huntington, New York, **2001**, 83–107.
11. O. Ivanciuc, T.S. Balaban, and A.T. Balaban, *J. Math. Chem.*, **1993**, 12, 309.
12. D. Plavšić, S. Nikolić, N. Trinajstić, ad Z. Mihalić, *J. Math. Chem.*, **1993**, 12, 235.
13. D. Ciubotariu, PhD thesis, 1987, Timisoara, Romania; D. Ciubotariu, M. Medeleanu, V. Vlaia, T. Olariu, C. Ciubotariu, D. Dragos, and C. Seiman, *Molecules*, **2004**, 9, 1053.
14. K.C. Das, B. Zhou, and N. Trinajstic, *J. Math. Chem.*, **2009**, 46, 1369.
15. M.V. Diudea, *J. Chem. Inf. Comput. Sci.*, **1997**, 37, 292.
16. L. Feng and A. Ilic, *Appl. Math. Lett.*, **2010**, 23, 943.
17. I. Gutman, *Indian J. Chem.*, **1997**, 36 A, 128.
18. B. Lucić, A. Miličević, S. Nikolić, and N. Trinajstić, *Croat. Chem. Acta*, **2002**, 75, 847.
19. K. Xu, *Discrete Appl. Math.*, **2012**, 160, 321.
20. K. Xu and K.C. Das, *Discrete Appl. Math.*, **2011**, 159, 1631.
21. B. Zhou, X. Cai, and N. Trinajstić, *J. Math. Chem.*, **2008**, 44, 611.
22. M.R. Darafsheh, *Acta. Appl. Math.*, **2010**, 110, 1225.
23. H. Shabani, A.R. Ashrafi and M.V. Diudea, *Croat. Chem. Acta*, **2010**, 83, 439.
24. H. Shabani, A.R. Ashrafi and I. Gutman, *Studia UBB Chemia*, **2010**, 55, 107.
25. A.R. Ashrafi, H. Shabani, M.V. Diudea, *MATCH, Commun. Math. Comput. Chem.*, **2013**, 69, 151.
26. A.R. Ashrafi, H. Shabani and M.V. Diudea, *Studia UBB Chemia*, **2010**, 4, 137.
27. F. Buckley, F. Harary, *Addison-Wesley, Reading, MA*, **1990**.